# The application of time-lapse microgravity to investigate and monitor subsidence related to salt dissolution

**Thesis submitted in accordance with requirements of Keele University for the degree of Doctor in Philosophy by Michael William Branston**

**May 2003**

# Abstract

Subsidence of the ground surface due to the removal of support either through man's mining activity or natural dissolution of rock occurs throughout the world. In Cheshire, subsidence related to salt extraction has occurred in various forms for centuries, the most frequent and devastating occurring in the $18^{th}$ and $19^{th}$ centuries. Subsidence in Cheshire has restricted the industrial development of areas with a history of salt extraction and jeopardised the stability of urban areas.

It is important for the remediation of such sites, that the cause of subsidence and it's state of development is established. Increasingly, practitioners are looking toward cost effective, non-invasive techniques to rapidly assess subsidence afflicted areas.

This thesis investigates the potential of one such technique, time-lapse microgravity. Microgravity has become established as a tool for use during site investigations where the characterisation of sub-surface density contrasts is required. The objective of this thesis is to develop this technique into a tool for the characterisation and monitoring of areas experiencing surface subsidence.

Preliminary trials were conducted at Preesall Brine field (Lancashire) and Keele University (Staffordshire) to verify that time-lapse microgravity was an accurate and viable technique. A case investigation was conducted at an urban site in Northwich, Cheshire known to be experiencing subsidence related structural problems. Gravity modelling and inversion techniques were employed to identify the causative body's dimensions and monitor its development over a four-year period.

Further filed trials were carried out at Marston, Cheshire. A major mass deficiency was identified as cause of the subsidence in the area using gravity modelling techniques but sub-surface mass movement was not identified during the monitoring period.

Interpretation of passive microseismic data, acquired alongside the time-lapse microgravity surveys, has provided information on the mechanism of failure responsible for the subsidence recorded at the test sites.

This work has shown that time-lapse microgravity is a viable, cost effective, non-invasive monitoring technique that is beneficial in the assessment and characterisation of subsidence affected areas as well as providing information valuable to the assessment of the remediation of such areas.

# Acknowledgements

Firstly, I would like to thank Professor Peter Styles for his insightful and enjoyable supervision during this Ph.D. It is largely down to his style of supervision that I have enjoyed my time at Keele so much. Thanks also go to the rest of the Applied & Environmental Geophysics Research Group at Keele University for their support and friendship. Special thanks go to Paul Baggaley, Richard McGrath and Duncan Bate for their enthusiasm and help in the field.

Special thanks goes to Sam Toon for his continued IT support during my research and to Ian Stimpson for his valuable contributions to the structure and content of this document.

I would also like to thank Kevin Wardle and Jim Ronson at ICI, as well as the local farm tenants at Preesall, for their time and understanding during the Foot and Mouth crises. I am also grateful to Peter Skinner at WS Atkins for his time and input during my investigations in Northwich.

I would like to express my gratitude to my family for their support and encouragement as well as giving special thanks to Julie Marshall for everything she has given me over the last three years.

This Studentship was funded by NERC, Reference number: 19/99/ES/6, with CASE sponsorship by ICI.

# Contents

**Abstract** ..... i
**Acknowledgements** ..... iii

**Chapter 1-Introduction** ..... 1
1.1 Introduction ..... 1
1.2 Thesis overview ..... 4
1.3 Summary of the aims and objectives of the thesis ..... 7

**Chapter 2-Literature Review** ..... 8
2.1 Introduction ..... 8
2.2 Accounts of subsidence in salt ..... 8
2.3 The use of microgravity in engineering investigations ..... 10
2.4 Previous examples of time-lapse microgravity ..... 15
2.4.1 Introduction ..... 15
2.4.2 Geotechnical applications ..... 15
2.4.3 Applications in the study of volcanoes ..... 19
2.5 Sources of error during a microgravity survey ..... 20
2.5.1 Instrument error ..... 20
2.5.2 Atmospheric effects ..... 22
2.6 The use of passive seismicity in salt cavern monitoring ..... 25
2.7 Other techniques used in the detection of underground voids ..... 30
2.8 Conclusions ..... 34

**Chapter 3- Microgravity Theory and Survey Protocol** ..... 36
3.1 Introduction ..... 36
3.2 Newton laws ..... 37
3.3 Units of gravity ..... 42
3.4 The constituent parts of the Earth's gravity ..... 42
3.5 Application of gravity surveying ..... 44
3.6 Criteria for detection ..... 44
3.7 Instrumentation ..... 45
3.7.1 Lacoste and Romberg D meter ..... 45
3.7.2 Scintrex CG-3M ..... 48
3.8 Sources of error in the Lacoste and Romberg microgravity meter ..... 50
3.8.1 Errors ..... 50
3.8.2 Creep error from spring rheolity ..... 50
3.8.3 Periodic error ..... 50
3.8.4 Levelling errors ..... 51
3.8.5 Variations in external temperature ..... 51
3.8.6 Barometric effect ..... 51
3.8.7 Magnetic field effect ..... 52
3.8.8 Vibration ..... 52
3.8.9 Wind ..... 54
3.9 Survey procedures ..... 55
3.9.1 Introduction ..... 55
3.9.2 Survey objectives ..... 55

3.9.3 Sample interval ..... 55
3.9.4 Acquisition along a profile ..... 56
3.9.5 Acquisition using a square grid ..... 57
3.9.6 Acquisition using a radial grid ..... 57
3.9.7 Station selection ..... 57
3.9.8 Determination of survey point geographical co-ordinates ..... 59
3.9.9 Acquisition protocols ..... 61
3.9.9.1 Taking a reading ..... 62
3.9.9.2 Procedure for the acquisition of microgravity data ..... 63
3.9.10 Re-ranging of a gravity meter ..... 64
3.9.11 Weather ..... 65
3.10 Statistical analysis of station spacing ..... 65
3.11 Precision ..... 73
3.11.1 Survey precision ..... 73
3.11.2 Keele Gravity Range ..... 74
3.12 Gravity reduction ..... 81
3.12.1 Reduction ..... 81
3.12.2 Drift correction ..... 81
3.12.3 Free air correction ..... 83
3.12.4 Bouguer correction ..... 83
3.12.5 Terrain correction ..... 84
3.12.5.1 Hammer method ..... 84
3.12.5.2 Parker method ..... 85
3.12.5.3 Plouff method ..... 85
3.12.6 Tidal correction ..... 86
3.12.7 Latitude correction ..... 88
3.12.8 Data manipulation ..... 89
3.13 Inherent problems associated with the interpretation of gravity data ..... 90
3.14 Enhancement of gravity anomalies ..... 92
3.14.1 Isolation of gravity anomalies ..... 92
3.14.2 Fourier analysis ..... 95
3.14.3 Continuation ..... 97
3.14.4 Matched wavelength filters ..... 100
3.14.5 Savitzky-Golay filters ..... 100
3.15 Modelling and interpretation of gravity anomalies ..... 100
3.15.1 Gravity modelling ..... 100
3.15.2 Depth estimates ..... 101
3.15.3 2.5D Modelling ..... 104
3.15.4 Thickness estimates ..... 104
3.15.5 Estimation of total anomalous mass ..... 105

**Chapter 4- Field Trials at Preesall Brine Field ..... 107**
4.1 Introduction ..... 107
4.2 The geology of Preesall ..... 110
4.2.1 Sherwood sandstone ..... 110
4.2.2 Mercia mudstones ..... 111
4.2.2.1 Hambleton mudstones ..... 112
4.2.2.2 Singleton mudstones ..... 112
4.2.2.3 Kirkham mudstones ..... 112
4.2.2.4 Preesall salt ..... 113

4.2.2.5 Breckells mudstones ..... 113
4.3 *A-priori* data ..... 114
4.3.1 History of Preesall salt field ..... 114
4.3.2 Subsidence in Preesall salt field ..... 117
4.3.4 Hydrogeological assessment of Preesall salt field ..... 119
4.3.4 Risk assessment ..... 121
4.4 Forward modelling of the gravity response ..... 124
4.5 Testing of radial grids ..... 128
4.6 Acquisition of microgravity at brine well 64 ..... 131
4.6.1 Reconnaissance profiles ..... 131
4.6.2 Acquisition on a radial grid ..... 133
4.6.3 Further microgravity acquisition within Preesall brine field ..... 139
4.7 Gravity change at brine well 64 ..... 140
4.8 Topography change ..... 144
4.8.1 Independent levelling ..... 147
4.9 Gravity modelling ..... 147
4.9.1 Upward continuation ..... 147
4.9.2 Euler deconvolution ..... 149
4.9.3 2.5D Modelling ..... 152
4.9.4 Thickness estimates ..... 155
4.10 Conclusions ..... 163
4.10.1 General conclusions ..... 163
4.10.2 *A-priori* data ..... 163
4.10.3 Microgravity ..... 163
4.10.4 Modelling of gravity signal ..... 164
4.10.5 Original aims ..... 165

**Chapter 5-The Application of Time-Lapse Microgravity at Peter Street, Northwich ..... 167**
5.1 Introduction ..... 167
5.2 Field procedures ..... 171
5.3 Gravity results ..... 174
5.3.1 Correcting for the gravitational effect of buildings ..... 176
5.3.2 Microgravity acquired around the area of principle subsidence ..... 181
5.3.3 The change in gravity at Peter Street ..... 185
5.4 Topographic results ..... 191
5.5 Resistivity profiling ..... 197
5.6 Discussion ..... 200
5.7 Intrusive investigation ..... 201
5.8 Modelling of the gravity signal ..... 205
5.8.1 Depth estimates ..... 206
5.8.2 Thickness estimates ..... 209
5.8.3 2.5D Modelling ..... 213
5.8.4 Area outside the principle zone of subsidence ..... 219
5.9 Conclusions ..... 222

**Chapter 6-The Application of Time-Lapse Microgravity along the Trent and Mersey Canal, Marston ..... 225**
6.1 Introduction ..... 225

6.2 Previous work ..... 229
6.2.1 Site investigation at the Lion Salt Works ..... 230
6.2.2 GEMA ..... 231
6.2.2.1 Basic introduction to GEMA ..... 231
6.2.2.2 Results and conclusions of the GEMA programme ..... 233
6.3 Microgravity investigation at the Trent and Mersey Canal ..... 237
6.3.1 Survey procedure ..... 237
6.3.2 Gravity data ..... 243
6.3.3 The terrain effect of the surrounding topography ..... 246
6.3.4 Filtering of gravity data ..... 248
6.3.5 Borehole data ..... 250
6.3.6 Modelling of gravity data ..... 252
6.3.7 Time-lapse microgravity ..... 258
6.3.8 Summary and conclusions ..... 264
6.3.9 Future work ..... 267
6.4 Second site in Marston area ..... 268
6.4.1 Introduction ..... 268
6.4.2 Survey procedures ..... 269
6.4.3 Gravity results ..... 270
6.4.4 Modelling o gravity data ..... 273
6.4.5 Conclusions ..... 277

**Chapter 7-Characterisation of a Site in Northwich Using Microgravity ..... 279**
7.1 Introduction ..... 279
7.2 Borehole data ..... 283
7.3 Gravity forward modelling ..... 288
7.4 Field procedures and processing ..... 291
7.5 Gravity results ..... 297
7.6 Modelling of gravity data ..... 299
7.6.1 Depth estimates ..... 299
7.6.2 Thickness estimates ..... 302
7.6.3 Mass deficiency ..... 307
7.7 Further processing ..... 307
7.8 Further intrusive investigation ..... 311
7.9 Conclusions ..... 313

**Chapter 8-Passive Seismic Monitoring of Cavities in Salt ..... 316**
8.1 Introduction ..... 316
8.2 Passive microseismic monitoring at Preesall brine field ..... 317
8.2.1 Phase 1 ..... 317
8.2.2 Phase 2 ..... 329
8.3 Passive microseismic monitoring at Peter Street, Northwich ..... 333
8.4 Passive microseismic monitoring at Northwich town center ..... 340
8.5 Discussion and conclusions ..... 349

**Chapter 9-Conclusions ..... 354**
9.1 Introduction ..... 354
9.2 Aim 1-Viability of time-lapse microgravity ..... 354

9.3 Aim 2-Precision of time-lapse microgravity ..... 354
9.4 Aim 3-Suitability of microgravity to identify the causes of subsidence ..... 355
9.5 Aim 4-The role of time-lapse microgravity ..... 355
9.6 Aim 5-Further testing of the viability and application of microgravity and time lapse microgravity ..... 356
9.7 Implication of this work and suggested future work ..... 356

# Chapter 1

# Introduction

## 1.1 Introduction

Problems associated with subsidence due to hydrological changes in the sub-surface occur throughout the world. The scale of subsidence can range from slumps of a few centimetres to rare catastrophic occurrences resulting from the collapse of entire mines e.g. the 1994 Retsof salt mine collapse in the Genesee Valley, New York.

In the Cheshire basin, the extraction of salt from the deposits became a major industry in the 18$^{th}$ and 19$^{th}$ centuries, bringing employment and great prosperity to the area. However, with this great prosperity came widespread subsidence. Poor mining practices and the difficulty in stopping water ingress resulted in the catastrophic collapse of many mines in the area at this time.

Although these incidents in Cheshire declined with the change in extraction technique from dry mining and natural brine pumping to controlled brine pumping, the mining activities of the 19$^{th}$ century and their associated subsidence has scarred the landscape. Development of towns such as Northwich have been hindered as vast areas to the north of the town, which were once thriving industrial areas, are now unsafe to build on or require extensive engineering which restricts development because of costs.

The problem of subsidence is also currently hindering the redevelopment of areas within the town. The structural integrity of existing buildings is under threat from continuing subsidence, damaging property prices as well as services and posing a potential treat to life.

The UK Government has major initiatives in urban regeneration to remediate these 'brown-field sites'. The Government's FORESIGHT programme: Natural Resources and Environment; Non-Invasive Assessment for Waste and Contaminated Land, states:

*"The ability to protect and enhance the environment relies on the capacity to understand, describe and map sub-surface properties on many scales. Foresight aims to stimulate advances in non-invasive techniques to provide better means of assessing and monitoring environmental change. This will underpin more rational response strategies to contaminated land issues by government, industry and the public. There is a growing need for real-time monitoring techniques to determine which zones require remediation within a site. These changes will drive the need for improved site assessment and the provision of new tools and techniques for land remediation. Government, local authorities, industry and business need advanced assessments of these hazards to help shape rational response strategies"*

Other strategies, which address the problem of subsidence, are been implemented across the world. These include the European Unions initiative, ROSES (Risk of Subsidence due to Evaporite Solution) which aims to predict and manage risk associated with areas underlain by evaporites across Europe.

Microgravity is the measurement of minute variations in the Earth's gravitational field. It can be used to investigate the sub-surface density distribution across both urban and rural areas and is not effected by cultural interference. Anomalies in the gravitational field are the result of changes in the sub-surface density and can be caused by natural cavities or solution features (such as karst in limestone), or man-made features such as storage tanks etc.

With the microgravity technique it is possible to identify the size, depth and density contrast of the body responsible for the gravity anomaly and consequently, microgravity has become an extremely useful tool for the investigation and characterisation of brown-field sites.

In relation to the ongoing subsidence problems in Cheshire, microgravity can be used to identify the cause of the subsidence and provide a fast, non-intrusive characterisation of the problem areas. Using the characteristics of the gravity anomaly it is possible to differentiate between subsidence that is caused by natural solution of salt and that which is a legacy of the dry mines of the $18^{th}$ and $19^{th}$ centuries. Such information has enormous benefit in assessing the requirement for further intrusive investigation and by targeting such investigation, has the potential to vastly reduce the associated costs.

The identification of the cause of the subsidence (i.e. a cavity or solution feature) is only the first objective of a site characterisation program. The stability and potential hazard posed by the migration to the surface and possible collapse of such a feature is an integral part of the remediation process. Time-lapse microgravity is a technique in which repeated microgravity surveys can be used to identify sub-surface density contrasts and monitor their development over time. The use of time-lapse microgravity to track the development of sub-surface density contrasts can provide a fast, real-time, cost-effective, monitoring technique, which has little or no impact on the residents or environment.

Although microgravity surveys have become accepted practice in site investigations over the last ten years, time-lapse microgravity remains a relatively new discipline although examples of its use exist in the literature. Repeated microgravity surveys were used by Poeter (1990) to locate textural heterogeneities within the cone of depression caused by pumping in an unconfined aquifer. Pool and Eychaner (1995) also used time-lapse microgravity to monitor the movement of groundwater. In this case

temporal-gravity surveys were used to directly measure aquifer-storage change and estimate values of specific yield. A forward inversion was performed by Hare et al. (1999) to investigate the potential of time-lapse microgravity to monitor the success of a proposed water injection in the Prudhoe Bay reservoir, Alaska.

However, until recently (Rybakov et al, 2001), time lapse microgravity has not been used to detect and then monitor areas of low density in unstable environments. Rybakov et al. used repeated microgravity surveys to monitor the evolution of sinkholes at the western edge of the Dead Sea. It is the aim of this thesis to investigate the potential of time-lapse microgravity in geotechnical applications.

In order to assess the feasibility of time-lapse microgravity surveys, field studies have been carried out at a site in Lancashire where cavity migration is monitored by other means, enabling validation of the results. Repeated microgravity surveys have also been acquired on stable ground in order to establish the achievable precision of a time-lapse gravity survey. An integral part of this study into the application of time-lapse microgravity as a geotechnical solution, is the use of case studies around Northwich, Cheshire.

## 1.2 Thesis overview

This chapter provides an outline of the aims, objectives and structure of the thesis. Chapter 2 then continues to outline the application of microgravity as documented in pre-existing literature. Chapter 2 will also briefly explore the role of microseismics in the monitoring of cavity stability.

Chapter 3 will review the protocols that need to be followed for the successful acquisition, processing and interpretation of microgravity data. A detailed description of the correct survey procedure will also be included, as good survey technique is vital to the

success of a microgravity survey. The behaviour of microgravity meters under varying conditions will also be explored in this section, including analysis of survey repeatability.

Chapter 4 will introduce the Preesall brine field, which has been used to assess the feasibility of time-lapse microgravity for the monitoring of cavities within salt. The Preesall brine field was in production until the middle of the 20$^{th}$ century. The area has experienced subsidence related to the extraction of salt for over a century but it is the continuing monitoring program, implemented by ICI, which enables the assessment of the time-lapse microgravity technique. The data collected by ICI has been used to constrain the interpretations derived from the time-lapse microgravity surveys and assess the success of the technique.

The first of the case studies based around Northwich is presented in Chapter 5. This chapter details a geophysical investigation close to an area within the town that has experienced surface subsidence for over twenty years. Microgravity has been used to locate the body responsible for the subsidence and identify its probable origin. Time-lapse microgravity has been used to monitor the development of the causative body over a four-year period. Secondary geophysical methods have been used to constrain the dimensions of the body and aid in the geological interpretation.

In chapter 6, two case studies are presented from the area around the village of Marston, just north of Northwich. This area has been scarred by the decline of the salt extraction industry. Large subsidence pools (flashes), which developed as a result of excessive salt extraction by dry mining and brine pumping have now been developed into wildlife sanctuaries. However, continuing subsidence effects the Trent & Mersey canal, once the main route for exporting the salt mined in that area. A program of time-lapse microgravity has been acquired across one of the worst effected areas of the Trent & Mersey canal. Interpretations are drawn from the gravity data as to the cause of the

subsidence and the potential risk of further subsidence and surface collapse. A second, complementary microgravity investigation has been conducted along a stretch of road in a similar area. Information about the location of this survey is restricted because of commercial sensitivity but the geology and history of the area link it with the canal site.

Chapter 7 is a record of work instigated to characterise a site in Northwich after a void was discovered during routine work to repair a collapsed retaining wall. The site is located on the north bank of the River Dane in an area previously thought to be uneffected by salt dissolution. Microgravity has been used to help investigate the extent of the void and to target further invasive drilling, resulting in a full risk assessment of the site. Invasive investigation has been used to support the interpretations drawn from the microgravity data.

Microseismology has long been established as an effective way of assessing and monitoring the ground stability in an area. Microseismic monitoring has been carried out in conjunction with the time-lapse microgravity surveys in Preesall and Northwich. Chapter 8 reviews the successes of this work in identifying the seismicity of the areas as well as discussing the possible source mechanisms and mode of failure.

The results and conclusions of this thesis are interpreted in chapter 9. The practicality, success and application of time-lapse microgravity surveys are discussed in the context of applied and environmental site investigations.

## 1.3 Summary of the aims and objectives of the thesis

| | Aims and Objectives | Methodology | Results |
|---|---|---|---|
| 1. | Assess the viability of time-lapse microgravity surveys in environmental and geotechnical applications | Field trials in an actively subsiding area. Validation of results by data acquired with existing monitoring system | Chapters 2 and 4 |
| 2. | Establish precision obtainable during a time-lapse microgravity survey | Repeated surveys across stable land at Keele University and field trials at Preesall | Chapter 3 and 4 |
| 3. | Ascertain whether microgravity can be used to identify the cause of subsidence in areas underlain by salt | Field trials in subsidence effected areas supported by invasive investigations | Chapter 5 |
| 4. | Identify the role that time-lapse microgravity can play in the monitoring of subsidence | Peter Street case studies in Northwich | Chapters 5 |
| 5. | Further testing of the viability and application of microgravity and time-lapse microgravity to the investigation and monitoring of subsidence. | Case studies in Northwich, supplemented with invasive investigation where possible | Chapters 6 and 7 |

# Chapter 2

# Literature Review

## 2.1 Introduction

This literature review begins by outlining the cause, form and effect of subsidence found in salt deposits, primarily in the Cheshire Basin. The detection of voids by the successful use of microgravity in engineering applications is then discussed and previous examples of time-lapse microgravity are presented.

Passive seismicity has often been used for the monitoring of cavern stability. A review of the use of passive seismic monitoring for the characterisation of salt cavern stability is presented as well as successful examples of void detection by other geophysical techniques.

## 2.2 Accounts of subsidence in salt

Mid-Cheshire consists of three salt and chemical manufacturing towns; Middlewich, Winsford and Northwich. The district's major industries (salt and chemical manufacture) are both dependent on salt as a raw material. Exploitation of the salt deposits has been accompanied by serious subsidence, caused by the mining of rock salt and the pumping of brine. Subsidence in the salt fields tends to be more widespread than in coal mining districts. The solubility of salt and the long distances over which brine flows to the pumping shafts cause subsidence to occur at points distant from the productive areas (Wallwork, 1956).

Brine pumping overtook mining in terms of salt production in the late $18^{th}$ century. Currently natural brine is only extracted at Marston and Wincham near Northwich but it remains impossible to accurately predict the amount or place where subsidence is going to

occur. Today, 99% of brine extracted in Cheshire is by controlled solution mining from chambers formed within the salt below dry rock head (Bell et al., 2000).

Bell (1988) and Bell et al. (2000) discusses in detail the subsidence associated with the extraction of salt in Cheshire by mining and brine pumping. Much of the subsidence is a legacy of the late 18th century boom period when poor mining practices often led to roof collapses and the early closure of many mines. The increasing popularity of natural brine pumping and "bastard brine" pumping (the pumping of brine from flooded mines) lead to unpredictable widespread subsidence caused by drawing fresh water into contact with the salt, accelerating the dissolution process. Subsidence of this form often occurred up to 8km from the pumping stations. The nature of the subsidence depended on the geology of the area and the distribution of the pumping stations. Flashes, or water filled hollows formed by the collapse of strata, formed when brine pumps were arranged in a line concentrating the brine runs into one broad channel. They can be up to 10m deep and 70m wide. In areas with stronger overlying stratum, subsidence would be related to the formation of cavities beneath the surface. Collapse of these cavities would leave small hollows at the surface about 6m in diameter. It is this form of subsidence that currently poses a hazard to the area as the location and development of these cavities is unknown.

The discontinuation of most near-surface mining and brine extraction in Cheshire has enabled the hydrogeological system to begin re-balancing itself. It is possible that as natural groundwater flows are re-established through the disrupted salt fields further subsidence will occur. Recent geochemical sampling has shown that brine from springs is entering the rivers in the Cheshire salt field again (Cooper, 2002). The continued subsidence in the Cheshire salt

field caused by the deterioration of disused salt mines is necessitating programs of remediation for such mines.

Wassman (1980) describes subsidence resulting from solution mining of salt in the area around Hengelo in the Netherlands. Cavities produced in the salt have become interconnected. Wassman found that some cavities tended to collapse several years after pumping had ceased and noted that brecciation had taken place in the overlying Red Beds of Bunter age. Brine from the cavities in the underground salt permeated into the overlying marl, rising by capillary action. This caused a reduction in structural strength of the marls, resulting in material collapsing into the cavity. Void migration took place and, depending on the bulking factor of the rocks involved, could move into the overlying clays, causing pronounced subsidence. In some cases, void migration does not reach the surface as the propagating void becomes choked with collapsed material. Additional ground movement can then be attributed to consolidation in the brecciated marls. This is responsible for the slowly decreasing, but long lasting, subsidence.

## 2.3 The use of microgravity in engineering investigations

One of the first uses of microgravity in engineering investigations was by Arzi (1975). He used microgravimetric surveys to verify bedrock soundness at the foundation of a nuclear power plant, delineate a zone of small cavities and trace grout emplacement at the foundation of a large cooling tower.

He points out that the difference between the usual large-scale gravity surveys and microgravimetric surveys for engineering applications is significantly more than a mere scaling down of the grid spacing and precision tolerances. In addition to the smaller scale, the

special physical environments for such microgravimetric surveys require careful revisions of field procedures as well as data reduction and interpretation.

Arzi concludes, "Where properly applied, microgravimetric surveys – usually in conjunction with selective drilling – yield reliable sub-surface information at a high resolution that is still limited by the gravimeter noise".

Arzi suggests that the operator should strive to increase the density of the coverage rather than repeating readings at the base station, because time expenditures on readings are a critical factor in survey economics. Also microgravimetry should not be attempted where prior information indicates geological noise will blur a weak signal, where terrain is very irregular or where stable positioning of the meter is impossible. This is sound advice from which to base the design of a basic microgravity survey. However, it is now possible for a skilled operator to acquire microgravity data in these areas. Although repeat readings are time consuming, they are a valuable tool in the quality control and assurance of the data, giving support and confidence to the geological interpretation.

Butler (1984) presents two case histories of the use of microgravity and gravity gradient techniques to delineated two cavities, at depths of 20m and 30m respectively. Results of the use of vertical gradient survey using a tower are also presented.

In the first case study at Medford Cave, the scope of microgravimetric surveys was tested. A Lacoste and Romberg model D meter was used on a grid of points approximately 80m by 80m with a 3m spacing over the target and a 6.1m spacing elsewhere. The base station was observed every hour and the meter was used in a tidal recording capability during the night for comparison with the field base station drift data.

Two types of gravity-gradient maps were generated. Ring and Centre point (spatial filtering) techniques were utilized to compute first (vertical gradient) and second derivative maps from the gravity data. The second derivative was produced using the Elkins (1951) residual method and produces a map closely resembling a residual gravity map. The vertical or first derivative map was produced using an equation due to Baranov (1975).

It was found when comparing the different techniques along a profile that the gravity and second derivative had similar capabilities but that the first derivative was able to resolve the sources of the anomalies better.

In the second case study at Manatee Springs, the feasibility of gravity gradient survey techniques was investigated using a tower totalling 1.63m in height with four survey platforms. It was found that each set of measurements took 15 to 25 minutes to complete so the ground station was reoccupied at the end of each sequence and the data drift corrected. Butler found no obvious indications of an anomaly that could be caused by the main sub-surface cavity system.

Results of drilling at the Manatee Springs site confirm that the large magnitude, short spatial wavelength anomalies which appear in the measured interval vertical gradient profiles were due primarily to relatively shallow (<6m) density anomalies such as clay pockets and limestone pinnacles. The lower amplitude, longer spatial wavelength anomalies which appear in the measured horizontal gradient were due to deep (>25m) main cavity system.

Butler concludes that a much taller tower (>6m in height) with measurement stations several feet above the ground would be required to have any chance of detecting the small vertical gradient caused by the cavity system. Therefore the usefulness of vertical gradient

surveys using towers of manageable height (1-4m) is primarily limited to exploration of shallow targets (<10-15m).

Al-Rawi et al. (1989) tested the applicability of microgravimetric surveys for determining the thickness and shape of a salt deposit by carrying out field measurements. The results indicate that the method can be applied successfully if a few boreholes are available as control points to define the local regional field.

The microgravity method has also been used to detect two shallow, sub-surface abandoned mines in northern New Jersey (Ghatge 1993). Gravity data were collected along profiles and modelled before the negative gravity anomalies were investigated using either trenching or drilling. In both areas of investigation (Lawrence Iron mine and the Schulyer Copper mine), the results of the gravity modelling were confirmed by the ground investigations.

Patterson et al., (1995) use microgravity to investigate dissolution subsidence at Ripon, Yorkshire. Dissolution of gypsum is prevalent around Ripon so the construction of a new government office required a phased investigation of the area including the acquisition of microgravity data. Microgravity surveys were carried out both inside and outside of the existing building revealing a negative anomaly with a peak amplitude of -74μGal. Subsequent invasive investigation confirmed the existence of a breccia pipe caused by gypsum dissolution.

Case histories using the microgravity technique to detect cavities are presented by Bishop et al. (1997). Bishop describes the successful use of microgravity to detect sub-surface voids of mining or karstic origin in urban environments. In one example the gravitational effect of surrounding buildings greatly effected the interpretation of the gravity data. To

correct for this, gravity was acquired in an identical housing estate on an identical grid. The second survey was shown to have solid foundations with the sub-surface being free from voids. This data set was then used to correct the first survey for the terrain effects of the buildings by simply subtracting the second survey from the first. In this way the terrain effect of the buildings were separated from the gravity data, identifying anomalies from sub-surface voids.

In 1998 a microgravity survey of the upstream and downstream switchyards of the Wilson Dam power plant was performed by Yule et al. (1998). The objective was the detection of sub-surface cavities or other anomalous conditions in the switchyard foundations that could threaten the stability of switchyard structures. The microgravity survey and treatment of the terrain effects led to the development of residual gravity maps that allowed identification of low density areas which might effect the condition of the foundations. The drilling program was guided by anomaly size and depth estimates and encountered zones classified as voids, mudzones, or very soft zones as expected from the low gravity readings in these areas. The microgravity surveys allowed the formulation and execution of a limited and rational foundation investigation plan in a difficult and dangerous drilling environment.

Qianshen et al. (1996) presents a thorough review of the microgravity technique. Topics reviewed include forward modelling and survey design as well as field acquisition and data reduction.

## 2.4 Previous examples of time-lapse microgravity

### 2.4.1 Introduction

In recent years, work has been carried out on the possibility of time-lapse microgravity. This is the use of repeated microgravity surveys to detect changes in the local gravitational field. Such changes could be the result of sub-surface mass changes and the identification of such changes has applications in fields such as oil extraction, groundwater extraction, geotechnical engineering and the study of volcanic activity.

### 2.4.2 Geotechnical applications

Measurements were made by Ervin (1986) to determine if gravity changes could be identified as precursors to earthquakes and to investigate the hypothesis that there is a casual relationship between water loading and earthquakes. Variations in the gravitational difference between most pairs of stations had a standard deviation of 15 μGal and may be attributed to random error. However, the gravitational difference between three station pairs exhibited a temporal change of approximately 45 μGal. Reader error was tested by having one survey crew reoccupy a line for four successive weeks. The standard deviation for the resulting differences was 15 μGal.

The three possible causes of this variation are changes in sub-surface water mass, elevation changes due to variable surface loading caused by fluctuation in river stage, and elevation changes produced by tectonic activity. Ervin concludes that although the data are insufficient to completely resolve the problem, changes in river stage appear to be the dominant mechanism.

Poeter (1990) investigated the use of microgravity for the delineation of textural heterogeneities. Repeated microgravity surveys were used to locate textural heterogeneities within the cone of depression caused by pumping in an unconfined aquifer. To utilize this technique, a carefully controlled microgravity survey was conducted before pumping began and a second survey was conducted after the cone of depression has stabilized. The difference in the gravity was calculated and plotted to reveal the gravity anomaly, which indicated the geometry of aquifer heterogeneities in the de-watered zone. The magnitudes of the anomalies of interest were close to the detection limit of the gravity meter. Importantly, correction for terrain, latitude, and elevation was not necessary because such corrections cancel out when the gravity meter is placed at the same station in both surveys. This substantially reduces potential sources of error in the survey. Butler (1984) states that for such a survey, the potential error is of the order of 5 μGal under ideal conditions and 10 μGal if the survey is conducted on soft ground, in wind, or in an area where there is ground motion from passing trucks.

Poeter emphasizes that, "accurate gravity readings require strict attention to details that influence precision. Firm footing must be established at each station (e.g. concrete pad) and the elevation of each pad should be measured as accurately as possible. Elevation changes due to subsidence must be measured and the gravity reading corrected. Errors due to the influence of a magnetic field can be prevented by orientating the gravity meter to the same distant point for all readings".

In 1993, an investigation was begun to assess the utility of temporal-gravity surveys to directly measure aquifer-storage change and estimate values of specific yield (Pool and Eychaner 1995). The field site was the Pinal Creek basin, which is an alluvial basin in central Arizona. The results of the investigation indicate that temporal gravity measurements were

useful in estimating storage change and specific yield in the alluvial aquifer. Changes in gravity at six wells ranged from less than 2 μgal near a perennial stream reach, to 158 μGal in an area of large water level change. The standard deviation of the measured change in gravity ranged from 1.6 to 5.9 μGal, which is equivalent to 0.13 to 0.46 ft of water. Sources of error were caused by inaccurate approximation of solid-Earth tides, atmospheric effects, and non-linear instrumental drift.

The gravitational effects of water content and mass in the unsaturated zone were not monitored during the study. However, one area may have been affected by a nearby pipe leak that occurred the day before the survey was acquired as the ground was wet across a large area. Excess water in the unsaturated zone appears to have caused an increase in gravity of about 5 μGal.

In 1999, Hare et al. performed a model study for the Prudhoe Bay reservoir in Alaska. Forward and inverse gravity modelling was carried out on a suite of reservoir simulations of a proposed water injection in the Prudhoe Bay reservoir, Alaska. Surface gravity observations were used to monitor the progress of a gas-cap waterflood in the reservoir at 2500m depth. Differences in the gravity field in time reflect the changes in the reservoir fluid densities. Preliminary field tests indicate that a survey accuracy of 5-10 μgal can be achieved using a modified Lacoste and Romberg G meter. Forward modelling predicts variations in surface measurements of 100 μGal after 5 years of water injection and 180-250 μGal after 15 years.

Hare et al. suggest that a baseline survey should be performed prior to the waterflood. Subsequent gravity survey data are then subtracted from the base line data in order to obtain the gravity anomaly associated with the change in fluid distribution. Relocating stations to within 1m allows the latitude correction to be neglected. The gravity sampling pattern

consisted of radial transects with a station spacing of approximately 600m, augmented by a coarser 1200m grid of stations. The paper suggests that a multi-stage field experiment must be conducted in order to assess the sources of non-experimental error.

Regional time lapse gravity was conducted in the north Netherlands for many years. Gelderen et al. (1999) report that gravity observations made over the Groningen gasfield (900km$^2$ in area) from 1978 onwards were reanalysed and a new survey was carried out using Lacoste and Romberg model G meters. The observed gravity changes obtained during four surveys spanning an 18-year period were compared with the gravity effect due to natural gas extraction computed from the reservoir model and the production data. The trends obtained from observed and calculated gravity changes agreed well within their expected error margins. Detailed field procedure was implemented, including the use of two instruments operating in separate closed loops so that different observers and instruments measured all points. Careful account was also taken of land subsidence and the effect of any subsidence (1cm/year) was removed by means of free air reduction to the 1978 station height.

Rybakov et al. (2001), applied time-lapse microgravity to monitor the development of sinkholes in carbonate rocks. Problems associated with sinkhole development cause serious concerns in land use planning in the Dead Sea area. The time-lapse microgravity technique was successful in predicting collapse hazards along a road section and monitored their evolution over time.

### 2.4.3 Applications in the study of volcanoes

In recent decades, systematic microgravity studies over some 20 active volcanoes in Central America, Iceland, Italy, Japan, Papua New Guinea and the USA have provided data on sub-surface mass redistribution associated with volcanic activity. Concurrent data on ground deformation are essential to the unambiguous interpretation of gravity changes (Rymer, 1994).

Rymer used repeated high-precision gravity observation across potentially active areas to look for small time-varying features of the substructure. She reports that "As experience of an area increases there is the possibility of characterizing eruption precursors". A second purpose was to calculate the sub-surface mass and/or density changes associated with eruptions.

The author reports that a precision of 10-15 μGal is required across survey networks and this places extreme demands on the instrument and operator. However, Lacoste and Romberg instruments have the potential to achieve this precision when used with extreme care. During dynamic gravity surveys in volcanic areas, small changes in gravity and height with time are usually measured at a range of stations and compared with unchanging reference points on at least two separate occasions.

Rymer concludes that realistic estimates of mass and density change may be derived when concurrent elevation control is available; the precision of height determinations need only be 4-5cm given that gravity is realistically only measurable to 10-15 μGal in the field. I would suggest that when possible, the surveyor should strive to attain height measurements with a repeatability of <1cm in order to improve the quality assurance of the survey.

Rymer et al. (1993 and 1994) report on gravity and ground deformation measurements that were recorded on Mt. Etna between 1989 and 1993 in conjunction with seismic data. During this period extensive fracturing was occurring which culminated between 1991 and 1993 with the largest lava eruption this century. The 1989-90 period was marked by initial gravity increase (up to 100μGal) at stations near the summit. At the same time, elevation data indicated progressive deflation of the summit region. There is no obvious correlation between these data sets and the changes in height are much smaller than required to explain the variations in gravity. Gravity data also indicated 400μGal increases at the summit stations and a zone trending S-SE in which gravity was increased by 100μGal.

The magma intrusion was essentially aseismic; seismic earthquake sequences occurred between February and May 1991, but the sources were deep (7-20 km). The combination of seismic, gravity and ground deformation evidence, suggests vesiculation and expansion of frothy magma and/or downwards fracture propagation and magma seepage. Pre-eruption vesiculation has been inferred previously using microgravity at andesitic stratacones where only 1-2% change in the degree of vesiculation accounts for the observed changes of ~100μGal.

## 2.5 Sources of error during a microgravity survey

### 2.5.1 Instrument error

Rymer (1989) attempts to quantify the sources of error on a single gravity difference measurement using Lacoste and Romberg instruments. A combination of external effects, reader effects and instrumental effects are shown to produce a maximum error for a single reading of approximately 23 μGal and a minimum of 7 μGal. Single difference measurements

have corresponding errors of approximately 33 μGal and 10 μGal respectively. Evidence is also presented to demonstrate the importance of thermal and mechanical tares which are best removed from field data by isolating step functions using repeat reading rather than by always assuming linear drift. Below is a summary of some effects and their associated errors.

Carbone and Rymer (1999) demonstrate that calibration changes of the order of 1000ppm for Lacoste and Romberg meter G-513 can occur. The technique used by L&R to calibrate the instruments assumes that the value of gravity and the spring constant do not vary. Instead a variable mass is applied to the beam with the vertical distance between the virtual pivot of the beam and the point of suspension of the spring needed to zero the beam position being determined. The calibration is then checked on an established and stable line at Cloudcroft (Lacoste and Romberg, 1998).

Tests by Carbone and Rymer (1999), using a number of L&R instruments, have indicated that the calibration is not the same for all meters. For an experiment of this type, where several meters are tested in one period on a given calibration line, it cannot be determined whether the differences in the calibration reflect the accuracy of the manufacturer or whether each meter has changed its calibration through time.

Using 15 years of microgravity data collected around the world with G-513 it was demonstrated that meter G-513 was stable for 7 years but that there have been two large changes of the order of 1000ppm that have each taken place over a period of several months. The changes occurred during 1985/86 and 1994/95 with no significant change in the intervening years. Although the mechanism that caused these calibration changes has not been identified, it has been shown that both failure of the o-ring seals and causes linked to servicing can be ruled out.

Debeglia and Dupont (2002) conducted several experiments on the accuracy of a Scintrex gravity meter. Calibrations were made between French relative and absolute base stations from which estimates of the uncertainties of the calibration factors were established as $10^{-3}$ for calibration on an old gravity net and $10^{-4}$, for a high amplitude absolute base line. The authors believe this to be sufficient for a microgravity survey.

Continuous gravity recordings were used to enable the estimation of the stability and accuracy of the instruments. It was found that some of the time variations of gravity measurements were not entirely removed by standard processing procedures. The accuracy of corrected gravity measurements is mainly limited by inadequate corrections of tidal effects. However, comparisons of continuous and simultaneous recordings from two fixed gravimeters have shown that they are coherent and in phase (Debeglia and Dupont 2002).

### 2.5.2 Atmospheric effects

Merriam (1992) considers the effect that atmospheric pressure has on the value of gravity measured at the Earth's surface. When considering time-lapse microgravity, effects such as terrain and longitude can be neglected, as they will not change over the monitoring period. However, effects such as pressure, that are inconsistent between surveys need to be investigated.

The transform functions between atmospheric pressure change and microgravimetric change are found to be relatively insensitive to the details of the model atmosphere. However, they are dependent on the temperature at the base of the column, and on the relative height difference between the base of the column and the gravity station. The total signal that global pressure systems contribute to gravity is about 30 μgal, of which about 90% is produced by

the atmosphere within 50km of the gravity station. A zone between 50 and 1000km contributes a couple of μgal, as does the remainder of the globe. Within the local zone (<50km) pressure changes rapidly in time, but is spatially coherent, so that hourly observations of pressure and temperature are sufficient to compute an accurate correction.

Local Admittance = -0.356 μgal/mbar. Accuracy of barometer = 10μbar.

Temperature Admittance = +0.013(T-15°)μgal/°C

Where T = temperature.

Goodkind (1986) examines the records of 7 superconducting gravimeters at five different locations in California and one in Boulder, Colorado. After the removal of tides and the gravitational attraction of the atmosphere, fluctuations over periods of a few days and several months were observed at all sites. These fluctuations had peak amplitudes of 10 μGal. In most locations the causes of these aperiodic variations were not determined. However, at the Geysers geothermal field, much of the gravitational variation is correlated with seismic activity, re-injection rate and rainfall. Measurements of this type were not possible prior to the development of the superconducting gravimeter and consequently these results provide the first evidence for gravity variations at the magnitude and time scale presented.

Goodkind states that the atmospheric effect can at times be removed to better than 1 μGal by fitting and subtracting the pressure record. When the fit is good, the coefficient ranges between 0.2 and 0.4 μGal/mbar. When other gravity variations of comparable magnitude are present, Goodkind recommends that the pressure signal is removed with a fixed

coefficient of 0.3 μGal/mbar. At locations where weather patterns are violent and irregular, the effect of the atmosphere cannot be removed as successfully because gravity can reveal the approach of an air mass of different density before it is directly overhead.

Goodkind also investigates the effect of groundwater on gravity. He states that in principle, variations of groundwater levels would have a relatively large effect on gravity. He presents an example in which an infinite slab of water, in material of 10% porosity, produces an acceleration of 4.2 μGal/per meter of thickness. The results from the Geysers demonstrate the importance of monitoring ground water and rainfall if gravity changes due to other causes are to be identified. During heavy rainfall at this site, gravity increases of 0.54 μGal per cm of rain were observed.

In addition to his laboratory measurements Goodkind made some differential measurements with instruments separated by a distance of 7km. Both locations were within 1km of the ocean but at different distances and elevations above it. If the periodic signals at tidal frequencies are removed from each record individually, the remaining signals have peak excursions of 6 μGal. The source of these signals is suggested to be the atmosphere. Goodkind found that the correlation between the two instruments separated by 7km was indistinguishable from that between the two instruments located in a laboratory. The conclusion of this work is that the influence of the atmosphere on gravity difference measurements over a range of 10km will be of the order of 0.1 μGal. Thus differential measurements such as monitoring of magma chambers, groundwater reservoirs and subterranean cavities can be made to this precision if two gravity stations are used and are separated in the order of 10km scale. As well as correcting for atmospheric variations the

gravity data must also be corrected for groundwater effects in order to isolate and interpret other non-tidal gravity variations to this precision.

However, Debeglia and Dupont (2002) summarize that meteorological and hydrogeological effects have no influence on microgravity surveys because they correspond to very weak variations when considered over the entire measuring program.

## 2.6 The use of passive seismicity in salt cavern monitoring

Passives seismic monitoring has long been established as an effective way of monitoring the stability of sub-surface cavities. Its application in the monitoring of rock failure and mine stability within evaporites is summarised in this section.

In November 1978, the Los Alamos National Laboratory installed a triaxial downhole geophone at the Mound Strategic Petroleum Reserve, a salt dome near Freeport Texas. This was installed at a depth of 592m. The orientation was not controlled but later determined using calibration shots. A second geophone was used at the surface to identify events originating from the surface. Albright and Pearson (1981) report that seismic activity started soon after the start of the depressurisation and reached a peak 5 days later before it rapidly died off. Nineteen locatable microearthquakes with magnitudes between –1 and –2 were observed during and after depressurisation. A high majority of the events recorded did not contain the requisite information to allow event location. This was because the direct transmission path of these events to the geophone would have to be through the cavern. As a consequence, the shear-wave portion of the signal would be lost and the compressional wave portion attenuated and refracted by the cavern/salt interface making location of the event impossible. However, because the shear-wave spectra of these events were characterized by

well-defined corner frequencies the authors were able to calculate the radius of the rupture surface, the seismic moment, and the stress drop from the source spectra.

Important conclusions derived from this study are that comparatively small changes in the internal pressure of oil storage caverns may be enough to cause failure in the salt near the cavern walls and that downhole microseismic surveys can locate zones near large underground excavations that are undergoing rock failure.

Gehle and Thoms (1981) monitored acoustic emissions from a pressurized borehole in rock salt. The borehole was located in the Cote Blanche salt mine in south Louisiana. The acoustic emissions (AE) signals received demonstrated a pronounced increase in activity at the crossing of a distinct pressure threshold. Some correlation of increased AE to salt movement was also detected. While the test performed did not yield AE that were precursory to fracture, it did clearly display a rise in AE at fracture.

The results of the experiments performed by the Bureau of Mines at the Galena Mine, Wallace Idaho, suggest that geophones used for frequency analysis should be mounted in holes drilled far enough into the country rock to be past fractures near the surface and to be away from drift resonance caused by the overlying strata (Rowell and Yoder 1981). The authors conclude that if frequency and energy analysis are important, considerable forethought must be used before geophones are located and mounted within a mine matrix as the mount can resonate. The size of the rock mass to which the geophone is attached and the presence of cracking and faulting in the nearby country rock can also effect the signal. Proximity to mine openings may also cause undesirable resonance.

The Potash Corporation of Saskatchewan Mining Limited has undertaken research to determine whether commercially available technology can provide advanced warnings of

collapse. The research objective was to determine if the roof fall warning capabilities of the Microseismic Roof Fall Warning System as demonstrated in coal mines is translatable to potash ore bodies.

As part of this work, Laboratory work was undertaken at the University of Saskatchewan. Cubes of potash ore were loaded to failure while being monitored by "Rock monitors". As loading to each successive increment occurred, event counts would rise rapidly to a peak and then fall off to a level at or near background.

It was also found that a correlation exists between count activity and applied load. A marked similarity was noticed between the shape of the graph of Applied load verses cumulative events and the usual behaviour of stress/strain curves (Vance 1983).

Microseismic monitoring was also applied to test for the Kaiser effect (Kaiser, 1953). Specimens were loaded to a level below the yield strength, unloaded, and reloaded to above the previous level. If the Kaiser Effect were to hold, then a distinct change in event count behaviour would be observed upon reloading. On the basis of the results Vance concludes that the Kaiser Effect was observed in the Potash ore specimens tested.

During underground testing a warning level energy/event ratio anomaly was given seventeen minutes before a roof fall of 20 tons. After this initial success, three additional groundfalls occurred over the next week. During that time none of the occurrences were accompanied by a warning level signal. However, the three failures were accompanied by clear unambiguous energy/event ratio anomalies.

Hente et al. (1985) used both microseismic observations and mine survey results to monitor Asse rock salt mine. They found that these methods complemented each other well. Microseismic monitoring has the advantage of providing information about inaccessible

regions as well as being able to observe continuously. Whereas monitoring of gradual displacements, which are especially important in salt, are best achieved by surveying. The observed microseismic activity from the Asse salt mine, as well as the measured displacements were interpreted as being due to creep of rock salt from the bottom of the mine towards the open rooms. The array used 7 vertical component geophones. The acquisition was event-triggered and recorded at 1482Hz (these were added to by 4 horizontal component geophones). Difficulties were encountered when using the horizontal components for location as information at different stations turned out to be inconsistent in most cases. Spectral analysis also produced spurious results. The cause of this is thought to be distortion of the signal due to the excavations. The measured displacements would suggest a subsidence in the top part of the mine together with an even greater uplift in the mine floor.

Measuring of microseismic events has been carried out at the former potash mine at Hope since early 1984 (Heick and Flach, 1989). Analysis of the data suggests an immediate temporal relationship between brine introduction and the onset of microseismic activity.

Elf-Atochem has been solution mining a salt formation in southern France for twenty years. Once brine production had ceased, the assessment and monitoring of the stability of deep caverns (from 1900m to 2800m with diameters of around 30m and a height of 500m), presents a problem. Maisons et al. (1997), present a paper which confirms the accuracy of downhole permanent seismo-acoustic technology to monitor the sealing process. The microseismicity has been characterized and located using triaxial hodogram analysis, however, the microseismicity shows many clusters of seismic doublet events allowing the use of relative analysis.

The microseismicity has yielded useful data on the geomechanical behaviour of the site and identified that the seismicity is associated with brine flow. The seismicity induced by the salt leaching process is a means to detect weak zones that could again become active after closure. A closure test reveals that a direct relationship exists between the seismicity and the bleeding of brine from the caverns.

The microseismic monitoring network consisted of only one downhole triaxial geophone anchored at a depth of 1800m and four sub-surface triaxial geophones cemented in small shallow boreholes 25m below the surface. However, the very small magnitude (seismic moments of $10^8$ Nm to $10^{10}$ Nm) and depth (>2000m) precluded the recording of most of the events from the surface.

The triaxial hodogram method of location consists of determining the P-wave arrival direction and the source-transducer distance. The direction in space of the velocity vector for a given linearly polarized P wave can be characterised by two angles: azimuth and inclination. The best way to study this trajectory is to model it by computing the covariance matrix over a time window and then calculate the Eulerian angle. The source to geophone distance is computed from the time delay between P and S waves. In these applications the time window used to analyse particle trajectory and thus to calculate azimuth and inclination is systematically fixed to the first period of the P-wave onset. The S-wave arrival time is picked up when the radial-radial angle between the P-wave velocity vector and a moving velocity vector is greater than 80°. Ray tracing was not applied due to a general lack of velocity information (Maisons et al., 1997). This paper gives a very detailed account of its results, matching the different stages of well closure with characteristic microseismicity.

## 2.7 Other techniques used in the detection of underground voids

Beres et al. (2001) conducted ground-penetrating radar and microgravimetric surveys in the southern Jura mountains of western Switzerland in order to map sub-surface karstic features. By using small station spacing and careful processing of the geophysical data, and by modelling these data with topographic information from within the cave, accurate interpretations were achieved. The authors found that the two techniques complemented each other extremely well. For example, microgravity can complement GPR methods for accurately delineating a shallow cave section and GPR methods can be complementary in determining cavity depths and in verifying the presence of off line features and numerous areas of small cavities and fractures.

The limitation of GPR is its penetration. Sharma (1997) suggests that ground radar penetration is of the order of 20m, although this may increase to 50m under ideal conditions of low conductivity (e.g., in dry rocks and frozen ground), and decrease to less than 2m in materials of high conductivity (such as wet clay and silt). This limits the use of GPR to the detection of shallow targets in the urban British environments where the majority of sites are underlain by several meters of fill consisting of silts and clays and is wet for much of the year.

Lange (1999), used electromagnetic, gravity and natural potential methods to map the structure and ground water patterns beneath valley alluvium and determined the geophysical expression of the caverns at the surface. Although the resolution of the gravity survey was only 1mGal, due to severe terrain effects, two of the three cavern passages were successfully expressed as gravity lows at the surface.

The spectral analysis of surface waves (SASW) method is an earthquake seismology technique that has recently been adapted for shallow applications. The SASW method is based

on the fact that surface-wave velocity in a layered medium is dispersive. The surface-wave velocities in a medium depend on the stiffness and density of that stratum. Therefore, for small variations in density, the stiffness profile of a layered medium can be inverted from the dispersion curve of surface waves. An air filled underground void represents a significant change in stiffness from the surrounding medium. The interaction between surface waves and an underground void causes late time amplification of the surface waves and results in an anomalous high energy response for certain frequencies over the location of the void. The potential of this method has been demonstrated by both laboratory and field tests by Phillips et al. (2000).

The main limitations of the SASW method are problems with the inversion algorithms (used to determine the depths to boundaries between different layers) when dealing with inclined layers and reflections of body waves. Depth of penetration is limited because of the difficulty of generating large wavelengths ($\lambda$>30m) with high signal to noise ratio. On the other hand, SASW is more sensitive to certain anomalies than conventional seismic methods based on travel time.

Gritto and Majer (2000) present a numerical study that investigates the possibility of inverting seismic data for the location and volume of a cavity. The data is generated using an exact solution for the scattering of elastic waves in a sphere, whereas the inversion is based on the low frequency Mie approximation to the exact solution. A correlation analysis is used between these solutions to solve the inverse problem in two steps. First, the location of the cavity is determined, before the volume is estimated in a second step. Adding correlated and uncorrelated noise tests the robustness of the results. This method is found to be robust as long as the cavities are well determined while the estimates of the radii are most susceptible to

noise and the deviation between approximation and exact solution. The Mie approximation can be applied whenever a spherically shaped cavity is the target of the investigation.

The advantage of knowing the elastic parameters *a-priori* reduces the problem to a 2 parameter estimation for the location of the centre and the radius. The correct phase information provides the location of the cavity and therefore is susceptible to variations in the background velocity. The radius of the cavity is determined by the amplitudes of the scattered wavefield, and therefore is affected by data noise, even if the noise is uncorrelated. However, a carefully selected source receiver geometry which provides enough coverage to reduce uncorrelated noise, can be effectively used even under extreme noise conditions (Gritto and Majer, 2000).

El-Behiry and Hanafy (2000) used geophysical techniques to map the vertical extension of a sinkhole. Two open holes (about 0.5m$^2$ each) were discovered shortly after excavations in an engineered site located at the 15$^{th}$ May City, 35Km south of Cairo, Egypt. Visual inspection could not reveal much information on the spatial extensions of the two holes. Dual antenna GPR , Dipole-Dipole multi electrodes resistivity profiling, and P-wave seismic refraction surveys were carried out to outline the extensions of these holes. GPR data revealed a depression feature that gave rise to the exact detailed outlines of the sinkhole (6m long, 4.5m wide, 1-2m deep) in addition to numerous sub-surface voids (mostly at depth range of 0.5-1.5m) and fractures. The medium containing the two holes was identified by seismic refraction as highly fractured limestone filled with spoil material (540-1200 m/s). It had a thickness of 1-2m and overlaid intact limestone bedrock (3800 m/s). 2-D inverse resistivity models could not delineate the sinkhole itself due to the electrode separations used (a=5m, 10m). However, the resistivity surveys were successful in identifying two high resistivity

(20,000 Ohm) anomalies that originated from the base of the sinkhole to a depth of 8m and trend to the south. These anomalies are interpreted as fractured zones.

Noel and Xu (1992), describe the successful process of cavity detection through the use of electrical resistivity tomography. The method differs from conventional electrical resistivity surveying in that a large array of electrodes are used and by recording the maximum number of independent measurements that are possible on the array.

When conducting the survey it is assumed that measurement relate to the region situated at the mid point of the array, at a depth equal to half the electrode spacing. In this way it is possible to build a vertical section of the sub-surface by expanding the array about its midpoint.

Yaramanci (2000) investigated the exploration and monitoring of underground waste disposal sites in rock salt using resistivity-imaging techniques. The presence and migration of water has been studied in the research mine in Asse, north Germany using a multi-electrode array and current steps of up to 800V. Recent developments in hardware, inversion schemes and petrophysical interpretation of the resistivity enable reliable and useful measurements to be conducted with direct current resistivity.

Schoor (2002) used 2D electrical resistivity imaging to detect sinkholes in South Africa. The author concludes that the technique is well suited to the detection and mapping of known sinkholes. The technique is also capable of discriminating between developing sinkholes, where the target is primarily conductive weathered material and mature sinkholes, comprising resistive air-filled cavities.

However, Burton and Maton (1975), indicate that where the depth of a cavity is equal to its diameter, the maximum disturbance in the resistivity profile is only about 10% of the

background level. As noise frequently exceeds this value, cavities at depths greater than twice their average dimension (such as old mine workings) are usually not recorded limiting the use of the resistivity technique to the detection of cavities at shallow depths.

## 2.8 Conclusions

The literature shows that the microgravity technique has been successful in detecting sub-surface density contrasts in a wide variety of applications. Through the application of careful survey procedure it is now possible to attain precision, which enables the survey to greatly assist in the interpretation of sub-surface geology and risk assessment.

Time-lapse microgravity shows great potential as a tool for the monitoring of sub-surface mass changes in geotechnical investigations. Time-lapse microgravity has been successfully applied to monitor aquifer recharge, water flood operations in oil reservoirs and mass changes resulting from volcanic activity. More recently the technique has been applied during the assessment of collapse hazards on the western shore of the Dead Sea.

Passive seismic monitoring is an established tool for the monitoring of stresses associated with cavern stability. Microseismic and acoustic events within evaporites have been extensively studied and the use of passive seismic monitoring has been proven to be beneficial in the assessment of risk associated with ground collapse.

Microgravity is not the only non-invasive geophysical technique that has been successful in the detection of sub-surface cavities. Methods such as GPR, resistively imaging and SASW have successfully identified sub-surface cavities but their depth of penetration restricts the application of these techniques to the investigation of shallow sub-surface features (<10-20m). Microgravity has the potential to record anomalies from sub-surface

cavities at much greater depths and consequently microgravity has a wider range of applications. However, the integration of other geophysical techniques has the potential to reduce the ambiguity associated with gravity modelling and improve the overall interpretation.

# Chapter 3

# Microgravity Theory and Survey Protocol

## 3.1 Introduction

Sir Isaac Newton first published his ideas on the laws of gravitation in *Principa Mathematica* in 1687. Since then the mutual attraction between all masses has been recognised as a universal phenomenon and accounts for the fact that a body when released near the Earth will fall with increasing velocity. The rate of increase in velocity of the body is called the gravitational acceleration (g). This would be a constant value on the surface of the Earth if the Earth were a perfect sphere of uniform concentric shell structure. However, the Earth is not of this form. It is not spherical, it is not uniform and it also rotates. These factors all contribute to the variation in gravitational acceleration that we see on the Earth's surface.

This chapter details the basic concepts necessary for the study of gravity for engineering applications. The calculation of gravity and the units of measurement are discussed in section 3.2 and 3.3 respectively (modified from Sharma, 1997). The contributing factors of the Earth's gravitational field are explained in section 3.4 at which point the relatively small portion that is used for engineering applications is highlighted. The application of microgravity and the criteria for detection are then introduced in sections 3.5 and 3.6.

The instrumentation used in microgravity surveys is highly specialised as a result of the precision required during a survey. The instrumentation used during this survey is described in detail in section 3.7, with the possible sources of error outlined in section 3.8.

In order to attain the precision and accuracy that the microgravity instruments are capable of, the acquisition procedure during a microgravity survey needs to be standardised and carefully implemented in order to keep systematic errors to a minimum. A detailed account of the correct survey procedure necessary for a microgravity survey is presented in section 3.9. In addition, the use of statistical analysis to select station spacing is included in section 3.10. This section analyses the effect grid location has on the measured anomaly and shows how the recorded value can often be far less than the theoretical anomaly. The precision of microgravity surveys is discussed in greater detail in section 3.11. The work carried out into the precision of repeated microgravity surveys on the Keele Gravity Range is discussed here. This section outlines the expected level of precision for the subsequent time lapse microgravity surveys.

Section 3.12 outlines the required reductions to remove the external effects described in section 3.4, leaving the portion of the Earth's gravitational field created by the near surface inhomogeneities, the interpretation of which was the initial reason for the microgravity survey. The inherent problems associated with the interpretation of gravity surveys and the possible way in which gravity anomalies can be enhanced and modelled are discussed in sections 3.14, 3.15 and 3.16. Section 3.16 describes the techniques which have been used extensively in this study for the interpretation of the measured anomalies.

## 3.2 Newton's laws

The following discussion on the calculation of gravity is modified from Sharma (1997).

The force of attraction, F, between two point masses m and m' , separated by a distance, r, is given by Newton's Universal Law of Gravitation:

$$F = G\left(\frac{mm'}{r^2}\right)r_1 \qquad (3.01)$$

where $r_1$ is a unit vector directed from m towards m' (when F is acting on m), and G is the gravitational constant which has a measured value of $6.672 \times 10^{-11} Nm^2 Kg^{-2}$ in SI units. The force exerted on a body at the Earth's surface is due to the attraction of the Earth. When the effects of rotation and non-uniformity of the shape and density of the Earth are neglected (as if it were a sphere of uniform concentric shell structure), the force exerted by the Earth on a body of mass m can be obtained from Eq.(3.01) as

$$F = G(M_E m / R^2)\bar{r}_1 \qquad (3.02)$$

where $M_E$ is the Earth's mass. $R_E$ is the Earth's radius, and $\bar{r}_1$ is a unit vector directed from m towards the centre of the Earth.

The gravitational force is also given by Newton's Second Law of Motion, $F = mg$, where g is the acceleration that would be caused by the gravitational pull of the Earth if the body were allowed to fall freely. Thus acceleration due to gravity (g) can be expressed as equivalent to the force exerted by the Earth on a unit mass, and can be expressed as

$$g = F / m = G(M_E / R_E^2)\bar{r}_1 \qquad (3.03)$$

where $\bar{r}_1$ is a unit vector directed towards the centre of the Earth. The SI unit for acceleration due to gravity, g, is $ms^{-2}$. In the c.g.s system the unit for g is $cm/s^2$. This unit is referred in geophysics as the Gal in honour of Galileo.

The gravitational potential, U, due to a point mass m at a point P, at a distance r from m, is defined as the work done by the gravitational force in moving a unit mass from an infinite distance to the final position at P. In geodesy and geophysics, the sign convention is to take U to be positive quantity; its magnitude is given by

$$U = Gm/r \tag{3.04}$$

The potential function, U, plays an important part in the theory of attraction; the negative derivative of U gives the gravity attraction in the corresponding direction. Thus

$$g_r = -\frac{\partial U}{\partial r} = \frac{Gm}{r^2} \tag{3.05}$$

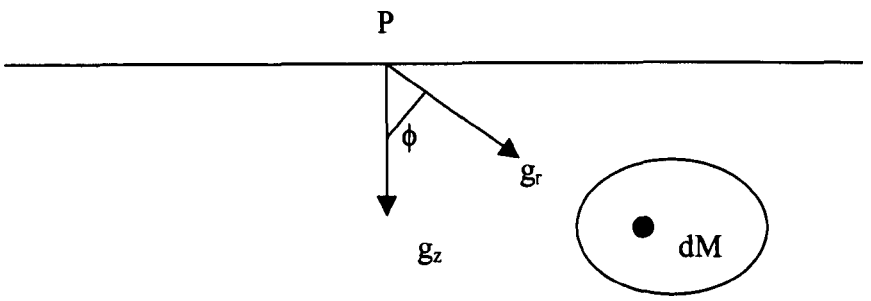


*Fig 3.1. Gravitational attraction g and its vertical component $g_z$ at a point P due to a mass M.*

The gravity attraction due to a generalised mass distribution (Figure 3.1) is the vertical sum of attractions produced by all point masses, because they do not generally act in the same direction. It is the vertical component of gravity attraction, $g_z$, (henceforth written simply as g), that is measured. This is calculated at a point P by the integral equation

$$g = G\int_M \frac{dM}{r^2}\cos\phi = G\int_V \frac{\rho\cos\phi dV}{r^2} \qquad (3.06)$$

where dM is the mass of a volume element dV of density $\rho$ at a distance $r$ from P.

Considering the point P located at $\alpha, \beta, 0$ and the mass element at x,y,z, we can write $dM = \rho dxdydz$. In this coordinate system, Eq.(3.06) can be written as

$$g = G\iiint \frac{\rho z dxdydz}{r^3} \qquad (3.07)$$

where $r = [(x-\alpha)^2 + (y-\beta)^2 + z^2]^{1/2}$

If the variation in mass distribution is two dimensional (2-D), which occurs when a body composed of elements each of constant cross-section dS striking infinitely in a horizontal direction (say from + ∞ to -∞ in the y direction, perpendicular to the plane of Fig 3.1), the above equation reduces to

$$g_{(2-D)} = 2G\iint \frac{\rho z dxdz}{r^2} \qquad (3.08)$$

where $r = [(x-\alpha)^2 + z^2]^{1/2}$

These are the basic equations for calculating the gravity effects of bodies of uniform density. Use of Equations 3.07 and 3.08 make it possible to obtain closed analytical expressions for the gravity effects of bodies of regular shape such as sphere, cylinders, horizontal slabs etc. (Table 3.1).

| Geological form | Geological Structure | Gravity Formula | Depth Rule |
|---|---|---|---|
| Sphere | compact bodies | $\Delta g = \frac{4\pi GR^3\Delta\rho}{3z^2}\frac{1}{[1+(x^2/z^2)]^{3/2}}$ | $z = 1.305x_{1/2}$ |
| Horizontal cylinder (infinite strike) | ridges, valleys, tunnels | $\Delta g = \frac{2\pi GR^3\Delta\rho}{z}\frac{1}{[1+(x^2/z^2)]}$ | $z = 1.0x_{1/2}$ |
| Narrow cylinder (infinite depth extent) | volcanic necks, plugs | $\Delta g = \pi GR^2\Delta\rho/(x^2+z_1^2)^{1/2}$ | $z_1 = 0.58x_{1/2}$ |
| Vertical sheet (infinite strike) | thin dykes | $\Delta g = 2Gb\Delta\rho\left[\frac{\ln(x^2+z_2^2)^{1/2}}{\ln(x^2+z_1^2)^{1/2}}\right]$ | $z_1 \approx 0.4x_{1/2}$ |
| Horizontal slab (semi-infinite0 | near vertical faults | $\Delta g = 2Gt\Delta\rho\phi$ | $z = 1.0x_F$ |
| Infinite slab (Bouguer slab) | sedimentary basins, plutons, ice caps | $\Delta g = 2\pi Gt\Delta\rho$ | $t = \Delta g / 2\pi G\Delta\rho$ |

*Table 3.1 Note: $\Delta g$ is the gravity anomaly ($m/s^2$) due to a density contrast $\Delta\rho$ ($kg/m^3$); $G = 6.672\times10^{-11}$ (Si units); x,z,R, respectively denote horizontal distance along the profile, depth to centre or median plane of the source, and its radius; $x_{1/2}$ is the half-width of the anomaly; $z_1, z_2$ are, respectively, depth to the top and bottom of the source; $\phi$ is the angle from the horizontal of the point of the observation to the median plane of the semi-infinite slab; $x_F$ is the horizontal distance over which the fault anomaly falls from $0.5\Delta g_{max}$ to $0.25\Delta g_{max}$; t is the thickness (depth extent) of the slab; b is horizontal thickness of the vertical sheet. Taken from Sharma (1997).*

## 3.3 Units of gravity

The basic c.g.s. unit of acceleration used to describe gravity is the Gal, named for Galileo. This unit and its subdivisions commonly used by many geophysicists are defined as.

1 Gal = 1cm/s²

1 mGals = $10^{-3}$ Gal

1 μGal = $10^{-6}$ Gal

The SI unit of acceleration is

1 m/s² (= $10^{5}$ mGal = $10^{8}$ μGal).

1 gravity unit (gu) = $10^{-6}$ $ms^{-2}$ = 1μ$ms^{-2}$

1 gu = 0.1mGal = 100 μGal

For the majority of this work gravity values will be described in μGals.

## 3.4 The constituent parts of the Earth's gravity

Microgravity is a specialist discipline and requires instrumentation that is capable of measuring the Earth's acceleration due to gravity to one part in one billion. Equally important are the acquisition procedures without which it is not possible to acquire good data. The interpretation is limited by the quality of the raw data.

If the main constituents that make up the Earth's gravity field are broken down it can be seen exactly how accurate the instrumentation and procedure for acquiring gravity needs to be.

The total acceleration due to the Earth's gravity is approximately 9.83 Gals which is ~983,000,000 μGal. The mass of the Earth accounts for ~974,899,700 μGal. The equatorial radius of the Earth is 21km greater than the polar radius which contributes

~5,000,000 μGal. The difference in elevation between the highest mountains and the deepest oceans contributes ~3,000,000 μGal. A further ~100,000 μGal is accounted for by regional geology and crustal structure. Importantly, for the acquisition of microgravity data, the Sun and the Moon contribute rapidly varying 100 to 200 μGal. The remaining 100 μGal is a result of inhomogeneity within the near surface strata, and it is this that is measured and interpreted in the discipline of microgravity surveying for environmental and engineering applications.

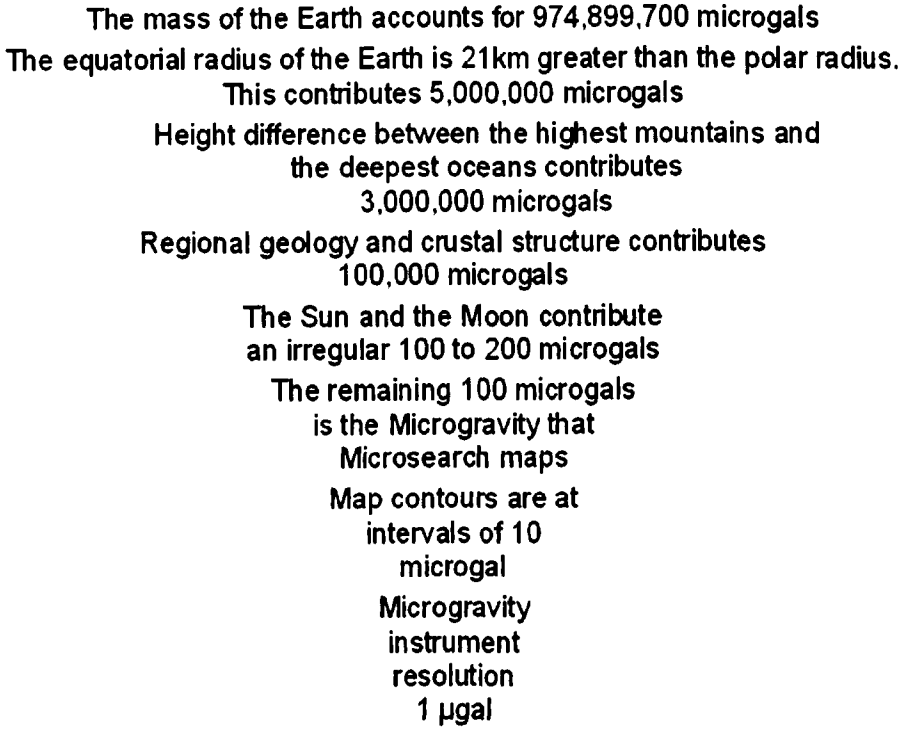


*Fig 3.2. The constituent parts of the Earth's acceleration due to gravity. This "gravity triangle" illustrates the small fraction of the gravitational effect that is measured during a microgravity survey.*

## 3.5 Applications of gravity surveying

Gravity is measurable all over the globe and the signal that is recorded is a summation of all the density variations surrounding that point on the surface at which we record the measurement. The gravity is not shielded or distorted in the way in which electromagnetic fields may be, although signals from individual sources may be superimposed with each other and mask their individual signals.

Gravity surveying has many uses on many scales. It can be used to investigate features on a tectonic plate scale (1000's km) or it can be used to investigate small archaeological features such as kilns (a few m). Between these two extremes is a wide range of applications. The fundamental questions that needs to be answered when a gravity survey is designed are the scale of the feature to be investigated, its lateral and vertical extents and, importantly, the expected density variation. These parameters can be used to calculate a theoretical anomaly that can be matched against the limits of resolution of the gravity survey. This information can be used to decide whether to proceed with the survey and if so, aid the survey design.

## 3.6 Criteria for detection

Several criteria must be satisfied before a gravity survey is undertaken. These criteria will establish whether a gravity survey is likely to be successful and satisfy its objectives. First, the target body must vary in density from the background material in the direction of the survey, i.e. laterally not vertically. If the body just causes variation in density vertically it will not be detected because it does not deviate from the concentric shell model and there will be no variation in gravitational acceleration between stations. In order to investigate such a body a borehole gravity survey would be required where the

field is sampled vertically. Second, the anomaly generated must be large enough to be detected. Meter resolution and expected noise must be considered at this stage. Third the anomaly generated must be more able to characterise the target body than other geophysical properties (magnetism, resistivity, etc.) otherwise gravity is not right tool for job (although a gravity survey could be used in conjunction with these other techniques to further constrain the anomalous body).

## 3.7 Instrumentation

### 3.7.1 Lacoste and Romberg D meter

Almost all the early absolute and relative determinations of gravity used some form of swinging pendulum (Sharma, 1997). The period of its swing being related to g by

$$T = 2\pi\sqrt{\frac{l}{g}} \tag{3.09}$$

where T is the period, l is the length of the pendulum and g is the acceleration due to gravity.

However, quicker and more accurate instruments have since been developed and so the pendulum has assumed a secondary role of measuring absolute gravity at primary base stations or being used for the calibration of other gravity measuring instruments. One example of this is the FG5 absolute gravity meter. An absolute gravity meter measures the acceleration of gravity directly by observing the free-fall of a reflective corner cube in a vacuum. Position is measured with an iodine laser and time with an atomic clock. The value for ***g*** is thus determined in terms of atomic constants that are assumed stable over periods of centuries (Bilham, 1999). This is in contrast to the spring-based relative meters which observe gravity differences in time or place.

Today all microgravity surveys in geophysical exploration use relative measuring instruments. These machines measure how gravity varies with relation to a fixed point, a base station. The basic principle of the relative gravity instrument is a very sensitive spring carrying a constant mass. A small change in gravity, $\Delta g$, causes the weight of the mass $((g+\Delta g)m)$ to change resulting in an increase or decrease in the length of the spring, $\Delta L$. To attain a precision of 10 μGal, the fractional change in the spring length $\Delta L/L$, must be measured to a precision of one part in $10^8$ (Sharma, 1997).

For the majority of the microgravity measurements made during this study a Lacoste and Romberg Model-D Gravity meter has been used. The Lacoste and Romberg gravity meter uses a zero-length spring to support a beam, which has a mass at one end and a frictionless hinge at the other i.e. a spring system in which the effective length (L) is zero when measured from a fixed point, Figure 3.3 (Lacoste and Romberg, 1998). The meter is read by nulling the mass position, i.e. returning the beam to its original position, by the use of a fine adjustment screw. The relative changes in gravity are measured by the number of rotations (or parts thereof), required to null the beam. This must be done with great accuracy and is accomplished with a series of levers. The levers are moved by a high precision screw, which in turn is rotated by a gearbox, which is connected to the nulling dial (Figure 3.3).

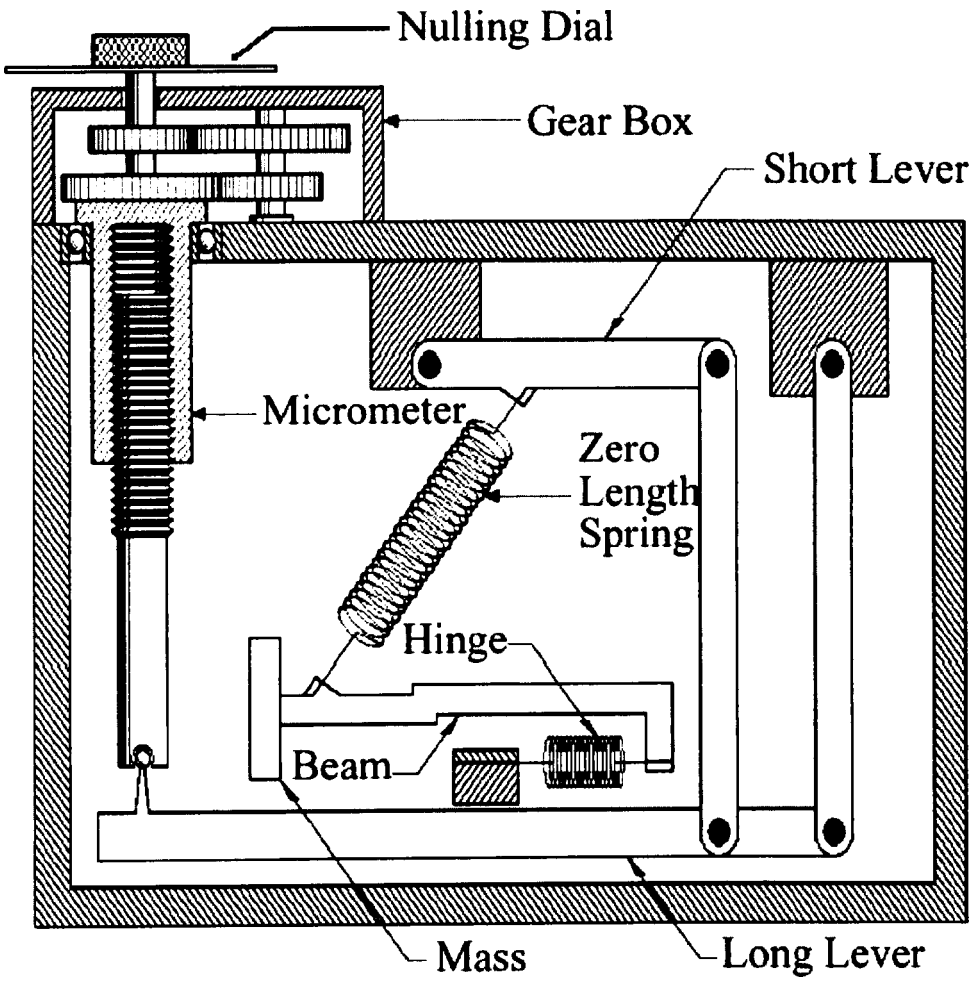


*Fig 3.3. Internal workings of a Lacoste and Romberg gravity meter. Taken from the Lacoste and Romberg manual (1998).*

The Lacoste and Romberg (L&R) gravity meter is made of metal parts. This increases the durability of the instrument but as the thermal expansion and contraction of metals is greater than that of Quartz used in other gravity meters, the L&R meters must be correctly maintained at a constant temperature. The frame with the spring and beam apparatus is placed in an insulated container where battery powered electrical heating coils maintain the temperature between 47 and 55°C to within 0.002°C using a thermostat.

The L&R D meter has a theoretical sensitivity of 1μGal. During a survey, when the meter is exposed to the elements, an accuracy of 3μGal is rare because of external effects and a value of 6-8μGal is more common. If the ambient noise level is large (wind, traffic, soft ground etc.), then the accuracy can deteriorate to 10-20μGal (the effects of ambient noise is explained in greater depth in the following section).

### 3.7.2 Scintrex CG-3M

During this study it became necessary to use a second type of microgravity instrument, the Scintrex CG-3M. The Scintrex CG-3M is an automated gravity meter whose sensitive element is composed of a quartz spring with its elongation counterbalance by an electrostatic force (Debeglia and Dupont, 2002). Its measurement range is 7000 mGal and its resolution 1 μGal. The relative value of g is determined by a series of measurements recorded at a sampling frequency of 1Hz. Generally, the series ranges between 60 and 120 readings depending on external noise. Based on individual readings and after the rejection of deviant values (individual values that deviate from the average by more than four times the standard deviation), the gravity meter provides the arithmetic mean of the n individual measurements and their standard deviation, SD. Assuming a normal noise distribution the measurement error is estimated by err=SD/□n. This error incorporates the instrumental error associated with the acquisition system plus any seismic noise effecting the measurement spring at different frequencies. The device is equipped with tilt and internal temperature sensors, and the data are corrected in real time from the observed variations. These different parameters are stored in memory and can then be transferred to a computer. The gravity meter can be operated in field (measurements

activated manually) or cycling mode (continuous measurement activated automatically at a regular interval (Debeglia and Dupont, 2002).

During the recording of a reading the Scintrex gravity meter will show variations in the calculated measurement error. These variations are generally a result of modification in the surrounding environment in the same way as the L&R D meter and the measures outlined in the following section can be applied to the Scintrex CG-3M. Changes in the levels of the instrument can cause fluctuations on the calculated error as can passing urban traffic. Seismic and meteorological interference can also increase the error. An effective way to reduce this measurement error is to increase the duration, and consequently, the number of measurements used to calculate the error. If this is not successful the survey should be stopped until such a time that the external effects have reduced enough to allow the acquisition of accurate data.

## 3.8 Sources of error in the Lacoste and Romberg microgravity meter

### 3.8.1 Errors

It is important for the gravity meter operator to be aware of the likely causes of error within the instrument and the effect that the external environment has on the quality of data so that he can adjust his technique in order to minimise their effect.

### 3.8.2 Creep error from spring rheolity

The L&R gravimeter uses a static, zero length spring. A visco-elastic Kelvin solid or Hooke solid can simulate the springs kinetic characteristics. In some instruments the reading varies with time after the clamp has been released. Qianshen et al. (1996), report that his L&R, meter D-28 requires several days to stabilise after readjusting the range. This has major consequences on the speed and accuracy at which a survey can be acquired. This problem has not shown in the data acquired by D-141. It is, however, standard procedure to leave D-141 unclamped for at least half an hour after being transported to site, in order that it may "stabilise". This procedure is described in greater detail later in the chapter.

### 3.8.3 Periodic error

It has also been reported by Qianshen et al. (1996), that many instruments have a periodic error associated with the mechanism of the operating system. The periodic errors of L&R D type meters are caused by errors in the centring of the internal gear system. Obviously, the amplitude of this error is different with individual instruments and Qianshen et al. report that they can be up to several μGal.

### 3.8.4 Levelling errors

The L&R D meter is fitted with bubble levels as standard. These have 50 seconds of arc per scale divisions and consequently the gravity meter tilting by 0.5 divisions would cause an error of 5μGal or more. It is therefore essential that electronic levels be fitted and used if the meter is to be used for the acquisition of microgravity data.

### 3.8.5 Variations in external temperature

Readings may be affected by sharp fluctuations in temperature. Qianshen et al. report that for the L&R D-28, a 5μGal change in reading is experienced with a temperature discrepancy of 8°C. Larger errors are also possible from sharp temperature variations. For example he measured an 8μGal error in D-96 when the temperature changed from 30 to 35°C.

### 3.8.6 Barometric effect

When considering the Earth's gravitational field at this level of accuracy it is also necessary to consider the effect that the weight of the atmosphere has on the gravity meter. Merriam (1992) considered the effect that atmospheric pressure has on the value of gravity measured at the Earth's surface. Merriam has found that the total signal that global pressure systems contribute to gravity is about 30 μGal, of which about 90% is produced by the atmosphere within 50km of the gravity station. A zone between 50 and 1000km contributes 1-2 μGal, as does the remainder of the globe. Within the local zone (<50km) pressure changes rapidly in time, but is spatially coherent, so that hourly observations of pressure and temperature are sufficient to compute an accurate correction.

Local Admittance = -0.356 μGal/mbar.

Accuracy of barometer = 10μbar.

Temperature Admittance = +0.013(T-15°)μGal/°C

Where T = temperature.

The amplitude of this effect is not large enough to concern larger scale gravity surveys. It is also not large enough to warrant the extra cost that would be incurred during a routine site investigation. During a time-lapse survey the re-observation of stable base station at the beginning and end of each day will correct for the majority of the effect leaving only the variation in pressure during the day uncorrected. Although this it not ideal it is the most cost effective solution.

### 3.8.7 Magnetic field effect

The effect of magnetism on the L&R D meter is small as it is equipped with dual layer magnetic shielding. However, if time lapse surveys are being carried out it is good practise to take each reading with the meter in the same orientation for each subsequent survey. Any erroneous effects that local or regional magnetic fields may have on the meters accuracy will thus be reduced.

### 3.8.8 Vibration

Vibrations are the biggest source of error encountered during a microgravity survey. Due to the mechanics of gravity meters and the fact that the relative increase or decrease in the length of a spring is being measured any sort of vibration is likely to

disrupt the accuracy of the survey. Transportation of the meter will effect its accuracy even though the spring is clamped. If it is being transported by car then efforts should be made to reduce its exposure to vibration and shock as much as possible. If the meter is to be used shortly after transportation then a settling period should be observed in which the meter can recover from the journey. Fortunately, the distances travelled during a microgravity survey are small. However, the longest period of transportation during a survey is usually from the survey station back to the base station at the end of the survey period. Care must be taken here and sufficient time allowed for the meter to settle as the base station readings are the most critical readings, and an error in these is likely to disrupt large portions of the survey. This problem is particularly acute when using the Scintrex CG-3M gravity meter. When carrying the CG-3M distances greater than 15m between stations, time must be given for the meter to settle as the CG-3M readings will drift before settling (usually decreasing). A 2 - 3 minute settling period is normally sufficient for distances around 20m.

Vibration from the ground also brings considerable errors and frustration. During operation in the vicinity of a road or carriageway, vibrations from passing traffic will have the effect of making the beam oscillate. It is possible to correct for this visually if the meter has a galvanometer attached to the beam read out as the operator can estimate about which point the beam is oscillating about. However, if an MVR is being used (a system, for use with L&R model G meters, where the voltage required to return the beam to its null position is displayed and recorded, eliminating the use of the nulling dial to record the value of gravity and increasing the precision of a L&R G meter to a level comparable to a L&R D meter) it is difficult to gauge which point the beam is oscillating. In some cases a reduction in the amount of oscillation has been found if the meter has been orientated with its long axis perpendicular to the road.

In addition to traffic secondary vibrations are caused by pedestrians. In many cases pedestrians are kept away from the area of investigation, but in some instances the non invasive nature of microgravity is used to its full and a survey may be acquired without the need to close off an area to the public. In this case then a curious member of the public is likely to disrupt the meters levels, hindering the acquisition of the survey.

One benefit of the zero length spring suspension is that it is relatively insensitive to longitudinal and transverse vibrations (Harrison 1960, LaCoste 1967). Consider the spring to be made of identical masses with segments of weightless zero length spring between the masses. The top of the spring is attached to A and the bottom of the spring is attached to B. Since spring segments are zero length springs, the forces each spring exerts on the adjacent masses are proportional to the spring length. Therefore if the masses are equally spaced vertically, the vertical component of force exerted on each mass will be zero regardless of its horizontal position or horizontal motion. (LaCoste and Romberg, 1998).

As well as these local ground vibrations, the vibration caused by local or global earthquakes will have the effect of lowering the meter's accuracy. Little can be done to prevent this other than note the time of occurrence and wait for the oscillations to cease, which could be several hours.

### 3.8.9 Wind

The main problem with wind is the effect it has on the stability of the levels. Steps can be taken to shield the instrument with a wind break or the operators body. However, it is more productive in many cases to cease acquisition until the conditions improve.

## 3.9 Survey procedures

### 3.9.1 Introduction

This section attempts to describe and discuss the procedures necessary to acquire accurate and precise microgravity data. Poorly acquired data can significantly reduce the possibility of an accurate and effective interpretation of the results and can subsequently reduce the likelihood of the survey satisfying its objectives.

The identification of the surveys objective will be discussed before moving on to the selections of sample interval and grid layout. The selection of individual stations within the grid and the determination of the stations co-ordinates is covered before protocol for the taking of a reading on a L&R D meter is outlined. Finally, the procedure for acquiring microgravity data is discussed.

### 3.9.2 Survey objectives

As discussed earlier, it is important to identify the purpose of the survey as a primary concern. Knowing the expected lateral and vertical size of the target body will help decide the scale of the survey including the sample interval. Appreciation of the effect that the local environment will have on the survey will also help eliminate difficulties in the planning stage. Knowledge of the density contrasts involved will determine the required survey accuracy and whether a 1D or 2D survey is appropriate.

### 3.9.3 Sample interval

There is no hard and fast rule for the station spacing or grid spacing in 2D surveys (d). However, considerations when deciding on the spacing include; depth of target and subsequently the half width of the expected anomaly. Ideally, at least 5 data points are required within the half width of the anomaly, however, this is not possible for shallow

targets. The size of the area to be surveyed is another consideration as the depth of the target body dictates the sample spacing it may be impractical to survey a large area due to the time it would take to complete the survey. Although time and costs are considerations, it would be folly to choose a spacing that is unlikely to detect the anomaly being investigated. It may be necessary to decide on the number of points that can be acquired and thus the feasible survey area, rather than the area of ground that would ideally be covered. Finally, the setting out process needs to be as easy as possible so fewer errors are made while marking out the grids. This is particularly important for repeat surveys when many of the survey points may be destroyed and so require re-installation. Spacing of survey points is statistically analysed in section 3.10.

### 3.9.4 Acquisition along a profile

The gravity profile is the simplest of acquisition templates. The profile is usually chosen for reconnaissance surveys or time limited surveys. Or to provide a series of several profiles across a feature of long lateral extent, such as a karst conduit, if the survey objective is to trace its position over large distances.

The profile should normally have an orientation perpendicular to the strike of the target feature. It is sometimes beneficial to vary the station spacing along the profile since the main area of interest can be sampled sufficiently while also extending the profile with a larger station spacing in order to sample the background field. This can be extremely useful for modelling and interpretation where corrections need to be made for local and/or regional geology.

### 3.9.5 Acquisition using a square grid

Locating gravity stations in a square or rectangle grid is particularly useful if the location of the target body is unknown. Square grids are commonly used in site investigations where the condition of the sub-surface is not known and the survey is being conducted to investigate whether any potential risk exists as a result of lateral varying density contrasts. Square grids enable simple uncomplicated setting out and acquisition as well as analysis of the gravity data along cross lines, perpendicular to the line of acquisition. Looking at crosslines in a survey is an effective way to quality control (QC) the data as any cumulative errors can usually be identified by a jump between adjacent points along the crossline. Using a square grid also means that the data is in a suitable format for griding directly by a contouring package.

### 3.9.6 Acquisition using a radial grid

A radial grid consists of a series of profiles originating from a centre point. This grid system is useful if the survey is around a feature of known dimensions such as a brine cavity or aquifer pump. Setting out of the grid is relatively simple using a theodolite or total station and the station spacing can be altered along each profile. In this way the spacing can be increased away from the centre point which, by design, would be the area of interest and consequently require a higher sampling frequency. This reduces the amount of data collected in "dead" areas away from the area of interest.

### 3.9.7 Station selection

Careful thought should be given to the position of each survey point and the surveyor should use their knowledge of gravity to site points away from features that

might adversely effect the value of gravity recorded at that point. Features the surveyor should be aware of are;

- Rugged country - the ground should be as flat as possible so that a stable contact can be made between the base plate and the ground. It may be necessary to flatten the ground before surveying.
- Soft ground – if the ground is soft or waterlogged it may not be possible to survey as stable levels will not be achievable. The Scintrex CG-3M has leg extensions for the base plate, which are used to penetrate the soft ground into firmer ground beneath. Occasionally, it is necessary to cut away the turf at station locations so that the meter can rest on the stable ground beneath.
- Exposure to strong winds – this is unlikely to effect individual points in an engineering investigation and so it is usually beneficial to suspend acquisition until conditions improve.
- Awareness of terrain effects – terrain effects drop off rapidly therefore moving a survey point a few metres away from buildings, holes etc. can reduce the effect of terrain and avoid processing at a later stage.
- Noise and vibration – traffic, people, maintenance will all have an effect on the quality of data acquired. It may be necessary to suspend access to areas likely to be effected by traffic etc. if the target body is on the limit of resolution.
- Services – it can be beneficial to avoid sitting survey points on or near known services such as inspection covers. At the very least their position should be noted, as they will tend to induce spikes in the gravity data.

### 3.9.8 Determination of survey point geographical co-ordinates

Accurate determination of the observation survey point geographical co-ordinates is an essential part to any microgravity survey. The co-ordinates of the stations need to be known in order that any anomalies detected in the survey can be related back to the ground. Ideally, the survey co-ordinates should be tied into a national survey grid. However, for small survey areas a floating grid, which is a grid that is not related to a national grid but set up for use in a local area, is sufficient. In this case it is essential to relate the grid to a permanent feature such as buildings or topographic features in order that survey points can be found again easily in the future if further investigation is required.

The free air correction (section 3.12.3) that is applied during the reduction of gravity data relies heavily on accurate height of the survey point positions. A 1cm error in the measurement of the station height will equate to a 3μGal error in the reduced gravity. It is, however, easy to eliminate this error by practising good survey procedure.

All of the topographic data in this thesis has been acquired with a total station (an instrument used for the accurate measurement of an objects position). With this, x, y, and z co-ordinates are measured with respect to a fixed point. Generally, a permanent survey nail is installed on site and acts as the topographic base station from which all the survey points and topography is related to. If subsequent topographic base stations are required they are set out from this master base station.

Ideally, the topographic data would be acquired concurrently with the gravity data. If the ground on site is reasonably level, it is possible to use a rotating laser level to determine the topography. If the ground is uneven, the topography will have to be acquired as a separate stage. If this is the case it is important to acquire the topography data as close

to the date of the gravity survey as is possible. It is also important to measure the exact position of the station point otherwise errors can creep into the gravity reduction.

During the acquisition of the topographic data it is good practice to make a sketch of the survey grid and note any missing points. In addition the p-code (short hand code used to identify the relevance of the measurement e.g. line and station numbers, fence, inspection cover etc.) and data point number should be noted for each gravity point. In this way there can be no ambiguity in matching the gravity point to the correct geographical co-ordinates.

If a secondary topographic base station has to be established during a survey, great care should be taken in order to avoid simple mistakes. The new base station should be established with either a survey nail or stake before being surveyed. Ideally, a tripod should be used to support the prism when sitting the co-ordinates of the new station. The co-ordinates of the new station should be written down together with the back-sight angle (i.e. 180° subtracted from the horizontal angle). In this way the total station can be checked to see if it is correctly recalling the information from its memory card as it is this procedure that is most likely to incur human error. If a mistake has been made it will become apparent when plotting the gravity station co-ordinates. Errors in the x, y, or z co-ordinates can be corrected with a simple transformation. Errors in the horizontal angle, incurred by either incorrectly inputting the back-sight angle, back- sighting to the wrong station or by the recall of the incorrect data point can be corrected by using the following formula to rotate the data:

$$x' = x\cos\theta - y\cos\theta \quad (3.10)$$

$$y' = x\sin\theta + y\cos\theta \quad (3.11)$$

where x and y are the current co-ordinates and x' and y' are the co-ordinates after being rotated by θ (Jeffrey, 1985).

Quality control is an important aspect of the topography survey because of its importance to the reduction process and the relatively large errors incurred in the gravity data. It is good practise to repeat 5-10% of the station points measured. Station heights should be repeatable to an accuracy of 5mm. Station co-ordinates are not as important to the reduction process and as a consequence an accuracy of 5cm is acceptable on the repeats. If more than one topography base station is used to survey the gravity stations then the loop should be closed (the surveyor should sight back to the original master base station from the final topographic base station) in order to give an indication of the cumulative error incurred when moving the topography stations. This error can then be redistributed around the survey stations in order to minimise jumps in reduced gravity or the survey can be repeated if the error is unacceptably high. i.e. over 2cm difference in height. Further explanation of surveying techniques is given in Banister and Raymond (1967).

### 3.9.9 Acquisition protocols

The actual acquisition of microgravity data is very simple. The operator need only remember a few simple procedures in order to operate the microgravity meter accurately. The key to successful acquisition is establishing a routine. In this way simple errors can be eliminated.

### 3.9.9.1 Taking a reading

To take a reading the operator needs to place the base plate on the ground as level as possible. On soft ground the plate should be stamped into the ground to stop it from sinking during the reading. This will also need to be done if the reading is to be taken on tarmac on a hot day. The meter should then be removed from the carry case. Care should be taken not to knock the meter on its way out of the box. If this does occur then a repeat base station reading should be taken in order to account for any tares which may have been incurred.

The meter should be placed on the base plate with the three adjustable legs sitting in the recesses on the base plate. These counter-sinks have been drilled specifically for this project and allow for the meter to be levelled on the same part of the base plate for each reading. This reduces errors caused by differences in elevation of the meter above ground level. If the ground is steeply sloping then it may be necessary to use the concave nature of the base plate in order to level the instrument.

The instrument should then be levelled using the adjustable legs that are located nearest the operator and to the operator's right. The levelling screw in the top left corner is fixed, again to keep errors caused by changes in elevation above the ground to a minimum. Once the instrument is level the spring can be released by turning the arrestment knob in the centre of the top panel anticlockwise. Looking down the eyepiece the operator should be able to see the beam being released from the left and oscillate briefly before settling on a position. The nulling dial should be used to bring the beam towards the reading line. The reading line value is usually displayed on top of the meter. If not, the manual should be referred to. In the case of the L&R D-141 meter it is 2.00. The beam should be made to approach the reading line from the left. When the beam reaches a position close to the reading line the operator can then use the electronic beam located just above the eyepiece

in order to achieve a more accurate reading. If the beam passes the reading line then the operator must start again and return the beam to the left hand side of the reading line before attempting to make a reading again. If the operator does not do this an error will be incurred in the reading caused by the slack in the gears and universal joint.

Once the operator is satisfied that the beam has been centred on the electronic reading line and that the instrument is still level, the counter reading and time of the reading are recorded. If the instrument is no longer level the reading procedure must be repeated. This procedure should be repeated three times for each station and the values should repeat to within 3 μGal. On stable ground with favourable weather it is possible to cut this down to two readings. The meter must then be clamped, by turning the arrestment knob clockwise and returned to the carrying case before proceeding to the next station and repeating the process.

#### 3.9.9.2 Procedure for the acquisition of microgravity data

First, a base station needs to be established. The base station readings are used to correct the acquisition data for instrumental drift and Earth tides. The base station readings are, as a result, extremely important to the accuracy of the acquisition data. Through personal experience, poor base station data can result in false correction of the acquisition data and therefore render the interpretation of such data incorrect. The base station site should be situated on level, stable ground, preferably concrete. It should also be sheltered from the wind and rain, as often, when the weather turns foul, the base station loop will still need to be completed.

A base station reading should be taken at the start of the day. The instrument should be given plenty of time for the spring to settle and as a rule should be left for 20-30 minutes, levelled and unclamped on the base station before the first reading is taken. At

least five readings should be taken from which a mean can be calculated. These five readings should all repeat to within 10μGal.

Throughout the survey the base station should be re-observed every hour. This is used to monitor and correct for instrumental drift as well as monitoring and correcting for Earth tides. A base station reading should also be taken at the end of the day to complete the days surveying. If this is not done then the last hours work is not usable.

Once an accurate base station gravity reading has been recorded the operator is free to collect data from the acquisition area. It is usual to collect the data on a grid or profile in a systematic order. In this way it is easier to spot and correct for tares and inaccurate drift corrections. It is also good practise to re-observe the station that was recorded just before the base station reading was taken before continuing with the acquisition. This will help identify inaccurate base station readings.

Random re-observation of 10% of stations should be acquired during a survey. These give a handle on the accuracy of the survey as a whole and the deviation should not exceed 5μGal or 25μGal depending on ground conditions and weather.

### 3.9.10 Re-ranging of a gravity meter

The LaCoste and Romberg model D meter has a limited range of 205 to 250 mGal in which it can measure gravity variation. This range is more than ample to measure microgravity over even very large sites and is equivalent to the change in gravity due to 1,200 m of elevation change. However, if a meter is to be used at a new site that is several degrees of latitude away from the previous acquisition site it will be necessary to re-range the gravity meter. This is done by setting the counter to mid range (1000.0) and balancing the meter by turning the coarse, re-ranging screw located under a small cover plate which is located on the top of the meter towards the centre. One turn of the coarse screw is about

74 mGal. The beam will move to the right if the screw is turned clockwise. When the meter is approximately balanced then the nulling dial can be used to complete the balancing of the meter. Once the meter has been ranged it should not be re-ranged during a survey except at a base station where the gravity has already been measured.

### 3.9.11 Weather

The LaCoste & Romberg model D and Scintrex CG-3m gravity meters are not waterproof. Care must be taken to avoid moisture from entering the instruments. It is possible to operate the instruments under an umbrella or similar cover if there is little or no wind. However, through personal experience the quality of data acquired when using the meter in this fashion is reduced because of the cramped position the operator finds themselves in. It must also be considered that, in the UK, with rain comes wind and changes in atmospheric pressure which, are again, likely to reduce the accuracy of the data recorded. Combining this with the fact that the operator is running the risk of ruining an instrument that costs in the region of £20,000 it is my opinion that the instrument should only be used in this manner to complete a base station loop.

## 3.10 Statistical analysis of station spacing

The vast majority of targets in microgravity surveys are three-dimensional bodies and it is important to consider the 3-D configuration of the anomaly in planning the data acquisition.

To detect shallow targets whose anomaly wavelength is short the choice of station spacing is at least as important as the resolution of the instrument. Most conventional forward modeling of theoretical anomalies assumes that the gravimeter will be located

exactly above the centre of the body and calculates theoretical anomaly amplitude on this basis. As the position of the body cannot be known *'a-priori'* this technique cannot be used as an accurate assessment of the likelihood of detecting that body as even a small movement away from the position of the peak of the anomaly can cause a very significant reduction in the amplitude recorded (Figure 3.4). Figure 3.4a shows the theoretical maximum anomaly calculated on a 1 m grid for a sphere of radius 1 m located at 2 m depth to centre and with a density contrast of -2.15 $gcc^{-1}$. On this basis, the gravity feature is easily detectable at 15 μGals , about 2 times the threshold value of the survey.

In order to determine whether this feature would actually be detectable in the field where knowledge of the position of the feature cannot be known a numerical simulation has been carried out. A random offset has been applied to a 3 m acquisition grid and the anomaly resampled onto this grid. Figures 3.4b shows the 3-D anomaly and a profile across its line of maximum amplitude. The anomaly has now dropped to about 7 μGal, just on the limit of resolution. This numerical simulation has been run 10000 times for random offsets in the x and y position of the 3 m sampling grid and the results displayed in Figure 3.5. The ranges of possible maximum amplitudes range from 5 to 15 μGal, with a mode at 8 μGal, the anomaly is therefore declared to be statistically detectable at this sampling spacing although there is a small probability that it will not be. This gives a much more robust estimate of the detectability of shallow features.

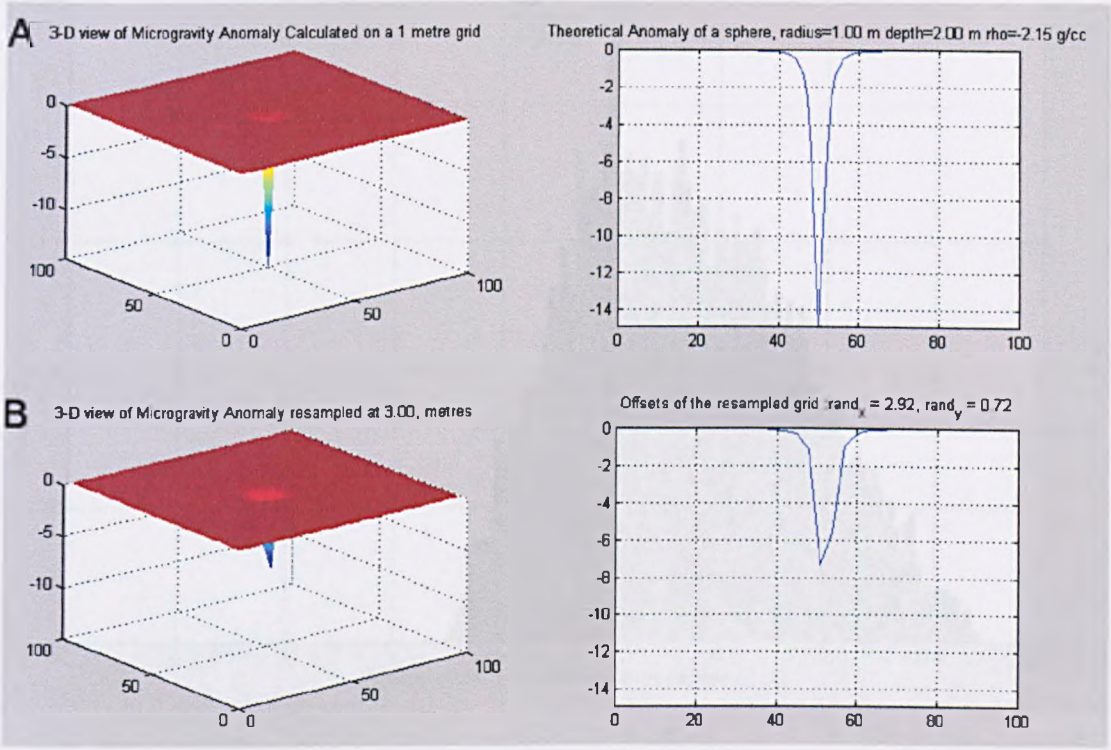


*Figure 3.4. a) Theoretical anomaly amplitude for a body with a radius of 1m, located at a depth of 2m with a density contrast of – 2.15 gcc$^{-1}$ on an acquisition grid of 1m spacing centered directly over the target body. The maximum amplitude is 15μGal.*

*b) Theoretical anomaly from the same body with an acquisition grid with 3m centres located randomly. The peak measurable amplitude is only 7μGal.*

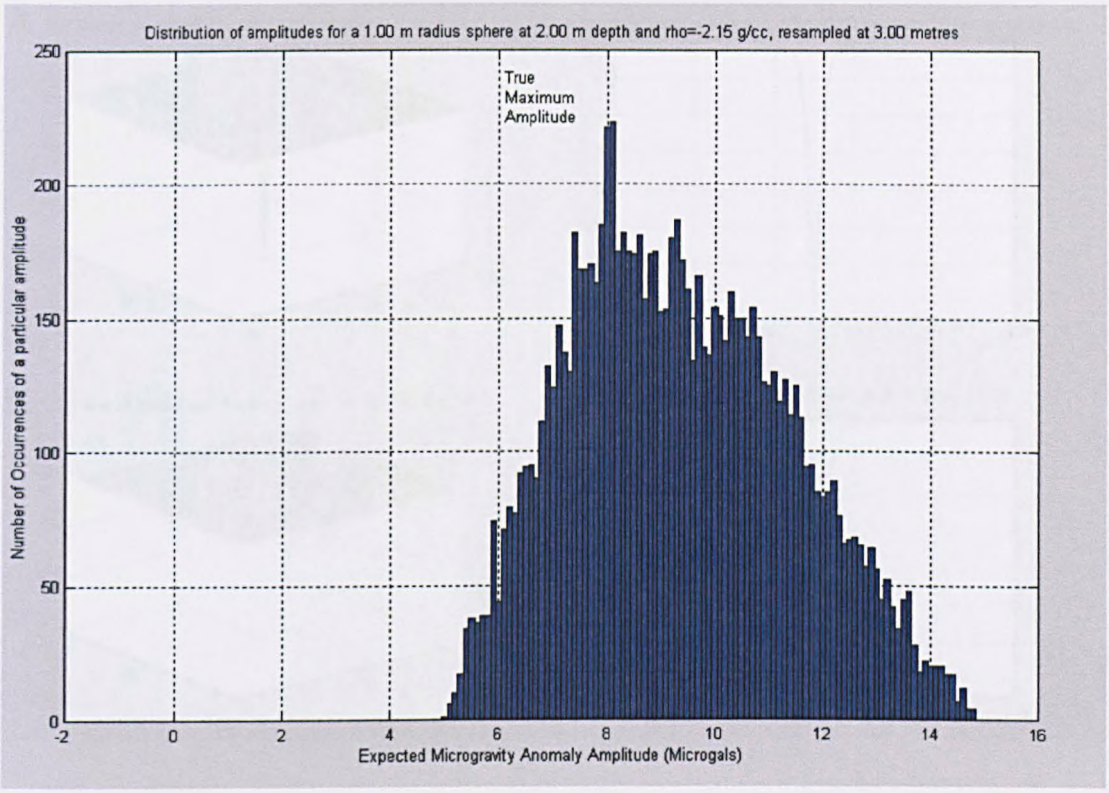


*Figure 3.5. Frequency distribution of the maximum amplitude detectable on a randomly sited acquisition grid with 3m centres. The mode of the distribution is 8μGal and a max of 15μGal. The body is said to be detectable on this acquisition grid.*

Figures 3.6 and 3.7 show the same analysis carried out for a 5 m grid spacing. It can be seen that for the particular sampling grid chosen at random in Figure 3.6b, the anomaly amplitude would only appear to be about 4 μGal, even though the theoretical maximum is about 15 μGal. The statistical analysis (Figure 3.7), shows that is even though it is theoretically possible to detect this feature, the probability is that it will lie beneath the threshold of detection for most realistic surveys at a 5 m spacing.

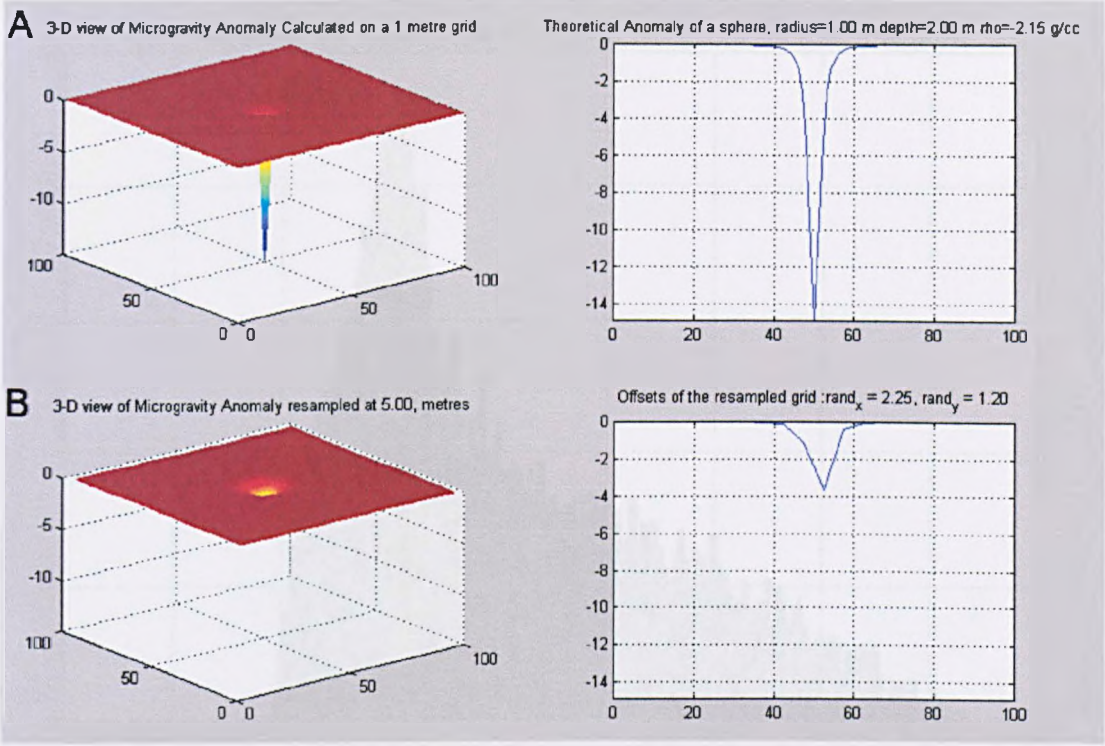


*Figure 3.6. a) Theoretical anomaly amplitude for a body of radius 1m located at a depth of 2m with a density contrast of – 2.15 g/cc with one m grid centred on the body. b) Theoretical anomaly for same body with an acquisition grid with 5m spacing located randomly. The measurable maximum amplitude would be ~4μGal. Therefore this body would be undetectable on a grid with 5m centres.*

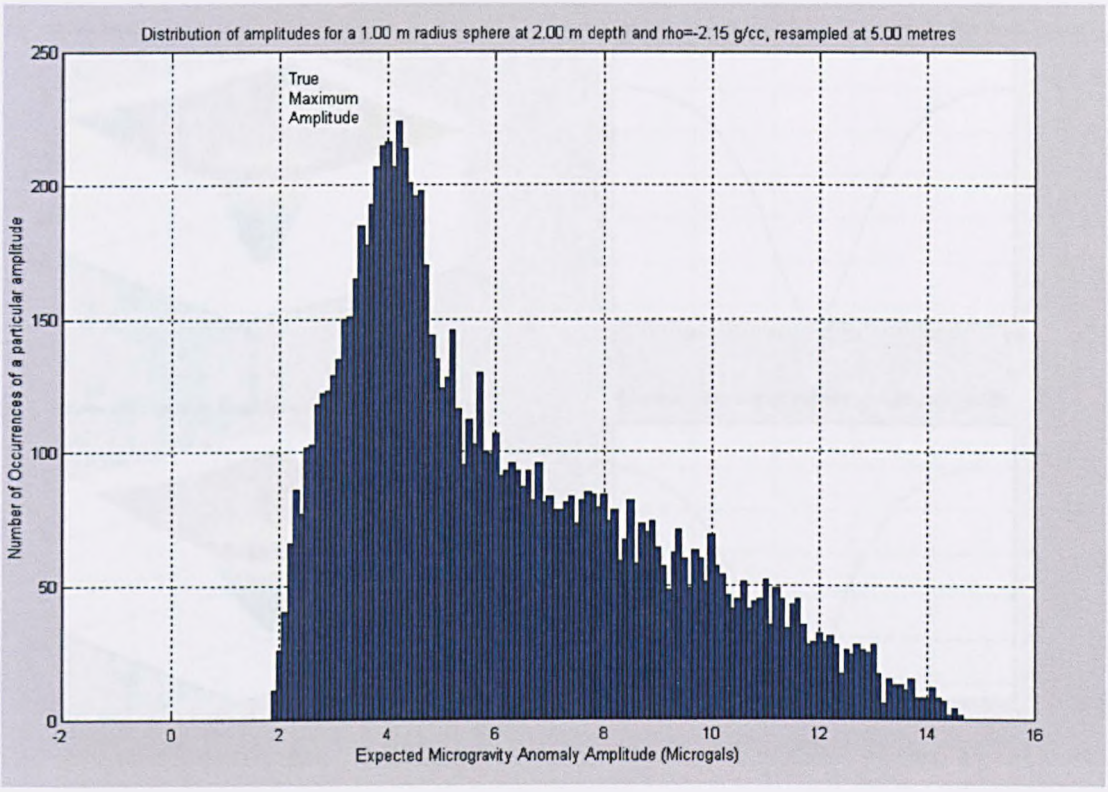


*Figure 3.7. Frequency distribution of the maximum amplitude detectable on a randomly sited acquisition grid with 5m spacing. The mode of distribution is 4μGal with a maximum detectable amplitude of 15μGal. The body is statistically unlikely to be detectable using this acquisition grid spacing.*

The effect becomes much less important for targets at greater depths because their anomaly wavelength becomes much greater than any sensible station spacing. This is shown in Figure 3.8 where a sphere of radius 4.3 ms located at a depth of 20 ms is resampled on a grid with 10m centres. The anomaly amplitude is very similar for the theoretical (a) and the random sampling grid (b).

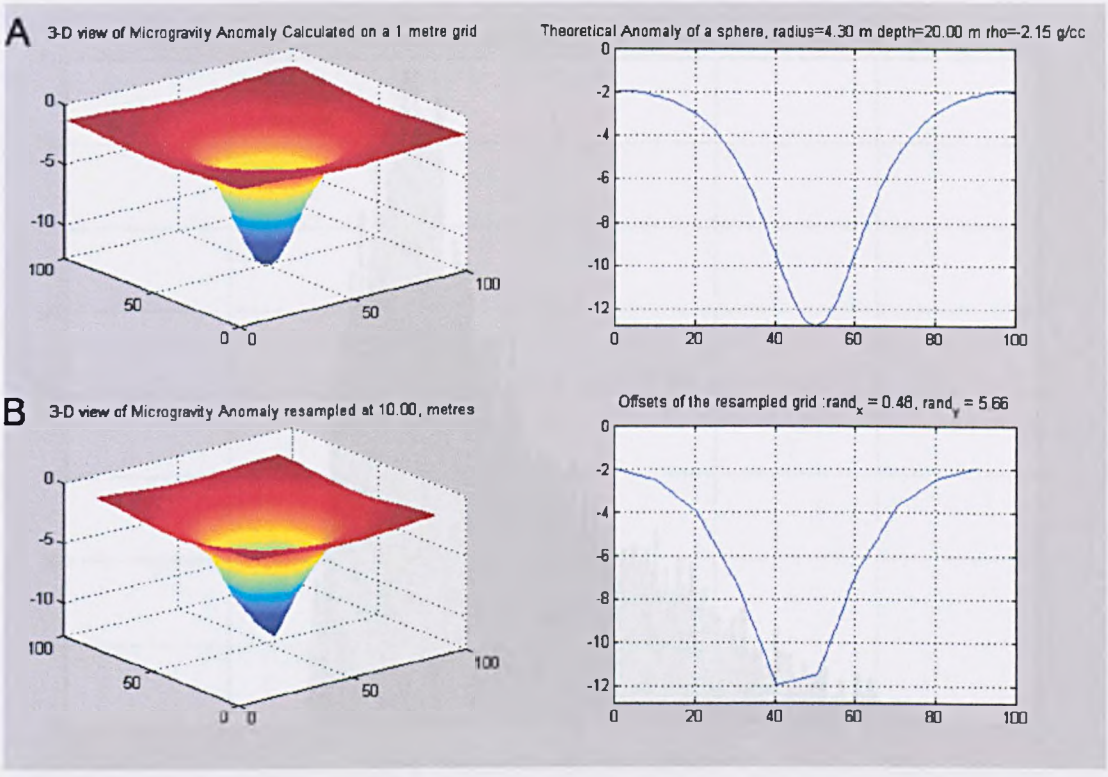


*Figure 3.8. Amplitude analysis for a body of radius 4.3m, located at 20m depth with a density contrast of -2.15 g/cc. There is little discernable difference in the measured amplitude between an acquisition grid with 1m spacing centred on the target body (a) and one with 10m spacing randomly centred (b).*

However, even at a 3 m station spacing, there is a limit of detection for small very shallow bodies. For a void which is 1 m below surface, the minimum detectable radius is about 0.75 ms (about 2.5 feet). The statistical analysis shown in Figure 3.9 shows that even though the theoretical maximum gravity anomaly is 21 μGal (3 times the threshold value) the expected measurable amplitude is likely to be about 6 μGal which is at the limit of resolution. Features smaller and shallower than this can be detected but only at very small station spacings of 2 ms or less and costs increase very markedly as station spacing decreases.

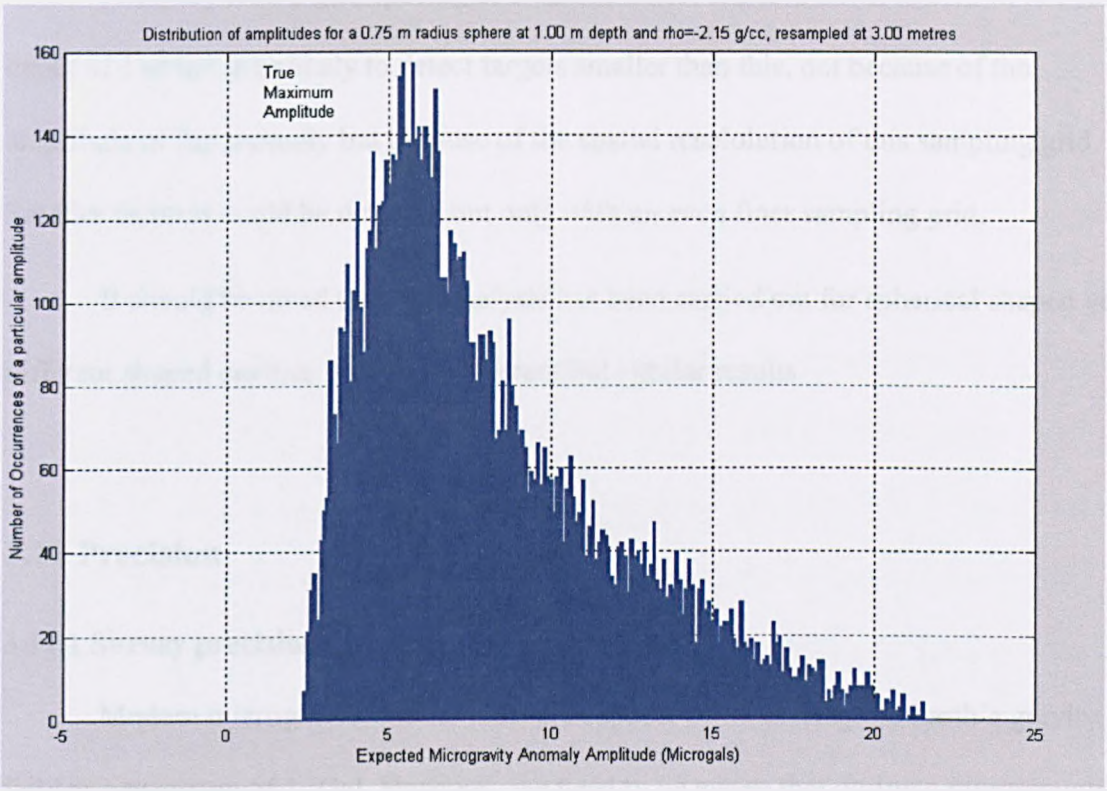


*Figure 3.9. Frequency distribution of the maximum detectable amplitude for a body with radius of 0.75m, a density contrast of –2.15 Mg/m³ and located at a depth of 1m. The resultant anomaly has been sampled on a randomly sited acquisition grid with 3m spacing. The distribution is positively skewed with a mode at 6μGal. This body is unlikely to be detected on this acquisition grid.*

Using this statistical procedure the detectability of spherical cavities with depth has been determined for both three and five m grid spacings.

At shallow depths there is a considerable difference between the resolving powers of a three and five m grid spacings which disappears for targets deeper than 4 m.

A survey with a five m grid spacing is unlikely to detect features smaller than 1.3 m radius at less than 2 m depth even though they are theoretically easily discernible but will detect targets of about 6 m radius down to depths approaching 30 m.

A survey with a grid spacing of 3 m will detect features down to 0.75 m radius at a depth of 1 m but is unlikely to detect targets smaller than this, not because of the amplitude of the anomaly but because of the spatial resololution of this sampling grid. Smaller features could be detected but only with an even finer sampling grid.

It should be noted that this analysis has been carried out for spherical shaped voids different shaped cavities will yield different but similar results.

## 3.11 Precision

### 3.11.1 Survey precision

Modern microgravity instruments are capable of measuring the Earth's gravity field to a precision of 1μGal. However, we need to be aware that during a microgravity survey the resolution attainable is constrained by factors apart from the precision of the gravity meter itself. As well as the contributing factors to gravitational noise discussed earlier in section 3.8 (wind, vibration etc.) the height of the survey point is a key contributor to the accuracy of the gravity survey. In order to achieve an precision of 1μGal the height of the survey station needs to be known to an precision of better than 1mm. An error of 3mm will in itself produce and error of 1μGal.

This kind of precision is technically possible for a topographical survey. However, it is important to assess what overall precision is sufficient for the survey. If the object of the survey is to map the structure of a sedimentary basin, a precision of 1μGal is not required. High resolution, engineering studies, however, require high degrees of precision as the target anomaly can be in the order of 10-15 μGal. Although the meter can theoretically record gravity variations smaller than this it is unwise to attempt to detect

target bodies producing anomalies lower than this because of the gravitational noise likely to be encountered during the survey.

### 3.11.2 Keele Gravity Range

When acquiring time-lapse microgravity it is important to be sure that if any changes in gravity are present that they are the result of mass change beneath the survey site and not the result of external factors. One of the most likely factors is subsidence. This can be accounted for by acquiring a new set of topographic data with each gravity survey. Other factors that can result in the misinterpretation of temporal gravity surveys are calibration errors if different instruments have been used to acquire the successive gravity surveys. If a single instrument has been used for the successive surveys (which is the ideal case), it is important to identify that no tares have occurred between surveys and if they have they should be identified and corrections applied to the latest data set as a datum correction.

In order to try and provide for some of these requirements of time-lapse microgravity a profile was set up at the School of Earth Sciences and Geography at Keele University. It is sited in a quiet location on ground that is stable, both on the long and short term. i.e. there are believed to be no geological structures beneath the site that are likely to change their gravitational signal over time and the material on the surface is solid and so the meter remains level. It consists of nine points with a 25m separation and runs down a slope giving it a total change in elevation of 10.021m.

The initial idea of the Keele Gravity Range (KGR) was to use it to check the calibration factors between instruments, particularly between a Scintrex CG-3M and a LaCoste and Romberg Model D. However, it was also realised that it would be beneficial to use it to establish the repeatability of microgravimeters over a period of a few months

and therefore determine what sort of errors are likely to be faced when attempting a time-lapse microgravity survey. It can also be used as part of the time-lapse survey to assess whether the instrument has experienced any tares during the period between surveys. Gravity was acquired on KGR on the dates given in Table 3.2;

| **LaCoste and Romberg Model D** | **Scintrex CG-3M serial # 610362** |
|---|---|
| 18/04/01 | 11/01/02 |
| 19/10/01 | 04/06/02 |
| 08/06/02 | |
| 27/07/02 | |
| 10/09/02 | |

*Table 3.2 acquisition dates of time lapse surveys on Keele Gravity Range*

Comparing the gravity values acquired with the L&R D-141 (Figure 3.10, Table 3.3 and Table 3.4) it can be seen that the average repeatability between surveys ($\Delta L$) ranges from 5.9μGal to 14μGal. The highest average repeatability is 20μGal after a period of 182 days (Table 3.4).

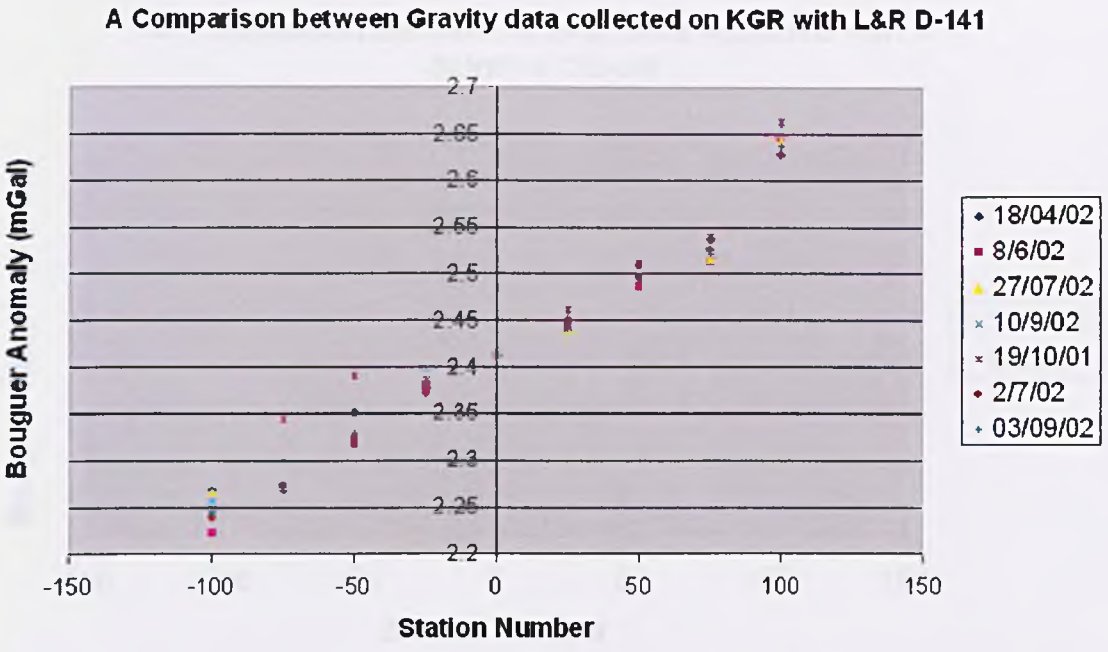


*Fig. 3.10. Graph comparing the gravity data acquired along the Keele Gravity Range with L&R D-141.*

However, survey points –50 and –75 from the survey acquired on the 19/10/01 and the 10/09/01 have disproportionately large deviations and would appear to be a result of an external factor. If these points are removed, it can be seen that the range of ΔL is reduced to 10.8μGal.

If the two surveys acquired with Scintrex CG-3M (serial #610362) are compared (Figure 3.11 and Table 3.5), it can be seen that the average difference between the surveys (ΔL) is only 2.1μGal.

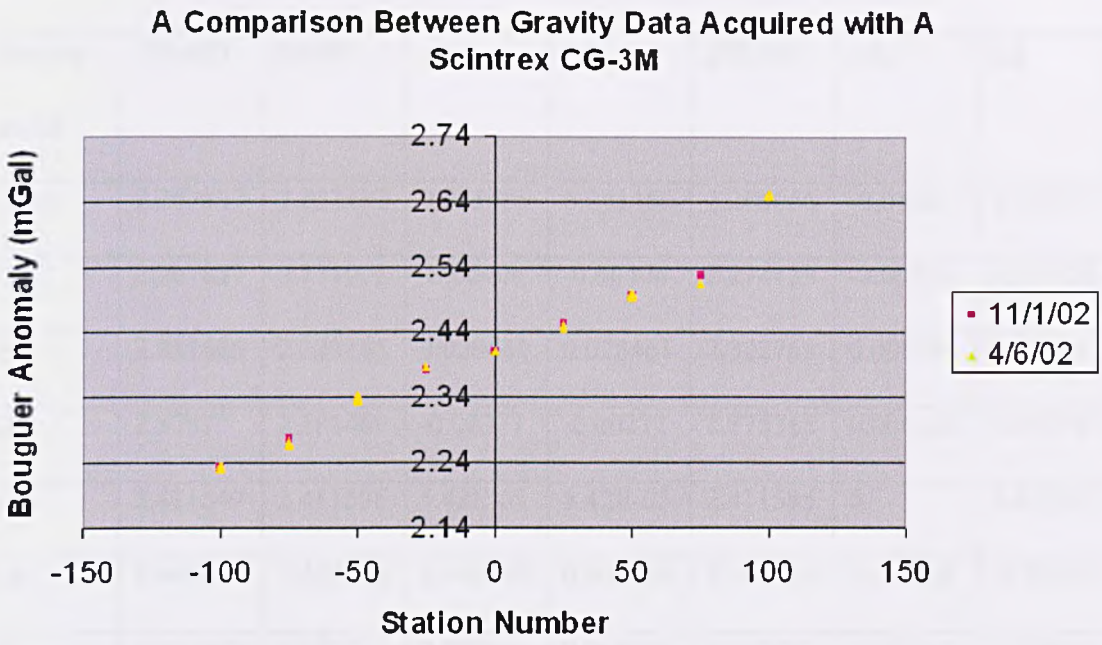


*Fig. 3.11. Graph comparing the gravity data acquired along the Keele Gravity Range with a Scintrex CG-3M.*

Comparing the Scintrex data acquired on the 04/06/02 with the L&R data, the repeatability ranges between 2.6μGal and 12.9μGal. This relates to the L&R surveys that were acquired on the 18/04/01 and 19/10/01 respectively.

| **Survey point** | **18/4/01** | **8/6/01** | **ΔL** | **ΔT** | **27/7/01** | **ΔL** | **ΔT** |
|---|---|---|---|---|---|---|---|
| **-100** | 2.267887 | 2.222432 | 0.045456 | 0.045456 | 2.266066 | -0.04363 | 0.001821 |
| **-75** | 2.267857 | 2.271922 | -0.00406 | -0.00406 | 2.274133 | -0.00221 | -0.00628 |
| **-50** | 2.351606 | 2.323145 | 0.028461 | 0.028461 | 2.322769 | 0.000376 | 0.028837 |
| **-25** | 2.3787 | 2.381469 | -0.00277 | -0.00277 | 2.375315 | 0.006154 | 0.003385 |
| **0** | 2.411649 | 2.411595 | 5.42E-05 | 5.42E-05 | 2.411595 | 0 | 5.42E-05 |
| **25** | 2.44041 | 2.439911 | 0.000499 | 0.000499 | 2.440461 | -0.00055 | -5.2E-05 |
| **50** | 2.495952 | 2.487337 | 0.008615 | 0.008615 | 2.500791 | -0.01345 | -0.00484 |
| **75** | 2.53723 | 2.513255 | 0.023976 | 0.023976 | 2.516893 | -0.00364 | 0.020337 |
| **100** | 2.628603 | 2.647324 | -0.01872 | -0.01872 | 2.643529 | 0.003795 | -0.01493 |
| **Av. point change** | | | **0.009056** | **0.009056** | | **-0.00591** | **0.003149** |
| **Gap between Surveys** | | | 50 days | 50 days | | 50 days | 100 days |

*Table 3.3 Results of repeated surveys on the Keele Gravity Range recorded with the L&R D-141 between 18/4/01 and 27/7/01. The values presented have been reduced to the Bouguer anomaly.*

*ΔL= latest change in gravity i.e. previous reading minus latest reading*

*ΔT= Total change in gravity i.e. first reading (18/0401) minus latest reading.*

| Survey Point | 10/9/01 | ΔL | ΔT | 19/10/01 | ΔL | ΔT |
|---|---|---|---|---|---|---|
| -100 | 2.2561735 | 0.009893 | 0.011714 | 2.248181 | 0.007993 | 0.019706 |
| -75 | 2.3002324 | -0.02610 | -0.03238 | 2.343697 | -0.04346 | -0.07584 |
| -50 | 2.3477278 | -0.02496 | 0.003878 | 2.391318 | -0.04359 | -0.03971 |
| -25 | 2.3984586 | -0.02314 | -0.01976 | 2.386719 | 0.01174 | -0.00802 |
| 0 | 2.4115945 | 3.32E-12 | 5.42E-05 | 2.411595 | -3.3E-12 | 5.42E-05 |
| 25 | 2.4562872 | -0.01583 | -0.01588 | 2.46232 | -0.00603 | -0.02191 |
| 50 | 2.5129548 | -0.01216 | -0.017 | 2.511761 | 0.001193 | -0.01581 |
| 75 | 2.5366404 | -0.01975 | 0.00059 | 2.541181 | -0.00454 | -0.00395 |
| 100 | 2.6581608 | -0.01463 | -0.02956 | 2.663177 | -0.00502 | -0.03457 |
| **Average point change** | | **-0.01408**<br>-0.01080 | **-0.01093**<br>-0.00998 | | **-0.00908**<br>0.000762 | **-0.02001**<br>-0.00921 |
| **Gap between Surveys** | | 43 days | 143 days | | 39 days | 182 days |

*Table 3.4 Results of repeated surveys on the Keele Gravity Range recorded with the L&R D-141 between 10/09/01 and 19/10/01. The values presented have been reduced to the Bouguer anomaly.*

*ΔL= latest change in gravity i.e. previous reading minus latest reading*

*ΔT= Total change in gravity i.e. first reading (18/0401) minus latest reading.*

*The highlighted values in the average point change are the resultant values if points –50 and –75 and deleted.*

| Station Number | 11/1/02 | 04/6/02 | ΔL |
|---|---|---|---|
| **-100** | 2.23364455 | 2.232909618 | 0.000735 |
| **-75** | 2.27798764 | 2.270018916 | 0.007969 |
| **-50** | 2.33558268 | 2.33937528 | -0.003793 |
| **-25** | 2.38324428 | 2.387074602 | -0.00383 |
| **0** | 2.41066192 | 2.411594566 | -0.000933 |
| **25** | 2.45419997 | 2.449027985 | 0.005172 |
| **50** | 2.49769401 | 2.498504367 | -0.00081 |
| **75** | 2.52804869 | 2.51530104 | 0.012748 |
| **100** | N/A | 2.652511073 | N/A |
| **Average point change** | | | **0.002157** |

*Table 3.5 Results of repeated surveys on the Keele Gravity Range recorded with the Scintrex CG-3M between 11/01/02 and 04/0602. The values presented have been reduced to the Bouguer anomaly.*

*ΔL= latest change in gravity i.e. previous reading minus latest reading*

Looking at the data acquired over the experimental period, it is not evident that any tares have occurred and therefore no correction need be applied to the time-lapse microgravity acquired during this period. This work has shown that if gravity surveys are to be compared and used in a time-lapse sense then a minimum error of at least 10.8μGal needs to be allowed if both surveys were acquired with a L&R model D meter. If the surveys are acquired with a Scintrex CG-3M then an error of at least 3μGal must be taken into consideration. If, however, the time-lapse surveys re repeated with different

instruments (i.e. L&R D141 and CG-3M serial #6103620) then a minimum error of at least 12.6μGal must be taken into consideration.

It is, however, worth noting that the cause of the large differences between repeat readings are probably a result of fluctuation in seasonal condition, particularly ground water level. If care is taken to repeat the survey at the same time of year then changes in gravity, which are a result of ground water fluctuations can be reduced. The installation of piezometers would make it possible to correct for the change in ground water level.

## 3.12 Gravity reduction

### 3.12.1 Reductions

The measured gravity differences recorded by the gravity meter between the base station and the acquisition grid are subject to several external effects that are not related to the sub-surface geology. In order for a valid geophysical interpretation to be made these effects must first be removed. The process of correcting for these effects is a well-established routine in any gravity survey and is often called reduction of data. The necessary corrections are (1) latitude correction, (2) free-air correction, (3) Bouguer correction and if the survey area requires it (4) terrain correction. As well as the above corrections, the instrument it self must be corrected for internal drift and Earth tides.

### 3.12.2 Drift correction.

As described earlier in section 3.7 the zero length spring used in the gravity instruments experience gradual change in reading with time. This drift is a result of the imperfect elasticity of the springs, which undergo an elastic creep with time. Drift can also result from temperature variations, which, unless counteracted in some way, cause

expansion or contraction of the measuring system leading to variations in measurements that are unrelated to gravity changes.

The correction for instrument drift is very simple and is based on repeated readings at a base station at recorded times throughout the day. A sample time between base station readings of one hour is normally used and the drift within this time is assumed to be linear. The meter reading is plotted against time throughout the day (Figure 3.12) from which the drift correction can be read off for a time *t* at which the field reading is taken and subtracted from the field meter reading for that respective time.

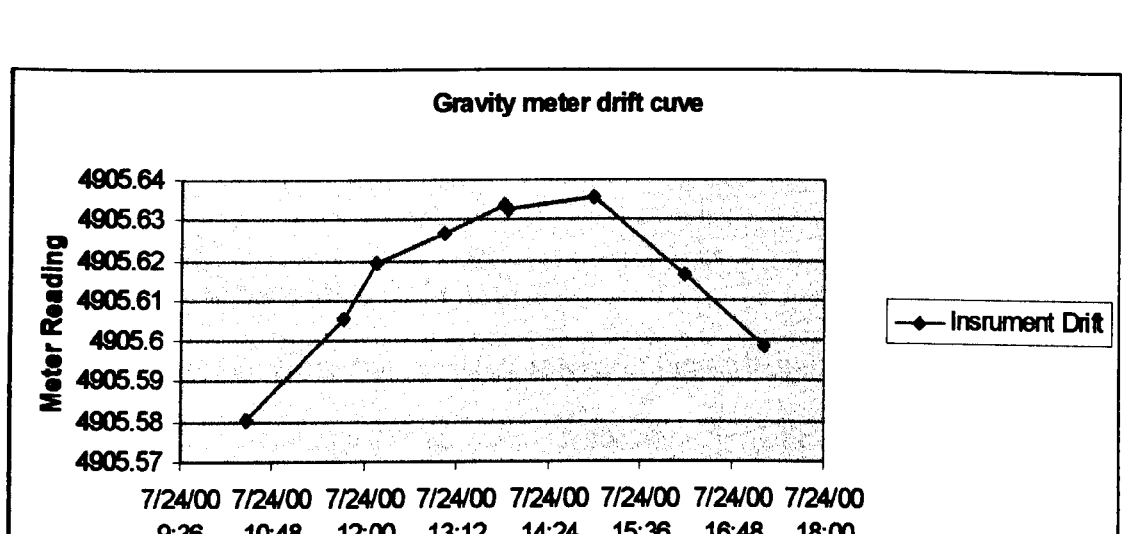


*Fig 3.12 Gravity meter drift curve for the 24th July 2000, taken from the microgravity survey of Brine well 64 in Preesall.*

### 3.12.3 Free air correction (FAC)

This correction takes into account the vertical decrease in gravity with increased elevation. The correction is based on the inverse square dependence of the acceleration due to gravity on the distance from a datum plane and can be written as

$$FAC = 308.6h \quad \mu\text{Gal} \tag{3.11}$$

where h is the elevation in metres.

The correction must be added to a gravity station which lies above the datum plane and subtracted if the station lies below the datum plane. In order to reach an accuracy of 1 μGal the elevation difference must be known within 3.3mm.

### 3.12.4 Bouguer correction (BC)

The free air correction accounts solely for the variation in height between gravity points. The Bouguer correction accounts for the attraction of material between a reference height and that of the gravity station. This can be approximated by treating the intervening rock material as an infinite horizontal slab, of a thickness equal to the elevation difference, Δh, between the reference base and the gravity station. If ρ is the density of the rock in $Mg/m^3$

$$BC = 2\pi G\rho h = 41.91\rho h \ \mu\text{Gal} \tag{3.12}$$

On land the BC must be subtracted, as the gravitational attraction of the rock between observation point and datum must be removed from the observed gravity value. It is therefore of opposite sign to that of the FAC. The net result of the combined Bouguer and

free-air correction is that g measured on the land surface decreases with height at a net rate of about 200 μGal/m (Sharma, 1997).

### 3.12.5 Terrain correction

The Bouguer correction makes the assumption that the topography around the gravity station is flat. This is rarely the case and for areas with significant relief a further correction, the terrain correction, is needed. A hill rising in the vicinity of a gravity station will tend to have an upward attraction due to the extra mass contained in the hill. This will have the effect of reducing the measured value of gravity. Similarly, a valley below the gravity station will also tend to reduce the measured value of gravity. In this case it is the missing mass within the valley that reduces the expected attraction due to gravity.

#### 3.12.5.1 Hammer method

The usual way for determining the terrain correction has been to use the method devised by Hammer in 1939. Using this method, the region around a station is divided into segments bounded by concentric rings at suitable intervals ($\phi$). The mean elevation difference, $\Delta h$, between each segment and the station is determined from a topographic map, regardless of sign. The terrain correction due to the attraction of the material in each segment is

$$TC = G\rho\phi\left[(r_2 - r_1) + \sqrt{r_1^2 + (\Delta h)^2} - \sqrt{r_2^2 + (\Delta h)^2}\right] \qquad (3.13)$$

There are various digital methods in which this process has been speeded up. Two such programs have been used within this study to calculate terrain correction where necessary. Both have been coded by Professor Peter Styles.

### 3.12.5.2 Parker method

The first of these programs is derived from the work by Parker (1995), and has been used in the surveys conducted during this study to calculate the terrain effects caused by topography. The Fourier-based method divides the area into two regions. The interior region is described as a cylinder (radius a) centred on each survey point and is excluded from the Fourier treatment. The attraction from the material within the cylinder is calculated directly by means of a quadrature scheme. The exterior integral is evaluated by Fourier methods (Parker, 1995). Examples of its use can be found in Chapters 6 and 7.

### 3.12.5.3 Plouff method

The second program has been used to calculate the terrain effect of buildings for use in surveys in urban environments. The program is based on calculating the gravitational attraction of a single rectangular prism (with uniform density and limits described by $x_1 \leq x \geq x_2, y_1 \leq y \geq y_2$ and $z_1 \leq z \geq z_2$) by integrating equation 3.14 over the surface of the prism (Blakely, 1996).

$$g(x,y,z) = -G\rho \int_{z_1}^{z_2}\int_{y_1}^{y_2}\int_{x_1}^{x_2} \frac{z'}{[x'^2+y'^2+z'^2]^{\frac{3}{2}}} dx'dy'dz' \qquad (3.14)$$

Where G is the gravitational constant. The body is arranged in Cartesian co-ordinates with z pointing downwards so that g increases in the direction of increasing z. The integral is simplified by moving the observation point to the origin.

Plouff (1976) provided a derivation of the equation 3.14, which is given in equation 3.15.

$$g = G\rho\sum_{i=1}^{2}\sum_{j=1}^{2}\sum_{k=1}^{2}\mu_{ijk}\left[z_k \arctan\frac{x_i y_i}{z_k R_{ijk}} - x_i \log(R_{ijk} + y_i) - y_i \log(R_{ijk} + x_i)\right], \quad (3.15)$$

where $R_{ijk} = \sqrt{x_i^2 + y_j^2 + z_k^2}$,

$\mu_{ijk} = (-1)^i(-1)^j(-1)^k$ (Blakely, 1996).

The program represents each building as a box. The height, width and length of the exterior wall are defined as well as the wall thickness and brick density. The program first calculates the effect of the area enclosed by the dimensions of the exterior wall (E). Using the wall thickness, a second box is defined which represents the interior of the building (I). The effect of this area is calculated and is subtracted from E. The result is the terrain effect created by the mass of the buildings walls. It is impossible to allow for the mass of the internal furnishings but the brick density can be modified to account for this. In practise, a process of trial and error is used to adjust the brick density until a good fit is achieved with the measured gravity data (e.g. Chapter 5).

### 3.12.6 Tidal correction

As well as the above effects, gravity measured during a survey varies with time because of periodic variation in the gravitational effects of the Sun and Moon associated with their orbits. In a high precision survey these effects must be corrected for.

There is a small but measurable gravitational effect of up to 240μgal, changing with time at a maximum rate of 50 μGal/hr at the Earth's surface due to its spin and the relative motion of the Sun and the Moon (Figure 3.13). The effect due to other celestial bodies is well below the limit of resolution for a field gravity meter (Rymer, 1989). This

variation can be predicted but the assumption of linear drift is invalid, therefore tidal corrections can not be ignored. Tidal gravity can vary as much as 1μGal/min.

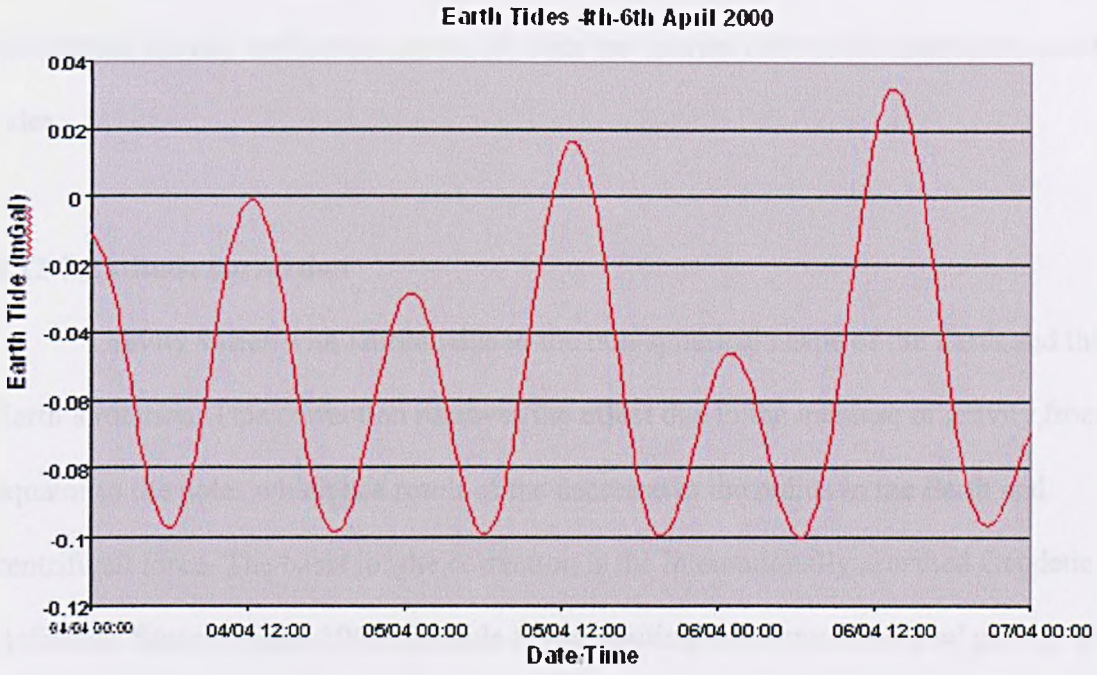


*Fig. 3.13 Example of fluctuation in gravity due to Earth tides.*

It is possible to predict the Earth tides using equation 3.16 but ideally it is advisable to record gravity continuously for at least a full day in the field location to check the prediction method used. Rymer (1989) discusses at length the cause and effect errors contained within the Earth tide correction, including the effect of phase differences between the observed elastic Earth and the predicted solid Earth tides

$$\Delta g = \frac{3GRM_m}{2D_m^3}\left(\cos 2\alpha_m + \frac{1}{3}\right) - \frac{3GRM_s}{2D_s^3}\left(\cos 2\alpha + \frac{1}{3}\right) \qquad (3.16)$$

where R = radius of rigid Earth

M = mass

D = distance

α = geocentric angle (Ferguson, 1992).

It is adequate for most microgravity surveys to correct for tidal variations by revisiting the base station at frequent and regular interval (of the order of one per hour). By revisiting the base station it is possible to monitor how the value of gravity varies throughout the day and hence correct for both the internal drift of the instrument and Earth tides.

### 3.12.7 Latitude correction

Gravity varies with latitude due to the non-spherical shape of the Earth and the Earth's rotation. This correction removes the effect due to the increase of gravity from the equator to the poles which is a result of the decrease in the radius in the Earth and centrifugal force. The basis for the correction is the internationally accepted Geodetic Reference System (GRS-1967) formula for computing the normal sea-level gravity at a latitude $\phi$.

$$g_\phi = 9.780318(1 + 0.0053024\sin^2\phi - 0.0000059\sin^2 2\phi) \text{ m/s}^2 \qquad (3.17)$$

The correction factor is zero at the equator and the poles and reaches a maximum at $\phi$=45°. The correction must be added to or subtracted from the measured gravity difference depending on whether the station is on a higher or lower latitude. Variations are typically of the order of 80μGal/100m for mid latitudes and as a consequence this correction is not usually applied for small microgravity surveys.

### 3.12.8 Data manipulation

Once the recorded gravity data has been "reduced" by the application of the corrections outlined above, it is necessary for the interpreter to check the quality of the data. By following a simple recipe the interpreter can determine the quality of their data beyond a simple measure of the repeatability of a gravity measurement.

- Normalise station elevation to the base station. i.e. subtract the elevation of the base station from all stations. This will reduce the elevation correction and result in a Bouguer anomaly centred around zero. It will also reduce the risk of errors being induced by the incorrect selection of the Bouguer density.
- Plot the Earth tide correction against the cumulative drift of the instrument. These values should be in the opposite sense and are an excellent way of identifying erroneous base station values as well as tares in the data.
- If the base station values have been identified as being very poor, possibly due to the poor selection of a base station site (wind, vibration etc.), it is possible to replace the drift with the tide correction calculated with Longman formula. This is a good way of salvaging data that would otherwise be unusable because of poor base station data. It is, however, not ideal as internal drift of the instrument is not corrected.
- Plot elevation of acquisition stations. This is used to identify any errors in the survey data. Although the offset of single points can usually be explained by ground conditions, systematic offsets can be identified by this method and usually attributed to topographic base station changes during the survey procedure. At this stage it is vital that a comprehensive field notebook has been kept. Identified errors should be corrected before further processing.
- Plot geographical co-ordinates of acquisition points. This should be completed by the surveyor as someone who hasn't been to the site is unlikely to be able to identify

systematic errors in the horizontal angle of the total station. Corrections should be made by using formulas 3.09 and 3.10.

- Plot the Free Air Correction against raw gravity for each survey point. The gravity data should be the inverse of the elevation correction. This is because the Free Air Correction has yet to be applied to the data and at this stage accounts for the vast majority of the variation seen in the gravity values. Plotting these two values enables the identification of suspect points. This is a way of easily identifying typing errors or misprints before further processing. Points that are identified should be corrected or deleted. This should be applied to cross-lines as well as in-lines.
- Finally, the interpreter should plot the Bouguer anomaly for in-lines and cross-lines. The variation in gravity should be smooth and gradual. If it is not, and there are points which do not follow the general trend, the data should be cross checked against the position of known service features such as inspection covers. In general, these points should be deleted, as they will confuse the overall gravity picture. If the data contains a high degree of oscillation then it is most likely a result of poor acquisition conditions (wind, vibration etc.) and a filter may need to be applied. Two of the most common filters are a moving point average filter or a low pass filter. A third type of filter that can be used is a Savitzky-Golay polynomial filter which fits a polynomial surface to the data set (section 3.15.3).

## 3.13 Inherent problems associated with the interpretation of gravity data

There are two main characteristics of the gravity field that make unique interpretation almost impossible. The first is the fact that the measured gravity and hence the reduced Bouguer anomaly is a result of the superposition of many mass distributions at various depths. From the gravity triangle described in section 3.4, the anomaly being

looked for is a very small part of the total gravity field. There is also the possibility that there are other gravity variations within the strata as well as the body in which the survey has been designed for. It is highly probable that the gravity anomaly is not the result of a single causative body but the sum of various bodies at various depths.

More serious is the difficulty in distinguishing the source from the effect, which is the problem with all potential field theory. For a given distribution of a gravity anomaly on or above the Earth's surface an infinite number of mass distributions can be found which would produce that anomaly.

Geological reasoning is required to reduce the infinite number of solutions down to a few plausible possibilities. *A priori* data such as the expected depth and/or density contrast of the feature can narrow down the likely possibilities further. Finally, the best way to substantiate the interpretation is to include a second method in the process of interpretation. In this way, techniques that use different characteristics of the gravity anomaly can be used to supplement one another. If lithological knowledge can be provided from drilling logs or seismic data, then the geophysicist can have a fair degree of confidence in his interpretation.

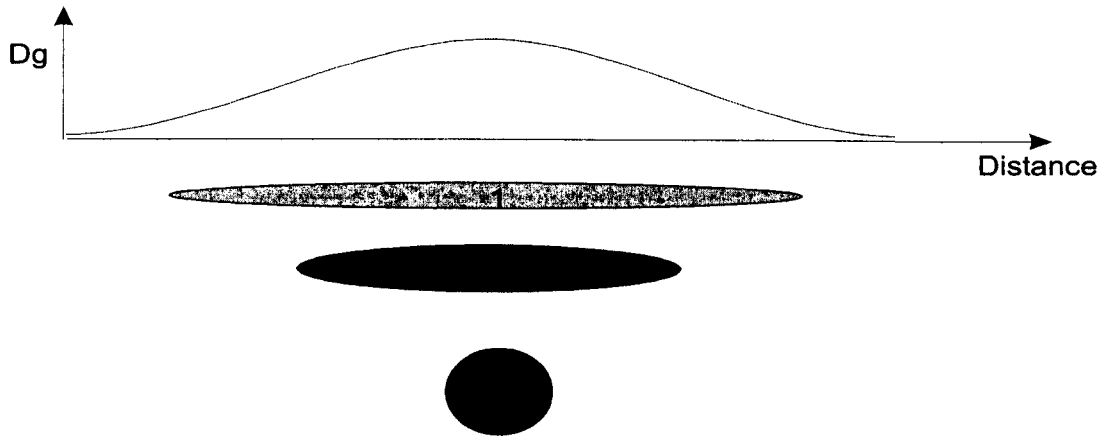


*Fig. 3.14. A diagram showing the ambiguity within gravity data. The anomaly shown (Dg) can be created by either of the three sources shown by varying the density contrast (Sharma, 1997).*

## 3.14 Enhancement of gravity anomalies

### 3.14.1 Isolation of gravity anomalies

The anomalies associated with a small near surface density contrast, for instance a target body in an environmental investigation, usually have a short wavelength and are laterally limited as shown in Figure 3.14. As a consequence of this characteristic, they tend to be masked by the larger wavelength gravity response associated with the regional geological structures which, have larger amplitudes and are detectable over greater distances.

To study the short wavelength (local) anomalies they are separated from the long wavelength (regional) response. The resultant signal is termed the residual and it is the isolation of the residual from the regional that is key to the interpretation of gravity data.

Residual fields have been calculated in this thesis by fitting a polynomial surface to the reduced Bouguer anomaly. The Bouguer data (Figure 3.15) is used to generate the mathematical surface giving the closest fit to the observed gravity field of a given order (Figure 3.16). This surface is then subtracted from the Bouguer data thus removing the regional trend and isolating the local anomalies (Figure 3.17). This method is free from subjective bias although the interpreter must keep in mind the geological feature they are using the fitted surface to correct for. In practical terms it is generally good practice not to exceed a polynomial order greater than 2. Since increasing the polynomial order will have the effect of reducing the amplitude of the remaining anomalies, as the surface becomes closer in form to the original data and more distant from a plausible geological scenario.

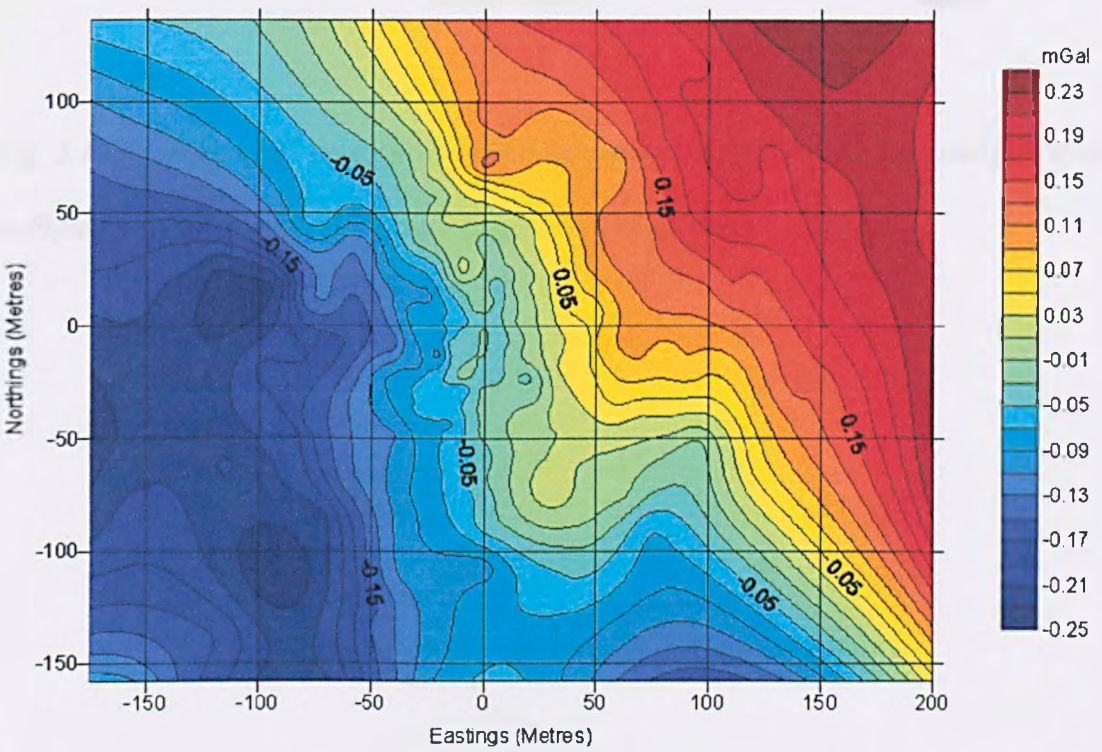


*Fig. 3.15 Example of reduced to Bouguer anomaly gravity data (taken from Preesall Brine well 64, acquired in 2000).*

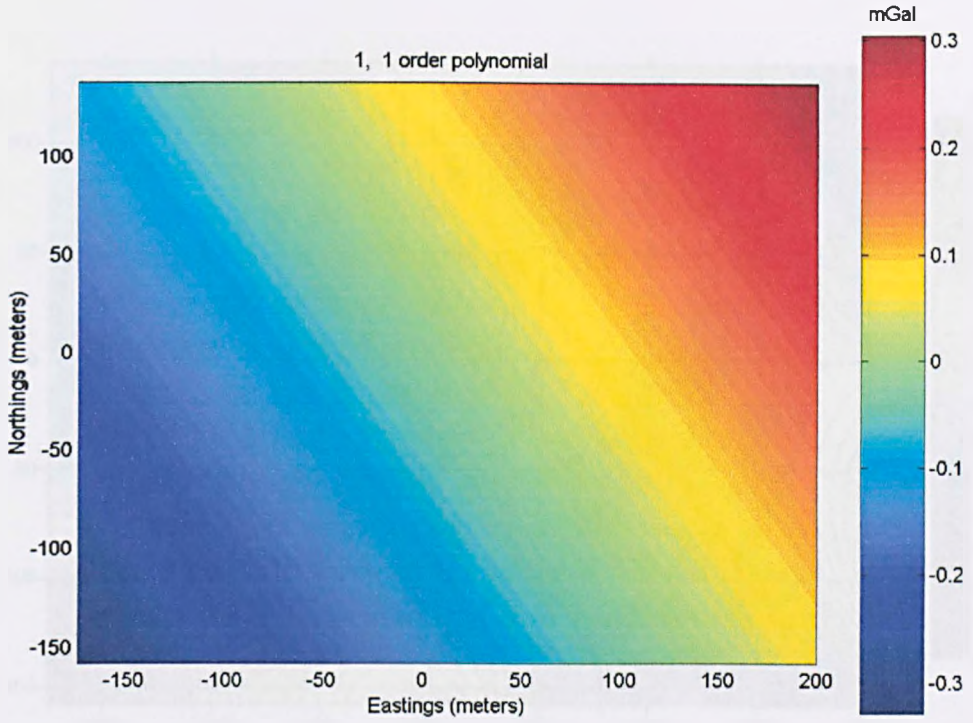


*Fig. 3.16 Example of 1st order polynomial that has been fitted to the reduced gravity data in Figure 3.15 (taken from Preesall Brine well 64, acquired in 2000).*

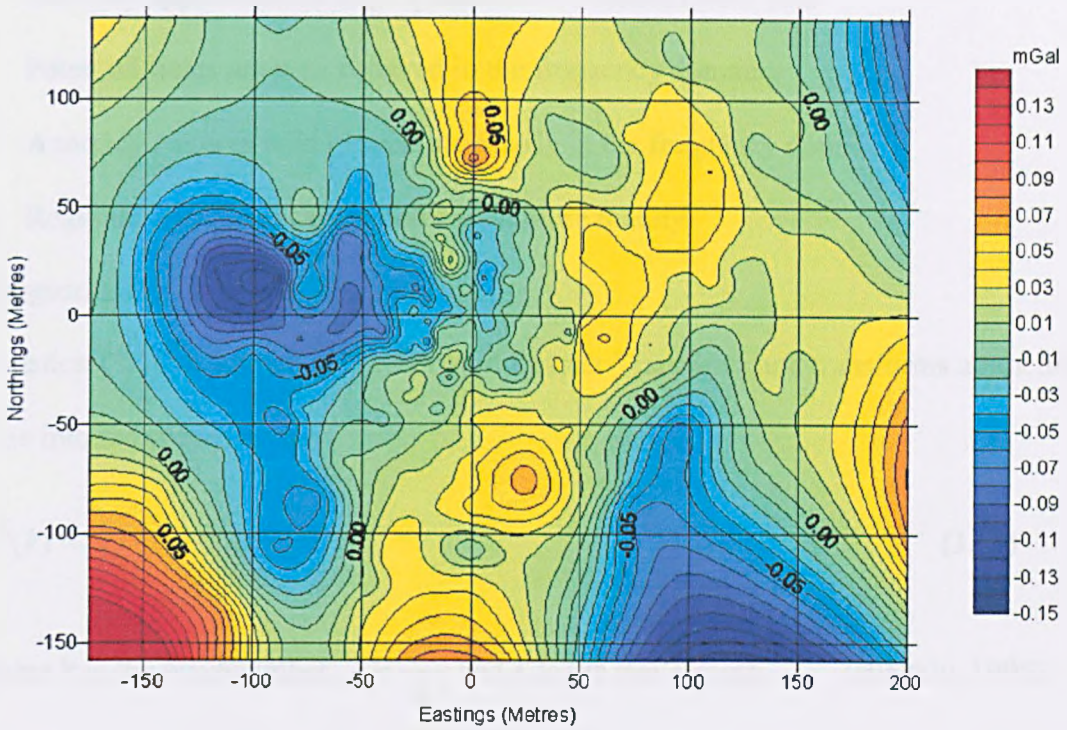


*Fig. 3.17 Example of a residual gravity anomaly. The 1st order polynomial has been removed from the Bouguer anomaly, effectively removing the effect of regional geology (taken from Preesall Brine well 64, acquired in 2000).*

### 3.14.2 Fourier analysis

Fourier analysis is a mathematical procedure by which a signal or continuous function is separated into its individual frequency components. These are sine-waves which are multiples of a fundamental frequency and have amplitude and phase coefficients. This technique is of particular use in the analysis of gravity data as the frequency domain offers some distinct operational advantages over the space domain.

These include

1. The easy application to large quantities of Potential field data
2. Potential fields are well behaved in the frequency domain
3. Anomaly patterns tend to separate clearly in the frequency domain
4. Regional separation can be automated more readily

(Ferguson, 1992).

Equation (3.18) is known as the Forward Fourier Transform and transforms a function of time into the space domain

$$F(k) = \int_{-\infty}^{\infty} f(x) e^{-ikx} dx \qquad (3.18)$$

where k is the wavenumber, $k = \frac{2\pi}{\lambda}$ and λ is the wavelength. (Blakely, 1996).

The reverse process can be achieved in a similar manner and is known as the Inverse Fourier Transform.

$$f(x) = \frac{1}{2\pi} \int_{-\infty}^{\infty} F(k) e^{ikx} dk \,. \qquad (3.19)$$

Both of these exist if f(x) satisfies inequality

$$\int_{-\infty}^{\infty} |f(x)| dx < \infty, \qquad (3.20)$$

that is if f(x) does not repeat itself over a finite segment of the x axis (Blakely, 1996).

The Fourier transform can be extended easily to functions of two variables. The Fourier transform of f(x,y) and its inverse Fourier transform are given by,

$$F(k_x, k_y) = \int_{-\infty}^{\infty} \int_{-\infty}^{\infty} f(x, y) e^{-i(k_x + k_y y)} dx dy, \qquad (3.21)$$

$$f(x, y) = \frac{1}{4\pi^2} \int\int F(k_x, k_y) e^{i(k_x + k_y y)} dk_x dk_y \,, \qquad (3.22)$$

where $k_x$ and $k_y$ are inversely related to wavelengths in the x and y directions, respectively: $k_x=2\pi/\lambda_x$ and $k_y=2\pi/\lambda_y$ (Blakely, 1996).

### 3.14.3 Continuation

Upward continuation is a mathematical method used to calculate the gravitational signal of a buried object if it had been measured at a higher or lower plane than it was originally.

Upward continuation uses the convolution theorem which states that the Fourier transform of the convolution of two functions is equal to the product of the transforms of the individual functions. This means that the result obtained by the convolution of any two functions can be calculated by taking the Fourier transform of each function, multiplying their relative transforms, and calculating the Fourier transform of this product (Ferguson, 1992).

The Earth's gravitational filed U can be shown to satisfy Laplaces equation in space which is given by

$$\frac{\partial^2 U}{\partial x^2}+\frac{\partial^2 U}{\partial y^2}+\frac{\partial^2 U}{\partial z^2}=0 \qquad (3.23)$$

Solutions of this can be obtained by separation of the variables and solving to show that a Potential field has the general form

$$g(x)=\sum_{k=1}^{\infty} A_k e^{ikx}\cdot e^{\pm kz} \qquad (3.24)$$

If the Potential field is calculated for height zero then

$$g(x)_{z=0}=\sum_{k=1}^{\infty} A_k e^{ikx}\cdot e^{\pm k0} \qquad (3.25)$$

which is equal to

$$g(x)_{z=0} = \sum_{k=1}^{\infty} A_k e^{ikx} \cdot 1 . \quad (3.26)$$

At any other height dz the following applies

$$g(x)_{z=dz} = \sum_{k=1}^{\infty} A_k e^{ikx} \cdot e^{\pm kdz} \quad (3.27)$$

which can be rearranged to give

$$g(x)_{z=dz} = g(x)_{z=o} \cdot e^{\pm kdz} \quad (3.28)$$

These calculations are readily performed using Fourier Techniques. The field is transformed into the wavenumber domain, then each Fourier coefficient is multiplied by

1. $e^{-kdz}$ for Upward continuation
2. $e^{kdz}$ for Downward continuation

before being inverted back to the spatial domain (Ferguson, 1992).

In this way the process of upward continuation, i.e. projecting the observed signal to a higher elevation can be used as an effective low pass filter. In this way high frequency noise associated with shallower near surface sources can be eliminated leaving the low frequency signal associated with deeper seated sources. This method of filtering can be more successful than a conventional low pass filter as it uses Laplace's equations rather than forcing the gravity signal to obey a different arbitrary set of laws which might be the case for a standard filter such as a Butterworth filter.

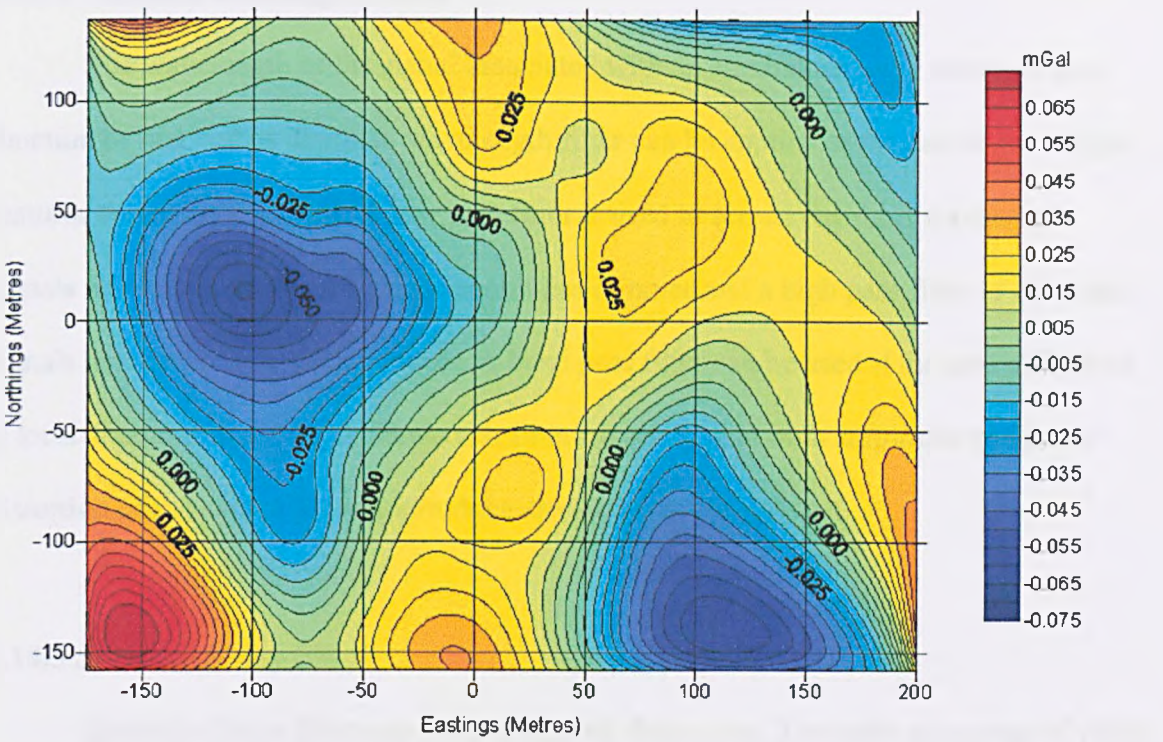


*Fig. 3.18 Example of Upward continued gravity data. The residual anomaly shown in Figure 3.17 has been upward continued by 15m. Note the smoothing of the anomaly (Taken from Preesall Brine well 64, acquired in 2000).*

Downward continuation is the opposite of this and effectively converts the observed gravity signal to what it would be if it had been acquired at a level close to the position of the sources. This can be an effective method in which to establish the depth of the source as once the continuation is projected to a depth greater than the major source the continuation begins to show extreme fluctuations as Laplace's equation is violated. In this way a good estimate of the depth of the source can be achieved. However, any noise sources, which are often of high frequency, are also amplified and this should be used with caution.

### 3.14.4 Matched wavelength filters

The wavelength of the signal associated with an anomalous body increases as a function of that bodies depth. A wavelength filter can be applied to the data to investigate features at particular depths. A low pass filter is used to screen out short wavelength signals associated with near surface anomalies or noise and a high pass filter to eliminate signals associated with deep features. A band pass filter can be used if the area of interest is located at mid-range depth. However, filtering can lead to both amplitude and phase distortion of the anomalies and introduce artefacts into the data set.

### 3.14.5 Savitzky-Golay filters

Savitzky-Golay filters are used to smooth data series. The main advantage of using a Savitzky-Golay filter over a moving average filter, is the smoothing of peaks defined by only a few points without loss of amplitude, broadening or change in slope (ADInstruments, 2002).

The filter performs polynomial least squares fitting inside a moving window. The higher the order of the polynomial the lower the degree of smoothing. The order of polynomial (p) must not exceed the frame size (f) and if the condition p=f-1 is met, no smoothing will occur.

## 3.15 Modelling and interpretation of gravity anomalies

### 3.15.1 Gravity modelling

Usually, the main objective of a gravity survey is to identify and delineate sub-surface density contrasts. In order to achieve this we need to use the key characteristics, gradient, wavelength, amplitude and position of the anomaly to assess the causative body's

size and location. There are four main interpretation techniques that can be used to achieve this goal.

### 3.15.2 Depth estimates

Euler Deconvolution is a method for locating the sources of potential fields based on both their amplitudes and gradients and an estimate of the probable geometry of the causative body (Thompson, 1982). The technique is based upon Euler's homogeneity relationship and differs from similar techniques in that no basic geological model is assumed. Euler Deconvolution can be applied and interpreted even when other modelling software cannot properly represent the geology. The technique is very appropriate for use in microgravity surveys where high-quality, closely spaced data are available. Successful interpretation of the results given by Euler deconvolution is partially dependent upon the interpreter's intuitive understanding the ambiguity associated with gravity interpretation and also partially dependent upon experience with model studies. Geological knowledge of the area may be required to choose between one or more clusters of solutions.

Potential fields such as gravity, magnetism and their spatial derivatives are said to be homogeneous of degree n as they satisfy Euler's equation (Blakely, 1996).

$$(x-x_0)\delta V/\delta x + (y-y_0)\delta V/\delta y + (z-z_0)\delta V/\delta z = -nV \qquad (3.29)$$

The derivative of the continuous field $V$ satisfies the above homogeneous equation of degree $n$ where $n$ is known as the structural index. This is an indicator of the fall off rate of the field with distance $r$ and depends on the geometry of the suspected body e.g. line, point, sphere or any combination of them and the particular potential field type. Hence, from a field which is measured at point $(x,y,z)$, the gradients in these directions can either

be measured or calculated. Knowing the values *(x,y,z)* and their derivatives at more than four points, and an estimate of *n*, the location of the causative body, ( $x_0$ $y_0, z_0$) can be solved by a least squares matrix inversion.

With gravity as the value for V a profile can be extracted from the grided data and the y-co-ordinate set to zero. The unknown factors are co-ordinates $x_0, z_0$ representing the distance along the profile and the depth of the point source. The predicted type of source is represented by *n*, the structural index.

Applying a window to three or more total field values and solving the derivatives will solve the unknowns $x_0, z_0$ and *n* exactly. Moving this window across the data obtains many solutions to the variables $x_0, z_0$. The solutions are plotted if acceptance criteria are met (usually if they are below a certain error value), showing the depth of the causative body together with its position along the profile. Only those locations that cluster as solutions from several window positions are considered significant.

However, it is best not to apply equation (3.29) directly to the data, as most anomalies require high structural indices whereas the lower structural indices provide better depth estimates (Thompson, 1982). Geological knowledge and experience of the area is used to estimate a structural index that best suits the situation and depth solution.

A second problem is that, with real data, anomalies are infrequently represented by point sources. This problem is overcome by using a large sample window of 4 or more data points. This produces many solutions to the variables from which the interpreter can identify the most realistic solution. Ravat (1996) describes how as the sample window increases in length, the relative variation in n decreases. and the solutions calculated from larger windows are less scattered. Therefore, a larger window tends towards a more confident depth estimate, although as pointed out by Reid et al. (1990), there is a trade off between window size and inclusions of effects from neighbouring anomalies.

It is known from potential theory that there is no unique inverse solution to the gravity problem. Therefore, the representation of anomalous gravity field as being due to a sub-surface distribution of simple density models is not unique. Euler deconvolution does not attempt to construct models of sub-surface density contrasts. It only helps the interpreter to construct these models by presenting a series of possibilities. The greatest strength of Euler deconvolution is that it is capable of resolving, and sometimes identifying, a wide variety of geological possibilities (Thompson, 1982).

Upward continuation (section 3.14.3) can also aid the interpretation of source depth by providing a clearer solution. Ravat (1996) suggests that if one can upward continue data to an elevation sufficiently high, the method will always yield accurate centroid locations. However, this approach depends greatly on the signal to noise ratio being high enough.

Filtering in the form of upward continuation, wavelength or polynomial filtering will generally improve the quality of the depth estimate by removing the high frequency noise from the data set. As the Euler method is dependent on gradients, it is highly sensitive to high frequency noise or jumps in the data. Rapid changes in gradient will lead to the incorrect sighting of solutions.

When considering the error incorporated within the Euler depth estimate Ravat's (1996) Figures and computations show that, in the average sense, most of the error is mapped into the depth error. This is because the gravity signal has much greater sampling in the horizontal plane. This results in errors in the horizontal plane being cancelled out in the process of averaging. Because the vertical plane cannot be sampled (unless borehole gravity measurements are made), this process does not occur in the vertical plane. Ravat (1996) also states that the physical error in location increases with source-to-observation distance. In environmental work, where source-to-observation distances tend to be small, this error is well within acceptable limits.

### 3.15.3 2.5D Modelling

Using the gravity-modelling computer program, GRAVMAG it is possible to model the probable cause of the gravity anomaly. GRAVMAG is a package developed by the British Geological Society to model gravity and magnetic anomalies based on the method of Talwani and Ewing (1960). The sub-surface volume of any shape created by the user is subdivided into horizontal polygons of equal depth increments. Taking the surface integral of each polygon gives the gravity per unit thickness of that polygon. Integrating the polygons with depth gives the total surface gravity at any surface point (Speed, 1970). In this way the user can build a series of polygons to match the original gravity anomaly by trial and error. As well as the size and depth of the polygons the user can define the density, density contrast and half strike of the body. The interpreter must use their understanding of the geological situation to produce the most plausible solution. Additional information such as logged boreholes can greatly improve the validity of the interpretation.

### 3.15.4 Thickness estimates

The third modelling technique used gives an estimate of the thickness of the causative body by inverting the gravity data using the method of Cordell and Henderson (1968). The program iteratively calculates the thickness of the causative body using the Bouguer slab equation by minimising the misfit between the calculated and observed anomalies. As with most iterative processes a three step procedure is implemented. The steps are as follows where the subscript (j) indicates the level of iteration and the superscript (k) denotes the number of iteration.

1. The field $g_j^{(k)}$ is calculated at each observation point due to all the blocks, assuming thickness from the previous iteration.
2. The residual $g_j - g_j^{(k)}$ is found at each observation point.
3. The infinite-slab approximation is used again to estimate a new set of thicknesses. The correction to each block is calculated using the ratio

$$\frac{t_j^{(k+1)}}{t_j^{(k)}} = \frac{g_i}{g_j^{(k)}}. \tag{3.30}$$

The data is interpolated onto a rectangular grid so that the sources can be investigated on three dimensions. The sources are modelled as a bundle of rectangular blocks, one per gravity value. Block thickness $t_j$, j=1,2...,N, is defined relative to a reference surface, e.g. the top or bottom of the blocks. (Blakely, 1996). This depth horizon to which the solution is pinned must be assigned, and the density contrast between the causative body and the host rock are assigned from other information such as borehole data.

### 3.15.5 Estimation of total anomalous mass

It is possible to estimate the missing mass that is associated with the presence of sub-surface voids. This is a particularly useful tool as it enables the total mass of material needed to remediate the sub-surface voids to be calculated.

Gauss's Theorem shows that,

$$M = \frac{1}{4\pi G} \int_s \int g_n \partial s \tag{3.31}$$

where; M is the total mass producing the anomaly; G is the Universal gravitational Constant; $g_n$ is the gravity component normal to surface which encloses the anomalous mass.

However, it is not possible to integrate over the whole enclosing surface. Instead only the upper hemisphere is used and the integral of gravity values on the Earth's surface becomes.

$$M = \frac{1}{2\pi G} \int_s \int g_n \partial s \tag{3.32}$$

To calculate the missing mass, the volume of the gravity anomaly associated with the void needs to be estimated. The anomaly map is digitised and divided into a series of cells. An average anomaly value is assigned to each cell. Summing the cell area multiplied by the average value gives the total anomaly value. Substituting numerical values into equation 3.32 gives the anomalous mass.

$$M = 23.9 \int_s \int g_n \partial s \tag{3.33}$$

Where M is in tonnes, $g_n$ is in mGal and s is in square metres. For the total mass of the anomalous body must be multiplied by the density factor, $p_a /(p_a - p_c)$. Where $p_a$ is the density of the anomalous material and $p_C$ is the density of the country or surrounding rock.

The result obtained is usually an underestimate of the actual value because of the problem associated with deciding where the anomaly merges into the background.

# Chapter 4

# Field Trials at Preesall Brine Field

## 4.1 Introduction

Preesall Brine field is located on the east bank of the River Wyre immediately south of Knott-End-on-Sea and directly opposite the fishing town of Fleetwood (Figure 4.1a and 4.1b). Preesall was originally the main focus of this research as it presented an opportunity to field test time-lapse microgravity surveys. As a result of its geology and long history of salt mining it posses the unusual attribute of unstable cavities whose dimensions were being monitored yearly by ICI. The presence of this monitoring system enabled the trial of the time-lapse microgravity technique in an environment in which it was possible to quality control the results obtained.

Primarily, it was hoped that it would be possible to tally the dimension and depth of the body responsible for the expected gravity anomaly with the figures already available from the yearly dipping and hooking observations by ICI.

Secondly, it was hoped to assess the accuracy of repeated microgravity surveys in field conditions by using the monitoring system already in place to check the results of the time-lapse surveys and to conclude whether time-lapse microgravity was a feasible tool for the monitoring of sub-surface mass movements.

It was also expected that the acquisition of microgravity surveys would add to and improve the information available on the current position and stability of the cavities monitored.

This chapter outlines the geology and history of the Preesall Brine Field before detailing the methodology and results of the time-lapse microgravity survey carried out between July 2000 and August 2002.


*Fig. 4.1a. Preesall Brine field is located in the NW of Lancashire on the Fylde coast. The brine field itself is situated between the village of Preesall and the River Wyre.*

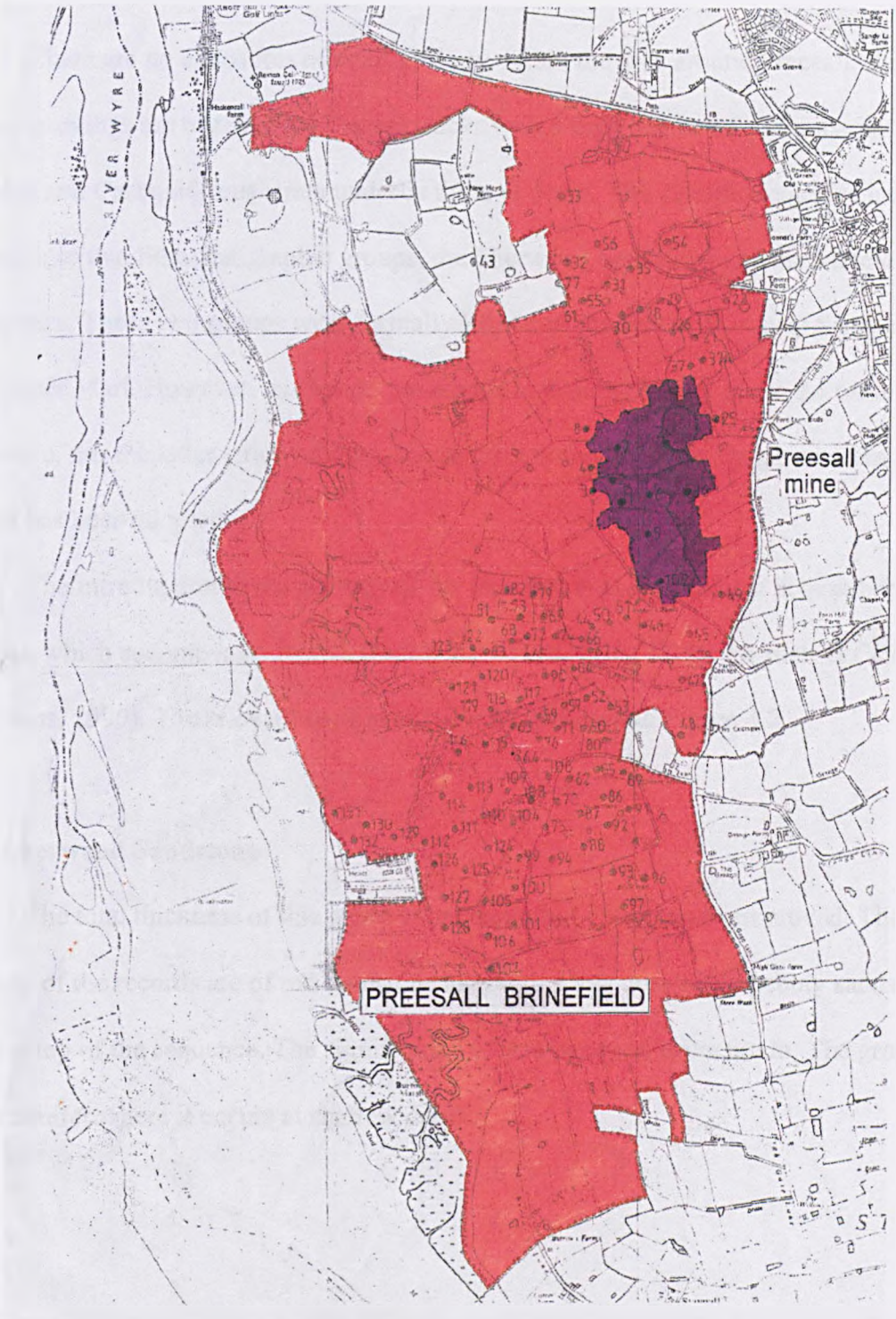


*Fig. 4.1b Map of Preesall brine Field. The orange area shows the extent of the extent of the area mined by solution. The Purple area shows the position of the original dry mine and the location of the brinewells and collapses*

## 4.2 The geology of Preesall

There are no exposures of solid geology within the area around Preesall. Sub-surface provings are restricted to Triassic rocks with a high degree of certainty that Permian and Carboniferous strata underlie these at depth. The Triassic sequence can be divided into two lithostratigraphic groups, the Sherwood Sandstone and the Mercia Mudstones. These two groups were formally known as the Bunter (Keuper) Sandstone and the Keuper Marl. However, as they do not equate in time with units given the same name elsewhere, nor the latter strictly a marl, the modern non-chronostratigraphic naming system has been adopted.

The introduction to the geology of the area that is presented here is based on the memoir, which accompanies British Geological Survey sheet 66 for the district (Wilson and Evans, 1990). The relevant section of sheet 66 is shown in Figure 4.2.

### 4.2.1 Sherwood Sandstone

The total thickness of this group is uncertain but 150m has been proved. The majority of the records are of red sandstone although a few note white pebbly sandstones near the top of the sequence. The significance of this variation is uncertain. The group is a major aquifer where it occurs at shallow depth.

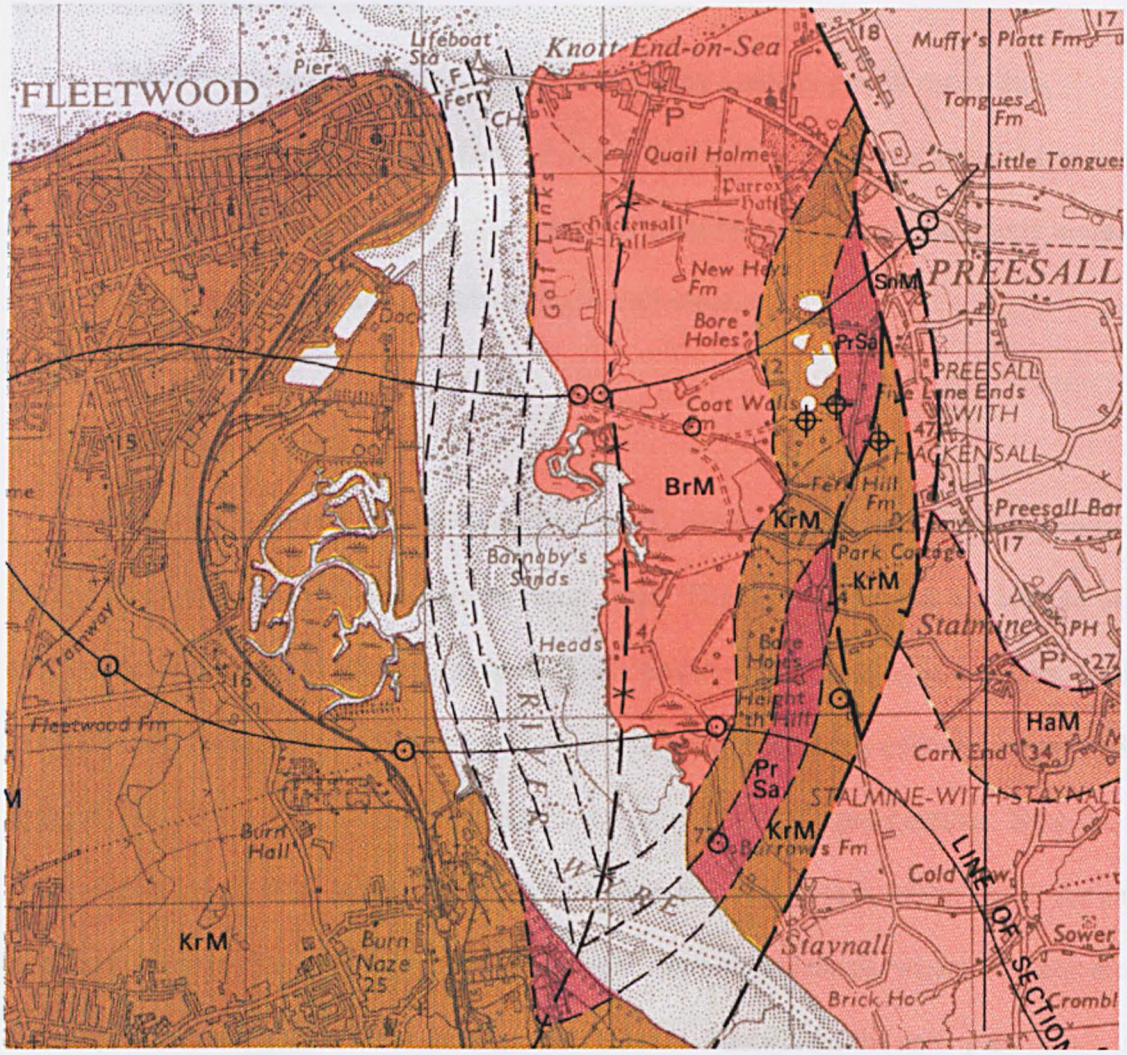


*Figure 4.2a Extract from the solid geology of the Blackpool area, sheet 66 (Wilson and Evans, 1990).*

### 4.2.2 Mercia Mudstones

The boreholes drilled as part of the exploration and production of the Preesall saltfield provide much of the data for this group. Their results have enabled the sequence to be subdivided.

#### 4.2.2.1 Hambleton Mudstones

These comprise of 20-35m of dominantly grey mudstone with many thin, intercalated siltstone bands particularly in their lower part. A persistent breccia lies near the base of the sequence. Above it mudcracks, current ripples, cross laminations, mud-flake conglomerates and salt pseudomorphs are all common.

#### 4.2.2.2 Singleton Mudstones

These comprise of 137-310m of dominantly red-brown, structureless or poorly bedded mudstones cut by ubiquitous gypsum veins. The thicker sections are located in the NW of the area. Shallow water indicators can be found where bedding is apparent. In the NW, thin salt beds lie near the base of the formation and have been collectively termed the Rossall Salts. Elsewhere, they are generally represented by collapse breccias. Near the top of the formation another group of salts, the Mythop Salts is present. In the south, the salt is represented by crystal growth within mudstones. Towards the north, where the salts are thicker, records suggest that the salts are also cleaner. Eastwards, the salts pass into solution breccias, and other breccias throughout the formation suggest the presence of further salts towards the centre of the depositional basin.

#### 4.2.2.3 Kirkham Mudstones.

This name has been given to a distinctive sequence of alternatively red-brown and grey-green well-bedded mudstones with many thin (c. 10mm) intercalations of siltstone and dolomitic siltstone, which become less significant in the NW. A detailed and precise correlation can be applied as this pattern is remarkably persistent. Over much of the area a thick solution breccia has been recorded from recent boreholes, and around the mouth of the Wyre this passes into the Preesall Salt Formation which divides the Kirkham

Mudstones into two in this area. The lower part averages 110m, thinning towards the SE, and contains up to 12 grey-green mudstone units each separated by poorly bedded, red-brown mudstones. These commonly contain gypsum nodules.

Above the Preesall Salt the colour variations are again present for up to about 120m at Preesall. However, the grey-green bands are thinner and less common than they are in the lower part of the formation. Microplankton are abundant below the Preesall Salt and are also recorded above it. This suggests a marine influence at the time.

#### 4.2.2.4 Preesall Salt

The Preesall Salt is preserved in a deep syncline between Preesall and the River Wyre. At its thickest some 185m of the formation has been proved. The formation is predominantly halite with a few persistent and thin mudstone partings. Towards the south of the saltfield, the unit thins and the individual salt beds are increasingly split up by more and thicker bands of mudstones.

#### 4.2.2.5 Breckells Mudstones

The Breckells Mudstones are largely structureless and dominantly red in colour. They succeed the Kirkham Mudstones in the deepest parts of the syncline and reach a thickness of 200m. Gypsum nodules are common, as are halite crystals, which are recorded together with halite veins and one thick bed of rock salt. Heavy brecciation at the top of the sequence suggests the former presence of another major salt horizon. Most of the formation is thus Ladinian in age and the only part of the sequence that is 'Keuper' in the German usage.

## 4.3 "A-priori" data

### 4.3.1 History of Preesall salt field

There is a long history of salt mining attached to the Preesall area. Salt was dry-mined in the area and during the 19th Century, Preesall was at the forefront of research into the application of controlled brine pumping. As well as the successful and well-documented, extraction of salt, the area underwent numerous investigations for purposes other than salt exploration. The following section is a brief description of some of the investigations implemented in the Preesall area and is taken from Strata Surveys Ltd Data Study, report number 7015/56. Compiled for ICI. The location of the boreholes is shown in Figure 4.1b.

1860 – Royal Engineers sunk borehole No 18 in search of water. The entire section with the exception of drift consisted of Keuper Marl.

1872 – Area mapped with a view to explore for hematite iron ore similar to that in Furness. Rock salt was discovered in borehole 2, with signs of the deposit in 8 and 9. Borehole 19 drilled by Fleetwood estate company.

1875 – Rev. Daniels and Daniel Elletson Esq. Sunk a shaft around borehole 2, to prove original sections. Some brine was recorded but there is no record of quantities.

1876 – Borehole 17 was bored and encountered red sandstone at a depth of 45ft below surface. Bunter Sandstone was present to a depth of 564 ft, and the end of hole. An abundant supply of fresh water was present. Previous investigations show the sandstone continues approximately 8 miles east of No 17 at a NW-SE trending fault.

1870's – Borehole 20 (plus others) were sunk. Borehole 20 showed weak brine and thin layers of salt.

1885 – Dry mine shaft No 2 was deepened to 610ft by the Fleetwood Salt Company. The salt was proved to be 340ft thick in layers of good and inferior salt and marl.

1888 – Salt Union Ltd was floated, combining Messers Fowler and Company, Solicitors of Westminster, London, with the exception of the saltworks at Middlesborough. This increased salt prices by 100% and up to 300% was common for their quantities.

June 1886 – Fleetwood Salt Co. given monopoly of the whole known reserves in the area.

1889 – The price of salt haulage was agreed for the next 42 years as 4 pence per ton, plus 2 pence per ton for tipping loose salt into ships. Preparation of the Preesall site for brine pumping was begun. This included draining of part of the salt marsh. Completion of railway sidings plus salt pans and stoves on the Fleetwood bank of the Wyre.

September 1889 – Drilling commenced at Borehole 21.

December 1889 - Rock salt was struck at 261ft and immediately the hole filled with brine to the same level as that in shaft No 2, thus proving a connection. As the mineral rights to these two boreholes were not co-owned, the use of these two boreholes for the extraction of salt by brine pumping was not possible.

1890 – The Fleetwood Salt Co. was purchased by United Alkali Company Limited.

December 1890 – Borehole 23 proved rock salt at 174ft thick. No brine was present and no connection to another borehole was suspected. An inner tube was inserted. Fresh water was pumped down and forced to rise up the outer case as brine. The recovered brine was then forced down borehole 21 for further enrichment. After 3 weeks the brine found a passage at the rock head and ceased to rise in borehole 23. This was the first example of "controlled" or "forced" brine pumping.

1891 – Borehole No 23 Collapsed leaving a flooded cavity of one third of an acre in extent and 40ft deep. Exploration of shaft No 2 of the dry mine was started by tunnelling. The quality of rock salt was equal to the average in Cheshire. However, there were layers of high grade salt. Initially, the shaft was at a depth of 470ft and ran SW for 266 yards were the salt ran out. A northerly tunnel was then commenced and ran to the boundary of the Elleston property. The tunnels were then used to make brine. Boreholes No 36 and 37 were sunk to introduce fresh water.

1893 – United Alkali Co. develop a mine at Preesall due to the large land subsidence in the Cheshire field and the resultant legislation.

1904 – The lower level mine was opened at a depth of 900ft below surface.

1920 – Extraction of brine from wells in the proximity of the shaft were ceased and sealed off. To compensate, extra brine was recovered from Shaft 2. However, repair and re-lineament of the shaft rendered the shaft to narrow to accommodate. Shaft 5 was sunk

away to the eastern boundary but a connection was made to shaft 2. No 5 shaft was sealed off due to loss of water to shaft No 2. However, too much damage had already occurred to save the mine.

1926 – Imperial Chemical Industries (ICI) was formed by the amalgamation of Brunner Mond and Company, Nobel Industries and the British Dyestuffs Corporation. The Elletsons still owned the mineral rights to the north of Preesall Salt Field.

1930 – Closure of the dry mine due to water seepage. ICI finally took over United Alkali Company just before the closure of the mine.

1934 – Surface subsidence forming a reservoir of brine. Several further subsidences have occurred forming the flashes to the west of Five Lane End.

1968 – ICI purchase outright the Elletson and Bourne estates covering the northern portion of the salt fields.

### 4.3.2 Subsidence in the Preesall salt field

Preesall Salt Field has suffered subsidence related to the exploration of salt for over a century. The early exploitation of salt by dry mining and the pioneering work in the development of controlled brine extraction has left a legacy of dramatic subsidence events. Below are listed some of the major collapses that have occurred in the area. The depth of the resulting flashes were recorded by Co-ordinated Surveys Limited in 1996 and are taken from Strata Surveys Ltd. report No 7015/56. "Geological Assessment" which was compiled for ICI (Harwood and Johnson, 1996).

1901 – Collapse of Brine well (BW) 28 and 29 at Northfield. No details of the brine caverns are available. The maximum depth of the flash is 18.8m.

1923 – Collapse of BW 54 at Westfield. Again no details of the brine caverns are available. The maximum depth of the flash is 27.7m.

1930 – Dry mine inundated with water and abandoned. Collapse of BW 21 to the north of the mine site.

1934 – The area to the north of the mines, shaft pillar collapsed. The maximum subsidence in this area is 28m, which is very similar to the presumed maximum working height of the mine.

1965 – Subsidence of BW 48. This subsidence is small and located alongside Back Lane to the west of Ivy Cottage. The maximum depth of the flash is 4.1m.

1974 – Collapse of BW 52 and 53. Minimum roof depth for BW52 before collapse is 80.9m. The maximum depth of the flash is 90m below surface with an average depth of 65m.

1994 - Collapse of BW 88. Roof rose to a depth of 67.3m below surface before surface subsidence was evident. The maximum depth of the flash is not known at this time.

### 4.3.3. Hydrogeological assessment of Preesall salt field

In order to assess the long-term stability of the Preesall Salt Field it is necessary to investigation the hydrogeology of the area. The main risk to the area is the continued dissolution of the salt deposits. For water to dissolve the salt there must be a source of water, inlets and outlets from the salt deposit as well as a path from the inlet to the outlet. A head to drive the flow must also be present. In 1997 Steventon and Dottridge of the Hydrogeology Group, University College London compiled a document reporting on the hydrogeology of the Preesall Salt deposits. This section summarises their findings.

Salt is considered impermeable as its crystalline structure is non-porous and its plasticity prevents fractures from remaining, however, it is soluble. Johnson (1981) identified four requirements for salt dissolution.

1. a deposit of salt
2. a supply of water unsaturated with respect to NaCl
3. an outlet for the removal of brine
4. energy to cause the water to flow through the system

In addressing these requirements, Steventon and Dottridge concluded that;

1. Salt is present at the site (Figure 4.2).
2. A number of routes may enable water to come in contact with the salt deposit.

These include:

- Water permeating through the boulder clay and collapsed Kirkham Mudstones above the wet rock head
- Water reaching the mine workings via the deep pits created by subsidence
- Water running down the Preesall Fault Zone to the salt deposits

- Unsaturated brine pumped into the mines via the well heads
- Water seeping down the boreholes

Approximately 75m³/day (27 000m³/ year) of water could be entering the salt by permeating through the boulder clay. 450mm of rain per year is available through ground water recharge of which 25 to 30mm per year will permeate through the boulder clay. The subsidence ponds are reported to contain water that is stratified, salty water being present at depth. This suggests that exchange of water is present between the ponds and the mine workings. Taking into account the surface area and the average rainfall and evaporation values, up to 32,500m² of fresh water could be coming into contact with the salt via the ponds.

3. No salt springs are known in the area so brine removal could be through three possible outlets.

- Removal of brine from the well head to keep the well at an approximate constant pressure. This practice is no longer continued
- Flow into the base of the ponds
- Flow into the estuary on the western limb of the syncline, providing head gradient and flow pathways exist

4. Only a small head gradient is present between the mean low water tide of the Wyre Estuary and the water level for fresh water inlet. However, there may be a greater

hydraulic pressure as the wells are maintained under a pressure head above ground level.

Steventon and Dottridge (1997) have identified that the Preesall Salt Field satisfies the criteria outlined by Johnson (1981). As a result of this the Preesall Salt Field is unlikely to stabilise and dissolution of the salt in and around the caverns will continue.

### 4.3.4 Risk assessment

In 1997 a risk assessment was carried out by Strata Surveys Ltd (Harwood and Johnson, 1996). This was stage 3 of a three-part investigation into the problem of cavity collapse in the Preesall salt field. The report identified that those cavities with a mudstone roof as being the cavities most likely to collapse and thus were labelled high risk. This is thought to be a similar situation to that which Wassman (1980) found at Hengelo in the Netherlands. At Henglo, some cavities tended to collapse several years after pumping gas ceased. In addition, brecciation had taken place in the overlying red beds of Bunter age. This claystone or mudstone loses its strength when wetted. Unfortunately, brine from the cavities in the underground salt permeates into the mudstone, rising as a result of capillary action. Eventually, this weakened material collapses into the cavity. Void migration then takes place and, depending on the bulking factor of the rocks involved, the void may move into the overlying clays. Pronounced subsidence occurs when this happens.

The hooking and dipping data collected by ICI at Preesall supports this, showing that the roof of BW88 was well above the top interface of salt and well into the mudstone. Hooking and dipping is a simple but effective way in which to assess the position of the cavity. A weight suspended from wire and attached to a drum driven by a motor is lowered down the borehole. The depth to which it reaches before the tension is released from the

wire is recorded. This is presumed to be the base of the cavity. Before the weight is lowered into the borehole a second length of stiff wire is attached to the weight so that it protrudes horizontally when the wire is suspended for a length that is larger than the diameter of the borehole lining. This is the hook. As the weight is retrieved and the wire wound back onto the drum, it is down to the skill of the operator to judge at which point the hook catches on the tube. Although this seems somewhat arbitrary, with experience a high level of accuracy can be achieved. It must be noted that this does not give a direct indication of the position of the roof of the cavity. The hooking data merely indicates the extent of the borehole lining. It is assumed, however, that when a collapse occurs that this event will damage the lining sufficiently to cause a break. There is obviously a high degree of error attached to this and this value should only be used as a guide.

It is understood that those cavities that have a salt roof intact have a roof migration rate that is much reduced to the mudstone roof cavities and in many cases appear to be stable. As a result of this observation, it became practice to control the depth and to a certain extent the position of the cavern roof with a layer of pressurised air. This limited the growth of the cavern and prevented it from encroaching into the overlying mudstone. Thus the caverns that will have the highest roof propagation rate and thus pose the highest risk of collapse are the solution cavities that were developed early in the century before the introduction of compressed air "blankets".

Using these criteria, the hooking and dipping data for those cavities with mudstone roofs have been studied to identify those cavities with high percentage decreases in the depth of the cavity floor and the hooking of the borehole lining.

| Year | 1990 | 1991 | 1992 | 1993 | 1994 | 1995 | 1996 | 1997 | 1998 | 1999 | 2000 |
|---|---|---|---|---|---|---|---|---|---|---|---|
| **BW #** | **44** | **44** | **44** | **44** | **44** | **44** | **44** | **44** | **44** | **44** | **44** |
| Dipper | 187.3 | 187.2 | 187.6 | 187.5 | 186.4 | 186.4 | 186.6 | 186.5 | 186.6 | 186.6 | 186 |
| Hook | 118.9 | 118.7 | 118.9 | 118.6 | 118.6 | 118.6 | 129.8 | * | * | * | * |
| A/L | 118 | 117.4 | 117.4 | 116.7 | 116.7 | 110.3 | * | 109.7 | 109.5 | 109.1 | * |
| **BW #** | **50** | **50** | **50** | **50** | **50** | **50** | **50** | **50** | **50** | **50** | **50** |
| Dipper | 191.1 | 191.5 | 189.8 | 189.7 | 189.7 | 189.7 | 189 | 188.6 | 187.2 | 184.3 | 181 |
| Hook | 128.9 | 130 | 129.2 | 129.5 | 129.5 | 129.8 | * | * | 125.3 | 115.6 | 106 |
| A/L | 129.2 | 129.2 | 127.9 | 128.6 | 128.6 | 125.2 | * | 124.3 | 125.1 | 122.5 | 105.9 |
| **BW #** | **64** | **64** | **64** | **64** | **64** | **64** | **64** | **64** | **64** | **64** | **64** |
| Dipper | 155.8 | 153.9 | 153.5 | 150.8 | 148.3 | 145 | 142.8 | 138.9 | 136.5 | 133 | 125.5 |
| Hook | 113.8 | 113.8 | 113.6 | 113.6 | 114.1 | 113 | 107.8 | 107.8 | 107.9 | 108.5 | 107 |
| A/L | 110.4 | 109.9 | 109.9 | 109.9 | 109.9 | 109.9 | 109.9 | 105.8 | 105 | 100 | * |
| **BW #** | **97** | **97** | **97** | **97** | **97** | **97** | **97** | **97** | **97** | **97** | **97** |
| Dipper | 152.8 | 153.3 | 150.6 | 149.6 | 150 | 150 | 156 | 146.5 | 145.6 | 146.5 | 144.4 |
| Hook | 112.1 | 112.1 | 112.1 | 112.2 | 112.3 | 112.3 | 112.5 | 112.6 | 112.6 | 112 | 112.2 |
| A/L | 109.2 | 109.2 | 107.4 | 106.2 | 105.5 | 103.5 | * | 101.1 | 100.1 | 98.9 | 97.9 |

* - Brine well (BW) not surveyed.

*Table 4.1 showing the depth below surface in metres of the cavity roof and floor for the four Brine wells thought to produce the largest change in gravity. Data provided by ICI.*

Based on the surveys carried out over the last twenty years by ICI, brine wells 44, 50, 64 and 97 were identified as the cavities most likely to produce a change in gravity during the monitoring period.

## 4.4 Forward modelling of the gravity response

Before work began in Preesall it was important to establish what scale of anomaly was likely to be created by the cavities present within the Preesall Brine Field. This would give information vital to the planning stage of the survey. At this site the dimensions of the cavities are already known. With this information the design of the survey can be tailored in order to achieve an optimum balance between coverage and sample rate.

Figure 4.3 shows the gravity response for BW64 in 2000. The parameters used in this model are taken from the ICI report "Survey of Obsolete Wells 2000". The parameters are;

**Top** 100m (carried over from 1999 as no hooking was attained in 2000)

**Base** 125.5m

**Radius** 25m

$\Delta\rho$ -1.2 $Mg/m^3$

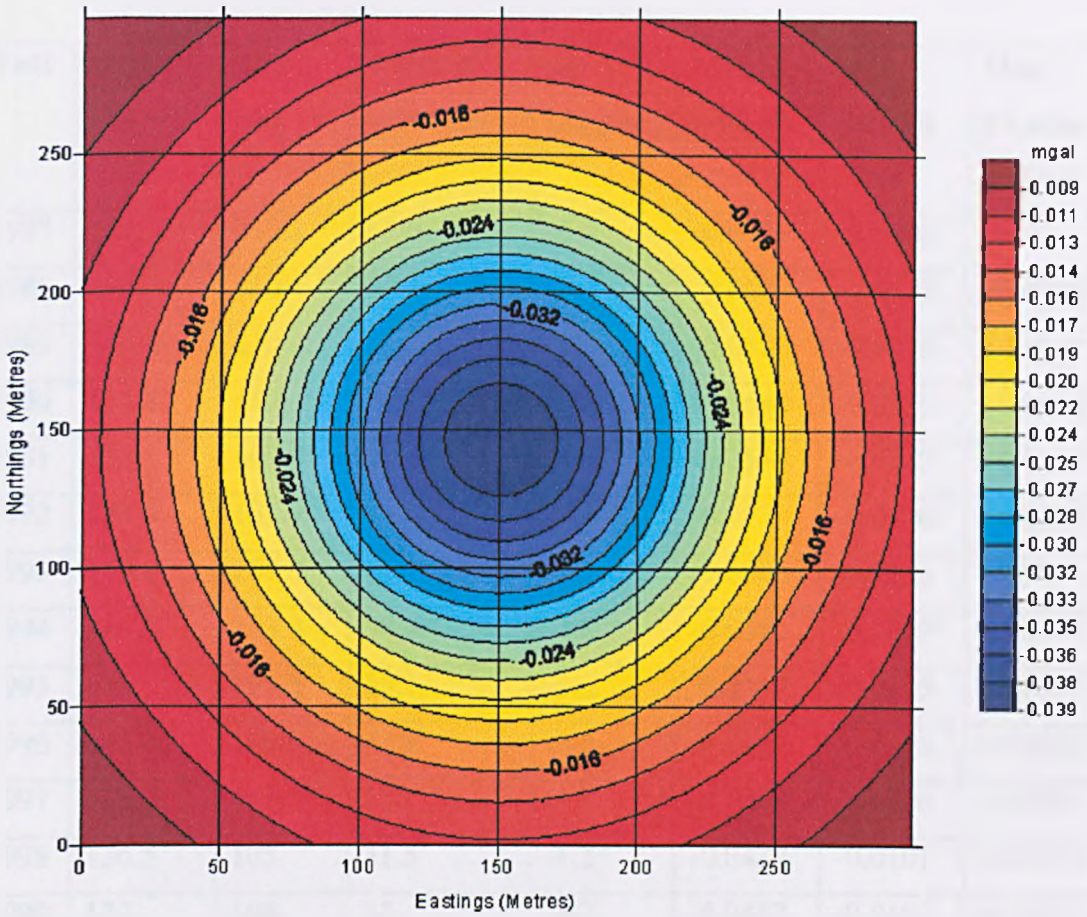


*Fig. 4.3 Forward model of the gravity response for Bw64 in 2000 Assuming a cylindrical shape.*

Figure 4.3 shows that the gravity anomaly for BW64 will tail off to an value below a microgravity threshold at a distance of 300m from the well head. It also shows that the maximum amplitude expected from the cavity associated with BW64 is 39µGal.

In an attempt to gauge how the gravity signal may vary over time, the gravity signal was calculated for BW64 for each of the last 13 years. This was achieved using the dipping and hooking data detailed the annual ICI report "Survey of Obsolete Wells".

Once the gravity signal is calculated for BW64 for each respective year the change in gravity for each step in time can be obtained. Table 4.2 summarises the findings.

| Year | Base (m) | Top (m) | Vertical extent (m) | $\Delta\rho$ ($Mg/m^3$) | Max (mGal) | Min (mGal) | Max Change (mGal) |
|---|---|---|---|---|---|---|---|
| 1987 | 165.9 | 110.3 | 55.6 | -1.2 | -0.0635 | -0.0190 | N/A |
| 1988 | 163 | 110.4 | 52.6 | -1.2 | -0.0609 | -0.0179 | +0.0026 |
| 1989 | 160.6 | 110.4 | 50.2 | -1.2 | -0.0588 | -0.0170 | +0.0021 |
| 1990 | 155.8 | 45.4 | 45.4 | -1.2 | -0.0544 | -0.0153 | +0.0044 |
| 1991 | 153.9 | 109.9 | 44 | -1.2 | -0.0534 | -0.0147 | +0.0010 |
| 1992 | 153.5 | 109.9 | 43.6 | -1.2 | -0.053 | -0.0146 | +0.0004 |
| 1993 | 150.8 | 109.9 | 40.9 | -1.2 | -0.0505 | -0.0136 | +0.0025 |
| 1994 | 148.3 | 109.9 | 38.4 | -1.2 | -0.048 | -0.0127 | +0.0025 |
| 1995 | 145 | 109.9 | 35.1 | -1.2 | -0.0447 | -0.0115 | +0.0033 |
| 1996 | 142.8 | 109.9 | 32.9 | -1.2 | -0.0424 | -0.0108 | +0.0023 |
| 1997 | 138.9 | 105.8 | 33.1 | -1.2 | -0.0450 | -0.0106 | -0.0026 |
| 1998 | 136.5 | 105 | 31.5 | -1.2 | -0.0437 | -0.0101 | +0.0013 |
| 1999 | 133 | 100 | 33 | -1.2 | -0.0487 | -0.0103 | -0.0050 |
| 2000 | 125.5 | 100* | 25.5 | -1.2 | -0.0395 | -0.0078 | +0.0092 |

*Table 4.2. Summary of the maximum gravity change for BW64 between 1987 and 2000. * Value carried over form 1999 as no hooking was obtained in 2000.*

A)

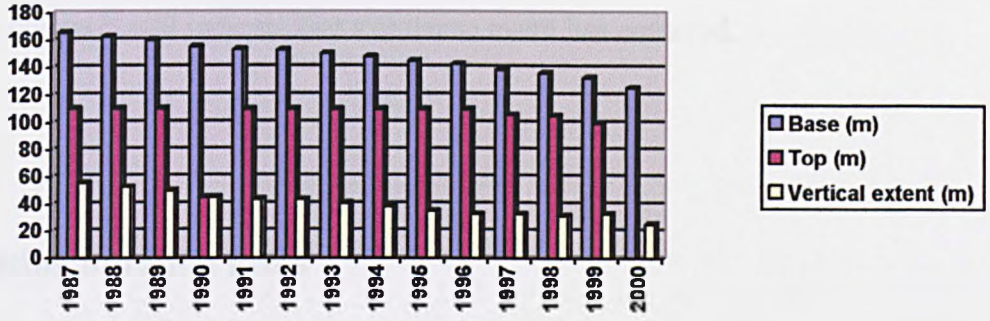


B)

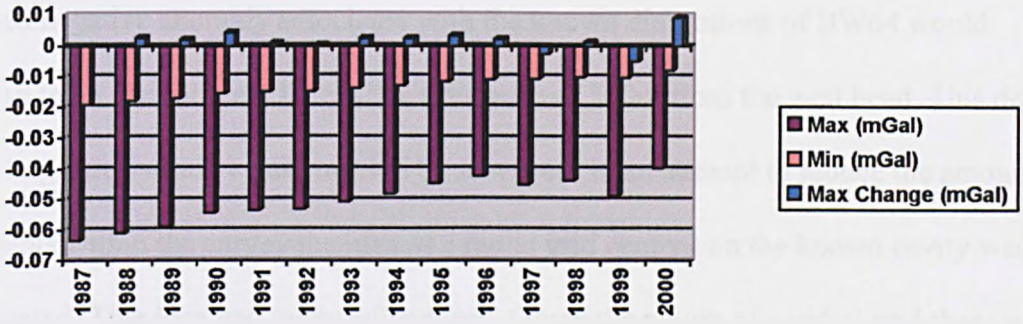


*Figure 4.4 Graphical representation of Table 4.2. A) Shows the variation in the cavities dimensions, base, top and vertical extent. B) is a plot of the associated gravity signal for the cavity.*

Figure 4.4 shows that the general trend for BW64 is that it is diminishing in size. The mechanism for this is a steady shallowing of the base. The maximum change in gravity is negligible and below the accuracy of a time lapse gravity survey. The general trend for the maximum change is that of a reduction in the maximum gravity signal. This is a result of the chamber size reducing as the base rises. There are two exceptions to this in 1997 and 1999 when there has been a rise in the top of the chamber of ~5m. This has resulted in an increase in the maximum negative anomaly.

In conclusion, this work outlines the fact that for an significant change in gravity signal to be detected in a three year monitoring period, a collapse event greater than

average will have to occur. In addition, any gravity change will be most apparent towards the centre of the known position of the cavity. Conversely, if a significant change in gravity occurs it will indicate that a collapse event has occurred.

## 4.5 Testing of radial grids

As discussed in the previous section, the design of the survey is vital to the successful acquisition of quality data. From the forward modelling it was apparent that the expected negative anomaly associated with the known dimensions of BW64 would diminish to an insignificant level after a distance of 300m from the well head. This defined a very large area which would need to be surveyed. In an attempt to reduce the amount of data points within the survey the idea of a radial grid centred on the known cavity was investigated. This idea had many advantages. Given the nature of a radial grid there is a concentration of data points at the centre, diminishing towards the edge of each limb. In this way a good coverage at the centre of the expected anomaly is achieved and a wider sample interval towards the edge of the expected anomaly occurs, up to and on to the background value. This is beneficial as demonstrated in the forward modelling, the maximum change in gravity signal is at or near the centre of the anomaly and little or no change should be detected on the limbs of the gravity anomaly, should a significant collapse occur. Consequently, with a radial grid the number of sampling points can be reduced within the survey as well as concentrating the data points around the key area of interest.

With this in mind a radial survey grid was designed. Since the expected change in gravity was predicted to be on the limit of resolution for a time-lapse gravity survey it was deemed necessary to over-sample the area around the centre of the known cavity. As the

change in gravity signal decreases with distance from the cavity centre, the station spacing was increased to reflect this, until the station at the end of each radial limb would be only present to sample the background reading due to local geology. Consequently, the radial grid was divided into three sections. The inner section samples the centre of the expected anomaly. It is this area that is expected to detect any change in gravity. The middle section samples the limbs of the expected gravity anomaly. The outer section is included to sample the background value of the local geology so that corrections can be made to remove trends in the gravity data caused by dipping strata.

In order to keep the laying out of the grid simple and avoid mistakes in the field, survey point spacings of 5m, 10m and 20m were chosen for the inner, middle and outer sections respectively with a 20 degree angle between each limb. Ideally, the length of the radial limbs would be 300m long in order to sample the entire anomaly. However, due to constraints imposed by the geography of the site, the maximum limb length was reduced to 200m. Consequently, the sections of each limb were divided up into inner 0-50m, middle 50-160m and outer 160 –200m domains.

Sampling the modelled gravity anomaly for 1997 tested the effectiveness of this grid system. The main concern was the effect that centring the grid away from the centre of the anomaly would have on the reconstruction of the anomaly. To answer this a Matlab routine was written, in which the sampling grid described above was laid over the 1997 anomaly at increasing offsets from the centre of the anomaly. From these discrete data points the anomaly was regrided and compared to the original anomaly. A random noise value of 15μGal has also been added to the model in order to simulate the conditions of an actual survey. This value is higher than what can actually be expected (~6μGal) but represents a worst case scenario.

With this it can be seen that the anomaly has been successfully restored even with the sampling grid at an offset of 45m from the centre of the original anomaly (Figure 4.4). At an offset of 65m (Figure 4.5), the anomaly is still distinguishable, although it has begun to loose its shape. This grid design was deemed to be satisfactory, as it was thought unlikely that a misalignment of the grid was unlikely to exceed 45m.

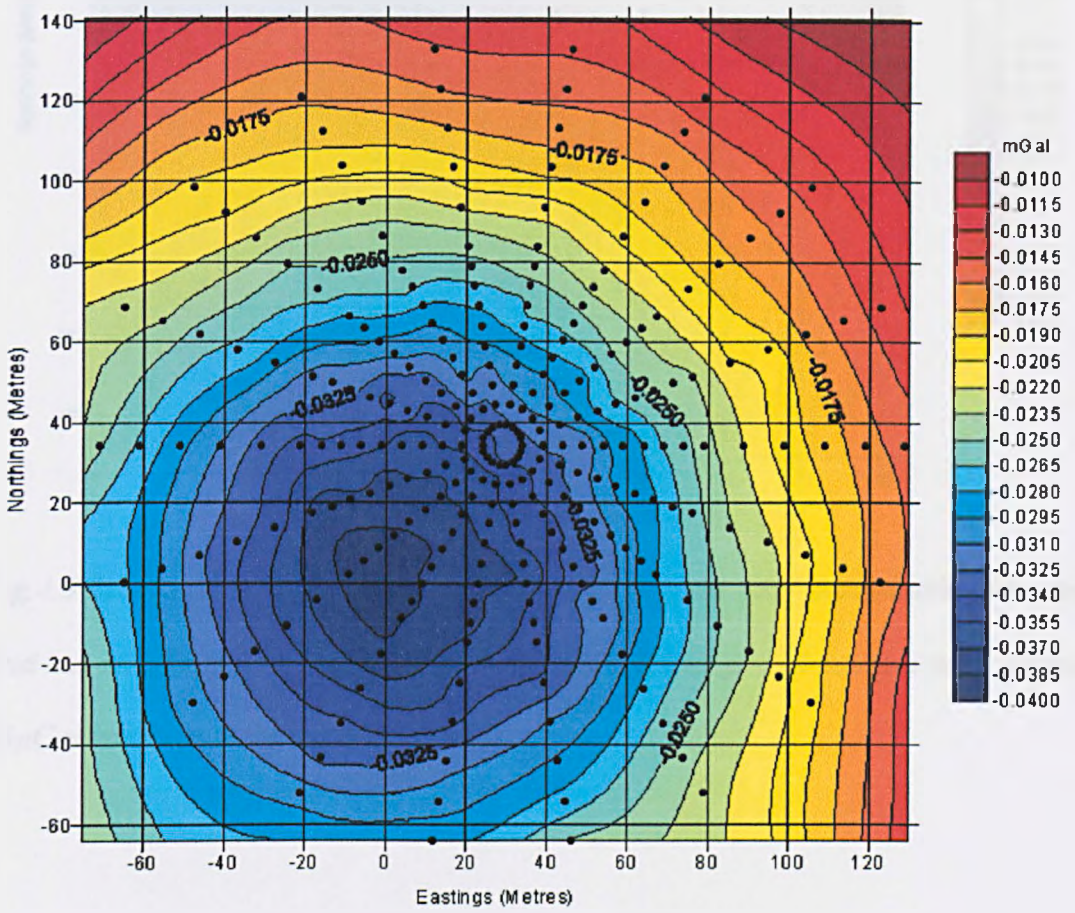


*Fig.4.4 Reconstruction of the expected anomaly using the 1997 parameters. The sampling grid has an offset of 45 ms form the centre of the original grid. A random noise element of 15μGal has been included in the model.*

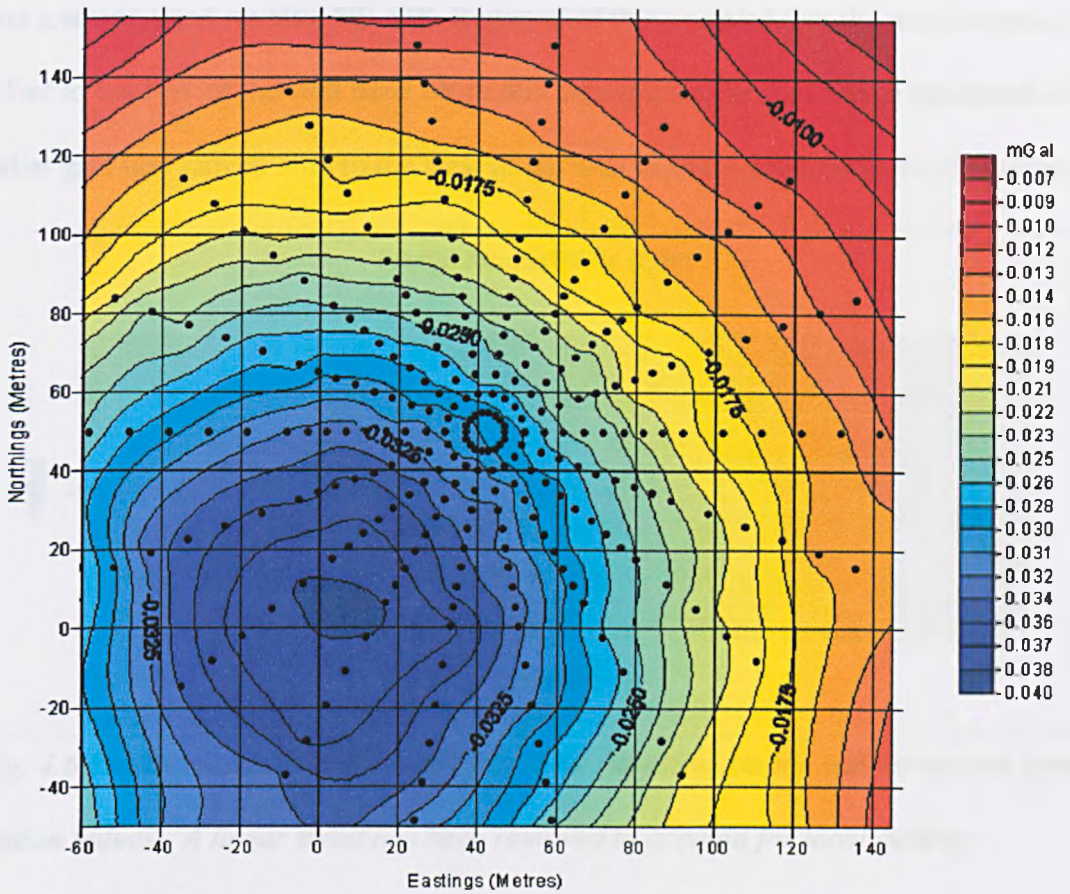


*Fig.4.5 Reconstruction of the expected anomaly using the 1997 parameters. The sampling grid has an offset of 65 m form the centre of the original grid. A random noise element of 15μGal has been included in the model.*

## 4.6 Acquisition of microgravity at brine well 64

### 4.6.1 Reconnaissance profiles

On the 27th of April 2000, two reconnaissance profiles were acquired across BW64. The objective of this was to ascertain that the gravity anomaly associated with BW64 was indeed detectable. The profiles were centred on the well head and were both 200m in length. They ran perpendicular to each other on bearings of 340°-160° and 70°-250°. The survey point spacing used was 10m. Reduction of the data showed that there

was a strong trend running NE-SW. Removal of this revealed that the main anomaly was offset to the NW of the well head. With this information the location of the centre of the radial grid was moved 30m to the west of the well head to compensate for this offset.

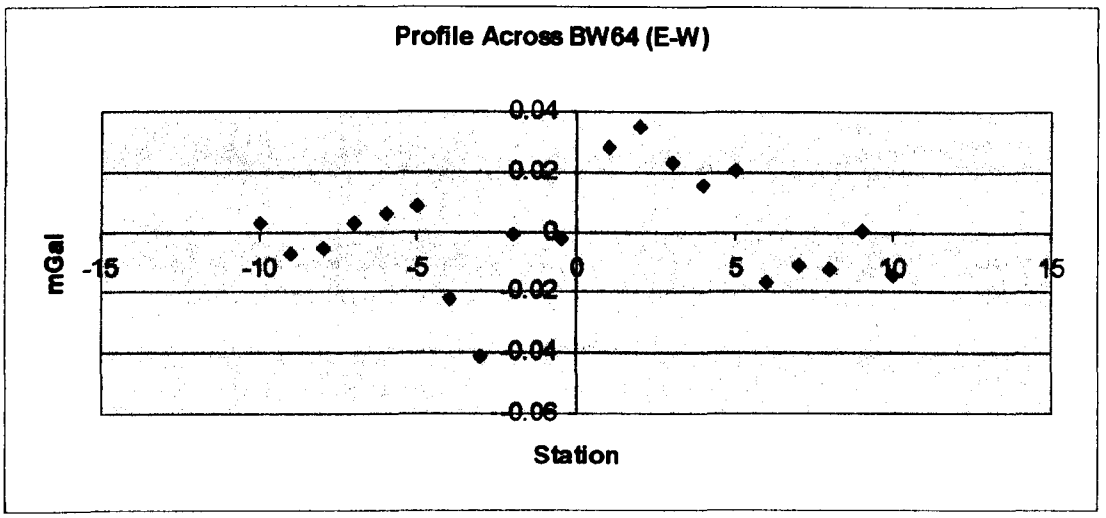


*Fig. 4.6 Profile running across Bw64 from east (negative station values) to west (positive station values). A linear trend has been removed to account for local geology.*

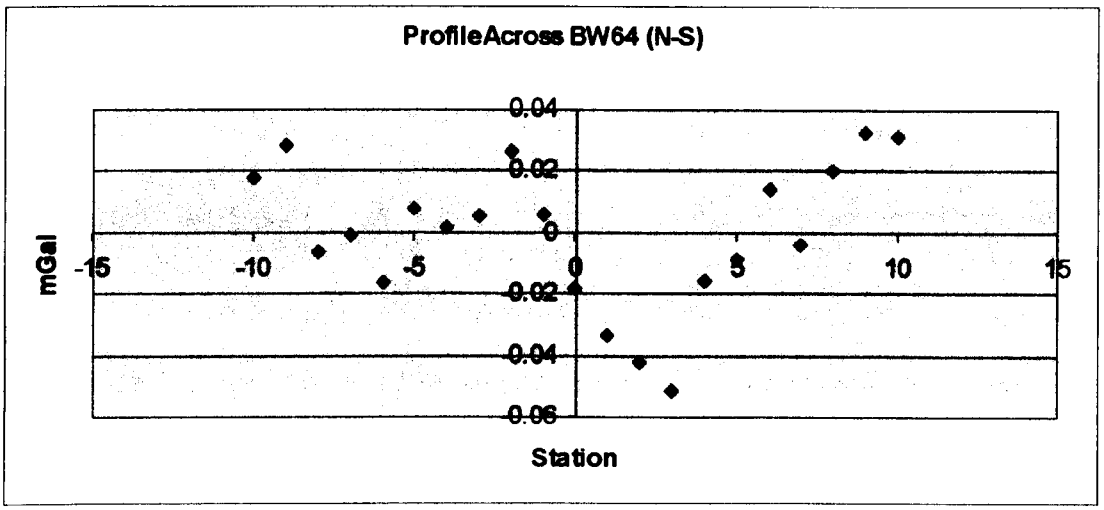


*Fig. 4.7 Profile running across Bw64 from north (negative station values) to south (positive station values). A linear trend has been removed to account for local geology.*

### 4.6.2 Acquisition on a radial grid

The grid described above was laid out in its entirety where local geography permitted. Its extent was contained within the two fields north of the track running west past Corcas Farm. A total station instrument was used to stake out the 50m, 100m, 150m and 200m stations at the correct angle after which the remaining stations were laid down using measuring tapes.

*Fig. 4.8 Looking north from BW88 towards BW64, Fleetwood can be seen in the background.*

Emphasis was put on marking the grid out in an accurate and repeatable manner as although it was intended to leave the grid staked out over the monitoring period, the areas outside of the compounds would have to be re-laid for future surveys. Ideally, each survey point would have been monumented (with a concrete base) so that gravity could be recorded on a firm and level surface. This was not possible , however, as the majority of Preesall Brine Field is agricultural and so disruption was to be kept to a minimum. Subsequently, the area within the compound was left staked out, but outside of the compound all markers were to be removed necessitating accurate reconstruction of the grid at a later date.

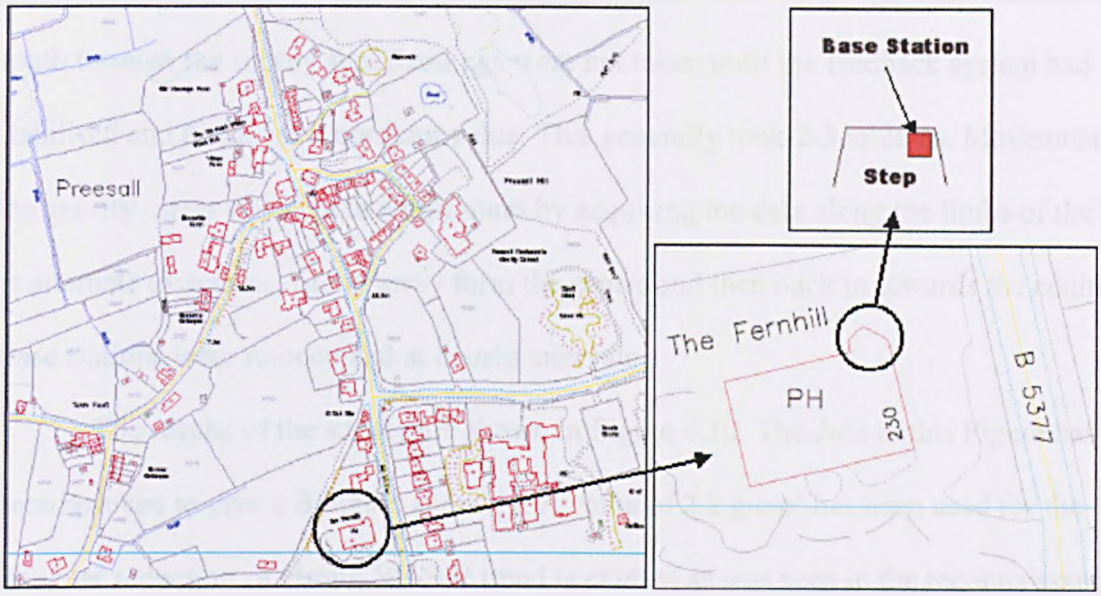




*Fig.4.9 Diagram detailing the position of the Fernhill base station. This base station is located away from the Brine Field and is used to correct for local changes in elevation and sub-surface mass at the local base stations (Grid Ref.: 336,696.72 447030.19).*

Since the intention was to use this site as a time-lapse monitoring site it was necessary to establish a base station on stable ground away from the area of investigation so all gravity readings were recorded relative to a constant datum. The base station was sited in Preesall Village at the rear of the Fernhill public house. This site was chosen as it is an obvious landmark and has a subsidence free history. The base station itself was sighted on a concrete step at the rear of the building (Figure 4.9).

Readings were taken at the beginning and end of each day. In this way the base stations located within the brine field are tied into this base station and so any changes in the local base stations due to subsidence or sub-surface mass change can be corrected.

The first survey across BW64 was acquired between the 20th and 24th of July 2000. A Lacoste and Romberg Model G meter with MVR feedback was used for the acquisition

(G-559). Local base stations were established on either side of the dyke that runs north south through the survey site. Readings were not taken until the feedback system had stabilised and displayed a constant value. This generally took 2-3 minutes. Movement of the gravity meter was kept to a minimum by acquiring the data along the limbs of the grid in alternate directions, firstly away form the centre and then back in towards the centre. Base stations were re-occupied at hourly intervals.

The results of the survey are shown in Figure 4.10. The data in this Figure have been reduced to give a Bouguer anomaly. A value of 2.2 g/cm$^3$ has been used for the Bouguer reduction. A strong NE-SW trend is evident as was seen in the reconnaissance profiles. This is a reflection of the fact that the brine field is located on the east limb of a syncline (see section 4.2).

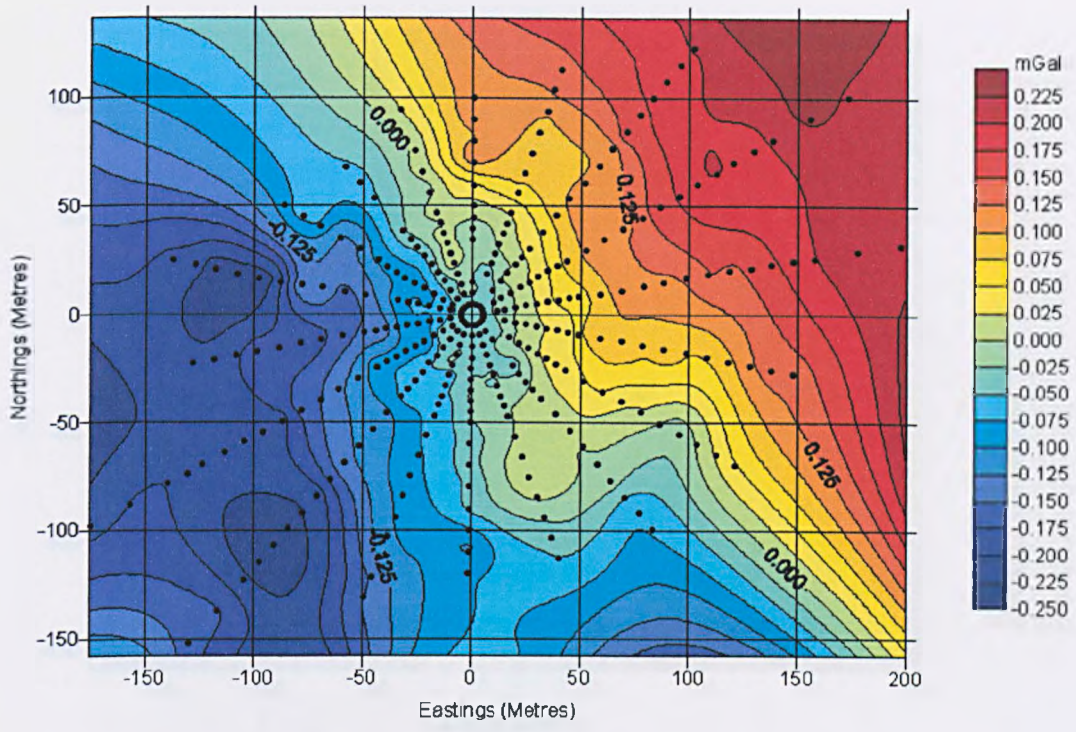


*Fig.4.10 Bouguer anomaly map for BW64. The local dipping strata cause a strong NE-SW trend.*

Removing this trend by fitting a 1st order polynomial surface (i.e. a plane) to the data produces a residual Bouguer anomaly map (Figure 4.11). The gravity lows become more apparent in this Figure as the strong regional trend has been corrected.

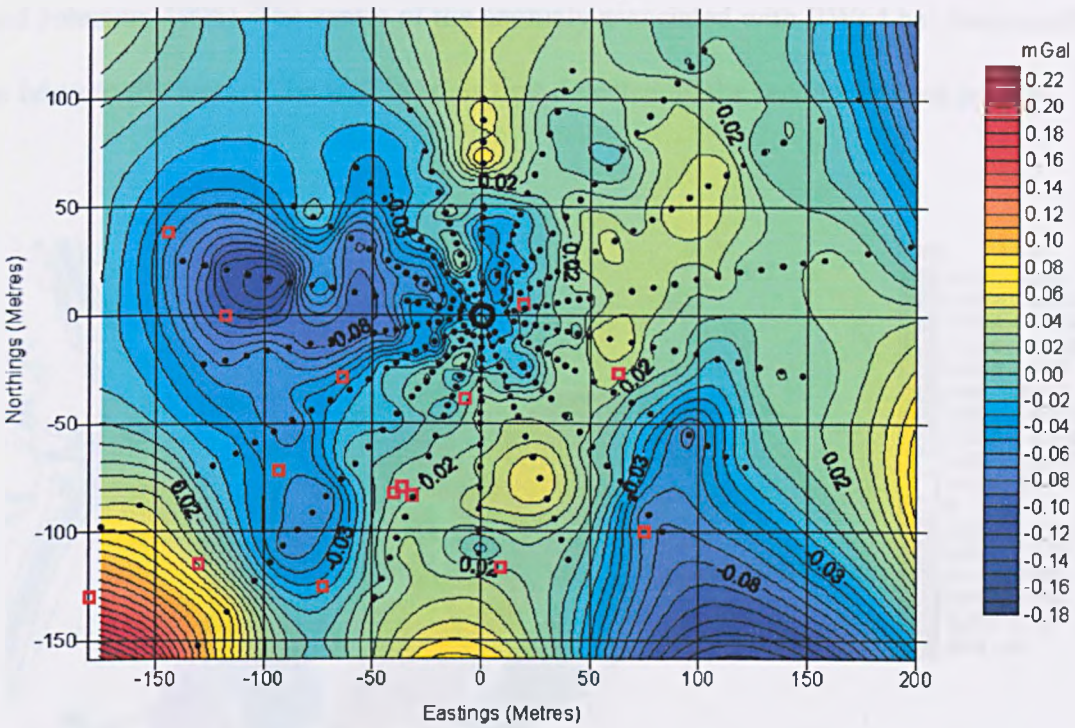


*Fig. 4.11 Gravity response across BW64 acquired in 2001. A 1st order polynomial surface has been removed from the data to account for locally dipping strata. Well heads are depicted by red squares.*

Figure 4.11 shows that the gravity low associated with BW64 has been detected. The presence of additional gravity lows, however, has had the effect of reducing the apparent size of the anomaly. The dominant anomaly is located at –100, 25. This anomaly is associated with BW116 shown in the Figure by the red square at –145, 40. Other high amplitude anomalies are located at –75, -100 and 75, -75. These are associated with BW113 and BW108 respectively.

Superimposing the gravity results onto a topographical map (Figure 4.12) the extent of the gravity anomaly can be seen. The gravity low in the NE of the map is related to the terrain and missing mass associated with the flash located in the top-right corner of the map. The flash (Aggleby's Pond) ranges between 65m and 90m in depth (Harwood

and Johnson, 1996). The centre of the anomaly associated with BW64 has been confirmed as lying to the west of the well head as first detected by the reconnaissance profiles.

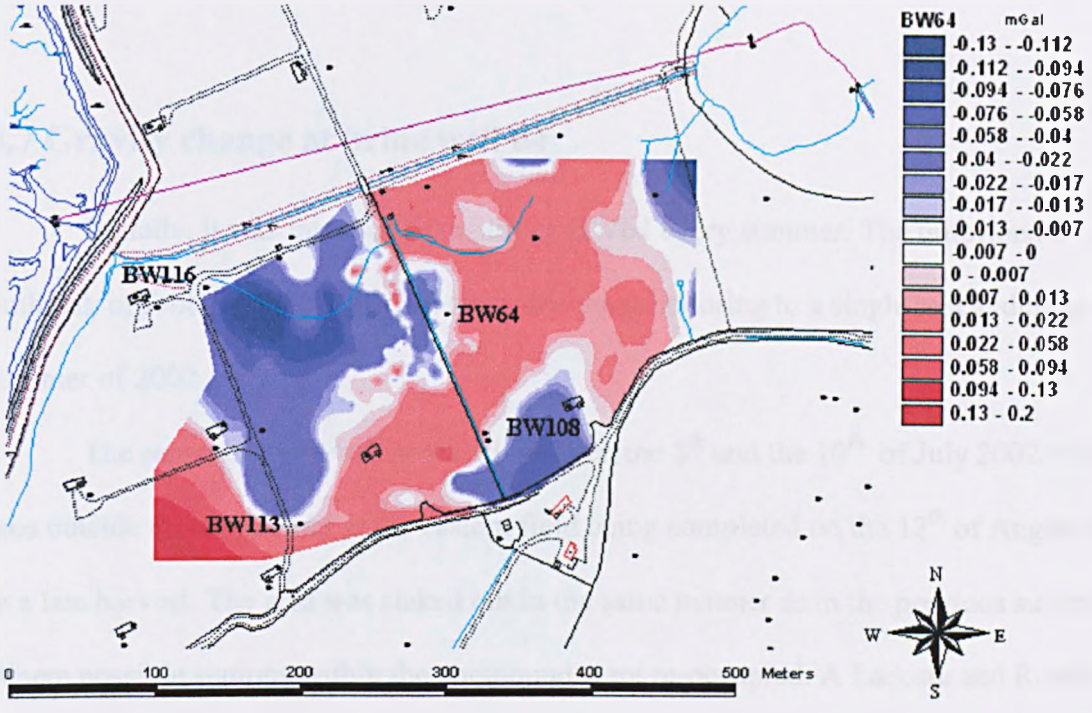




*Fig. 4.12 Gravity response for BW64 superimposed onto a topographical map.*

### 4.6.3 Further microgravity acquisition within Preesall brine field

Two further sites were identified as being at risk of roof collapse and subsequently of potential use for the assessment of the time-lapse microgravity technique. Microgravity data was acquired above Brine Wells 97, 44 and 50 at the same time as the 2000 BW64 data. The BW97 survey utilised a radial grid similar to BW64, whereas, BW 44 and BW50 were both covered by a single rectangular grid consisting of 518 points with a 10m grid spacing.

However, dipping and hooking investigation by ICI showed that the dimensions of these Brine Wells had not changed during the observation period and so follow up, time-lapse surveys were not acquired and consequently the data has not been included.

## 4.7 Gravity change at brine well 64

Initially, it was intended to re-survey BW64 every summer. The unfortunate outbreak of foot and mouth disease restricted the monitoring to a single repeat during the summer of 2002.

The second survey was acquired between the 8$^{th}$ and the 10$^{th}$ of July 2002 with the area outside the compound in the eastern field being completed on the 12$^{th}$ of August due to a late harvest. The grid was staked out in the same manner as in the previous survey. Where possible stations within the compound were re-occupied. A Lacoste and Romberg model D meter was used (D-141) for the acquisition of the gravity. The stations were occupied in the same sequence, using the same base stations. Readings were repeated a minimum of three times at each station, the repeatability being kept within 3μGal. Base stations were re-occupied at hourly intervals.

As before, a strong NE-SW trend was present and has been removed by fitting a 1$^{st}$ order polynomial surface to the data set. The resultant plot is shown in Figure 4.13. After removing the local geological response the same general features can be seen in the 2002 data that were present in the 2000 data set. The dominant anomaly is still located in the west of the grid. However, at first glance it appears to have diminished in amplitude. The other noticeable change is in the east of the grid. The anomaly associated with BW108 appears to have developed in a northerly direction towards the well located at 70, -25. The

region immediately to the north of BW64 appears to have also increased in amplitude and extent.

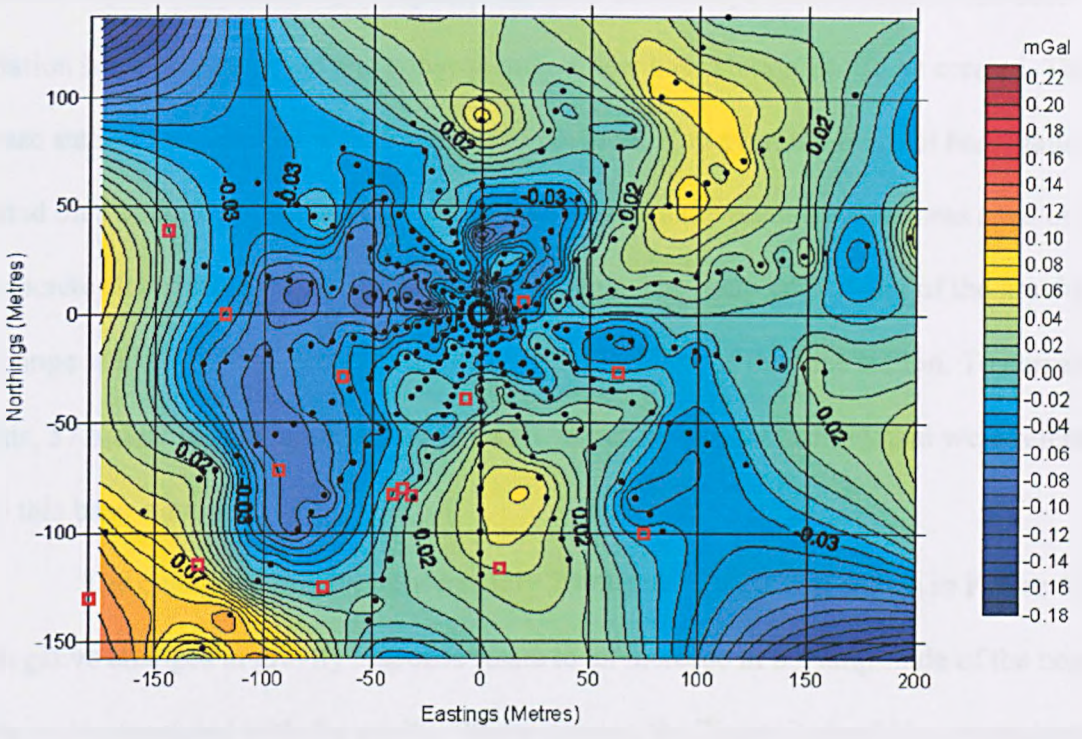


*Fig. 4.13 Gravity response across BW64 acquired in 2002. A 1st order polynomial surface has been removed from the data to account for locally dipping strata. Well heads are depicted by red squares.*

To investigate these apparent changes further, the respective Bouguer anomalies were subtracted from each other to produce a plot of the change in gravity over the two-year period. Without removing the strong NE SW trend caused by the local geology, the 2002 data set was subtracted from the 2000 data set. There is no need to apply terrain corrections in this scenario, as the relative change in topography is insignificant over the monitoring period. Consequently, the gravity variations induced by terrain are cancelled out.

The values of gravity recorded at the Fernhill base station are used to check whether the relative values recorded at the local base stations have varied between the respective surveys. In this instance the base station location used for the western part of the survey had increased by 57.8μGal. Between the surveys the location of this base station had been disturbed and consequently a new base station had to be created. The new base station was sited close to the original position. However, the original base station was sited on a concrete plinth set into the ground whereas the second station was sited on a concrete slab resting on the surface of the ground. The main constituent of the gravity change is likely to be a result of the change in elevation of the base station. To correct for this, 57.8μGal has been subtracted from all values in the 2002 survey that were referenced to this base station.

The change in gravity between July 2000 and July 2002 is shown in Figure 4.14. Negative changes in gravity response relate to an increase in the amplitude of the negative anomaly associated with the cavity. When viewing the Figure it should be remembered that changes outside of the grid are a result of edge effects and should be viewed with caution when considering variation in sub-surface mass distribution. From the analysis of the Keele gravity range data in Chapter 3 on the accuracy and repeatability of time lapse surveys, changes in gravity should only be considered significant if they exceed a value of ~15μGal.

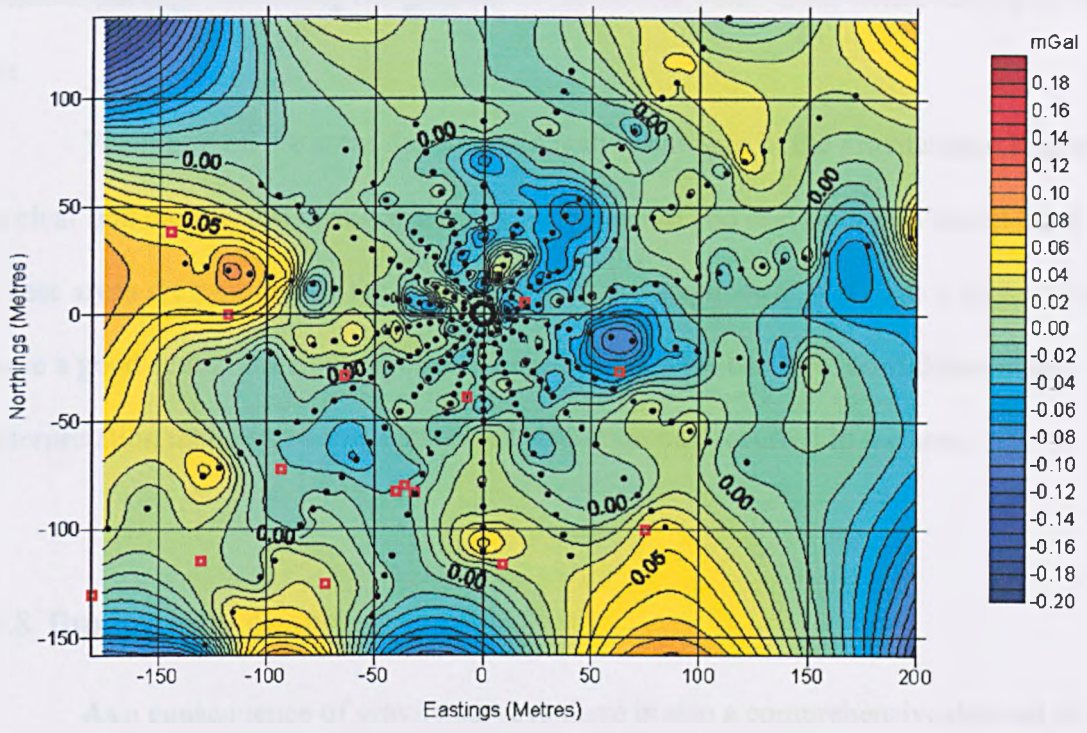


*Fig.4.14 The change in gravity response between July 2000 and July 2002. Negative changes relate to areas in which the negative anomaly associated with the cavity has increased in amplitude.*

With these three considerations in mind the main areas of change within the acquisition grid are located to the NE (negative), and west (positive) of the well head at BW64. Considering the positive changes first, the greatest change is located in the area around BW116. This area has undergone major re-landscaping during the interval between the surveys. In this time the farmer has excavated the area and laid a new field drain. As a result the changes in this area must be viewed with suspicion, as they are likely to be a result of changes in the terrain of that area. This landscaping is also visible in the topography change between the two surveys (Figure 4.15). The other positive changes lie at the edge of the acquisition grid. These cannot be investigated because of the sparse

distribution of the data and in the case of the anomaly at 80, -100, are exaggerated by the contour package continuing the gradient of the anomaly into areas where no data points lie.

Focussing on the areas denoted as negative changes in the gravitational response it is clear that the greatest changes are located to the NE and east of BW64's well head. These areas are sampled by the inner section of the acquisition grid an as a consequence have a good spatial distribution of data points. Hence we can have confidence in the interpretation that a sub-surface mass redistribution has occurred in the area.

## 4.8 Topography change

As a consequence of gravity surveys there is also a comprehensive data set of precise topographic data. These are acquired in order that the Free Air Correction and Bouguer correction can be applied to the gravity data as part of the Bouguer reduction. They are also useful in the study of areas liable to subside as they provide a valuable data set from which changes in surface topography can be identified and interpreted.

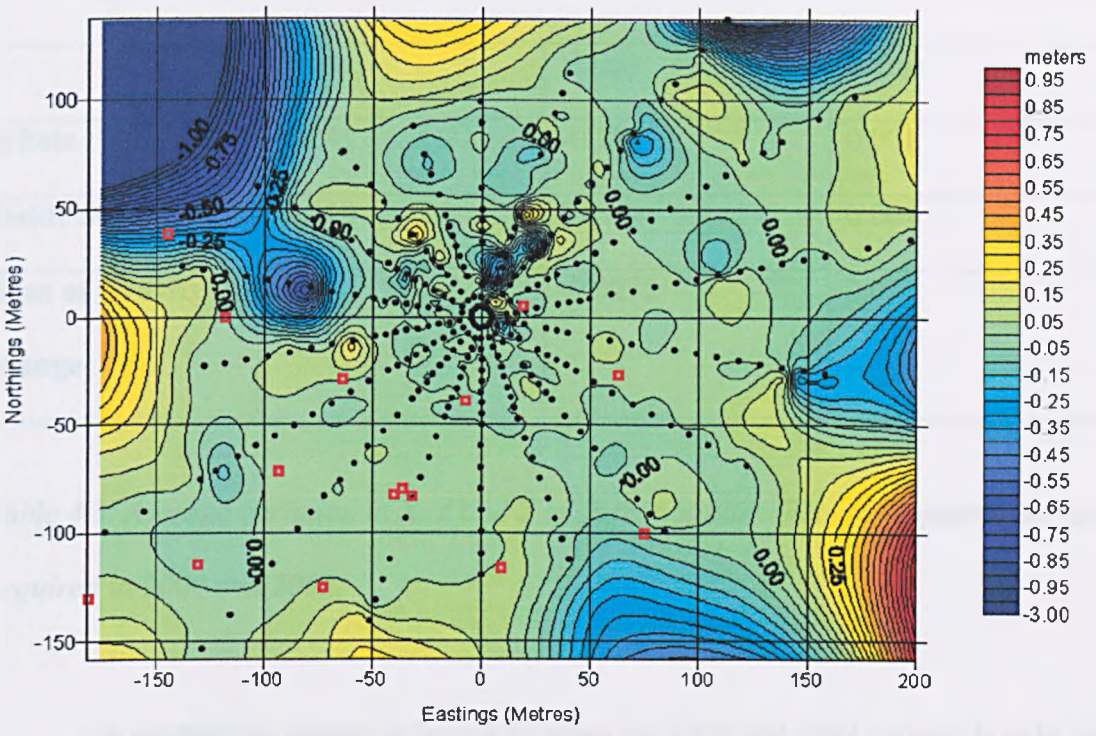


*Fig. 4.15 Map showing the height changes across the acquisition area between July 2000 and July 2002.*

Plotting the change in topography between July 2000 and July 2002 it is apparent that the majority of the area has not changed significantly in elevation (Figure 4.15). The areas of dramatic height change are located outside the data set and are thus a result of contouring artefacts. The main exception is at grid ref. –80,20, where a considerable negative is present. This is an area that has been reworked by the farmer in the period in between surveys and should not be considered as being related to the brine well.

| | X (m) | Y (m) | Z (m) |
|---|---|---|---|
| **Whole** | -0.045 | -0.124 | 0.001 |
| **Inside 50m** | -0.018 | 0.012 | 0.007 |
| **Area of Gravity change** | 0.495 | -0.0275 | 0.014 |

*Table 4.3. Average variation in X, Y and Z of gravity stations between topographic surveys acquired in 2000 and 2002.*

On average the change in height between the 2000 and 2002 surveys is only 1mm (Table 4.3). The variations in X and Y are slightly larger as is to be expected when surveying with a prism and pole. Inside the inner ring of the grid (inside 50m) the average variation in Z increases slightly to 7mm. For the area to the NE of the centre of the grid, where a gravity change has been recorded, the average variation is as high as 14mm. This is fourteen times above the average. Looking at the average error in X and Y, we see that for the area to the NE of the grid centre, the error is an order of magnitude greater than the grid average. This large lateral shift in station position is likely to be the cause of the relatively high change in Z instead of subsidence. This highlights the need for monumented stations, as without them the confidence in the interpretation is restricted. However, surface subsidence can not be ruled out.

However, this increased "error" in height in the area of greatest gravity change does not in itself explain the cause of the variation in gravity signal. A change of 0.014m will have a gravitational effect of 3μGal if we take into consideration the Free Air Correction and Bouguer Correction (Sharma, 1997). The anomaly present as a result of

subtracting the two surveys is of the order of 50-60μGal and consequently must be caused by offer factors.

### 4.8.1 Independent levelling

As part of the monitoring program at Preesall brine field, the well heads are periodically surveyed to identify if surface subsidence is occurring. Surveys were carried out in October 1999 and May 2002. During this period the ground level around Brine Well 64 has subsided by 0.0022mm as reported by R&D Engineering.

With this information we can confidently say that no significant subsidence has occurred in the area between July 2000 and July 2002.

## 4.9 Gravity modelling

### 4.9.1 Upward continuation

Before the size, shape and depth of the cavity associated with BW64 can be modelled it is necessary to remove the high frequency constituent of the gravity signal. In this instance this has been accomplished by using upward continuation. As described in Chapter 3, upward continuation uses a form of Laplace's equations to determine what the gravity signal would be if it was measured a given distance above the Earth's surface. In this way the signal from shallow, near surface features is filtered out as their signal will attenuate faster than that of deeper bodies. Consequently, it behaves in the manner of a low-pass filter but as it uses the principles of Laplace's equations the characteristics of the anomaly are retained.

Upward continuing the data by 15m i.e. calculating what the gravity signal would be if it had been acquired 15m above the surface, removes the near surface noise enabling the modelling of the remaining signal. This is effectively upward continuing the data by

three times the station spacing. The resultant gravity maps are shown in Figures 4.16 and 4.17. It is visibly noticeable that the high frequency aspect of the data has been removed.

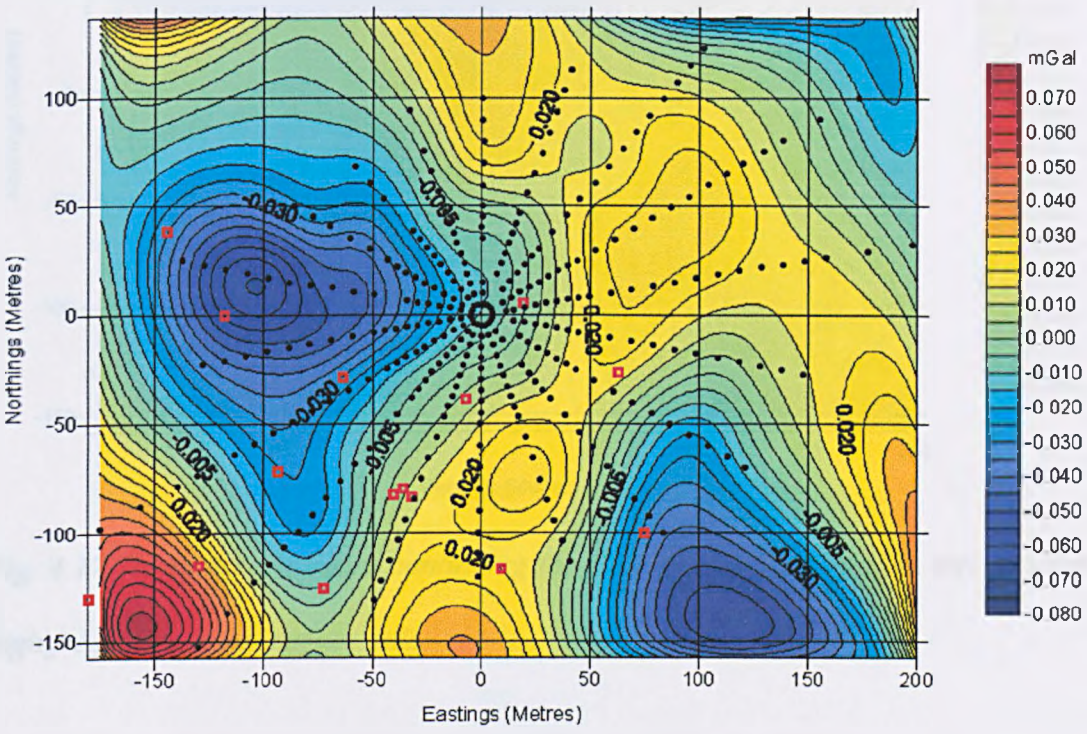


*Fig. 4.16 The result of upward continuing the 2000 gravity data by 15m. this removes the high frequency, near surface noise.*

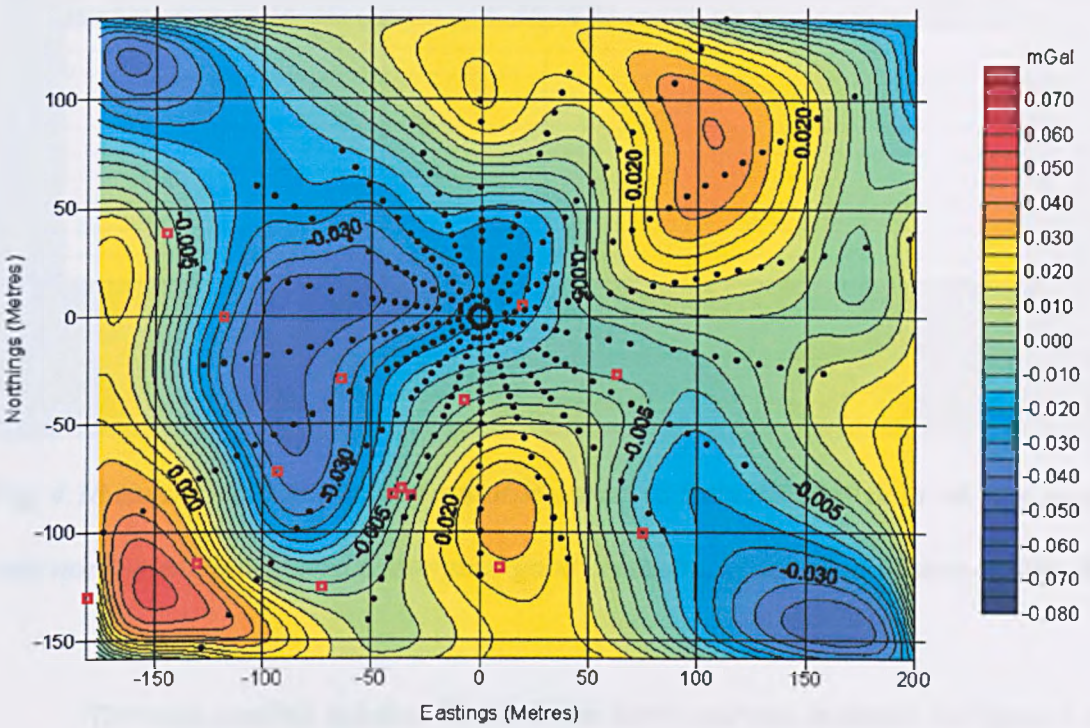


*Fig. 4.17 The result of upward continuing the 2002 gravity data by 15m. this removes the high frequency, near surface noise.*

### 4.9.2 Euler deconvolution

Extracting a profile from the upward continued gravity grids allows the application of Euler's equations to the data and uses the gradient of the anomaly to estimate the depth of the causative body. Extracting a profile that runs north-south along the zero Eastings samples the centre of the anomaly associated with BW64.

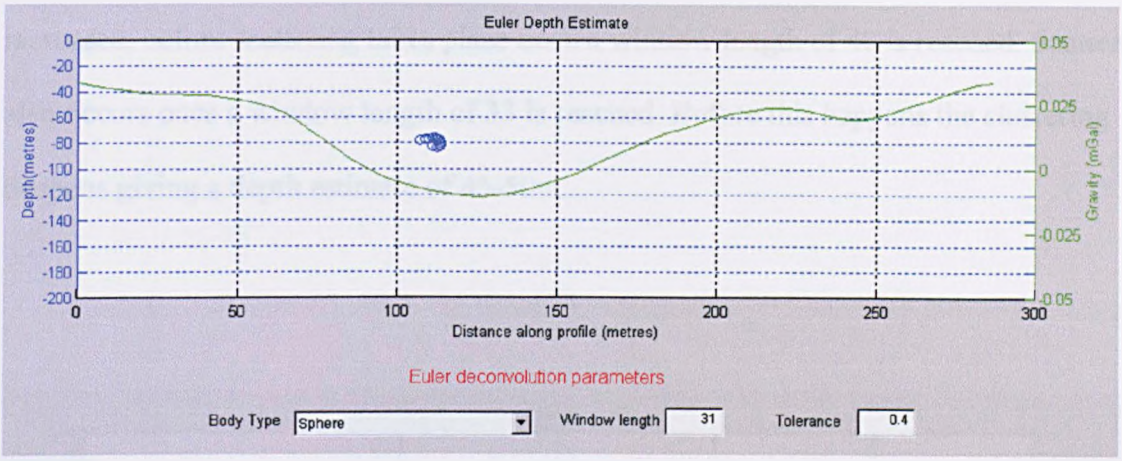


*Fig. 4.18 Euler Depth Analysis of a profile extracted from the 2000 data set. The profile runs north-south along zero Eastings. A good clustering of solutions is seen at 80m depth.*

The most credible solution for the Euler depth analysis, is shown in Figure 4.18. A depth of ~80m is shown by the tight clustering of solutions at approximately 115m along the profile. The parameters used for this estimate are a structural index of 2 (sphere), a window length of 31 and a tolerance of 0.4. The length of the frame window has a slight effect on the depth of the estimate. Increasing the window length broadens the cluster, while decreasing the window length shallows the estimate to a depth of 78m. Scattering occurs once the window length exceeds 36.

A second cluster of solutions is obtained by using a window length of 12. Again a structural index of 2 is used but this time the clustering of solutions places the top of the body at 85-90m. There is shallowing associated with the increase of the window length before scattering occurs at a window length of 15. Decreasing the window length has the effect of loosening the clusters before scattering occurs at a window length of 10.

If a structural index of one (vertical tabular body), is used, it is found that there is no clustering with the window length of 12. However, there is clustering if the window length increased to 36 and we find the depth estimate is reduced by 33m to a depth of 47m. Again, as previously, shallowing (to a depth of 44-48m) occurs if the window length is

increased, before scattering takes place once a window length of 40 is reached. Scattering also occurs once a window length of 33 is reached. Before this happens the clustering deepens giving a depth estimate of 45-50m.

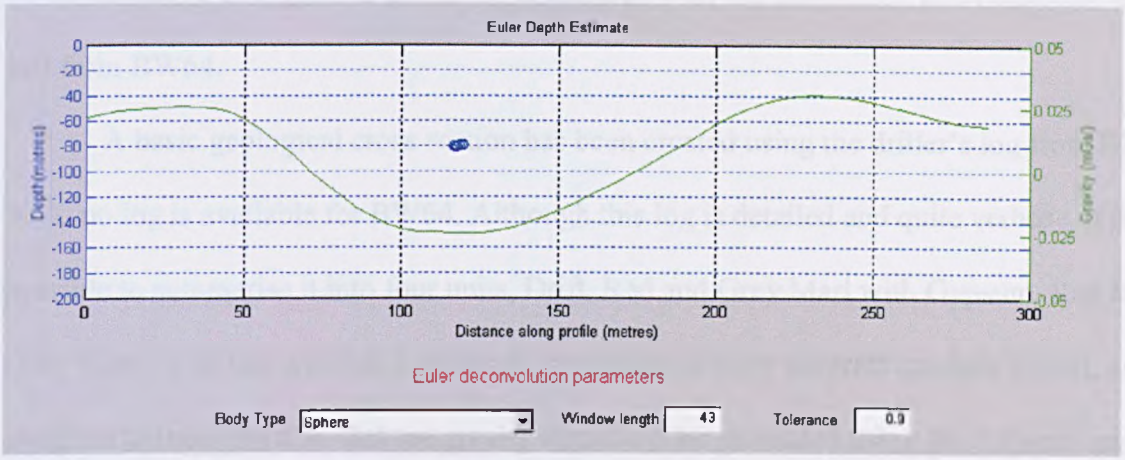


*Fig. 4.19 Euler Depth Analysis of a profile extract from the 2002 data set. The profile is the same as that used for the 2000 data set and runs north-south along 0 Eastings. A good clustering of solutions is seen a t 80m depth.*

A depth estimate of ~80m for the 2002 data is shown by the excellent clustering of solutions in Figure 4.19. This estimate was derived using a window length of 43, structural index of 2 (sphere) and a tolerance of 0.9. Increasing the window length results in a slight shallowing in the estimate to a depth of 77.5m. Scattering of the solutions occurs at a window length of 46. Decreasing the window length has the effect of deepening the depth estimate to 89m before scattering of the solutions occurs again. There are no other significant clustering at other window lengths or other depths.

Using a structural index of one (vertical tabular body), decreases the depth estimate by approximately 32m to a depth of 50m. Again increasing the window length shallows the estimate to ~38m. Scattering occurs at a window length of 55. Decreasing the window

length deepens the estimate to a maximum of 60m with a window length of 36. Scattering occurs after this. There are no other clusters of solutions at different window lengths.

### 4.9.3 2.5D Modelling

Using the solutions from the Euler depth analysis it is possible to model the extent of the causative body, that is the cavity associated with the dissolution and extraction of salt from BW64.

A basic geological cross section has been created using the driller's log from BW 90 as no log is available for BW64. Although this log is detailed and quite verbose, it is possible to summarise it into four units, Drift, Red and Grey Marl with Gypsum, Red and Grey Marl - first salt and Salt Rockhead. Properties (density contrast and half strike), are assigned to these units so that the gravity signal can be generated using the Talwani and Ewing (1960) method. The properties used in the model are summarised in Table 4.4.

Using the depth solutions generated by the Euler depth analysis the top surface of the cavity is fixed at a depth of 80m. The bottom of the cavity can also be fixed by using the dipping measurements. Both of these depths have a high degree of confidence attached with them. The dipping measurement (described earlier in this chapter) is likely to produce a true depth of the cavity base, unless it rests on a ledge of some sort which is unlikely in this scenario. The depth derived from the Euler Depth Analysis also has a high degree of confidence associated with it due to the tight clustering of solutions.

With these two variables fixed, the horizontal extent of the cavity can be established by matching the calculated gravity signal to the observed signal.

A density of 1 $Mg/m^3$ has been assigned to the material within the cavity as it is known to be water filled. With these parameters fixed the last variable is the cavity's lateral extent.

Figure 4.20 is an image of the model generated for the 2000 gravity data. It can be seen that a good fit has been achieved between the modelled and observed gravity signals. The calculated field does deviate from the observed field in the south, but this is related to gravity effects associated with another cavity which have not been modelled in this instance.

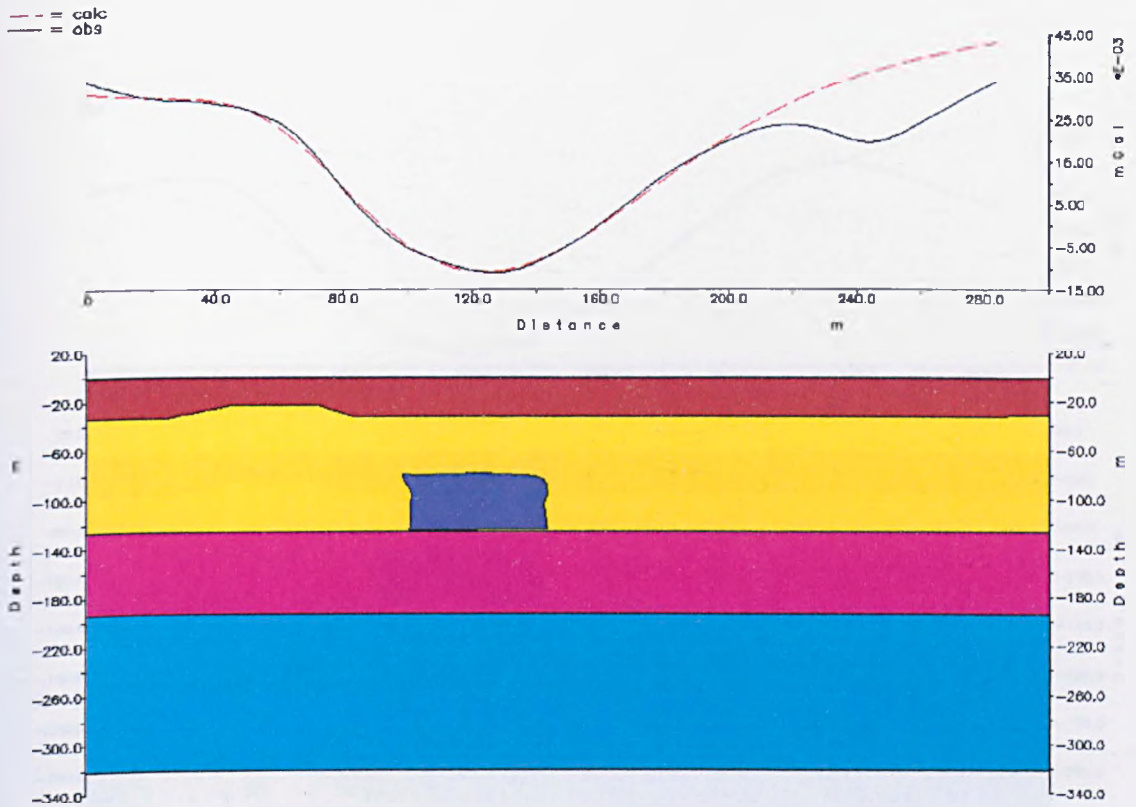


*Fig. 4.20 2.5D model of the 2000 gravity data set acquired over BW64. Polygon parameters are as summarised in Table 4.4. Gravitational effects associated with a secondary cavity cause the deviation from the observed gravity in the south of the profile.*

The 2002 gravity data set has been modelled using the same polygons and parameters. The Euler depth analysis suggests that no (or little) change in the depth of the top surface of the cavity has taken place. However, the anomaly has broadened and increased in amplitude by 10μGal. As the Euler Depth Analysis has given no indication of

the cavity propagating towards the surface, the increase in anomaly width and amplitude has been attributed to an increase in lateral extent of the cavity. The 2002 anomaly has therefore been matched by extending the cavity in 2000 by 10m to the north and 3m in the east west direction (i.e. the half strike of the body). A slight upwelling of the cavity floor has also been incorporated into the model. All other parameters and variables have been kept constant. The model is presented in Figure 4.21.

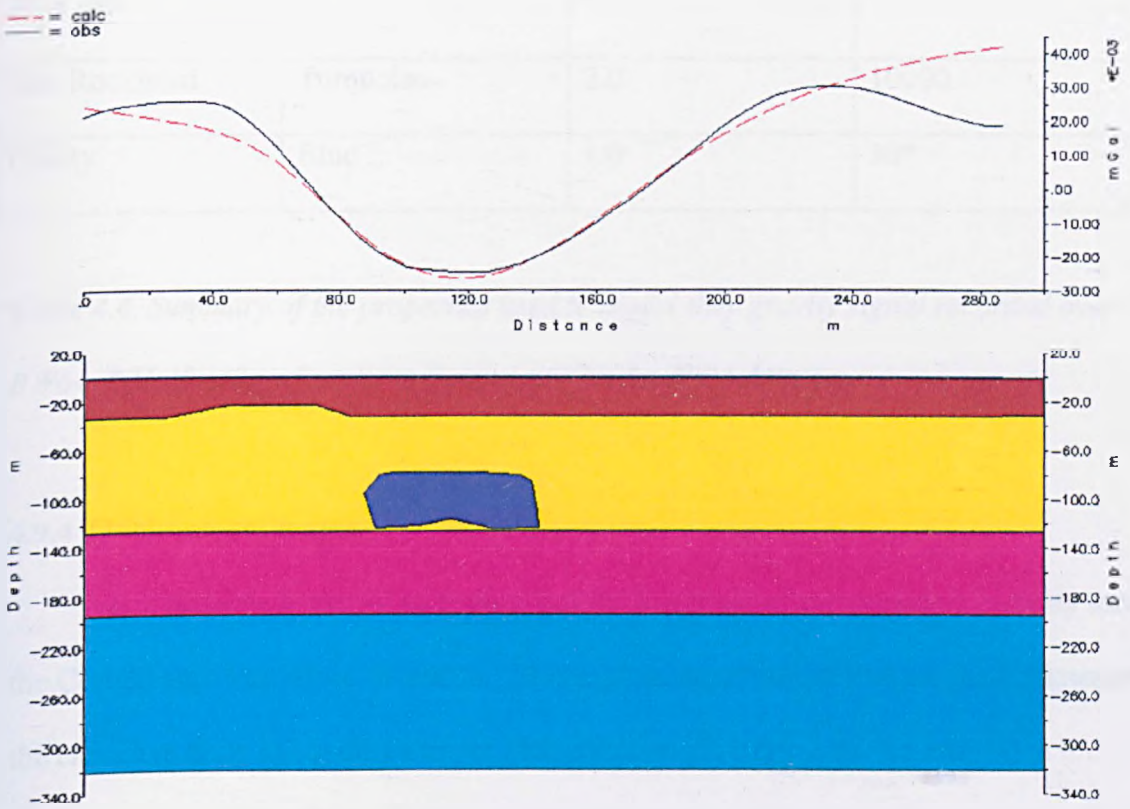


*Fig. 4.21 2.5D model of the 2002 gravity data set acquired over BW64. Polygon parameters are as summarised in Table 4.4. The cavity has increased in lateral extent to the north and in the east-west direction (i.e. in the plane of the page). Gravitational effects associated with a secondary cavity cause the deviation from the observed gravity in the south of the profile.*

| Geological Unit | Colour In Model | Density (Mg/m³) | Half Strike (m) |
|---|---|---|---|
| Back ground | White | 1.92 | 10000 |
| Drift | Brown | 1.8 | 10000 |
| Red Grey Marl with Gypsum | Yellow | 1.9 | 10000 |
| Red Grey Marl – First salt | Pink | 1.9 | 10000 |
| Salt Rockhead | Turquoise | 2.0 | 10000 |
| Cavity | Blue | 1.0 | 30* |

*Table 4.4. Summary of the properties used to model they gravity signal recorded over BW64. * Half strike of cavity increased to 33m for 2002 data set.*

### 4.9.4 Thickness estimates

It is possible to derive an estimate of the thickness of the causative body by using the Cordell and Henderson inversion. The program iteratively calculates the thickness of the causative body using the Bouguer Slab equation. The depth horizon to which the solution is pinned must be assigned, as must the density contrast between the causative body and the host rock. Using this method in conjunction with the depth estimates derived using the Euler depth analysis, enables a 3D image of the causative body to be created. Further details of the theory behind this method can be found in Chapter 3.

As described in Chapter 3, potential fields have many plausible solutions for the same problem. The Cordell and Henderson inversion has been conducted over a suite of values for the main two parameters. That is the depth at which the model is assigned and

the density contrast responsible for the gravity anomaly. Either the top or bottom of the model is fixed. So a suite of solutions can be created with the model being assigned a base level dictated by the dipping data (125.5m below surface). To complement this separate suites of solutions with the top of the model assigned depths dictated by the hooking and Euler data (100m and 80m below surface respectively) can be created. The Tables 4.5 and 4.6 detail the results of the iterations for the 2000 and 2002 data sets acquired over Brine Well 64.

The error (E) is a key consideration when considering the plausibility of the solution. Its unit is mGal and is a root mean square error of the difference between the observed gravity and the calculated gravity. The errors encountered with this data set are uncommonly high. However, the distribution and magnitude of thickness estimates derived from the iteration process are plausible.

From the solutions provided in Table 4.5 (2000 data set), it is evident that the thickness estimates do not match the recorded dimensions of the cavity (as recorded by ICI in 2000) for the density contrasts used. Fixing the base of the model at 125.5m below surface (taken from dipping measurement in 2000) we see that the maximum thickness for the area beneath the well head (area C Figure 4.22) is 18m. This puts the roof of the cavity at 107.5m. That is 7.5m beneath the hooking measurement taken in 2000 and 27.5m below the Euler depth estimate.

Assigning a depth of 100m for the top of the model (taken from hooking measurements in 2000) the maximum thickness is 16m for area C. This is 9.5m above the dipping measurement taken at the same time. The maximum thickness in area C with the top of the model pinned to 80m below surface (taken from the Euler Depth analysis) is 22m. This is 23.5m off the dipping depth of 125.5m.

It is possible to assign lower density contrasts than –0.7 $Mg/m^3$ to the model and this does indeed increase the maximum thickness, however, it also disrupts the distribution of the anomalous bodies. For instance assigning a density contrast of –0.4 $Mg/m^3$ to a model with its top surface pinned at 80m results in a maximum thickness of 31m being attained below the well head. However, it also results in the majority of the survey area having a calculated thickness of between 10 and 15m which is nonsensical. The model is also 14.5m above the measured base of the cavity. Therefore -0.7 $Mg/m^3$ has been assigned as the lowest density contrast for this experiment.

Looking at the errors encountered in the inversion, that is the error between the measured and calculated gravity values we can begin to explain the disappointing results. The error encountered in the inversion ranges between $2.4\Delta10^{-2}$ and $4.1\Delta10^{-2}$. That is a range of between 24 and 42 μGal, which is almost equivalent to the measured anomaly itself. As these errors are so large the result can only be used as a guide and not to investigate the cavities dimensions further.

| **Brine Well 64: 2000 Data set** | | | | |
|---|---|---|---|---|
| **Depth assigned to base of model 125.5m** | | | | |
| $\Delta\rho$ (Mg/m$^3$) | **A** | **B** | **C** | **E ($\Delta 10^{-2}$)** |
| -0.1 | 33 | 19 | 16 | 2.4 |
| -0.9 | 36 | 22 | 18 | 2.4 |
| -0.8 | 37 | 27 | 18 | 2.4 |
| -0.7 | 37 | 22 | 18 | 2.4 |
| **Depth assigned to top of model 100m** | | | | |
| $\Delta\rho$ (Mg/m$^3$) | **A** | **B** | **C** | **E ($\Delta 10^{-2}$)** |
| -0.1 | 26 | 16 | 13 | 4.1 |
| -0.9 | 34 | 17 | 13 | 4.1 |
| -0.8 | 34 | 20 | 14 | 4.1 |
| -0.7 | 38 | 22 | 16 | 4.1 |
| **Depth assigned to top of model 80m** | | | | |
| $\Delta\rho$ (Mg/m$^3$) | **A** | **B** | **C** | **E ($\Delta 10^{-2}$)** |
| -0.1 | 26 | 17 | 15 | 3.6 |
| -0.9 | 32 | 21 | 18 | 3.6 |
| -0.8 | 36 | 23 | 20 | 3.5 |
| -0.7 | 41 | 26 | 22 | 3.5 |

*Table 4.5. Table detailing the various solutions attainable for the Cordell and Henderson thickness inversion. The parameters that have been varied are the density contrast ($\Delta\rho$) between the host rock and the anomalous material and the depth at which the model is pinned as well as which surface of the model is pinned (i.e. top or bottom). Maximum thickness (m) has been given for the areas around anomalies A, B and C. The error (E) of the iteration is also given. Its units are mGal and give an indication of the success of the iteration.*

The Cordell and Henderson inversion technique has also been attempted after upward continuing the data set in an attempt to remove some of the near surface noise. Although the thickness estimates were similar to those recorded in Table 4.5 the definition and distribution of the causative bodies were lost. Thus the overall result contained less information than the data sets used to produce the results recorded in Tables 4.5 and 4.6.

The results obtained using the 2002 data set were of a slightly better quality (Table 4.6). With the base of the model fixed at 125.5m below surface the maximum thickness in the area of the well head (area C) ranged from 30m to 47m. That would place the top of the model at a depth of between 95.5m and 78.5m below the surface respectively. These end members fit the measured value of 100m (from hooking) and the estimated values of 80m (Euler Depth Analysis) well.

Fixing the top of the model to 100m also produced encouraging results. The maximum thickness ranged from 25m to 30m in the area around the well head which matches the measured base of the cavity (125m to 130m). Assigning a top depth of 80m for the model (taken from the Euler Depth Analysis) result in the maximum thickness in the area beneath the well head ranging from 22m to 33m This would place the bottom of the cavity between 102m and 113m below the surface. That is an error of 23.5m and 12.5m from the measured depth of the cavity below the well head.

These results suggest that the cavity roof is indeed at a depth of 100m below the surface and that the density contrast between the brine and the material that surrounds the cavity is between –0.1 $Mg/m^3$ and –0.8 $Mg/m^3$, although the large errors between the measured and calculated gravity fields reduce the credibility of these results.

The probable causes of the poor results derived from the Cordell and Henderson inversion are related to the high density of brine well cavities within the survey area i.e. the presence of BW116 and BW113, (Figure 4.12). The location of these cavities in the near vicinity of BW64 has effected the inversion process in two ways. First the gravity anomaly which results from BW64 cannot be properly resolved from the anomalies of BW116 and BW113. Consequently, the survey has not sampled the negative anomaly resulting from the superposition of these three cavities in its entirety. The inversion process understands that the gravity anomaly has not been sampled completely and

responds by moving mass out to the edges of the grid. This is evident in Figure 4.22. This results in the calculated thickness being an underestimate of the actual thickness as the mass at the edges has not been correctly assigned to the centre of the anomaly. However, the unusual situation present in the Preesall Brine field inhibits the full closure of the gravity anomalies that result from the brine cavities because of their close proximity to each other.

Further to this, the relative depth horizons of the cavities complicate the inversion. The inversion requires a reference surface be assigned (either the top or bottom of the cavity) at which the thickness is calculated. The roofs of BW116 and BW113 are located at depths of 290m and 270m below the surface, which is approximately 190m below the cavity, associated with BW64. This reduces the accuracy of the inversion because the program is trying to calculate the thickness of the causative body with reference to one depth horizon when in fact there are three. The success of the Cordell and Henderson inversion is greatly improved when the anomalous bodies are located along the same depth horizon.

| **Brine Well 64: 2002 Data set** | | | | |
|---|---|---|---|---|
| **Depth assigned to base of model 125.5m** | | | | |
| $\Delta\rho$ (Mg/m$^3$) | **A** | **B** | **C** | **E** ($\Delta 10^{-2}$) |
| -0.1 | 20 | 17 | 30 | 3.0 |
| -0.9 | 22 | 19 | 33 | 2.9 |
| -0.8 | 24 | 21 | 38 | 2.9 |
| -0.7 | 35 | 33 | 47 | 2.6 |
| **Depth assigned to top of model 100m** | | | | |
| $\Delta\rho$ (Mg/m$^3$) | **A** | **B** | **C** | **E** ($\Delta 10^{-2}$) |
| -0.1 | 17 | 15 | 25 | 3.7 |
| -0.9 | 17 | 15 | 23 | 3.7 |
| -0.8 | 20 | 17 | 26 | 3.7 |
| -0.7 | 23 | 20 | 30 | 3.8 |
| **Depth assigned to top of model 80m** | | | | |
| $\Delta\rho$ (Mg/m$^3$) | **A** | **B** | **C** | **E** ($\Delta 10^{-2}$) |
| -0.1 | 14 | 12 | 22 | 3.5 |
| -0.9 | 18 | 17 | 27 | 3.6 |
| -0.8 | 18 | 16 | 28 | 3.5 |
| -0.7 | 22 | 20 | 33 | 3.5 |

*Table 4.6. Table detailing the various solutions attainable for the Cordell and Henderson thickness inversion. The parameters that have been varied are the density contrast ($\Delta\rho$) between the host rock and the anomalous material and the depth at which the model is pinned as well as which surface of the model is pinned (i.e. top or bottom). Maximum thickness (m) has been given for the areas around anomalies A, B and C. The error (E) of the iteration is also given. Its units are mGal and give an indication of the success of the iteration.*

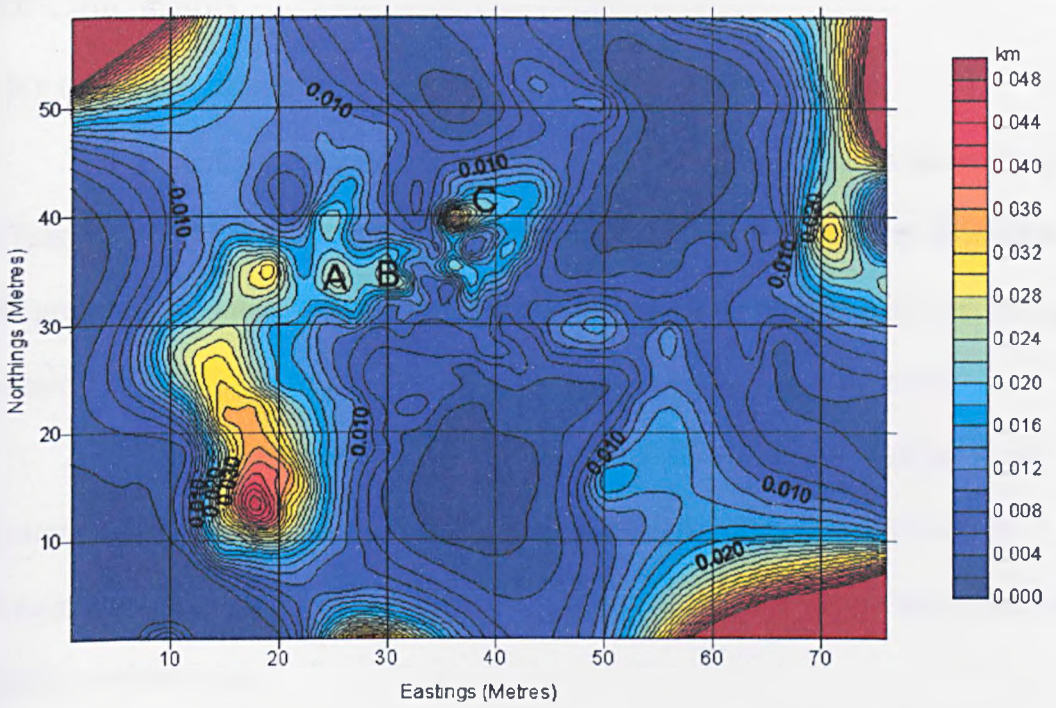


*Fig 4.22 Plot of the cavity thickness for the 2002 data. The base of the model has been fixed at 125.5m and a density contrast of –0.8 Mg/m$^3$ has been used. Areas A, B and C relate to Tables 4.5 and 4.6. Area C relates to the area below the well head where the dipping and hooking results are acquired.*

## 4.10 Conclusions

### 4.10.1 General conclusions

The aim of the work carried out in the Preesall brine field was to develop and test the feasibility and field accuracy of a time-lapse microgravity survey. The Preesall Brine field presented the unusual situation where caverns of known dimensions were being monitored regularly and through this monitoring were known to be unstable.

Although the size and timetable of collapse could not be predicted previous monitoring data could be used as a control to establish the potential of time-lapse microgravity in the continued monitoring of the Preesall brine field and other sites where unstable cavities exist.

A secondary aim for the microgravity survey at Preesall was to provide extra information and detail about the size, location and stability of brine cavities in areas where it had become impossible to monitor the wells in the conventional method due to the condition of the original borehole. It was also hoped that time-lapse microgravity could be established as a cost-effective alternative to the current method of monitoring.

### 4.10.2 A-priori data

The data provided by ICI suggested that the Brine Well most likely to provide a sizeable change in cavity dimensions was BW64. This brine well also had adequate access and so was selected as the main study area.

### 4.10.3 Microgravity

Through forward modelling it has been shown that it is possible to detect the gravitation anomaly generated by the missing mass associated with the brine extraction at

Brine Well 64. The maximum modelled anomaly was ~40μGal which exceeds the minimum resolution of a microgravity survey by some margin.

The survey around BW64 was rare in microgravity terms as the general location of the cavity was known and so acquisition on radial grid was tested. It was thought that a radial grid would reduce the number of acquisition points and provided a better coverage in the active area. The test showed the radial grid system to be successful in accurately sampling the gravity anomaly. In order that the radial grid be sited as close as possible to the centre of the anomaly, two reconnaissance profiles were acquired across the site. The centre of the grid was subsequently sited 30m to the west of the well head to account for an offset discovered it the location of the anomaly minima.

The initial survey in the BW64 area was conducted between the 20th and 24$^{th}$ of July 2000. It was successful in delineating the extent of the brine cavity. It also recorded the gravitational signal associated with the surrounding brine wells, especially that associated with BW116 to the west.

It was deemed, however, a success and so a second survey was acquired between the 8$^{th}$ and 10$^{th}$ of July 2002, finally being completed on the 12$^{th}$ of August because of access restrictions caused by the foot an mouth crisis preventing surveying in 2001.

### 4.10.4 Modelling of gravity signal

Euler depth analysis and 2.5D modelling using the GRAVMAG program have been used to establish the depth and size of the body. The Euler depth analysis show that the top of the body is most likely to be located at a depth of 80m. This result is the same for both the 2000 and 2002 surveys suggesting that little or no significant change has occurred in the height of the roof.

This is supported by the 2.5D modelling which also concludes that the slight change in the recorded gravity anomaly can be accounted for be increasing the half strike of the body by 3m. That is by increasing the lateral extent of the body and not the depth of the cavity roof. The hypothesis that the cavity has increased in lateral extent is supported by the decrease in gravitational signal in the area NW of the BW64 well head.

The results obtained from the Cordell and Henderson inversions were inconclusive. The model was in turn assigned depths equivalent to the base of the cavity (taken from dipping data 2000), the roof of the cavity (hooking data 2000) and the depth derived from the Euler analysis as well as a suite of density contrasts. Some combinations proved more successful than others, in particular assigning the model a top depth of 100m seemed to provide thickness that would coincide with the depths measured by the dipping method. However, the errors throughout the inversions were extremely high in the region of 40μGal (the same order of magnitude as the original anomaly) and therefore would lead the accuracy of the results to be questioned. Although these results can be used as a guide, their use in determining the true depth of the cavity roof is limited.

### 4.10.5 Original aims

With reference to the original aims of the work carried out on the Preesall brine field, the overall project was a success. The work had shown that the process of using time-lapse microgravity is feasible in a "field" environment.

The accuracy between the two repeated surveys were within the limits determined by testing on the Keele Gravity Range thus giving confidence that anything outside these limits was indeed a sub-surface mass change.

Modelling of the two data sets produced exceptional Euler solutions and showed that no change had occurred in the depth of the roof between the two surveys. There was,

however, a discrepancy between the estimated height and the height obtained by hooking. The quality of the Euler solutions suggests that the estimate is true and therefore the resultant height difference could be the result of the borehole casing extending into the cavity and is not flush with the cavity roof (thus giving a misleading hooking reading). A second interpretation is that bed separation has occurred above the roof of the cavity resulting in a quantity of missing mass above the cavity roof, offsetting the Euler depth estimate. Either interpretation highlights the fact that the cavity below BW64 is further advanced in its propagation than was first understood.

The Cordell and Henderson Inversion was relatively unsuccessful. Although the inversion produced figures for the thickness of the causative body that were of the right order of magnitude, it failed to provide conclusive results that matched either the data provided by ICI (i.e. that the cavity extended form 100m to 125.5m) or indeed supported the idea that the cavity roof was in fact at a depth of 80m and not 100m (Euler Depth estimates). The high errors encountered in the inversion are likely to account for this and so the technique should not be discounted from further investigations.

# Chapter 5

# The Application of Time-Lapse Microgravity at Peter Street, Northwich

## 5.1 Introduction

Peter Street is located in the east of Northwich (Figure 5.1a and 5.1b). It was built in the late 19$^{th}$ century at a time when Northwich was experiencing great prosperity from the salt industry. In recent decades residents have reported cracking and subsidence thought to be related to brine extraction. In 1985 the Cheshire Brine Subsidence Compensation Board, which has statutory responsibility for dealing with subsidence caused by brine extraction, demolished several houses in the area after they had become unstable (Figure 5.1a). However, residents still living in the area, report that the road and waste ground left by the demolition of the houses in 1985 are both suffering from subsidence and houses adjacent to this area are currently experiencing subsidence related structural problems.

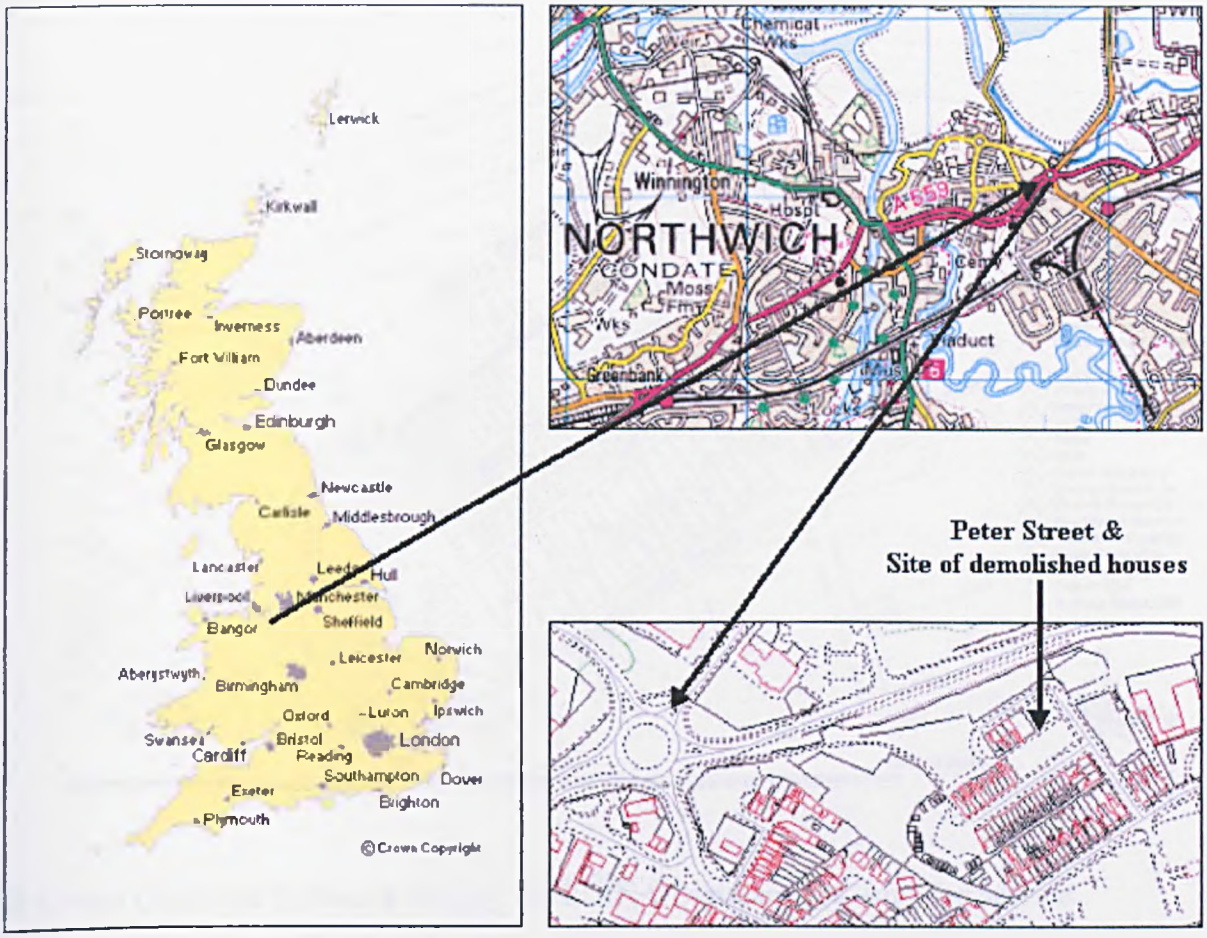




*Fig. 5.1a The site of investigation is located in the east of Northwich, just off Manchester Road*

The aim of the geophysical survey was to investigate the cause of the subsidence. It was important to establish whether the subsidence was related to mine workings in the area or whether it was a result of natural processes. Once the cause of the subsidence had been established it was hoped that an understanding of the stability of the area could be achieved and thus giving an estimate of the time scale under which the subsidence would continue and whether is would result in catastrophic collapse.

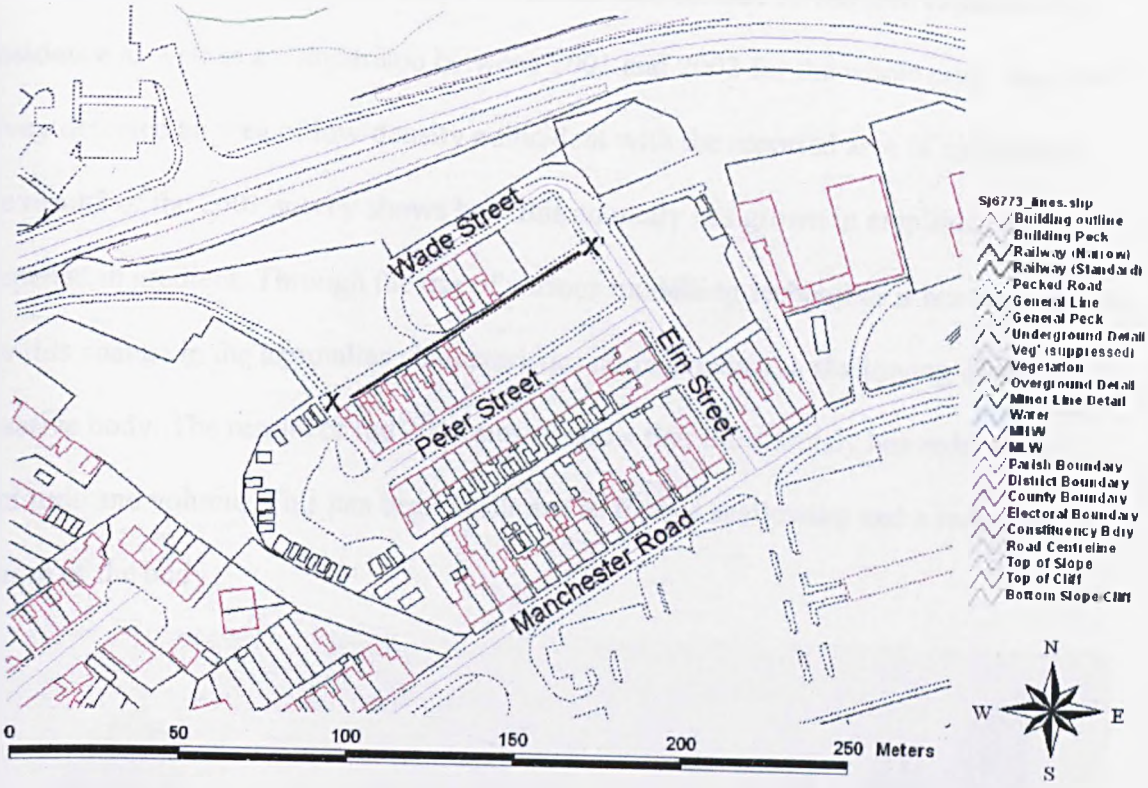




*Fig.5.1.b Street layout of the area being investigated.*

The microgravity technique was applied to the area, the application of the time-lapse technique allowing for an estimate of the ground stability. Resistivity profiles were also acquired over suitable areas of interest identified by the microgravity to constrain the geological characteristics of the causative body.

The microgravity surveys were acquired in the Peter Street area in 2001 and 2002. A data set acquired by Simon Emsley and Sarah Corrie of Golder Associates (UK) Ltd in 1998 on behalf of the Brine Compensation Board has also been incorporated to extend the period of monitoring. The 1998 survey covers an area approximately half the size of the subsequent 2001 and 2002 surveys. For the purpose of comparison with the 1998 data set the relevant portion has been extracted from the 2001 and 2002 data sets. This allows a

comparison between 1998, 2001 and 2002 for an area centred on the area experiencing subsidence as well as a comparison between 2001 and 2002 for the whole area. The 1998 survey detected an area of low-density coincident with the reported area of subsidence. The results of the 2001 survey shows how this anomaly has grown in amplitude and steepened in gradient. Through the use of various modelling techniques it has been shown how this change in the anomalies characteristics corresponds to a shallowing of the causative body. The results of the 2002 survey show that the anomaly has reduced in amplitude and volume. This has been attributed to further shallowing and a reduction in volume of the body.

*Plate 5.1 View looking NW from Elm Street towards Peter Street and Wade Street in the background. The waste ground in the foreground is the area left by the demolition of the houses in 1985.*

*Plate 5.2 View looking along X'-X. The area of principle subsidence can be seen where the cinder track dips by the trees.*

## 5.2 Field procedures

Before the 1998 survey, little was known about the cause of the subsidence in terms of size or depth. Preliminary speculation suggested that the cause of the subsidence was either due to the presence of unknown mine workings or solution features related to the pumping of brine. Microgravity data were collected on a 5 by 5-m grid giving a good compromise between resolution and site coverage. This resulted in approximately 130 points being collected over an area 92m by 47m.

The 1998 survey was acquired between the 21st and the 24th of July using a Scintrex CG-3M automated Microgravity meter. Base readings were taken at the start and end of each day and at hourly intervals in order to establish a drift curve for that particular

day. At every location 3 readings were taken in rapid succession to ensure repeatability of the measurements. Individual readings, consisting of 60 one-second samples, were taken over a period of one minute (Emsley and Corrie, 1998).

The 2001 survey was acquired between the $10^{th}$ – $13^{th}$ July using a Lacoste and Romberg D Meter (D-141). Base readings were taken at the start and end of each day and at hourly intervals throughout the day. Repeat readings were taken at each point to ensure repeatability and were kept within 3μGal. The topographic heights of the survey points needed for the free air and Bouguer correction were acquired to an accuracy of 2mm.

At the time the 2001 grid was laid out, nothing was known of the previous 1998 survey. Consequently, an exact match between the station positions was not achieved although a 5m by 5m grid was used and by coincidence a high level of correlation resulted.

The 2002 survey was acquired between the $10^{th}$ - $12^{th}$ of June. As far as possible the same grid as the 2001 survey was used to acquire the data. A Scintrex CG-3M automated Microgravity meter was used with base readings being taken at the start and end of each day and at hourly intervals in order to establish a drift curve for that particular day. Individual readings, consisting of 60 one-second samples, were taken over a period of one minute.

As part of the time-lapse monitoring a second base station and bench mark were set up at St Helens Church, Northwich (Figure 5.2), well away from the survey area on land that was considered to be stable and would not change during the period of monitoring. Ideally, an absolute gravimeter would be used to establish the absolute value of gravity at such a point, but this was not possible so it has been assumed that this base station has not changed during the monitoring period.

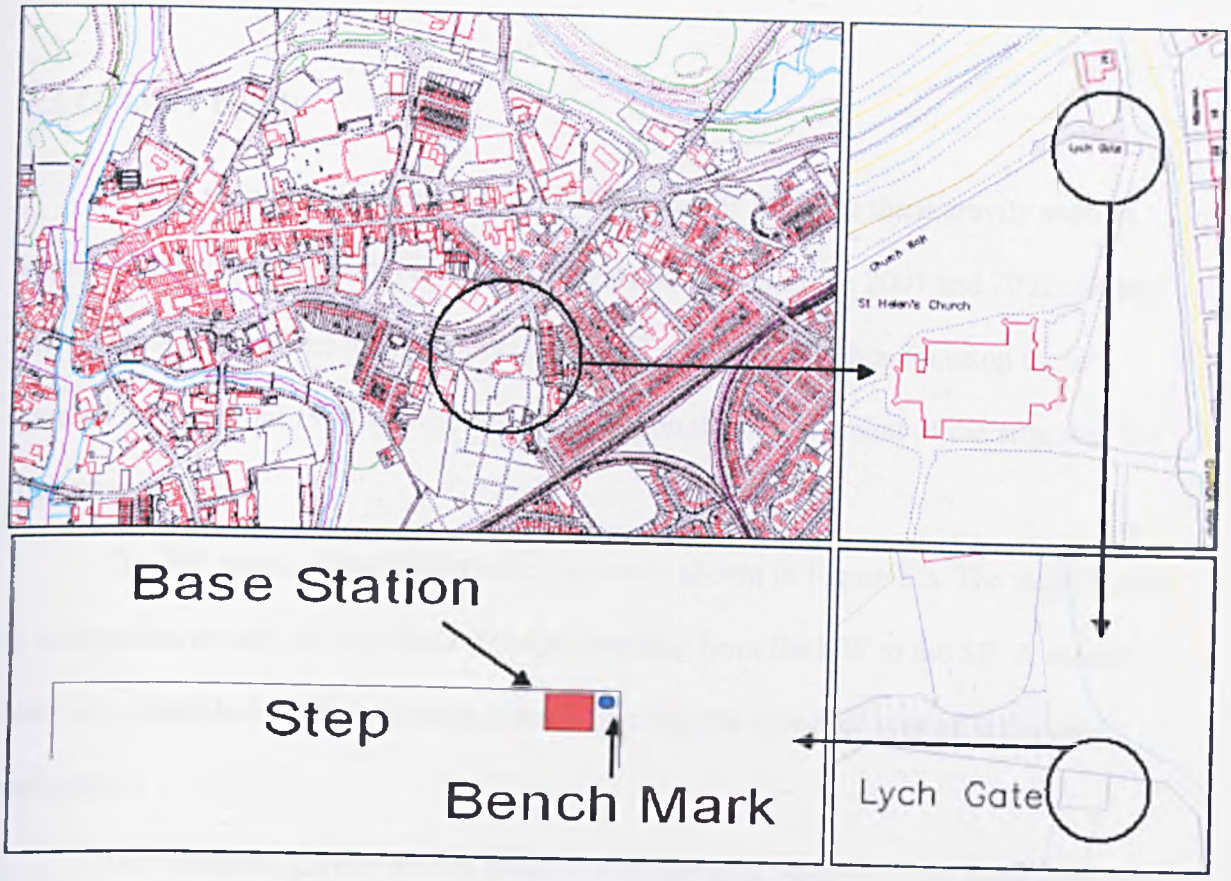




*Fig. 5.2 A control base station was set up at the St. Helens church, Northwich. It purpose was to allow for the correction of tares and drift between microgravity surveys of Peter Street (Grid Ref. 366,477.55 373,868.51).*

Gravity readings were taken at the St Helen's Church at the start and end of each day during the survey to assess whether the local base station at Peter Street had changed in value between the time-lapse surveys. Applying this correction ensures that each gravity survey is corrected for tares and subsidence between surveys.

All three surveys were processed in order to produce Bouguer gravity maps where the effect of drift, elevation and the influence of topography are removed. A value of 2.0 $Mg/m^3$ ($g/cm^3$) was used for the calculation of the Bouguer correction during the processing of each data set.

## 5.3 Gravity results

In this section it is intended to present the results from the three gravity surveys acquired in the Peter Street area. Initially, the whole extent of the 2001 and 2002 surveys will be presented and the main features discussed. The text will then focus on the area covered by the initial 1998 survey, concentrating on the development of the area over the four-year period.

The full extent of the 2001 gravity survey is shown in Figure 5.3. The main feature is a negative anomaly of amplitude -60μGal trending from the NW to the SE. A second anomaly branches off this and trends towards the NE, the principal area of recorded subsidence.

The change in gravity will be presented for the area centred on the subsidence for the period 1998 to 2002 before expanding to cover the whole area for the period 2001 to 2002. Here the evolution of the gravity signal over the monitoring period will be discussed with regard to the possibility of further subsidence.

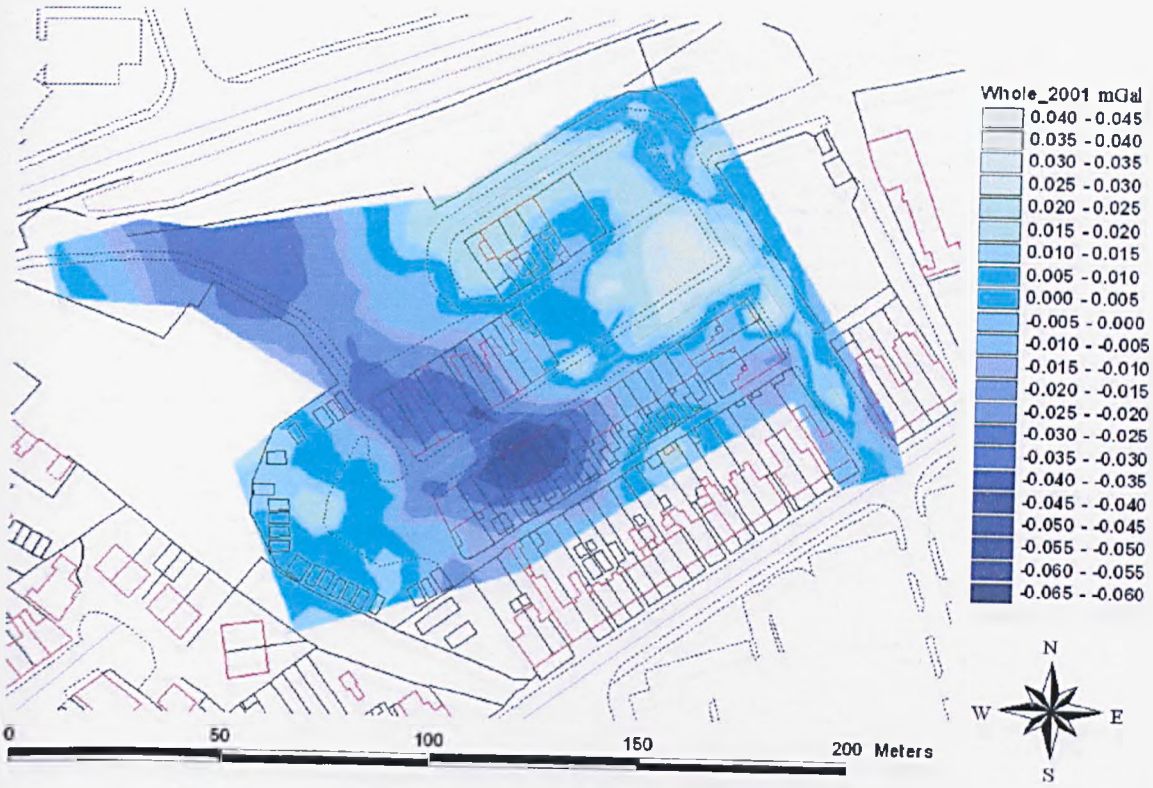




*Fig. 5.3 Contour map of the entire 2001 microgravity survey. Negative values of gravity are shown as dark blue. The main feature is a large negative anomaly (up to -60μGal) striking NW-SE across the survey area. A secondary negative anomaly can be seen to branch off this main anomaly up towards the NE towards the area in which the houses were demolished in 1985.*

The same features have been identified in the 2002 survey (Figure 5.4). The main negative anomaly that trends across the survey area in a NW-SE orientation is still present as is the secondary anomaly in the area where the maximum subsidence has been recorded.

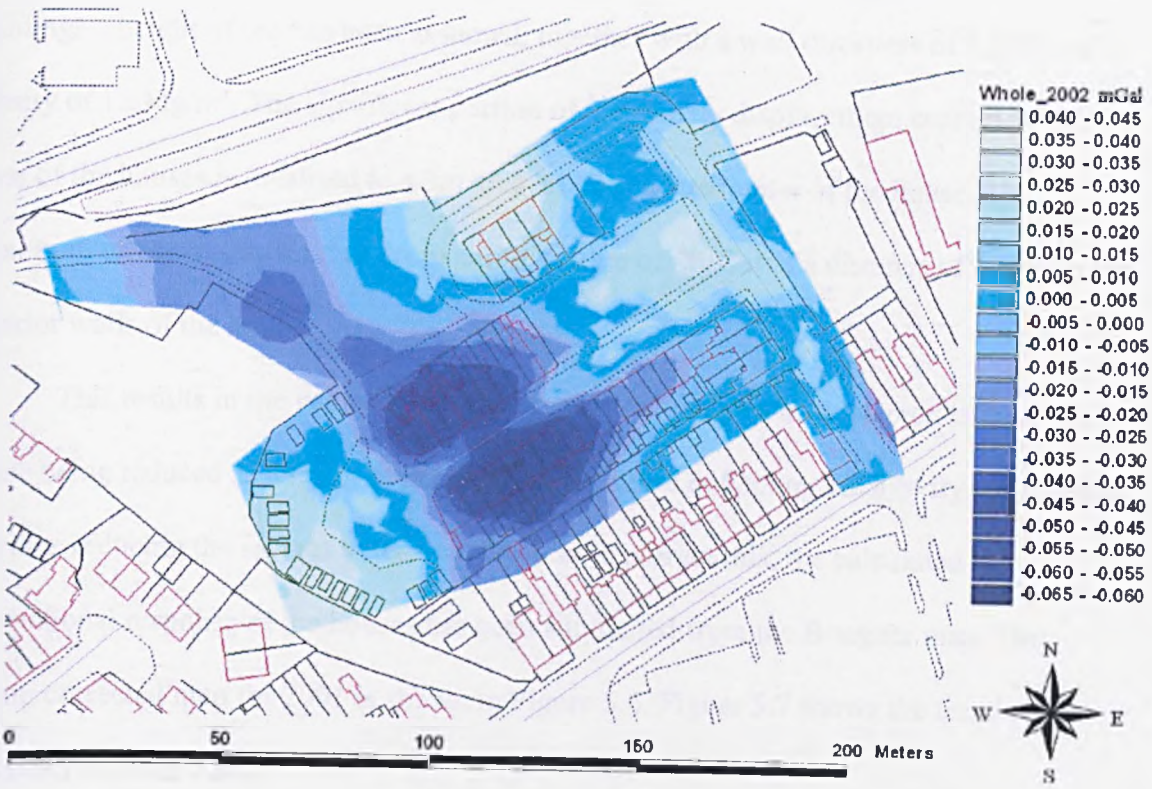




*Fig 5.4 The entire 2002 microgravity survey displayed as a contour map. Negative gravity values are denoted by dark shades of blue. The main feature identified in the 2001 survey can also be seen in this survey. That is a large negative anomaly trending NW-SE. Again a second linear anomaly can be seen to branch off this main anomaly towards the NE. However, the amplitude of this anomaly has become less negative over the monitoring period.*

### 5.3.1 Correcting for the gravitational effect of buildings

In this urban setting it is important to consider what effect the mass of the houses will have on the recorded gravity. In this setting, the houses can be treated as a terrain effect and so can be corrected for by applying a terrain correction (see Chapter 3). To investigate the extent and amplitude of the gravity anomaly caused by the house, the

terrain effect has been calculated and is displayed in Figure 5.5. In order to describe the buildings a height of 6m has been assumed, together with a wall thickness of 0.25m and a density of 1.6Mg/m$^3$. The significant portion of the gravity displacement created by the mass of the houses is localised to a 3m area around the perimeter of the house. The maximum effect is -25μGal but drops off to a value of -3μGal at a distance of 3m from the exterior walls of the house.

This results in the values of gravity recorded at stations in close proximity to the house being reduced as a result of the mass of the house deflecting the gravity meters mass and thus reducing the springs extension. In order to correct this, the calculated gravitational response of the houses has been subtracted from the Bouguer map. The terrain corrected map for 2001 is shown in Figure 5.6. Figure 5.7 shows the terrain-corrected map for 2002.

In both Bouguer gravity maps, a local trend dipping at 1.34 mGal / km to the SW was present. Owing to the small extent of the area, a first order polynomial was fitted to the data and removed from both data sets in order to highlight the local gravity anomalies.

The positions of the gravity stations for the 2001 and 2002 surveys are shown in Figure 5.5. It should be noted that no data was collected from the area occupied by the remaining houses. Anomalies, which appear within this area, are simply functions of the contouring process.

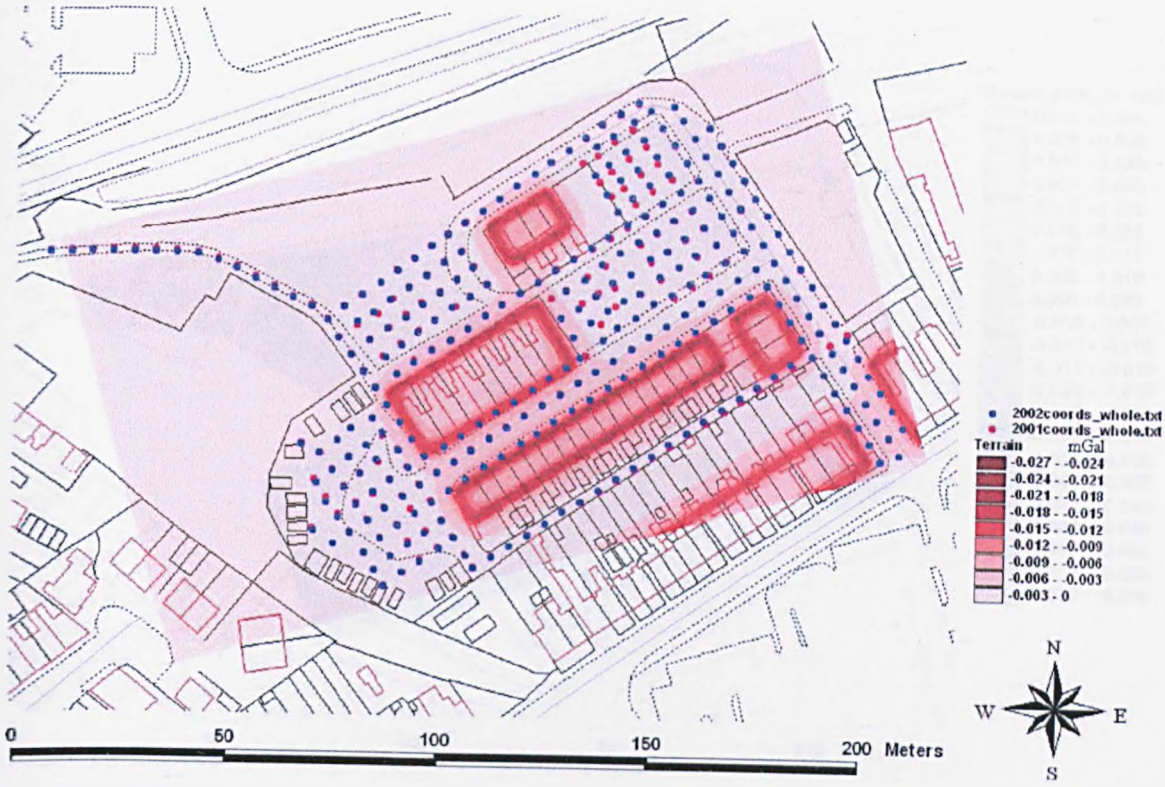




*Fig. 5.5 The gravity effect of the houses in and around Peter street has been calculated and is displayed here together with the station locations for the 2001 and 2002 gravity surveys. It can be seen that the gravity displacement caused by the mass of the house, although large, is quite localised.*

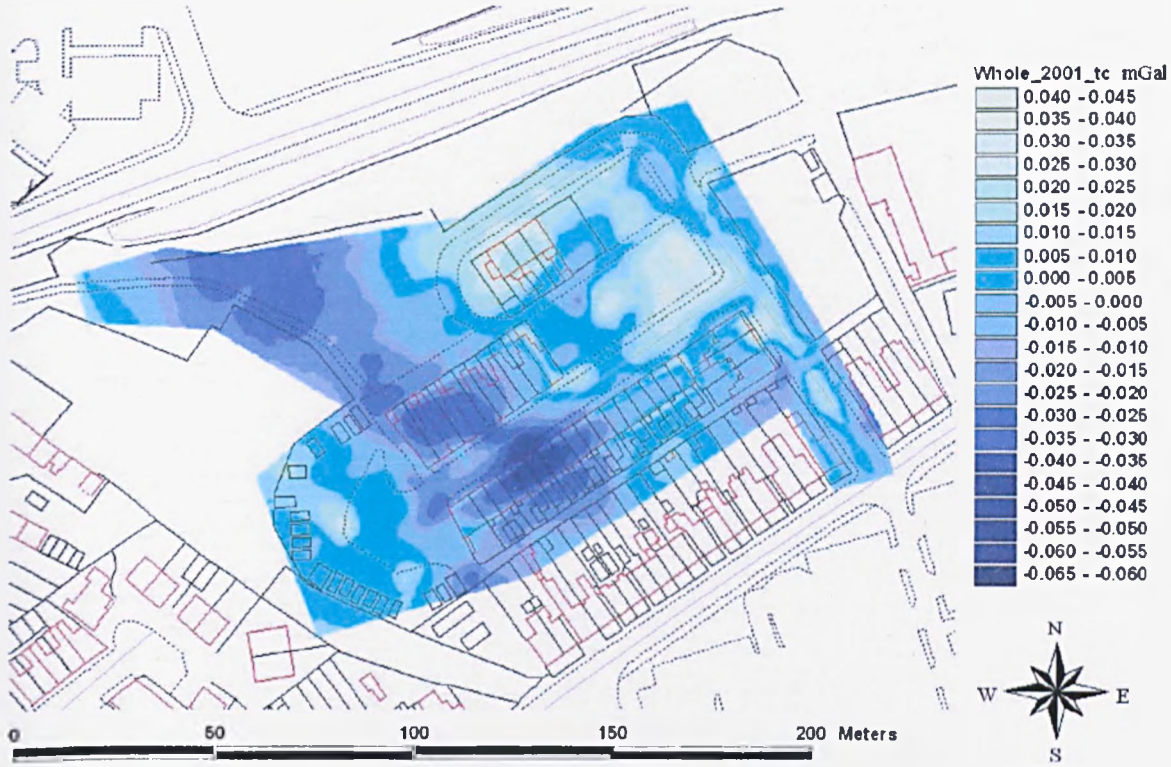




*Fig. 5.6 The Bouguer gravity map for the 2001 data set after the terrain effect of the buildings has been corrected for.*

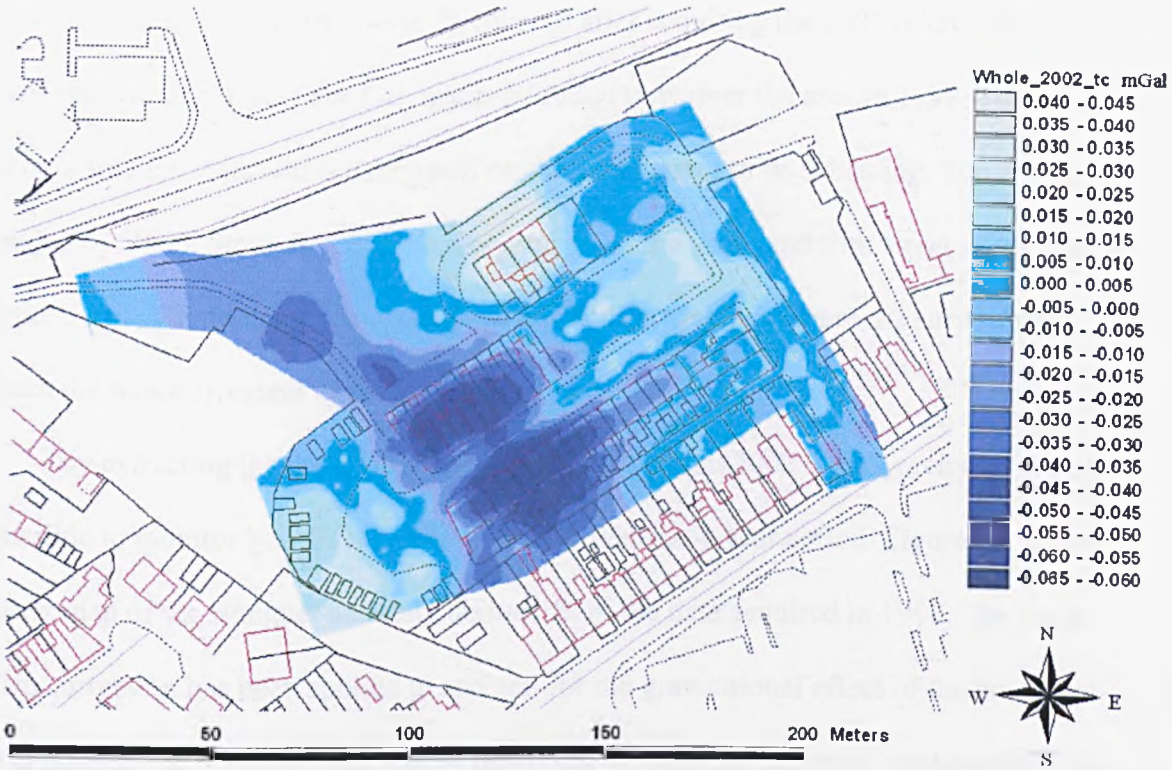




*Fig.5.7 The Bouguer map for 2002 after the terrain effect of the buildings has been corrected for.*

Once the gravitational effect of the houses has been subtracted, positive lineaments can be seen to run along the walls of some of the houses. Comparing these areas with the position of the gravity stations shows that they occur in areas where the stations are not located in close proximity to the buildings. Hence the effect of the buildings gravitation pull has not been recorded during the acquisition, resulting in the over correction of the recorded gravity values. In areas where the gravity stations do encroach on the buildings these positive lineaments can be seen to disappear, leaving undisturbed contours, confirming that the terrain correction has been successful.

### 5.3.2 Microgravity acquired around the area of principle subsidence

As mentioned earlier, it was discovered after acquiring the 2001 microgravity survey that Golder Associates Ltd. had acquired gravity over the area in 1998. The survey was on a smaller scale and concentrated on the area known to be subsiding. The area is bounded by Wade Street to the north, Peter Street to the south and Elm street to the east (Figure 5.1b). The footpath that extends in a NW direction away from the survey area defines the westerly extent of the area.

By extracting the coincident data from the 2001 and 2002 microgravity surveys it is possible to monitor how this area has evolved over the 4-year period. Figure 5.8 shows a contour map of the Bouguer anomaly derived from the data acquired in 1998. The same terrain correction has been applied to account for the gravitational effect of the houses as was applied to the previous data sets. A first order polynomial has been removed from the data set to account for localised geology. The same polynomial has been subsequently been removed from both the 2001 and 2002 data sets.

The 1998 microgravity survey detected a small negative anomaly (A) in the area of the experiencing subsidence. Its amplitude is approximately -15μGal and the anomaly extends in a NE-SW direction.

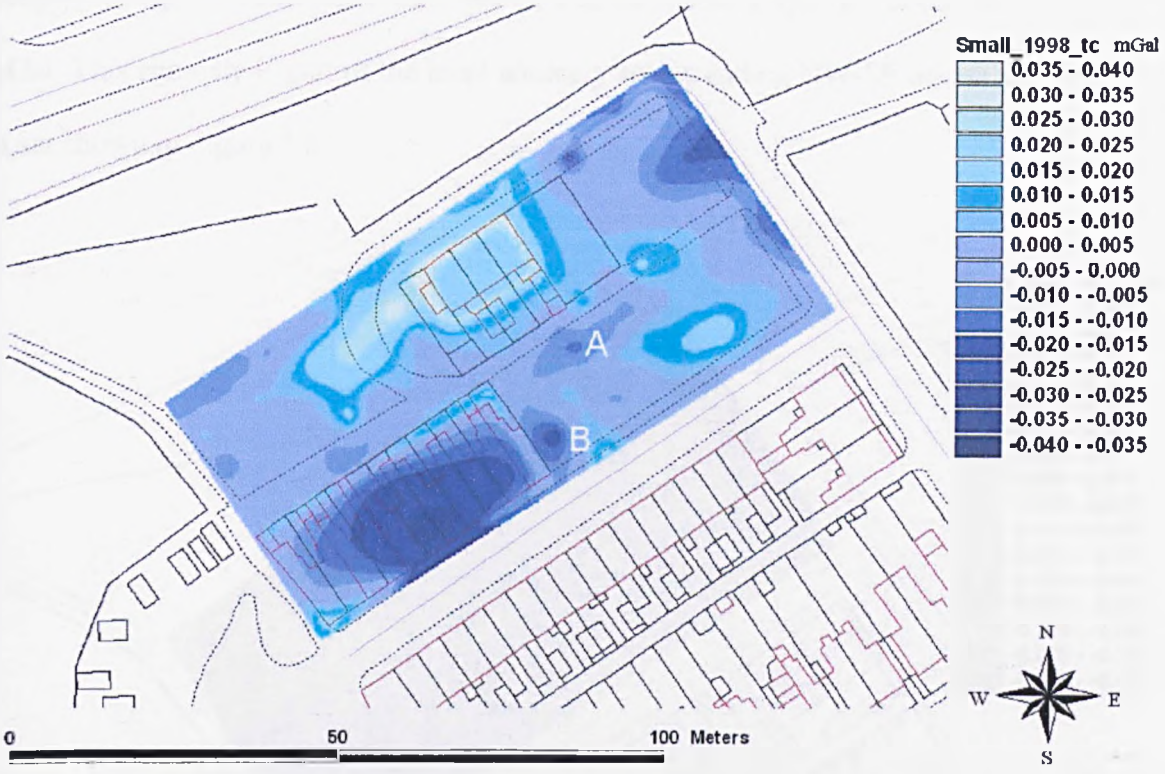




*Fig.5.8 A contour map of the gravity data acquired in 1998. A first order polynomial has been removed from the data after the gravitational effect of the buildings has been corrected for.*

A second, more localised anomaly (B), was recorded south of anomaly A. Anomaly B has an amplitude of -20μGal and is circular in extent.

Investigating the area of the 2001 microgravity survey that is coincident with the 1998 survey (Figure 5.9) it becomes evident that the area has been mobile between 1998 and 2001. Anomaly A has grown in amplitude and extent. Its amplitude is now -25μGal, and it has broadened towards the NE, extending onto the waste ground left by the demolition of the houses in 1985. Anomaly B is still evident although it appears to remain relatively constant in amplitude and extent. However, the area to the west has become

increasingly negative resulting in anomaly C. The maximum amplitude in this area is -20μGal. This anomaly is part of the large anomaly seen trending NW-SE across the 2001 data set shown in Figure 5.6.

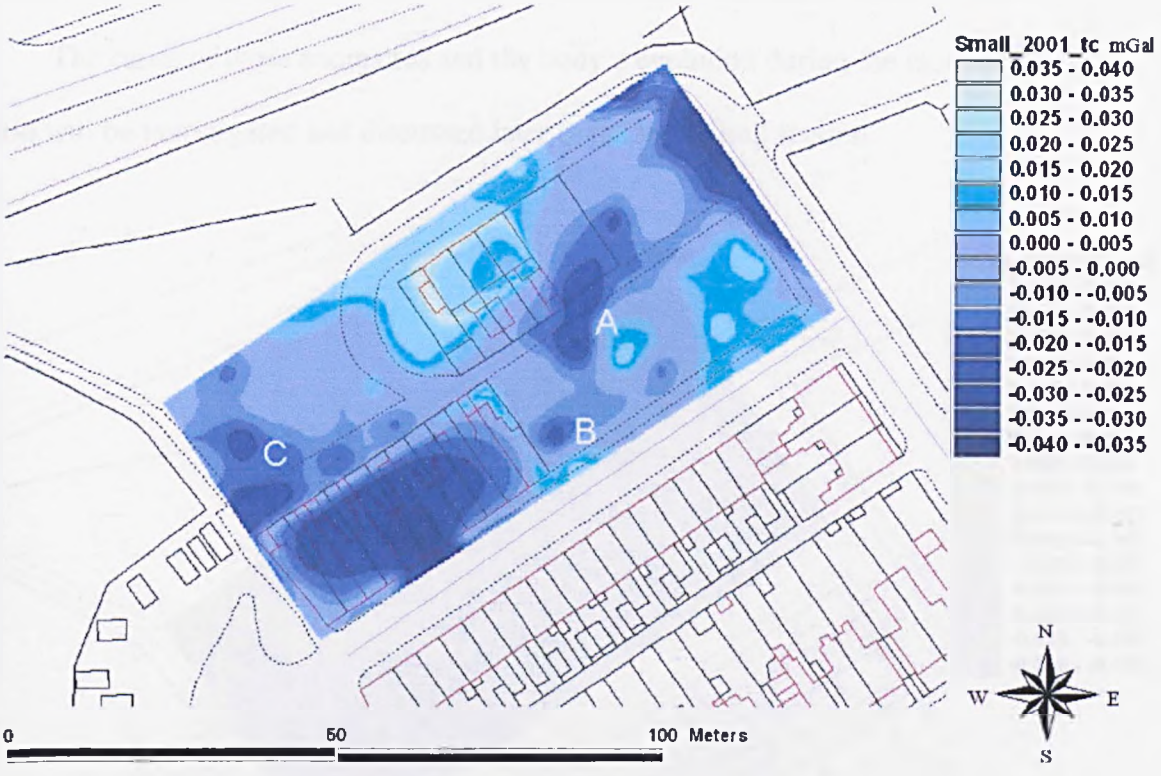




*Fig.5.9 A contour map of the gravity data extracted from the 2001 microgravity survey. A first order polynomial has been removed from the data after the gravitational effect of the buildings has been corrected for.*

Figure 5.10 shows the equivalent extract from the 2002 microgravity survey. Although the monitoring period is shorter, it is evident that the area has also been active during this period. Interestingly, anomaly A has decreased in amplitude to -12μGal. The cause of this will be investigated in the modelling section. Anomaly B remains consistent with the 1998 and 2001 surveys. Its amplitude and extent has remained relatively constant.

Alarmingly, anomaly C has continued its growth and now has an amplitude of -30μGal. The NE of the grid is the second area where the value of gravity has continued to decrease. Anomaly D appears to be the development of the NE extension of anomaly A seen in the 2001 survey. It has a large extent, some $20m^2$, with maximum amplitude of -35μGal.

The cause of these anomalies and the body's evolution during the monitoring period will be investigated and discussed later in the modelling section.

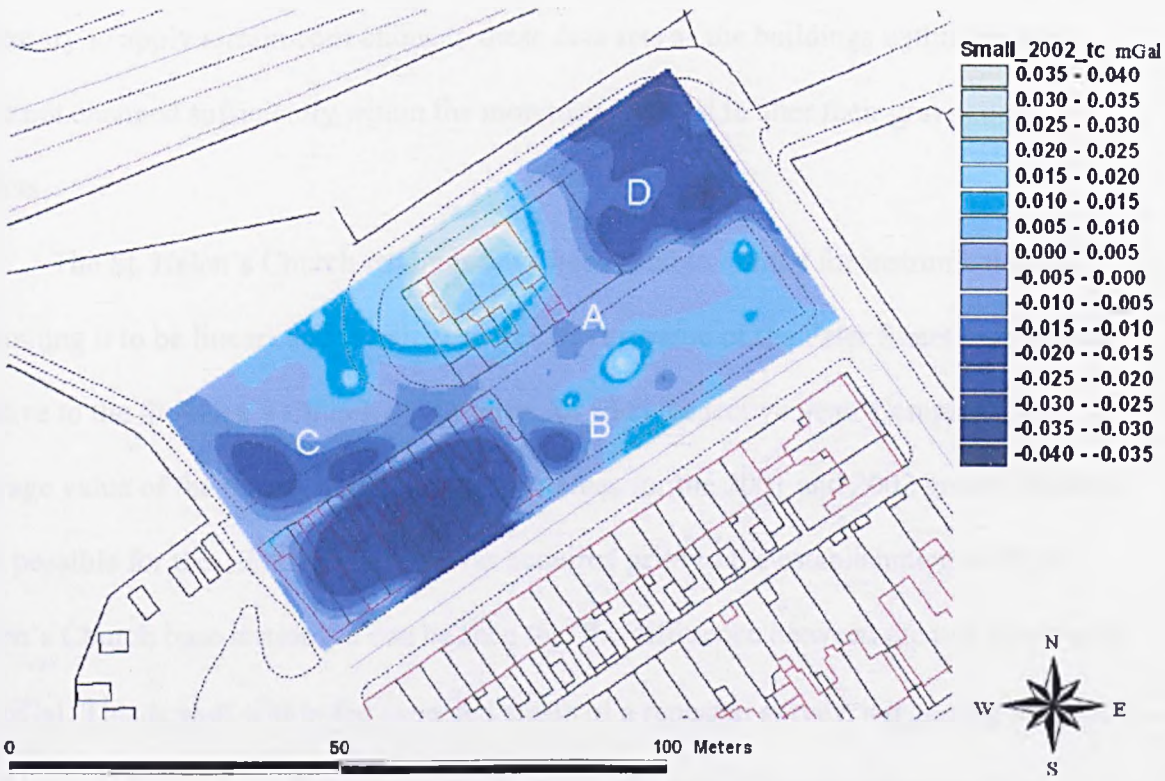




*Fig.5.10 A contour map of the gravity extracted from the survey acquired in 2001. A first-order polynomial has been removed from the data after the gravitational effect of the buildings has been corrected for.*

### 5.3.3 The change in gravity at Peter Street

By plotting the change in gravity it is possible to investigate the evolution of the gravity field in the area. Using the St. Helens church base station as a control it is possible to reduce the relative gravity measurements to the same datum before the most recent survey has the previous survey subtracted from it. The data sets used for this have not had any polynomial surfaces removed from them. It is important that the gravity data have been through exactly the same reduction steps to avoid systematic errors. It is not necessary to apply terrain corrections to these data sets as the buildings within the area have not changed sufficiently within the monitoring period to alter their gravitational effects.

The St. Helen's Church readings have been used to correct for instrument drift (assuming it to be linear) and to calculate the gravity value of the Peter Street base station relative to the St Helen's Church base station for each respective year. Comparing the average value of the Peter Street base station values for the 2001 and 2002 gravity surveys (not possible for the 1998 survey as it was acquired prior to the establishment of the St Helen's Church base station), it can be seen that the difference between the two surveys is 1.5 μGal. This is well within the expected errors of a repeated survey, suggesting that the local base station at Peter Street has not changed in the period between surveys. It is necessary to average the Peter Street values to account for Earth tides variations during the day (as the tidal variations are sinusoidal their average will be zero).

While comparing data sets from different years the more recent survey has always had the older survey subtracted from it. This results in increases in negative anomalies between surveys showing up as negative changes. Conversely, positive changes in gravity between surveys will show as a positive change on the difference plot.

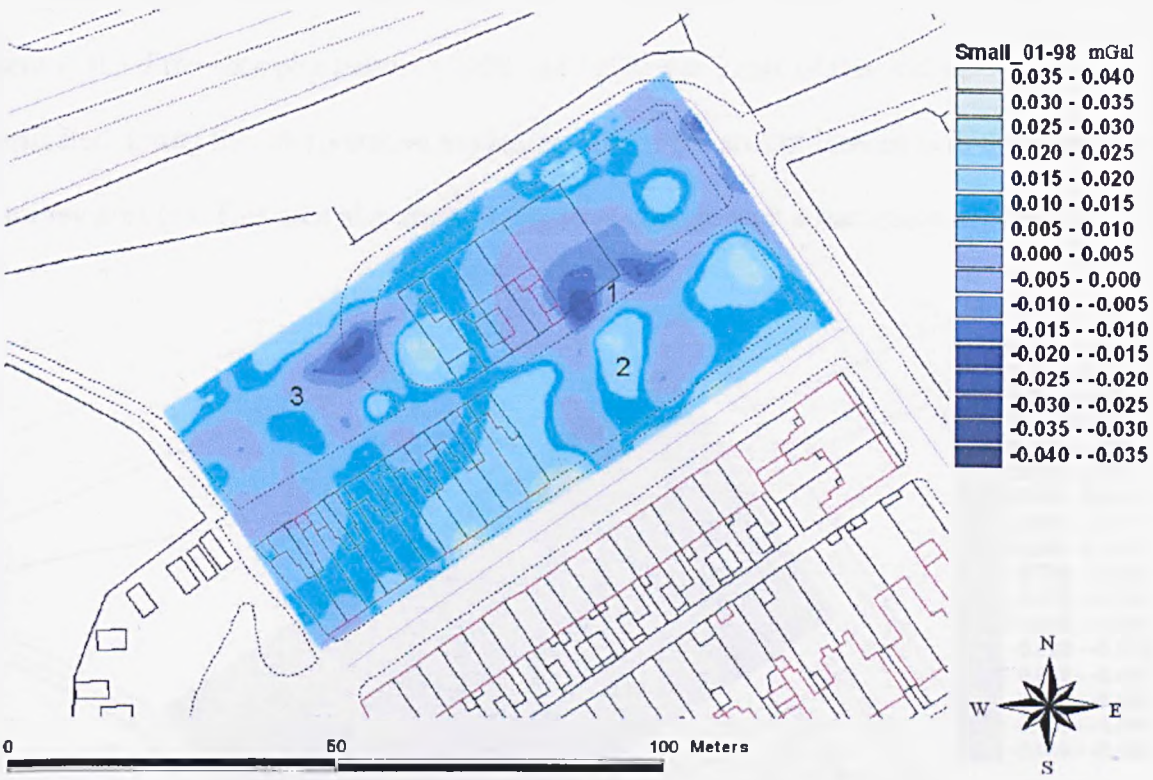




*Fig. 5.11 A contour map of the gravity change between 1998 and 2001. Both sets of data have been reduced using the same parameters before being contoured on to the same grid where a simple subtraction is calculated. Local geology and terrain corrections are automatically accounted for as their causes have not changed significantly over the monitoring period.*

Figure 5.11 shows that there is a high degree of negative change in the area around the principal subsidence (1). The area of negative change also extends southwards towards Peter Street. At its maximum a change of -35μGal has been recorded This is well above the expected error of a time-lapse microgravity survey (~15μGal), and so we must conclude that the causative body, or zone has been active during this time period.

Interestingly, there has also been a positive change in the area (2). This is also present in the difference plot between 2002 and 1998. The cause of this will be investigated during the interpretative modelling. The other area of interest is in the west of the survey area (3). This area also shows a negative change with a maximum of -25μGal.

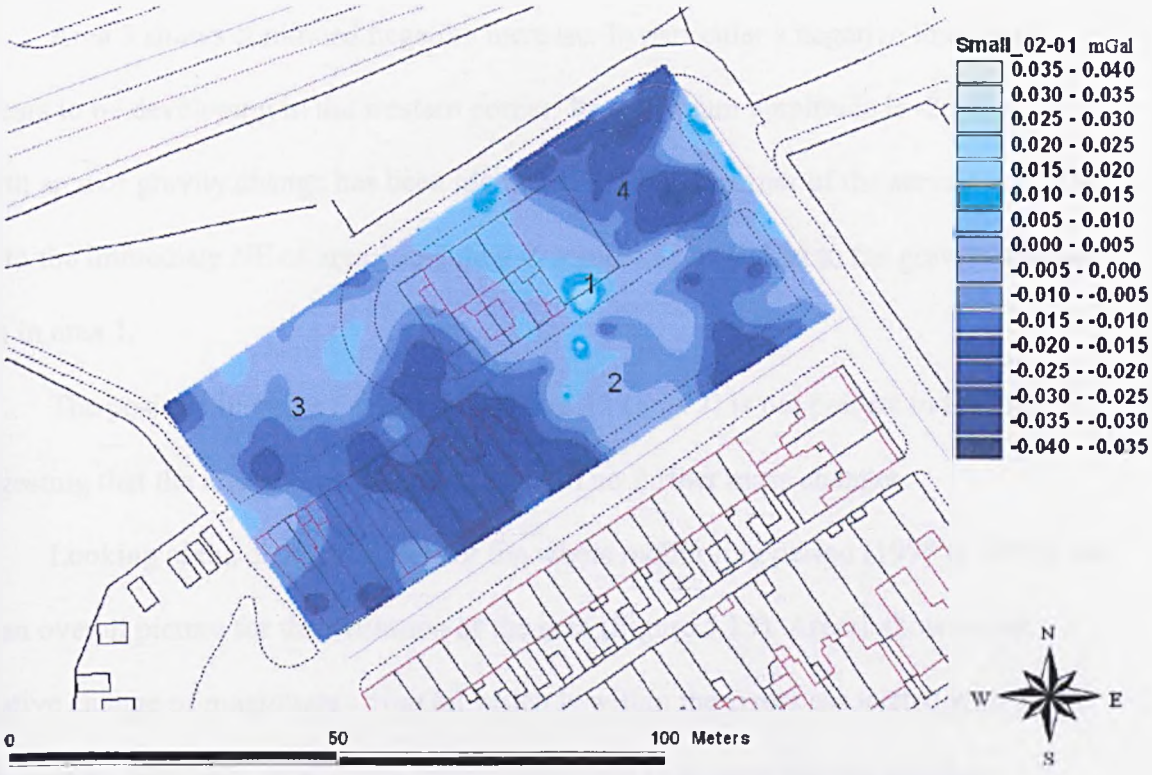




*Fig. 5.12 A contour map of the gravity change between 2001 and 2002. Both sets of data have been reduced using the same parameters before being contoured on to the same grid where a simple subtraction is calculated. Local geology and terrain corrections are automatically accounted for as their causes have not changed significantly over the monitoring period.*

Plotting the difference between the 2002 and 2001 microgravity surveys, shows how the areas identified in Figure 5.11 have evolved. Area 1 shows a decrease in negative

anomaly size i.e. the area has become more positive by approximately +10μGal. This is within the errors associated with a time-lapse microgravity survey, however, its spatial distribution also suggests that the area has been active between monitoring surveys. The possible cause of a reduction in the negative anomaly is investigated in the modelling section.

Area 3 shows continued negative increase. In particular a negative lineament appears to be developing in the western corner. Its maximum amplitude is -20μGal. A fourth area of gravity change has been identified in the NE corner of the survey grid. This lies to the immediate NE of area 1 and may in some way be linked to the gravity increase seen in area 1.

The positive increase evident in Figure 5.11 (area 2) is not present in this plot suggesting that the area has remained stable with no further mass changes.

Looking at the difference plot for the whole monitoring period (1998 to 2002), we get an overall picture for the evolution of the area (Figure 5.13). Area 1 shows a net negative change of magnitude - 10μGal which is within the errors associated with a time lapse survey. However, as we have intermediate data to suggest that the area has undergone increased negative change, we can be sure that this is in fact a real gravity change. If the intermediate data was not available the gravity change may be interpreted a result of re-surveying errors.

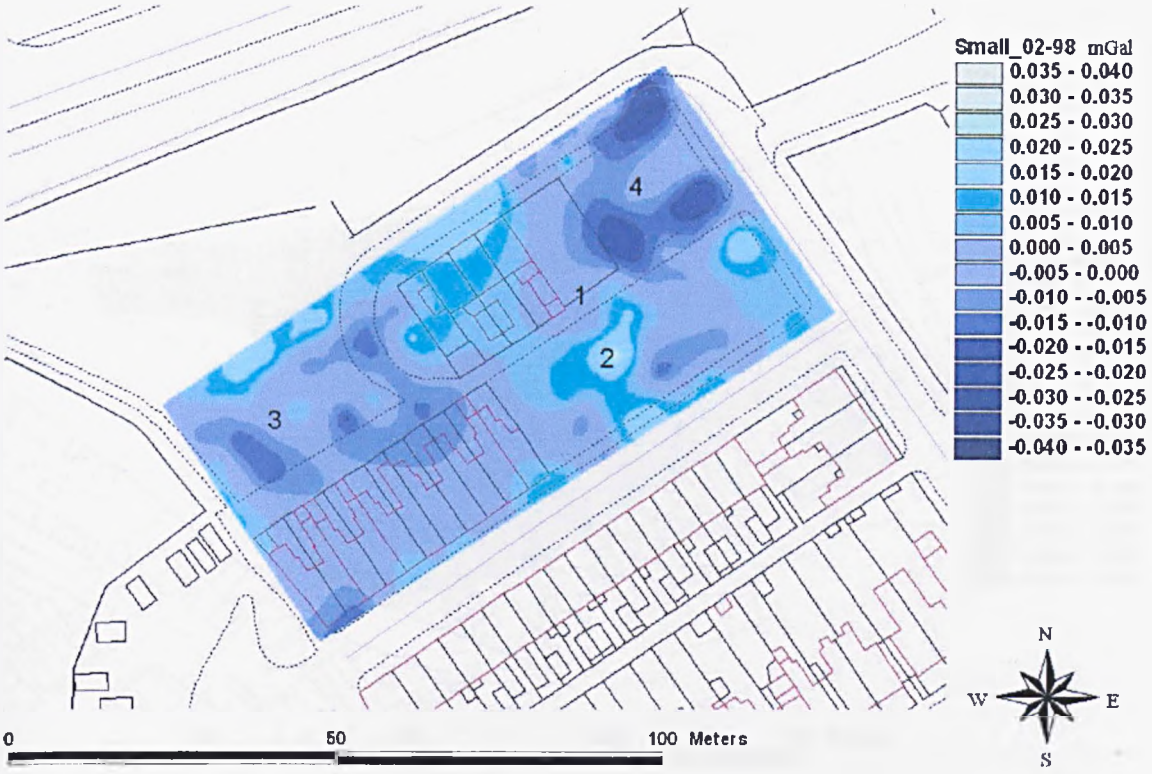




*Fig. 5.13 A contour map of the gravity change between 1998 and 2002. Both sets of data have been reduced using the same parameters before being contoured on to the same grid where a simple subtraction is calculated. Local geology and terrain corrections are automatically accounted for as their causes have not changed significantly over the monitoring period.*

Area 2 shows a net positive change. This again suggests that the change occurred between the 1998 and 2001 surveys. As its maximum amplitude is +35μGal it cannot be ignored and will be discussed in the modelling section.

The other areas of interest, area 3 and 4 show net negative increases of -15μGal and -20μGal respectively.

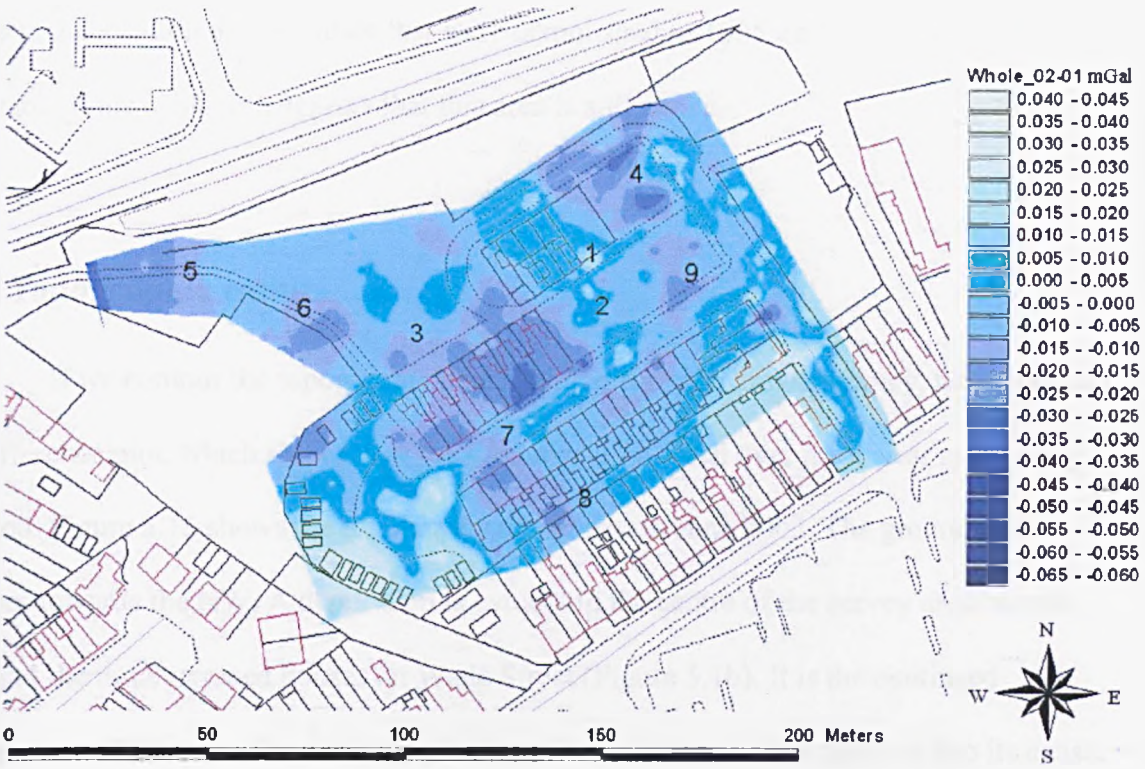




*Fig. 5.14 A contour map of the gravity changes between 2001 and 2002 for the whole of the survey area. Both sets of data have been reduced using the same parameters before being contoured on to the same grid where a simple subtraction is calculated. Local geology and terrain corrections are automatically accounted for, as their causes have not changed significantly over the monitoring period.*

Expanding the plot to look at the gravity changes over the entire area (Figure 5.14), we see that the increases in negative gravity are not confined to the area of principal subsidence. Of particular interest are the areas of gravity change trending NW-SE across the site, areas 5-8. The amplitude of these changes ranges between -15μGal and -25μGal (therefore above the expected error of the survey) but it is their spatial distribution that draws attention to the situation.

Area 9 would also appear to have links with area 4 and to areas south and east. This is the location of the houses that were demolished in 1985 after they had become unstable. This evidence suggests that this area is still active.

## 5.4 Topographic results

If we contour the topographic data acquired for each gravity survey, we can create a difference plot, which shows how the ground has subsided over the 4-year monitoring period. Figure 5.15 shows the topography of the area in June 2002. The ground gently slopes towards the NW. A depression is evident in the centre of the survey area centred around the three terraced houses on Wade Street (Figure 5.1b). It is the continued subsidence of this area that has brought about the geophysical investigation into its cause.

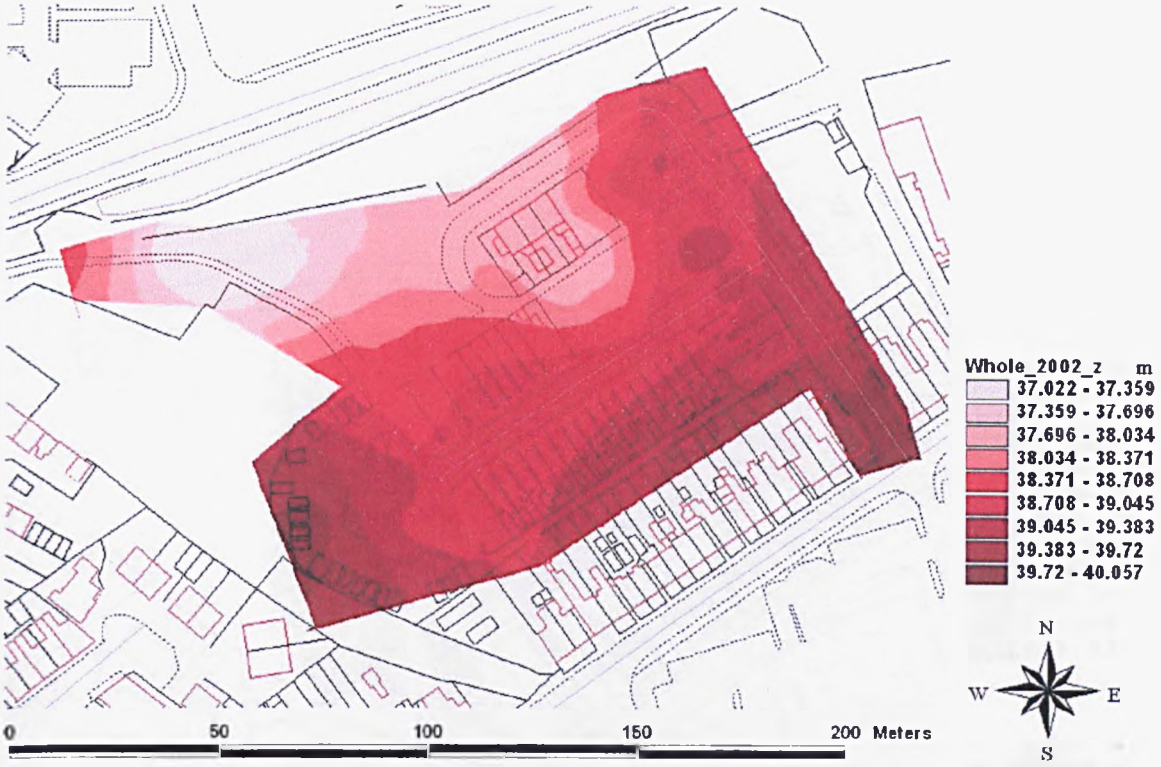




*Fig. 5.15 The topography of the area in 2002.*

Using the topographic data acquired for the microgravity survey we are able to calculate the change in topography in the area between 2001 and 2002. Figure 5.16 is a difference plot between the two data sets. It shows that the majority of the area has generally remained stable, with changes in height below ± 0.02m. Surprisingly, the exception to this is the area around the main topographic depression in the centre of the survey. In the period between the 2001 and 2002 microgravity surveys this area has increased in height by up to 0.15m.

We can investigate this further by plotting the topographic data for the area around the main depression. This enables us to track how the topography has changed between 1998 and 2002.

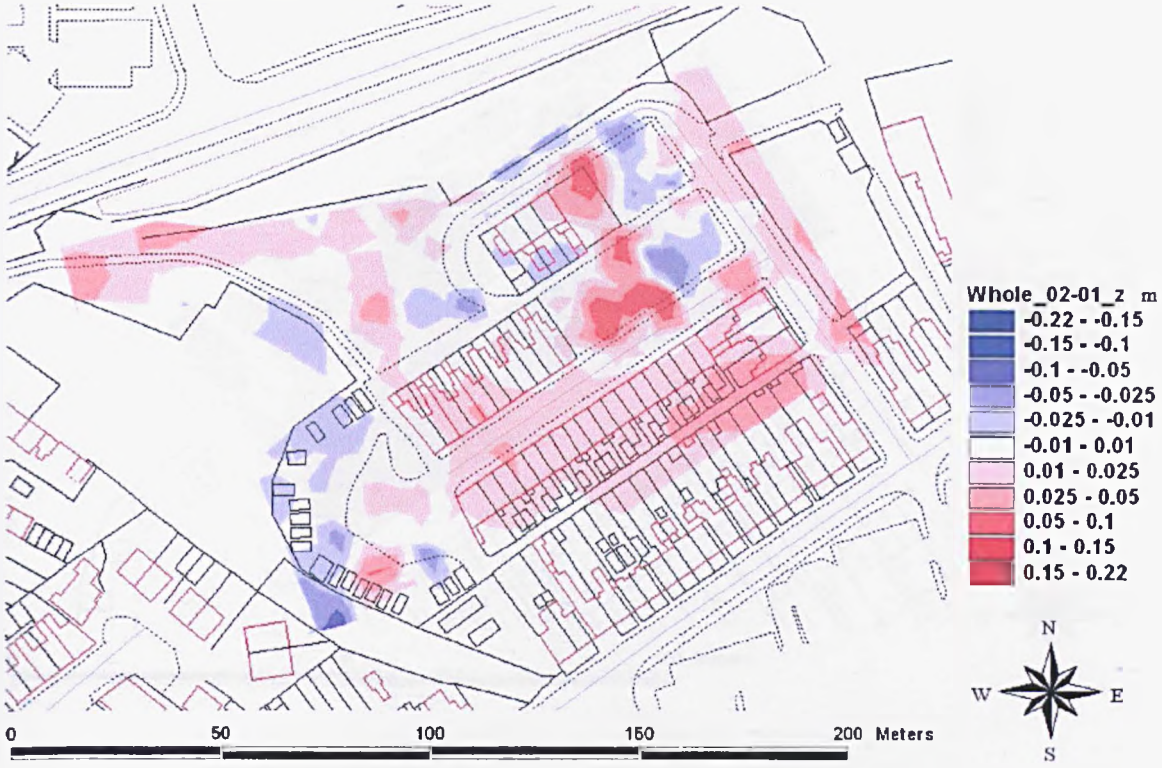




*Fig. 5.16 The change in height over the one-year monitoring period between 2001 and 2002 has been calculated using the topographic data from the gravity surveys.*

We can see that in the period between 1998 and 2001 there has been major subsidence in this area (Figure 5.17). The maximum amplitude of the subsidence is 0.22m. The area of subsidence stretches over approximately $30m^2$. In fact it covers an area greater than that covered by the negative gravity anomaly recorded in 2001 (Figure 5.9).

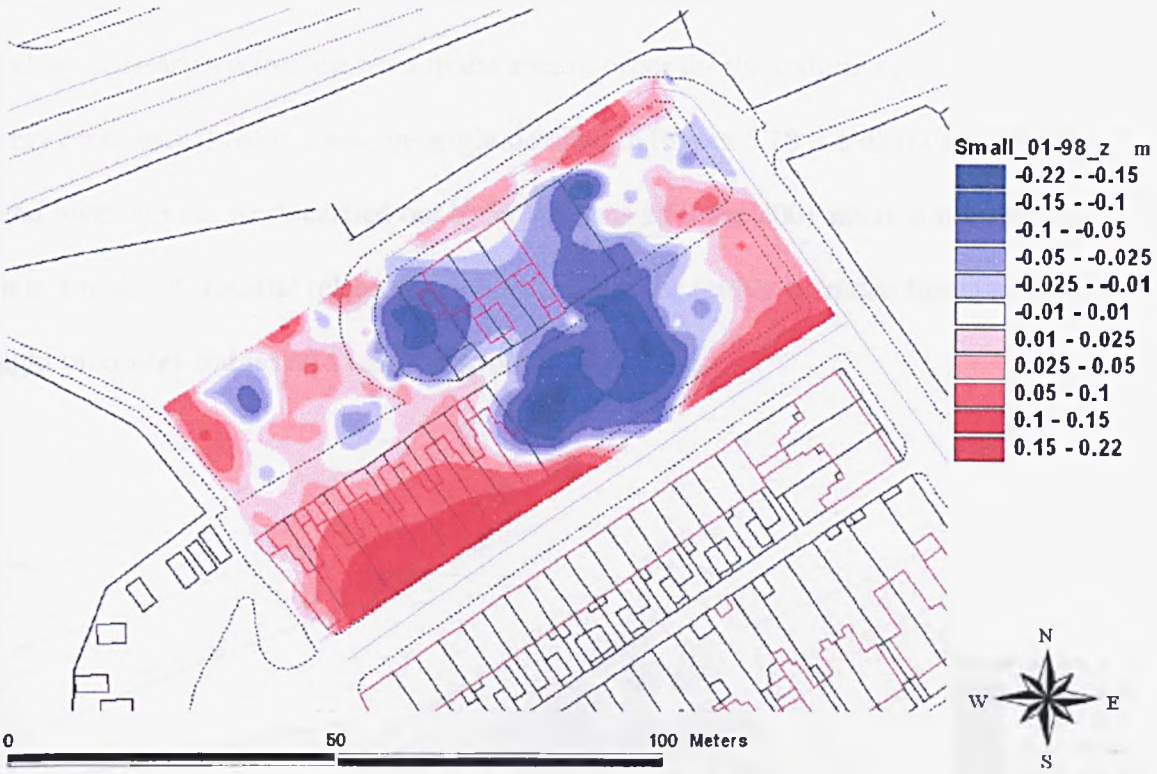




*Fig. 5.17 The change in height between the 1998 and 2001 microgravity surveys has been calculated using the topographic data from the gravity surveys. The areas of maximum subsidence are located around the site of the demolished houses.*

Looking at the equivalent plot for 2001 – 2002 (Figure 5.18) we see the increase in height of this area in more detail. The area in which the height has increased covers an area approximately half that of the initial subsidence. The likely cause of this surprising increase in height of an area that has a history of subsidence is related to the ground investigation work carried out by WS Atkins after the 2001 microgravity survey. As part of the ground investigation work a borehole was drilled in the area (see section 5.7) this required the resurfacing of the track running from Elm Street down to the first block of

terraced houses (an increase of between 0 and 0.05m has been recorded in this area). It was also necessary to clear the trees in the area in order for the drilling rig to gain access. It is my opinion that the increase in height detailed in Figure 5.18 is a direct result of the ground investigation work carried out by WS Atkins after the 2001 microgravity survey. i.e. it is a result of material related to the drilling process (either extruded from the hole or brought onto site) and is not a result of ground up-welling.

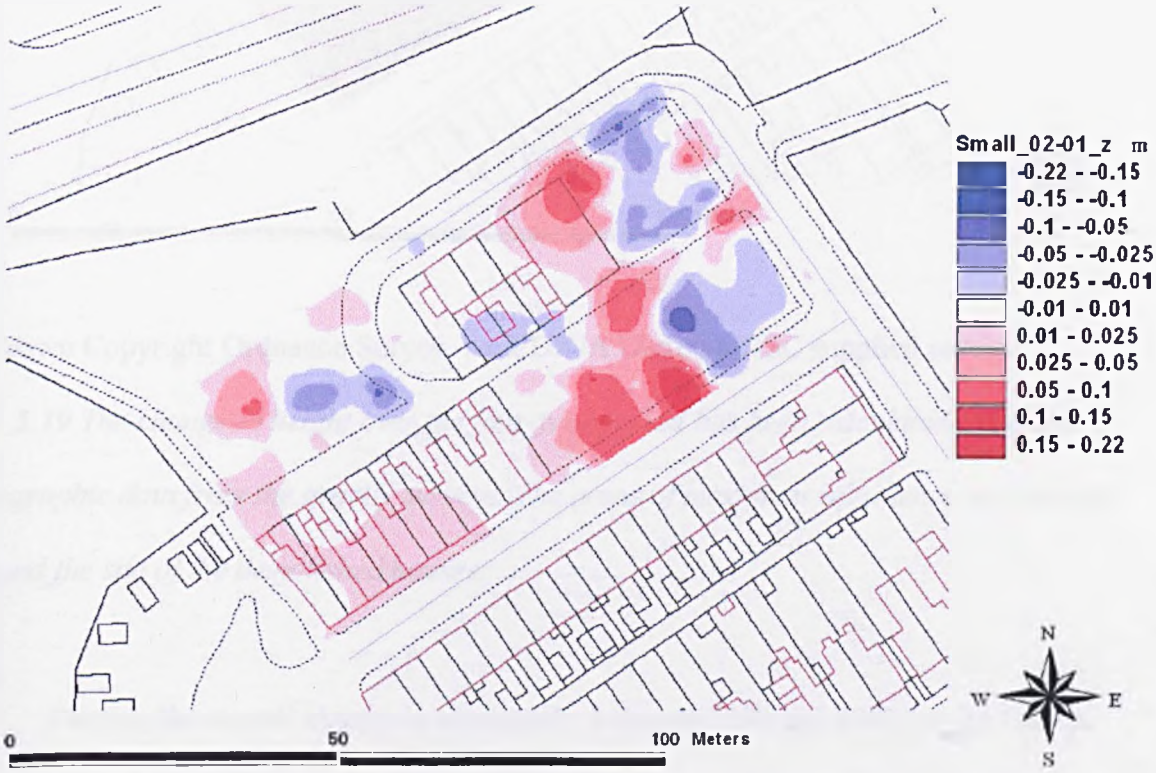




*Fig. 5.18 The change in height between the 2001 and 2002 microgravity surveys has been calculated using the topographic data from the gravity surveys. An area of increased elevation around the main subsidence depression is thought to be related to the ground investigation undertaken between the two surveys.*

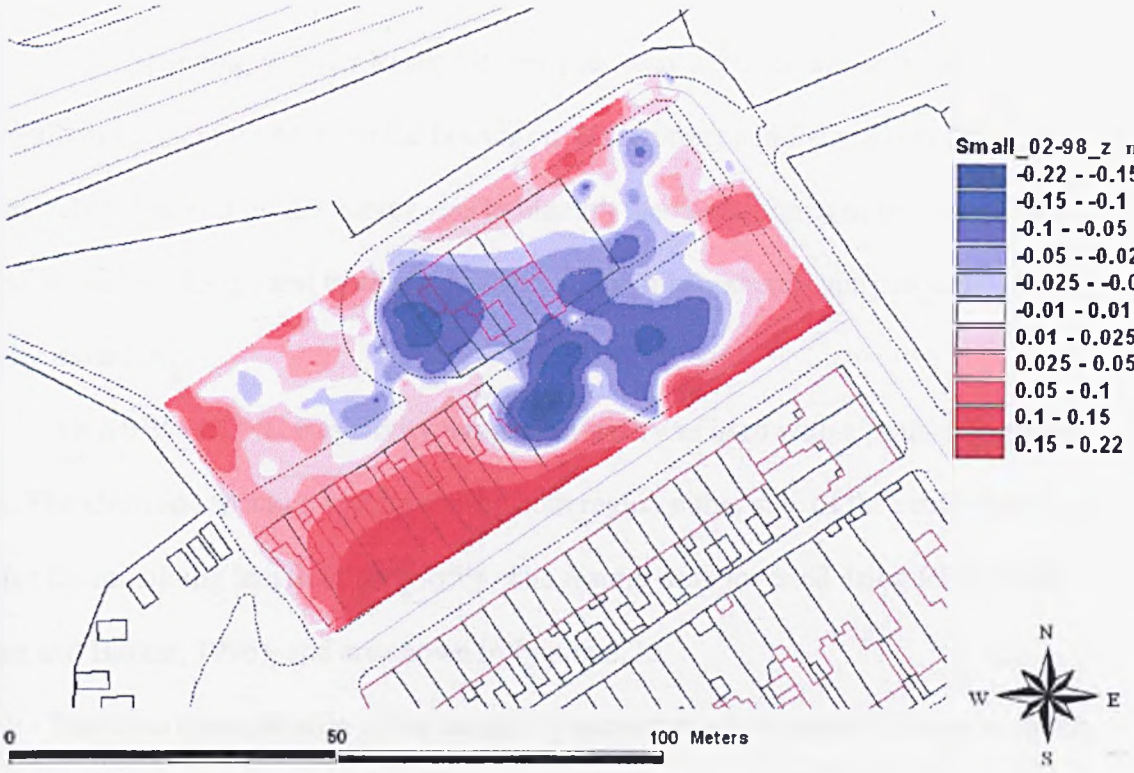




*Fig. 5.19 The change in height over the four-year period has been calculated using the topographic data from the gravity surveys. The areas of maximum subsidence are located around the site of the demolished houses.*

Plotting the overall change in topography between 1998 and 2002 we see that the net change in topography is a negative one representing a general trend of continuing subsidence in the area. The maximum subsidence in the area is 0.22m and extends over the majority of the waste land between the back of the terraces on Wade Street and Peter Street. The band of high values along the southern edge of the grid are caused by the offset between the 1998 survey points acquired along the gutter at the edge of Peter Street and the 2001/2002 survey points acquired along the pavement. The offset is ~0.1m which equate to the height of the curb.

## 5.5 Resistivity profiling

Two expanding Wenner Resistivity profiles were acquired along Wade Street and the cinder track running between the houses on Wade Street and Peter Street (X X' in Figure 5.1b). The aim of this survey was to identify the lateral limits of the source of the negative gravity change and to eliminate some of the inherent ambiguity associated with gravity modelling.

An ABEM LUND Resistivity Imaging system was used with a profile length of 80m. The electrode spacing was 1m for the 20m region either side of the centre point and 2m for the remaining length of the profile. The results were inverted using RES2DINV (Loke and Barker, 1996), and are shown in Figure 5.20.

The main characteristic of the resistivity section is a low resistivity zone at depth, with a near surface band of higher resistivity. The lower resistivity zone extends from about 2m to 15m with resistivity values of 9-30 Ωm, typical of clay rich material. The band of higher resistivity is generally confined to the top 1m and has resistivity values of 40-80 Ωm. This zone most likely represents the dryer, more resistive material which make up the cinder track along which the profile was acquired.

Within the section, there are two anomalous areas of higher resistivity. The main resistivity anomaly is located at 10-14m along the profile and has a maximum resistivity of 55 Ωm. This anomaly coincides with the location of the main negative gravity anomaly along profile X-X'. The second resistivity anomaly is located between –2 and –7m along the profile and corresponds to a small negative gravity anomaly. However, it is less significant as the maximum resistivity contrast is only 40 Ωm and the gravity anomaly has an amplitude of only 4μGal.

*Plate 5.3 Acquisition of the resistivity survey along X-X'. The near surface consisted of cinders and was extremely dry. Salt water was used to improve the electrical contact.*

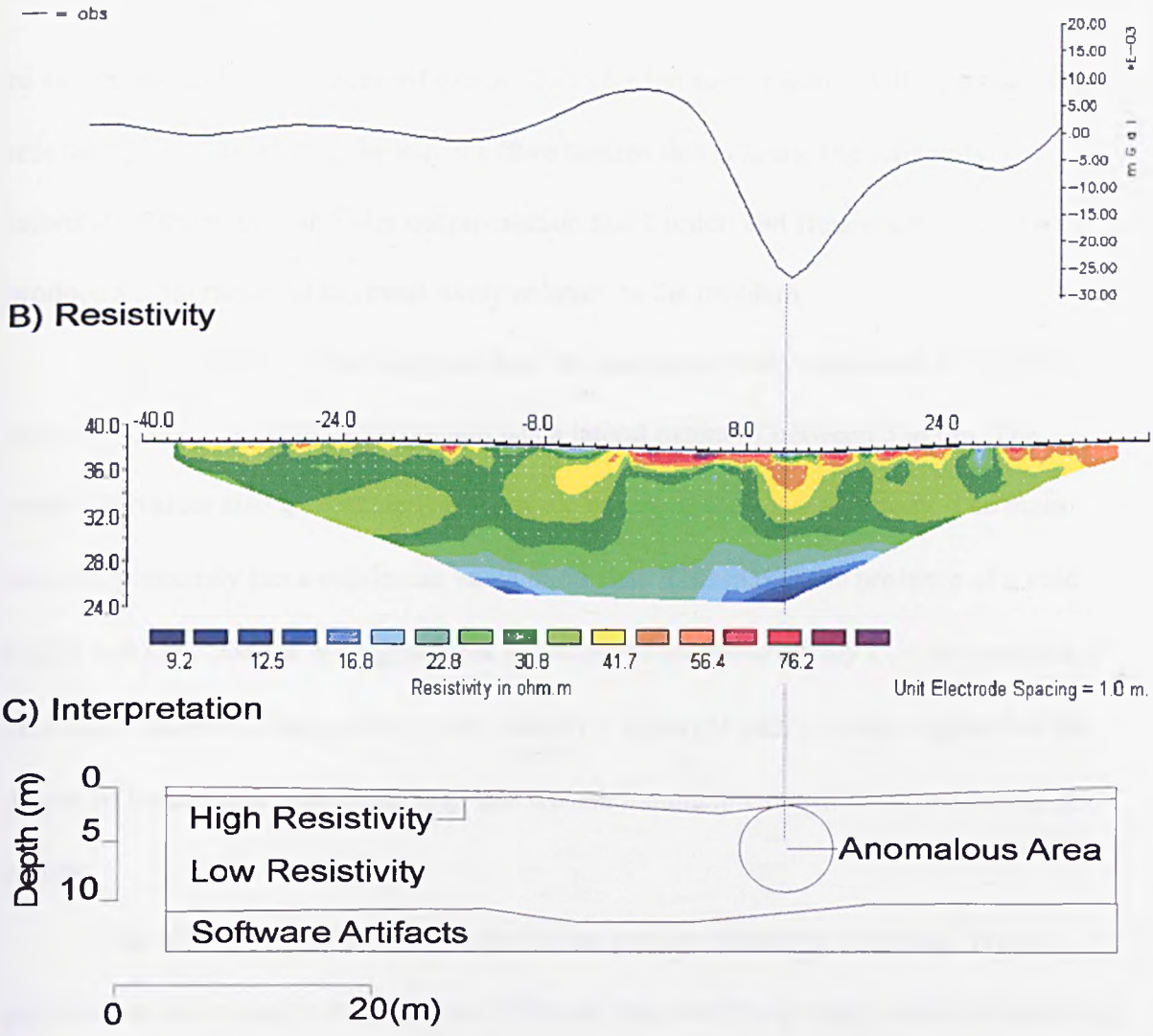


*Fig. 5.20 Plot showing the consistency between the gravity low and the anomalous area within the resistivity profile. A) Gravity profile extracted from the grided data. B) Resistivity profile acquired along XX' in August 2001. The left-hand axis is depth and relates to a local datum (ground level = 40m). C) Plot of the Schematic diagram of the qualitative interpretation that has been derived from the resistivity profile. It can be seen that there is a consistency between the gravity low and the resistivity anomaly. The simple interpretation has been used as a starting point for the 2.5D gravity model.*

## 5.6 Discussion

The interpretation of gravity data is by its nature non-unique. Many combinations of size, depth and density contrast can be found for the source which will reproduce the recorded gravity anomaly. The way we have tackled this is to use the resistivity information together with Euler deconvolution and Cordell and Henderson inversion to produce a 2.5D model of the most likely solution to the problem.

The resistivity section suggests that the anomalous body associated with gravity anomaly C lies at a depth of 3-10m and has a lateral extent of between 5 to 6m. The resistivity values also give an indication of the nature of the causative body. The main resistivity anomaly has a maximum value of 55 Ωm. This makes the presence of a void highly unlikely. Instead, it suggests that the cause of gravity anomaly C is the presence of brecciated material. The relatively low resistivity value (55 Ωm ) would suggest that the degree of brecciation is low and from this we can assume the density contrast would also be low.

This allows us to place constraints on the gravity modelling solutions. We can assume that the causative body is 5-6m wide and therefore the primary means of matching the observed wavelength of the gravity anomaly is to vary the depth of the body. We can also take into consideration that the resistivity section suggests that the top of the anomalous body is situated at a depth of 3 m.

We can further constrain the gravity model by taking into account the likely cause of the anomalous body. The area of Northwich has a long history of salt-related subsidence (Bell, 1975). Away from the main mines (as here) the principal cause of subsidence is the dissolution of salt at the wet rock head. This is caused by ground water coming into contact with the top of the salt bed and subsequently dissolving it. The cavity may then propagate towards the surface through a series of roof collapses, back-filling the cavity

with brecciated material. Compaction of the brecciated material by the weight of the overlying strata can then lead to subsidence at the surface. If we assume the body was created by this mechanism and has propagated towards the surface in a similar manner, we can limit the possible dimensions of the body during modelling.

## 5.7 Intrusive investigation

During August 2001 a borehole was sunk in the Peter Street area at the location shown in Figure 5.21. The drillers log enables us to add geological units to the 2.5D model. Estimates of the densities of the units have been assigned to the 2.5D model in order that a realistic geological model can be made within which the anomalous area can be placed. The log reports that the wet rock head aquifer was encountered at 23m depth and was under pressure (P. Skinner (WS Atkins), pers. comm.). It has been assumed that the anomalous body originates from the wet rock head and so its base has been assigned the same depth.

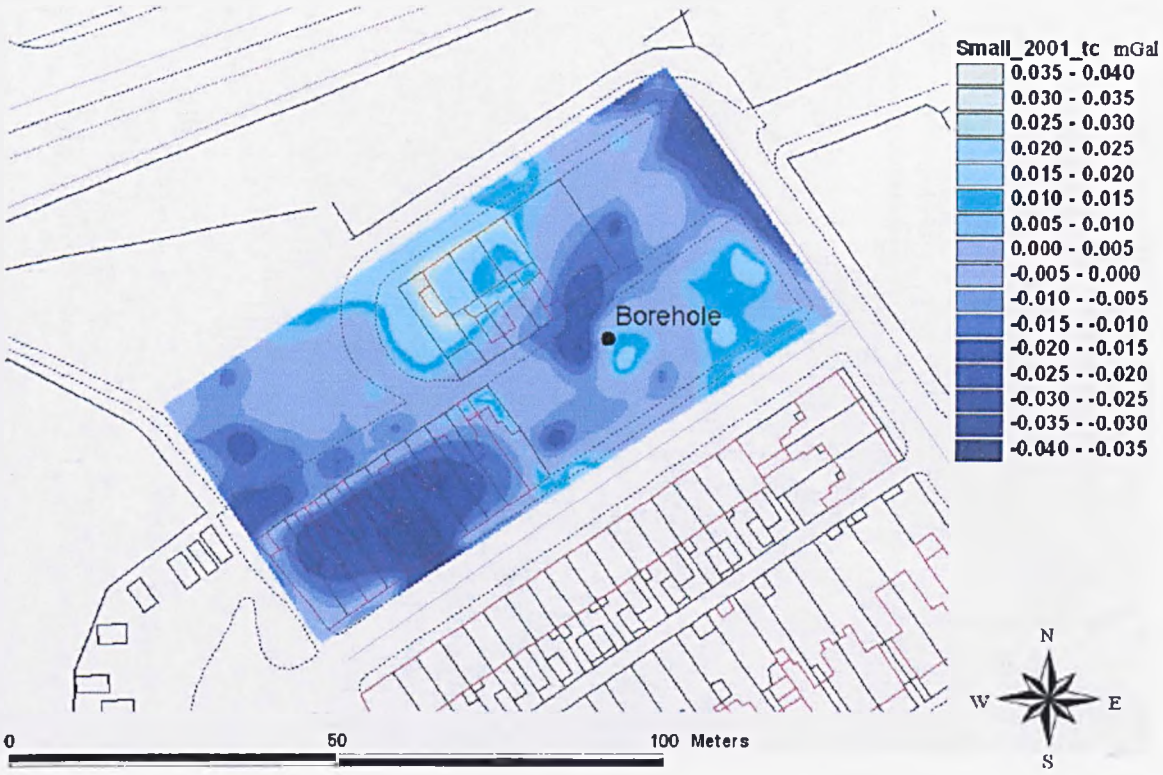




*Fig. 5.21 Figure showing the position of the borehole drilled in August 2001with the 2001 microgravity results overlain for comparison. Of note is the offset of the borehole from the negative maxima.*

Disappointingly, the borehole did not encounter a void. However, this could be a result of the location of the borehole, or indeed evidence that the causative body is a subtle transition into an area of lower density as opposed to a distinct boundary between strata and air filled void.

*Plate 5.4 Drill rig operating in the area south of the cinder track.*

| Depth (m) | Thickness (m) | Description |
|---|---|---|
| 0.0 | 1.3 | Made Ground |
| 1.3 | 1.7 | Soft light brown sandy clay |
| 3.0 | 7.3 | Stiff brown clay with sand bands |
| 10.3 | 0.7 | Gravel bed |
| 11.0 | 11.5 | Stiff dark brown boulder clay with silty sand bands |
| 22.5<br>23 | 1.5 | Weathered red marl<br>**Wet rock head aquifer encountered** |
| 24.0 | 17.7 | Red Marl |
| 41.7 | 52.3 | Salt |

*Table 5.1 Table presenting a summary of the driller's log. The location of the borehole is shown Figure 5.21.*

*Plate 5.5 Drill rig in amongst the trees. The house in the background front onto Wade Street. Evidence of the material responsible for the increase topography seen between 2001 and 2002 can be seen around the rig.*

## 5.8 Modelling of the gravity signal

Three modelling techniques have been applied to the three available data sets centred on the principal area of subsidence. The results of this have then been applied to the complete data sets, extending the interpretation to incorporate the whole area.

### 5.8.1 Depth estimates

Euler deconvolution is a method for locating the sources of potential fields based on both their amplitudes and gradients and an estimate of the probable geometry of the causative body (Thompson, 1982; Reid et al., 1990). The technique is appropriate for use in microgravity surveys where high-quality, closely spaced data are available (Chapter 3).

In this study, Euler deconvolution has been applied to several profiles, which have been extracted from the 2001, and 2002 data sets. The position of the profiles is shown in Figure 5.22. As a consequence of the large gaps in the data set caused by the presence of the houses, the application of 3D Euler Deconvolution to the whole data set was unsuitable.

In order to determine the correct depth for the body, Euler's equations have been solved for a range of structural indices. The results from this are shown in Tables 5.2 to 5.4. Profile 1 is coincident with the resistivity profile X-X'. The best agreement between the Euler depth solution and the resistivity section is obtained using a structural index of 0.6. However, all of the solutions lie within the dimensions of the body suggested by the resistivity section. Profile 2 runs across the same negative gravity anomaly but at a different orientation. Although data is missing from the start of the profile due to the houses, a good and credible solution is obtained. Profile 3 runs SW-NE across the negative gravity anomaly in the west of the grid that has shown continued enlargement during the monitoring period. The results obtained are again of a high credence and suggest that the causative body is at a similar depth horizon to the body responsible for anomaly A (profile 1). Profile 4 has only been extracted from the 2002 data set and the results from this are shown in Table 5.5. It has not been extracted from the 2001 data set as the gravity anomaly was not well enough established at that time. The results obtained from this profile suggest that the causative body lies at a deeper horizon although the

estimated depths are of the same order as those derived from the previous profiles The results for profile 1 extracted from the 1998 data set are presented in Table 5.2. The results from the other profiles are inconclusive for the 1998 data set because of the limited size of the anomalies.

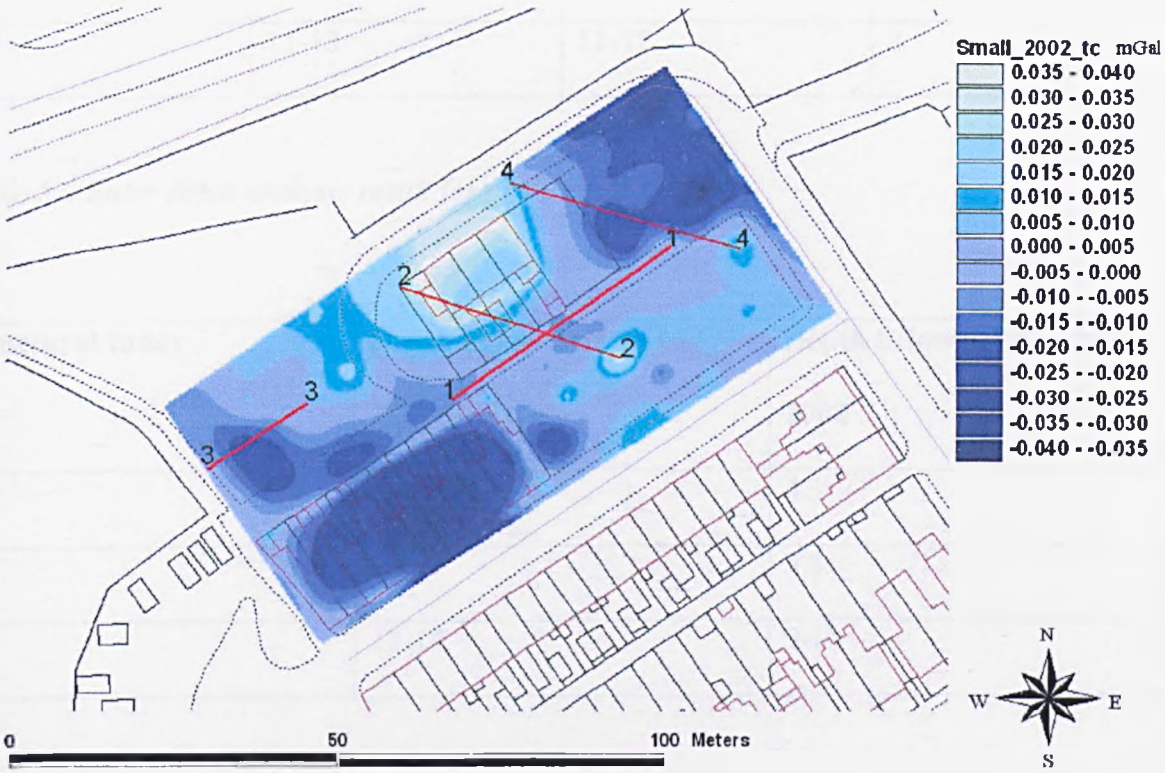




*Fig.5.22 Position of the profiles extracted for use in the Euler Depth analysis.*

| Structural Index | Depth below surface (m); 1998 | Depth below surface (m); 2001 | Depth below surface (m); 2002 |
|---|---|---|---|
| 0.6 | 4-6 | 3-4 | 3.25 |
| 1.0 | 6-8 | 5-6 | 5 |
| 2.0 | 11-13 | 11-12 | 8 |

*Table 5.2 Euler depth analysis result for profile 1.*

| Structural Index | Depth below surface (m); 2001 | Depth below surface (m); 2002 |
|---|---|---|
| 0.6 | 5.5-7 | 4.3 |
| 1.0 | 7.5-9 | 5.8 |
| 2.0 | 12-14 | 9-10 |

*Table 5.3 Euler depth analysis results for profile 2.*

| Structural Index | Depth below surface (m); 2001 | Depth below surface (m); 2002 |
|---|---|---|
| 0.6 | 2.6-2.9 | 3.8 |
| 1.0 | 3.6-3.7 | 4.6-4.7 |
| 2.0 | 6.2 | 6.8 |

*Table 5.4 Euler depth analysis results for profile 3.*

| Structural Index | Depth below surface (m); 2002 |
|---|---|
| 0.6 | 6 |
| 1.0 | 7-8 |
| 2.0 | 10.5-12 |

*Table 5.5 Euler depth analysis results for profile 4. (Applied to 2002 data set only)*

### 5.8.2 Thickness estimates

In order to give an indication of the thickness of the causative body and an estimate on its likely density contrast, the gravity data has been inverted using the Cordell and Henderson method (1968). The program iteratively calculates the thickness of the causative body using the Bouguer slab equation by minimising the misfit between the calculated and observed anomalies. The method requires assumptions about the depth horizon to which the solution is pinned and the density contrast between the causative body and the surroundings. By modifying these two variables a suite of solutions can be obtained for the thickness of the causative body. Table 5.6 summarises the maximum thickness obtained by inverting the 2001 data with solution horizons varying between 1m and 5m below the surface and density contrasts of between 0.1 $Mg/m^3$ and 1.0 $Mg/m^3$. The results suggest that for a body with a depth of 2-3m (as suggested by both the resistivity section and the Euler depth estimates), with a density contrast of between 0.15 and 0.3 is most likely to fit the geological situation present at Peter Street.

The lateral extent and thickness of the body responsible for anomaly A have been plotted for 2001 using a density contrast of 0.2 $Mg/m^3$ and assigning the top of the body to be 3m below the surface (Figure 5.23). The same process has been applied to the 2002 data set (Table 5.7). From this plot (Figure 5.24) we can see that the thickness of the body

responsible for anomaly A has decreased to a thickness of 5m. This represents a shallowing of the base of the body as the top surface remains fixed at 2m below surface. The area to the NE of the plot (area D) has been estimated as having a thickness of 8m. In reality this is probably an under estimate because the anomaly has not been closed which results in the inversion software compensating for mass which it believes to be outside of the grid of data. See Chapter 4 for a fuller explanation and discussion.

| **Density contrast Δρ** | **Depth to which the top of the solution is fixed (m) 2001** | | | | |
|---|---|---|---|---|---|
| | **1** | **2** | **3** | **4** | **5** |
| 0.1 | 27.9 | 30.5 | 33.4 | 36.9 | 41.0 |
| 0.15 | 11.6 | 12.5 | 14.7 | 16.0 | 17.5 |
| 0.2 | 7.6 | 8.3 | 8.7 | 9.8 | 10.5 |
| 0.3 | 4.8 | 4.9 | 5.2 | 5.7 | 6.5 |
| 0.4 | 3.4 | 3.6 | 3.7 | 3.7 | 4.2 |
| 0.6 | 2.2 | 2.2 | 2.4 | 2.4 | 2.6 |
| 0.8 | 1.6 | 1.7 | 1.75 | 1.8 | 1.9 |
| 1.0 | 1.3 | 1.3 | 1.35 | 1.4 | 1.5 |

*Table 5.6 Maximum thickness predictions derived from the Cordell and Henderson inversion method for the 2001 data set.*

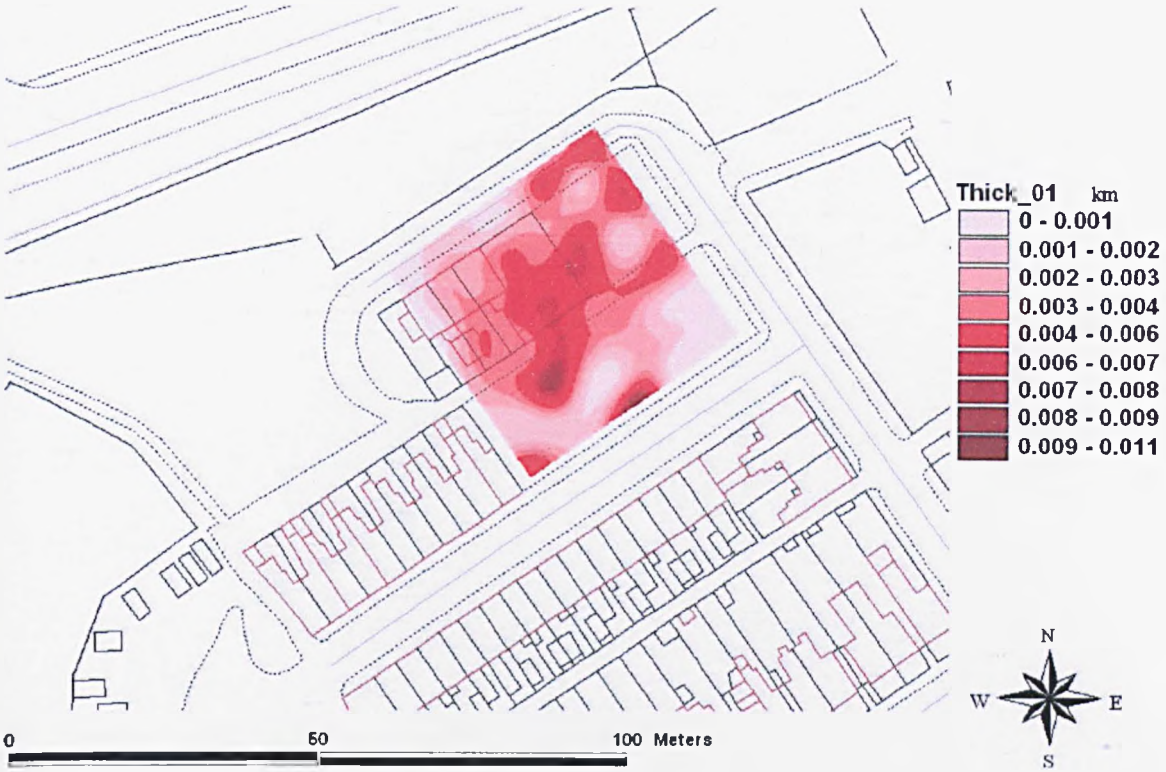




*Fig. 5.23 The thickness of the causative body related to anomaly A (2001). The top of the solution has been fixed at 3m below surface. The maximum thickness of anomaly A is 8m, i.e. the base of the body lies at 10m below the surface.*

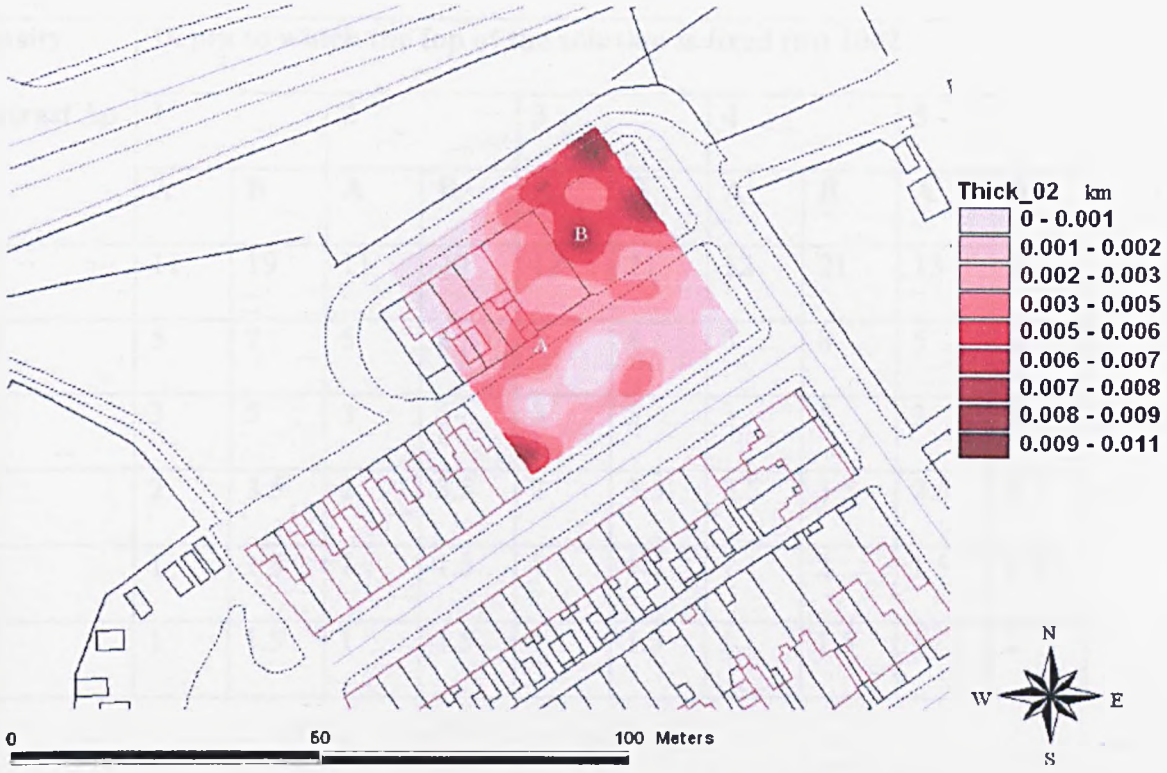




*Fig. 5.24 The thickness of the causative body related to anomaly A+D (2002). The top of the solution has been fixed at 2m below surface. The maximum thickness of anomaly A is 5m, i.e. the base of the body lie at 7m below the surface.*

| Density contrast Δρ | Depth to which the top of the solution is fixed (m) 2002 | | | | | | | | | |
|---|---|---|---|---|---|---|---|---|---|---|
| | 1 | | 2 | | 3 | | 4 | | 5 | |
| | A | B | A | B | A | B | A | B | A | B |
| 0.1 | 11 | 19 | 11 | 20 | 12 | 21 | 12 | 21 | 13 | 22 |
| 0.2 | 5 | 7 | 5 | 8 | 5 | 8 | 5 | 8 | 5 | 9 |
| 0.3 | 3 | 5 | 3 | 5 | 3 | 5 | 3 | 5 | 3 | 5 |
| 0.4 | 2 | 3.5 | 2 | 3.5 | 2 | 3.5 | 2.5 | 3.5 | 2.5 | 4 |
| 0.6 | 1 | 1.5 | 1 | 1.5 | 1 | 1.5 | 1 | 2 | 1.5 | 2.5 |
| 0.8 | 1 | 1.5 | 1 | 1.5 | 1 | 1.5 | 1 | 1.5 | 1 | 2 |

*Table 5.7 Maximum thickness predictions derived from the Cordell and Henderson inversion method for the 2002 data set.*

### 5.8.3 2.5D Modelling

Using the gravity-modelling package, GRAVMAG we are able to model the possible cause of the gravity anomaly. GRAVMAG is a interpretation package developed by the British Geological Survey to model gravity and magnetic anomalies based on the method of Talwani and Ewing (1960).

Figures 5.25 and 5.26 show two models created using GRAVMAG for the 2001 and 2002 data respectively. The modelled profile is profile 2, as used for the Euler Deconvolution (Figure 5.22). The geology has been derived from a borehole that was drilled in August 2001, its position is shown in Figure 5.21. The densities and unit names of the polygons used in the model can be found in Table 5.8.

The results from the Euler Deconvolution and the information gained from the resistivity section allow us to constrain the 2001 model by fitting the top of the body to a depth of 2-3m. The results from the Cordell and Henderson inversion suggest that the body responsible for anomaly C has a density contrast of between 0.2 Mg/m³ and 0.3 Mg/m³. These assumptions, together with the lateral extent derived from the resistivity section (5-6m) allow us to eliminate much of the ambiguity associated with gravity modelling.

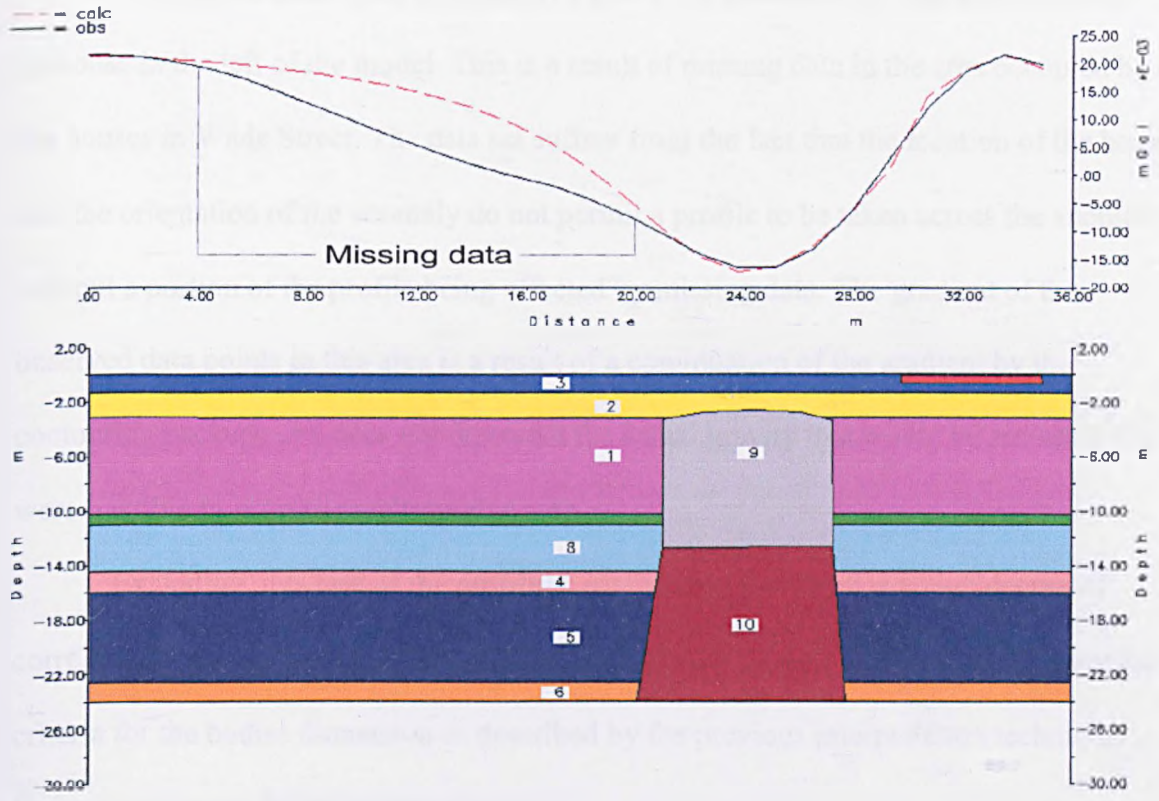


*Fig.5.25 2.5D GRAVMAG model for 2001. Polygons 9 and 10 are areas of low density. Polygon 10 represents the back fill of polygon 9. The red polygon to the right of the model is a near surface object of high density. The densities and geological interpretations of the polygons are listed in Table 5.8.*

The most plausible model which represents the 2001 data consists of thinly layered geological units cross cut by an upward propagating area of low density, polygons 9 and

10. These polygons represent a propagating area of loose material vertically above a second area of similar material but with a higher density, i.e. the material is passing from polygon 9 to polygon 10 where it compacts, thus increasing its density.

A third anomalous body is also included in the model. Polygon 11 (red rectangle in the right of the model) represents a near surface object that has a higher density than the surrounding geology. The origin of this object is uncertain although blocks of concrete are visible in the area on site.

A large deviation from the observed gravity is present in the calculated gravity response in the left of the model. This is a result of missing data in the area occupied by the houses in Wade Street. The data set suffers from the fact that the location of the houses and the orientation of the anomaly do not permit a profile to be taken across the anomaly without a portion of the profile being effected by missing data. The gradient of the observed data points in this area is a result of a continuation of the gradient by the contouring package and does not represent the actual gravity that would be recorded if it were possible to acquire gravity in this area.

Excluding this part of the profile, it can be seen that there is a high degree of correlation between the model and the observed gravity as well a the model fulfilling the criteria for the bodies dimension as described by the previous interpretation techniques, (i.e. resistivity and Euler deconvolution).

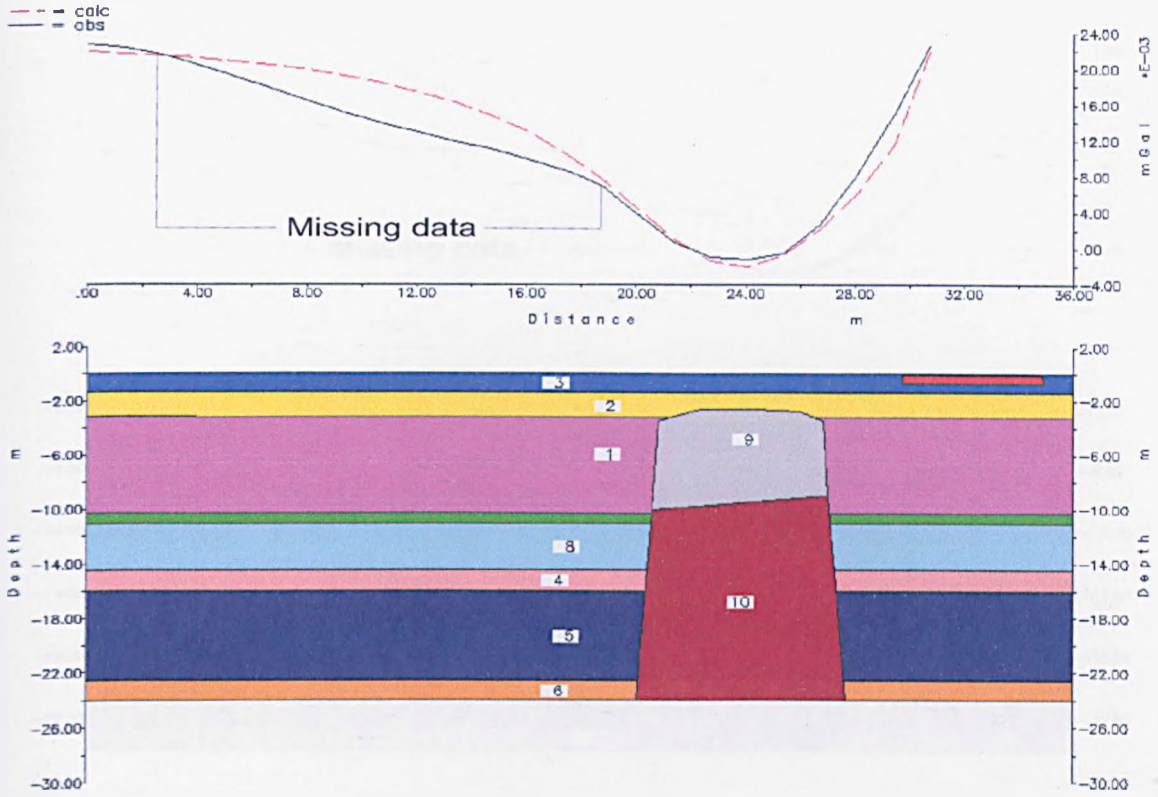


*Fig.5.26 2.5D GRAVMAG model for 2002. Polygons 9 and 10 are areas of low density. Polygon 10 represents the back fill of polygon 9. The red polygon in the right of the model is a near surface object of high density. The densities and geological interpretations of the polygons are listed in Table 5.8.*

Figure 5.26 shows the evolution of the 2001 model between the two surveys. It can be seen that the base of polygon 9 has shallowed and consequently the top of polygon 10 has also shallowed. The density of polygon 9 has increased, reducing the density contrast between the anomalous body and the surrounding material. This can be interpreted as the increased saturation of the material in the anomalous body or the influx of material from an adjoining area. This would require a link between the two areas and would have consequences on the future stability of this and surrounding areas.

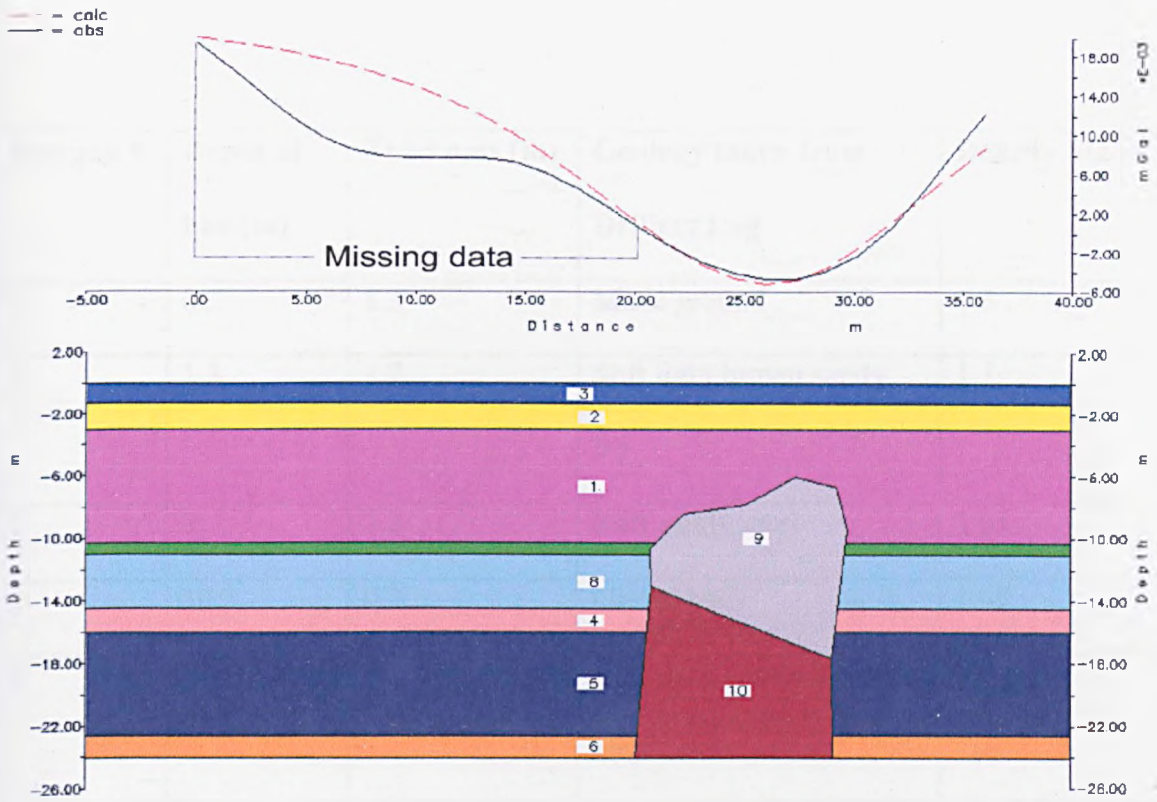


*Fig.5.27 2.5D GRAVMAG model for 1998. Polygons 9 and 10 are areas of low density. Polygon 10 represents the back fill of polygon 9. The near surface object of high density, represented by the red polygon, is not present in this model. The densities and geological interpretations of the polygons are listed in Table 5.8.*

The size of anomaly C in 1998 is less than 10 μGal and as such would normally be considered insignificant. However, using the information we have about the body in 2001 we can model the possible dimensions of the body in 1998 by assuming the bodies width and density has not changed dramatically over the 3-year period. Using the same parameters as the 2001 model, a good correlation between the observed and calculated gravity fields is attainable by increasing the depth of the body (Figure 5.27).

The high-density body, represented in Figures 5.25 and 5.26 by the red polygon, has not been incorporated in this model. This suggests that the object was introduced to the site between 1998 and 2001.

| Polygon # | Depth of bed (m) | Thickness (m) | Geology taken from Drillers Log | Density Mg/m³ |
|---|---|---|---|---|
| 3 | 0 | 1.3 | Made ground | 1.3 |
| 2 | 1.3 | 1.7 | Soft light brown sandy lay | 1.7 |
| 1 | 3 | 7.3 | Stiff sandy marl | 1.65 |
| 7 | 10.3 | 0.7 | Gravel bed | 1.65 |
| 8 | 11 | 3.5 | Stiff dark brown boulder clay | 1.72 |
| 4 | 14.5 | 1.5 | Wet silty sand | 1.65 |
| 5 | 16 | 6.5 | Stiff dark brown boulder clay with silty sand bands | 1.69 |
| 6 | 22.5 | 1.5 | Weathered red marl | 1.2 |
| 9 | Varies | Varies | Propagating area of low density | 1.25* |
| 10 | Varies | Varies | Backfill of polygon 9 | 1.45 |
| 11 | 0.0 | 0.75 | Near surface high density object | 1.8 |

*Table 5.8. Density values for Figures 5.20, 5.21 and 5.22. These values have been interpreted from the drillers logs. * value increases to 1.4 in Figure 5.21.*

### 5.8.4 Area outside the principal zone of subsidence

Euler depth analysis has been applied to the large negative anomaly trending NW-SE across the survey area by extracting data from profiles 5 and 6 (Figure 5.28). The results for the 2001 and 2002 surveys are presented in Tables 5.9 and 5.10 respectively. It is evident that significant shallowing of the causative bodies responsible for the gravity lows has occurred between the two surveys.

The Cordell and Henderson inversion technique has not been applied to the entire data set because closure of the anomaly trending NW-SE has not been obtained. This results in underestimates of the true thickness of the causative body. For a fuller discussion on the limitations of the Cordell and Henderson technique, refer to Chapter 4.

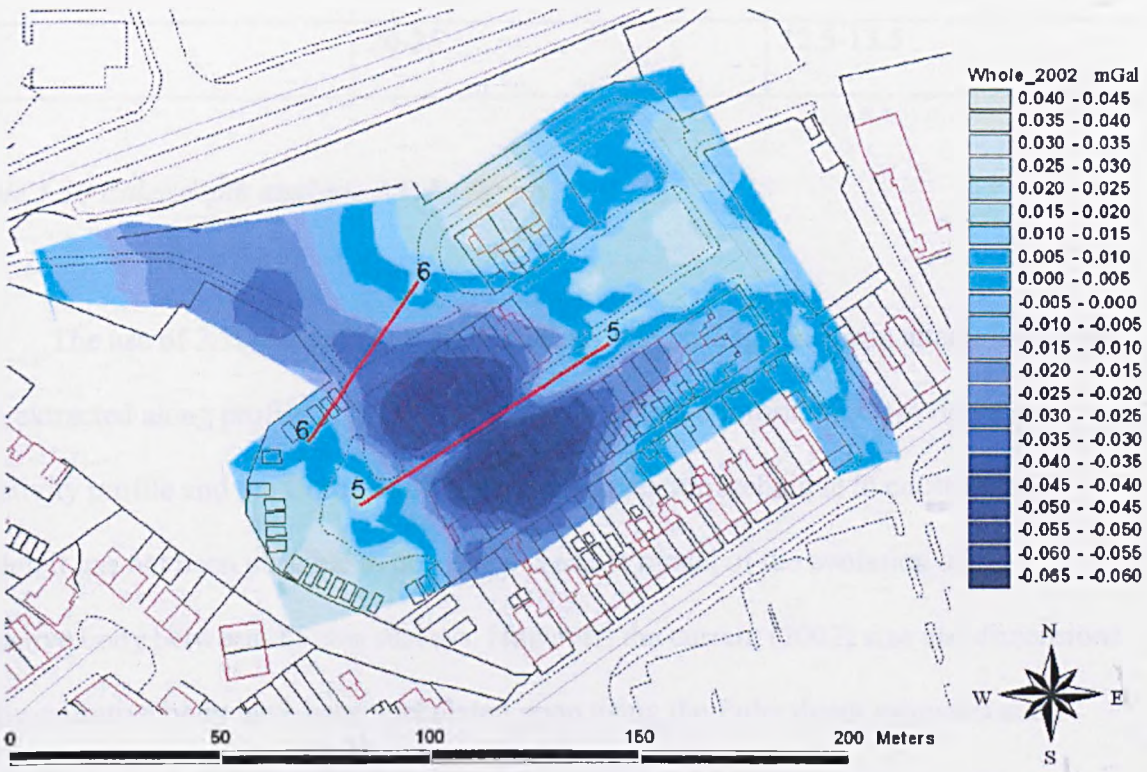


*Fig.5.28 Position of the two profiles used for the second phase of Euler depth analysis.*

| Structural Index | 2001 | 2002 |
|---|---|---|
| 0.6 | 12 | 6.5-7 |
| 1.0 | 15 | 8-9.5 |
| 2.0 | 20 | 12.5-14.5 |

*Table 5.9 Euler depth analysis results for profile 5.*

| Structural Index | 2001 | 2002 |
|---|---|---|
| 0.6 | 11-13 | 6-7 |
| 1.0 | 13.5-16 | 7-9 |
| 2.0 | 20-25 | 12.5-13.5 |

*Table 5.10 Euler depth analysis results for profile 6.*

The use of 2.5D modelling with the GRAMAG package has been attempted for the data extracted along profile 5. However, without the added information provided by a resistivity profile and the Cordell and Henderson inversion technique to constrain the model, it has not been possible to produce a credible model of the evolution of the causative body between the two surveys. However, the current (2002) size and dimensions of the causative body have been speculated upon using the Euler depth estimates and assuming the body is water filled (Figure 5.29). The densities of the polygons are described in Table 5.11.

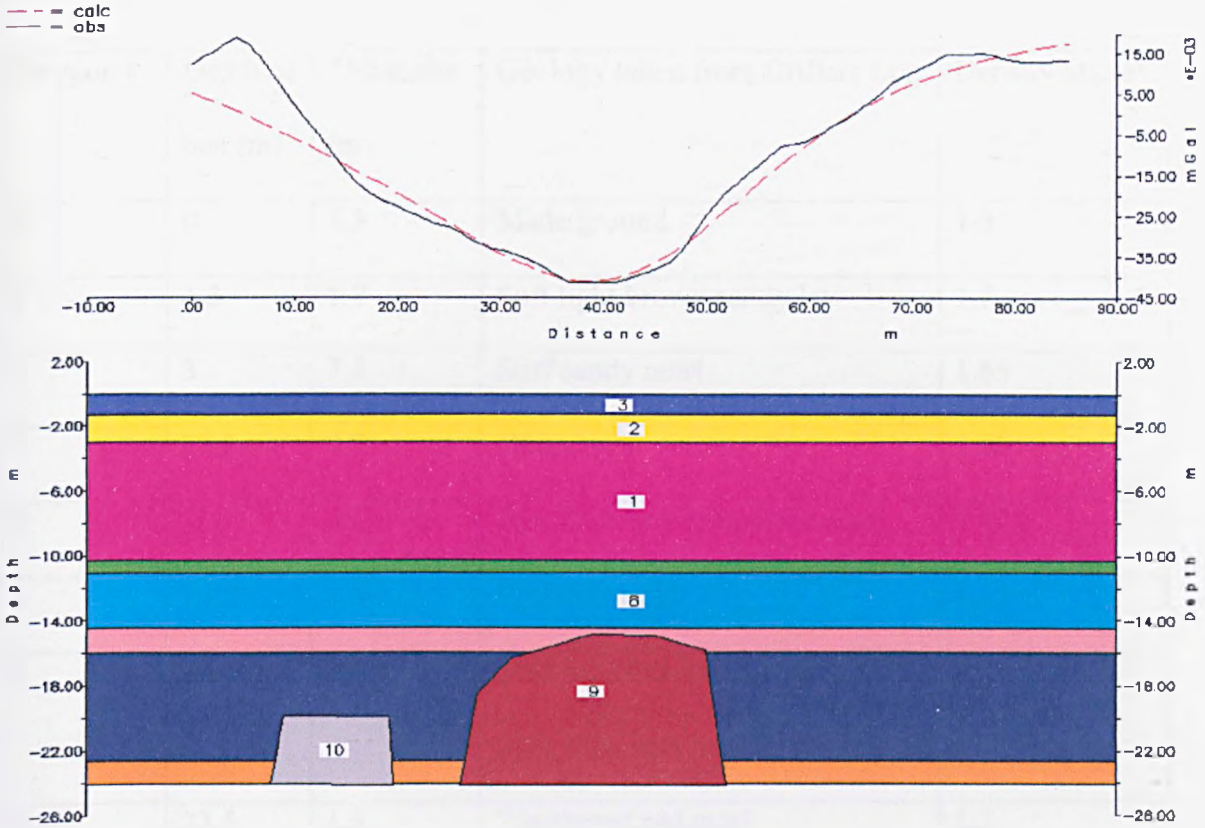


*Fig.5.29 2.5D GRAVMAG model for 2002, profile 5. Polygons 9 and 10 are water filled voids. The densities and geological interpretations of the polygons are listed in Table 5.11.*

| Polygon # | Depth of bed (m) | Thickness (m) | Geology taken from Drillers Log | Density Mg/m³ |
|---|---|---|---|---|
| 3 | 0 | 1.3 | Made ground | 1.3 |
| 2 | 1.3 | 1.7 | Soft light brown sandy lay | 1.7 |
| 1 | 3 | 7.3 | Stiff sandy marl | 1.65 |
| 7 | 10.3 | 0.7 | Gravel bed | 1.65 |
| 8 | 11 | 3.5 | Stiff dark brown boulder clay | 1.72 |
| 4 | 14.5 | 1.5 | Wet silty sand | 1.65 |
| 5 | 16 | 6.5 | Stiff dark brown boulder clay with silty sand bands | 1.69 |
| 6 | 22.5 | 1.5 | Weathered red marl | 1.2 |
| 9 | 15 | 9.0 | Water filled Void | 1.0 |
| 10 | 20 | 4.0 | Water Filed Void | 1.0 |

*Table 5.11. Density values for Figures 5.24. These values have been interpreted from the driller's logs.*

## 5.9 Conclusions

The area bounded by Peter Street to the south, Elm Street to the east, Wade Street to the north and the footpath to the west has subsided by a maximum of 23cm between July 1998 and July 2002. Microgravity surveys have shown that this subsidence is associated with negative gravity anomaly (A), interpreted to be a region of migrating lower density. Time-lapse microgravity has identified the area to be active in terms of sub-

surface mass movement. The technique has shown that this anomaly (A) has grown in size between 1998 and 2001 by 20-30μGal. A decrease in the negative anomaly between 2001 and 2002 has been explained by a shallowing of the base of the causative body together with a density contrast reduction thought to be caused by increased water saturation or lateral mass movement from the NE. Gravity modelling techniques indicate that the causative body now lies at a depth of 2-3m below surface and extends to the wet rock head at 23m below surface. It is unlikely that the body is an air filled cavity because of the relatively low resistivity values but is more likely a diffuse area of lower density consisting of brecciated material generated by cavity propagation.

It is apparent that the cause of the gravity negative is not related to mine workings. The size and distribution of the negative anomalies are too small to be caused by air/water filled mine workings. The borehole results also prove that there are no mine workings down to a depth of 100m below surface. I believe that the cause of the negative density contrast is a result of salt dissolution by ground water. With the information available it is not possible to distinguish whether it has been caused by the natural movements of ground water through the area or by the forced movement of ground water resulting from brine pumping.

In summary, I suggest a cavity has developed at wet rock head as a result of salt dissolution. Over time, this has migrated towards the surface, backfilling the space as it does so. This has resulted in a diffuse area of low-density material, extending from wet rock head up to 3m below surface with a lateral extent as shown by the thickness estimates. Surface subsidence has then effected the area as this material compacts. It is possible that the dissolution is a result of continuing brine pumping drawing fresh water into the system.

Interpreting the gravity changes outside of this area it is apparent that the main gravity anomaly trending NW-SE across the survey area has also been active during the monitoring period 2001-2002. Depth estimates suggest that this anomaly lies slightly deeper than the body responsible for anomaly A. As the depth estimates place the causative body at a depth above wet rock head, it is my opinion that the cause of the anomalies can be explained by the same process described above. However, the void is not as advanced as the previous example and so subsidence has not become evident at the surface. If the void continues to propagate towards the surface, the overlying strata will not be able to support itself and so will begin to subside. Depending on the size of the void below it at this time, the collapse could be catastrophic (if a large void is still present) or gradual, if the majority of the void has been filled with brecciated material as in the previous example.

In this environment, carefully acquired and processed time-lapse microgravity has proven to be a useful tool in the investigation and monitoring of an area affected by subsidence and can be used to determine the rate and extent of cavity growth.

# Chapter 6

# The Application of Time-Lapse Microgravity along the Trent and Mersey Canal, Marston

## 6.1Introduction

Marston is located to the north of Northwich on the B5075. Like Northwich the area is heavily associated with salt mining, and the canal here owes is existence to the salt industry (Wallwork, 1960).

The River Weaver was canalized in 1721 to serve the salt mines in the area. The banks of the canal saw further development of salt mines as transport was a major cost to the industry and so siting the mines on the canal reduced transportation costs dramatically. Figure 6.1 is an Ordnance Survey map published in 1872. In it can be seen the scale of the industry in that area. The Adelaide mine is perhaps the most significant, located where the road crosses the canal, but in this short stretch four other mines are located on the banks of the canal; Marston Old Mine, Pool Mine and Marston Hall Mine to the NW of what is now the B5075 and the Alliance works the SE.

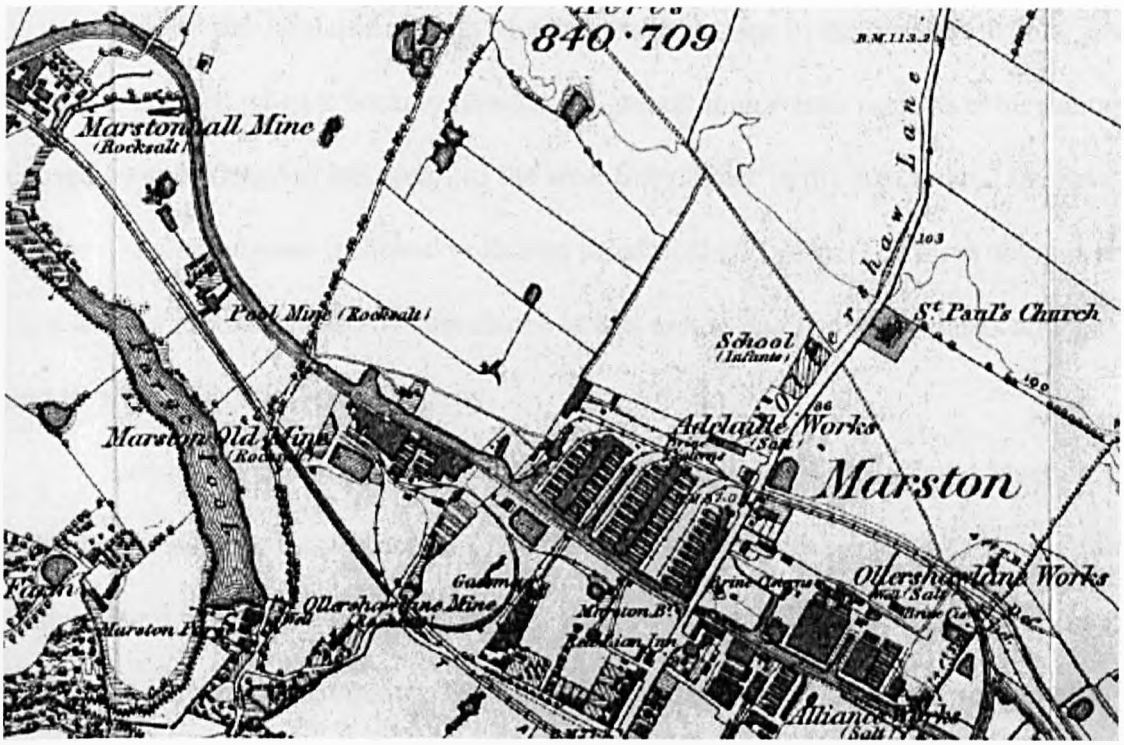


*Fig. 6.1 Ordnance Survey map published in 1872. On it can be seen the concentration of salt work on the banks of the Trent & Mersey canal. The road running NE across the Figure (Oltershaw Lane) is now the B5075. The Inn located where the road crosses the canal is now called the Salt Barge. North is at the top of the page; the scale is 1:4000.*

The mining of salt in Cheshire at this time was characterised by the large-scale collapses of mines (Bell, 1988). In 1840, seven flooded bottom rock mines were recorded in Marston and Wincham, eight in Dunkirk and two in Witton.

The collapse of the mines formed 'rock pit holes' which are large flooded craters. The abandonment of a mine brought added danger to its neighbors, and most of the area between Northwich Station and Marston Hall Mine was honeycombed with top and bottom rock mines (Bell, 1975). The proximity of the mines to one another and the waterways used in the carriage of rock salt increased the dangers of subsidence and the subsequent flooding of land in the vicinity of the mine.

In 1928 the Adelaide mine at Marston, the last mine in the Northwich area, was hastily evacuated when it became flooded. Of greater importance perhaps is the damage caused by subsidence to the canals of the area. Subsidence in the area around the River Weaver has had various technical problems for almost 200 years. The most obvious and very serious problem posed by subsidence in that area is damage to the banks and locks, and to bridges crossing the waterway.

Subsidence has occurred at all these points but it is at Wincham and Marston where subsidence has been most apparent. Here the canal passes over several flooded rock salt mines, and it is here that the most serious breaches of the banks have taken place. In an attempt to reduce costs of maintenance along the most severely damaged section of the canal, a new cut was opened in 1958 but parts of this cut are still suffering from ongoing subsidence. This is evident in the road bridge that crosses the canal. The bridge itself has had to be raised several times as the ground surrounding the canal subsides. Looking at Plate 6.1 several stages of construction can be seen including the last raise, approximately 50cm.

*Plate 6.1 The bridge built to carry the B5075 across the canal has had to be raised several times as a result of continuing subsidence. The previous level is shown by a line of light coloured bricks under the main carriageway.*

The first part of this chapter reviews relevant geophysical and site investigation work carried out in the Marston area previous to this investigation. After this the chapter is split into two sections; the first section reports on the time-lapse microgravity programme carried out on the banks of the Trent & Mersey canal. The second section details work conducted in a second site in the Marston area that cannot be named.

The first section, reporting on work carried out along the canal to investigate and monitor the continuing subsidence in that area, includes an outline of the survey procedure (Section 6.3.1), and the gravity results (section 6.3.2). Further sections detail the terrain corrections applied (section 6.3.3), the filtering of the gravity data (section 6.3.4) and

this the modeling of the gravity results (section 6.3.6) and the results from the time lapse monitoring (section 6.3.7) are discussed. A summary of the work and suggestions for further work are presented in sections 6.3.8 and 6.3.9 respectively

The second section has a similar structure to the first. A brief introduction (section 6.4.1) leads into the survey procedures (section 6.4.2) and the gravity results (section 6.4.3). Modeling of the data is presented in section 6.4.4 before the conclusions derived from this site are discussed in section 6.4.5

## 6.2 Previous work

There has been several investigations into the stability of the Trent & Mersey canal at Marston. In 1992 a site investigation was commissioned to assess the hazard posed by further subsidence of the mines in the area (Adams et al., 1992). It was proposed that the disused Lion salt works be preserved and consequently a detailed site investigation was necessary before restoration began.

In 1999 the area around Marston Old and Adelaide mines was used as a trial area for a new technique being developed by Dr. Sergey Levashov from the Ukraine. The technique is called GEMA (GeoElectricalMagnetic Application) and has successfully been used in the past to identify underground cavities, groundwater flows, pipeline leakage's, petroleum pollution plumes and hydrocarbon deposits.

Continuing monitoring of precise levels along the Trent and Mersey canal has been carried out by British Waterways. Analysis of this data highlights trends in the subsidence and identifies high-risk areas.

### 6.2.1 Site investigation at the Lion salt works

In 1992 a site investigation was commissioned to assess the hazard poised by further subsidence of the mines in the area (Adams et al., 1992). It was proposed that the disused Lion salt works be preserved and consequently a detailed site investigation was necessary before restoration began.

Desk studies by Adams et al. (1992) revealed that two economic halite beds, forming part of the Northwich Halite Formation, had been simultaneously exploited by relatively deep room and pillar workings and by brine well pumping at shallower depths. Records show that the Adelaide Rock Salt Mine, utilised room and pillar mining in the bottom bed at a depth from the surface of 103 m to the footwall, producing in seam voids of 5.6m in height. Brine pumping via several small diameter cased wells took place in the upper part of the top bed at depths up to 50m.

Geophysical acoustic methods were implemented, utilising 5 pre-drilled open boreholes. Compressional (P-wave) velocities were calculated from transit time and distance measurements, and relative amplitudes of the received waves were taken from the seismograph traces. In only one of the 5 boreholes drilled prior to the geophysical survey had there been a suspicion of the presence of a cavity.

Adams et al. (1992) conclude that the ground around the Lion salt works contains a significant number of unconsolidated zones and voids at depths from 50m upwards. Great variations in bulk density of the geological material at the site were due to a combination of natural solution at wet rock head, wild brine pumping and room and pillar mining.

### 6.2.2 GEMA

The aim of the 1999 project was to provide a challenging site in which to assess the performance of GEMA as well as providing Eutech Ltd. with additional information about the ground condition at the site.

The results produced by this project give an insight into the conductivity of the area as well as locating likely preferential flow paths and subsidence prone zones. Incorporating this information, enables us to support the subsurface model developed using the gravity data.

#### 6.2.2.1 Basic introduction to GEMA

This basic introduction to the geophysics behind GEMA is a summary of the work presented by John Lamont-Black in his report "On trial geophysical works on evaluation of the GEMA geophysical techniques in Northwich, Cheshire, UK July 6-7, 1999"

GEMA comprises of two electro-magnetic techniques which can identify the three dimensional position of subsurface bodies of anomalous apparent resistivity. Both techniques utilise the phenomenon of the natural polarisation of high resistivity objects in the natural electric field of the Earth and include:

1. The measurement of the Low-Frequency Components of the natural Electro-magnetic field of the Earth.

In the quasi-steady natural electric field of the Earth, anomalous objects with contrasting resistivity are manifested at the ground surface as anomalous values of intensity of the vertical component. This is a potential field and is represented at the ground surface by a distribution of ions strongly dependent on the structure of the local electric field. An increase or decrease in intensity of the field in certain areas leads to

concentration of ions of specific polarity. These areas relate to geological anomalies and the magnitude and polarity of change within these zones depends on resistivity contrast, size and depth of the anomalous bodies.

2. Electro-Magnetic Impulse Probing

Any object polarised in the natural electric field of the Earth forms ionic zones of different polarity in the near surface layer. Ions of certain polarity concentrate directly above the anomalous object and, depending on the depth of the object, the zone of ions of the opposite sign form. For bodies of regular geometry, an analytical relationship can be obtained between the depth of their occurrence and the distance between zones of different polarity.

The two zones are closely related, as they are reflections of the same anomalous object. It has been determined that a change in one of the zones will cause a similar change in the zone of opposite charge. Therefore by inducing impulse excitation of the ionic zone and switching the antenna to receiver mode, a signal from the ionic zone of the opposite charge is registered. The response signal is commonly presented as a spectrum of frequencies, which represent the restoration of the ion distribution following a deliberate disturbance in the form of an electromagnetic impulse. Each frequency has its own speed of propagation in a real medium and so by assigning parameters of the upper Earth layer, one can obtain analytical relationship between depth of the object and spectral characteristics of response signal. Performing a dispersion analysis for each survey position along a profile enables a cross section to be constructed, which can show positions of anomalous objects.

For a more detailed account of the theory behind the GEMA work the reader is directed towards Lamont-Black (1999).

#### 6.2.2.2 Results and conclusions of the GEMA programme

The work carried out during the test consisted of a reconnaissance of the whole area as well as four detailed studies based on this site overview. The report summarises that the results achieved with GEMA are somewhat ambiguous with regard to the detection of mine pillars and the dividing wall between the mines (the two main objectives of the survey). However, the reconnaissance survey did identify several "vertical structures of anomalously low apparent resistivity, some of which coincide with surface depressions or areas of known active subsidence or subsidence damage."

Of interest are the two or three situations, identified in the recognisance survey, where anomalously low apparent resistivity zones can be seen to extend laterally (Figure 6.2). These can be seen to cross the canal in two places, extending from the Marston Old Mine towards Adelaide mine. "From the shape of the anomaly and the relationship with the lake we may suggest that these zones of low resistivity may relate to underground brine flows."

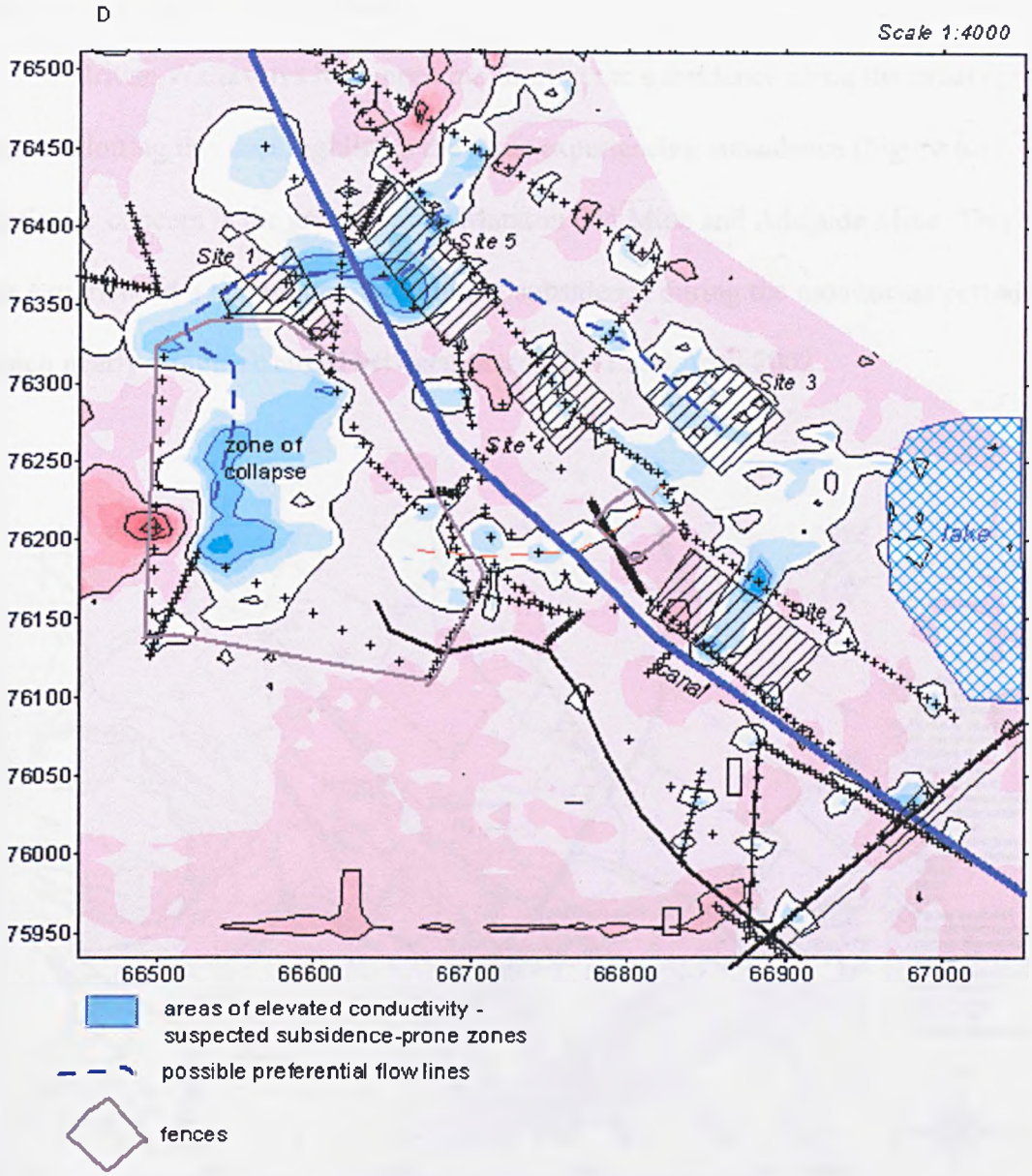


*Fig. 6.2 Reconnaissance survey carried out as part of the GEMA trials in July 1999. The light blue areas are suspect preferential flow lines. The fenced off areas correspond to Marston Old Mine (large area in the west) and Adelaide Mine (small area in the centre). Taken from Lamont-Black, (1999).*

### 6.2.3 Topographical monitoring

British Waterways have been monitoring the subsidence along the canal for several years. Plotting this data highlights the areas experiencing subsidence (Figure 6.4). Of particular concern is the area between Marston Old Mine and Adelaide Mine. This area has experienced a maximum of 400mm of subsidence during the monitoring period of which nearly 50mm occurred between March 2001 and April 2002.

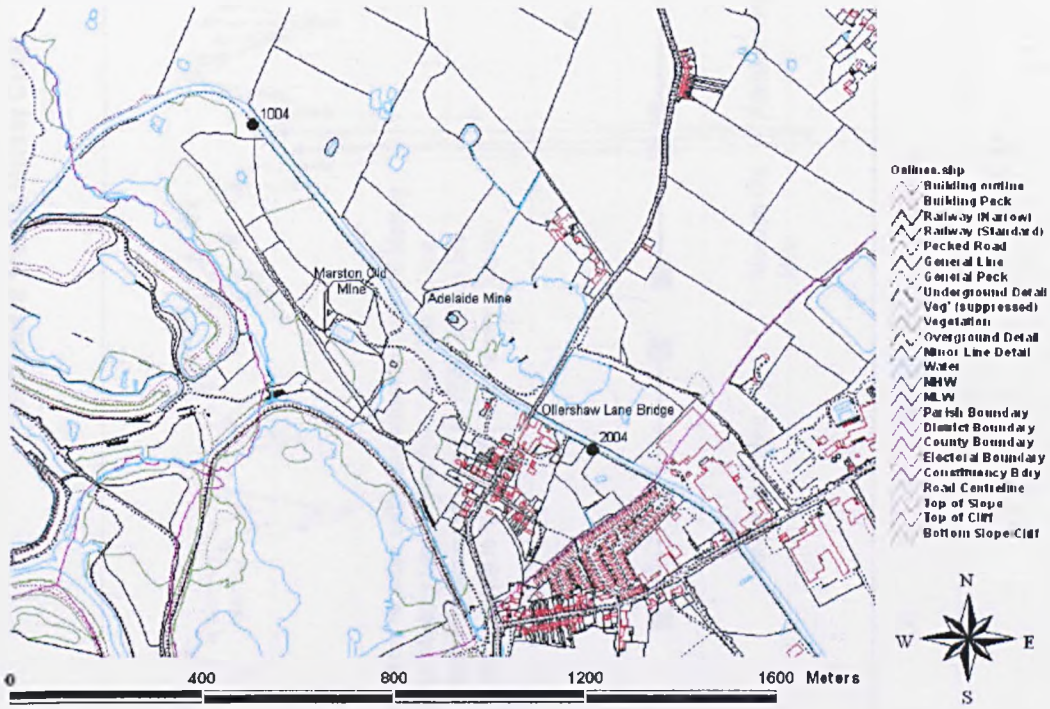




*Fig. 6.3 Map showing location of Marston Old Mine, Adelaide mine and Ollershaw Lane Bridge. Chainage 1004 and chainage 2004 are also marked for reference.*

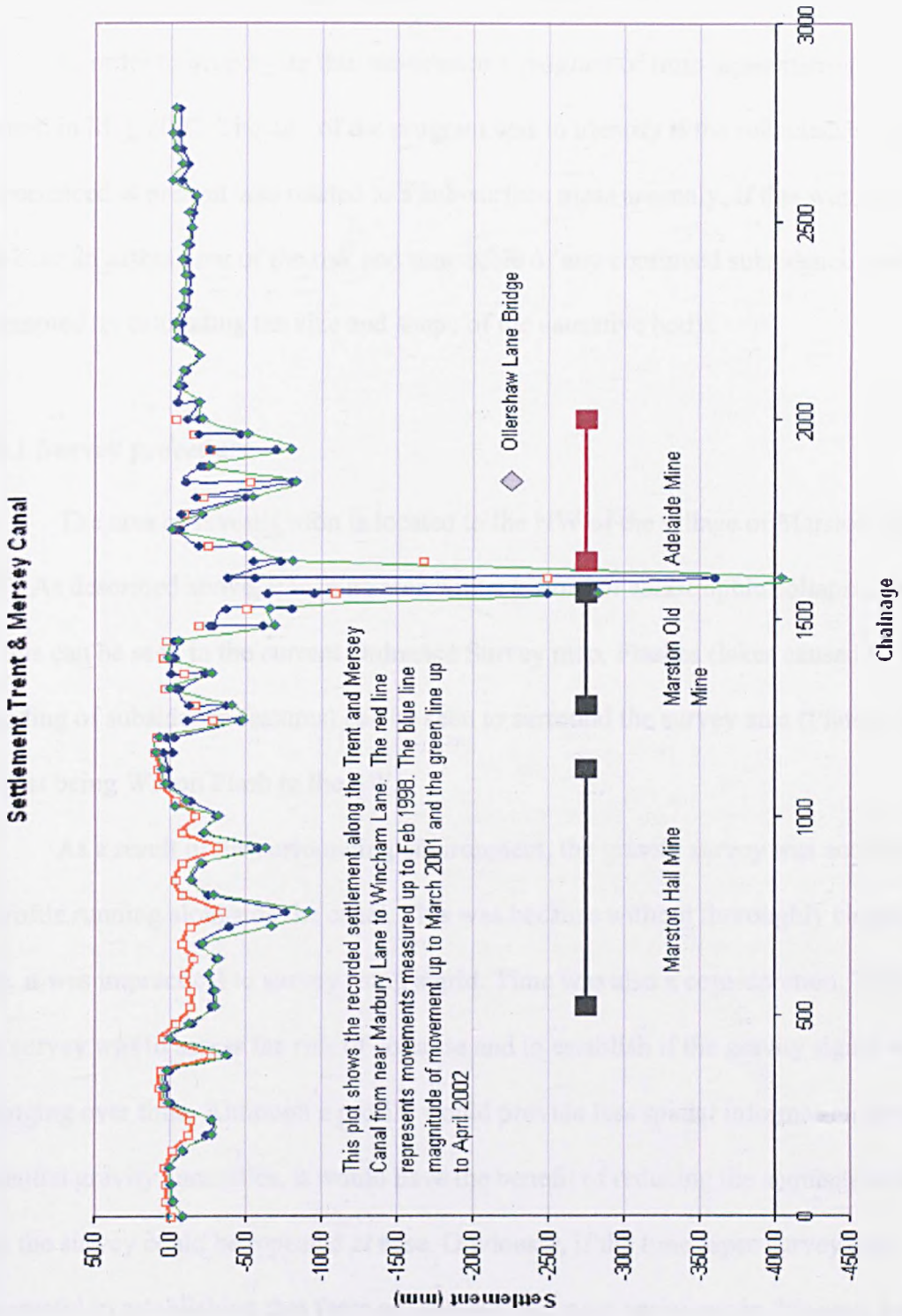


*Fig. 6.4 Plot of ground subsidence along Trent and Mersey canal. The area between Marston Old Mine and Adelaide Mine has experienced a maximum of 400mm subsidence. Data is provided by British Waterways.*

## 6.3 Microgravity investigation at the Trent and Mersey canal

In order to investigate this subsidence a program of time-lapse microgravity was started in May 2002. The aim of the program was to identify if the subsidence being experienced at present was related to a sub-surface mass anomaly. If this was found to be the case an assessment of the risk and time scale of any continued subsidence would be attempted by estimating the size and shape of the causative body.

### 6.3.1 Survey procedure

The area of investigation is located to the NW of the village of Marston (Figure 6.5). As described above, it is in an area with a history of catastrophic collapse. Evidence of this can be seen in the current Ordnance Survey map. Flashes (lakes caused by the flooding of subsidence features) can be seen to surround the survey area (Plate 6.2), the largest being Witton Flash to the SW.

As a result of the surrounding environment, the gravity survey was acquired along a profile running alongside the canal. This was because without thoroughly clearing the site, it was impractical to survey using a grid. Time was also a consideration. The aim of the survey was to assess the risk of collapse and to establish if the gravity signal was changing over time. Although a profile would provide less spatial information about the potential gravity anomalies, it would have the benefit of reducing the acquisition time so that the survey could be repeated at ease. Obviously, if the time-lapse survey was successful in establishing that there are sub-surface mass variations in this area, a more detailed grid could be acquired in order to provide the necessary data needed to characterise the site fully.

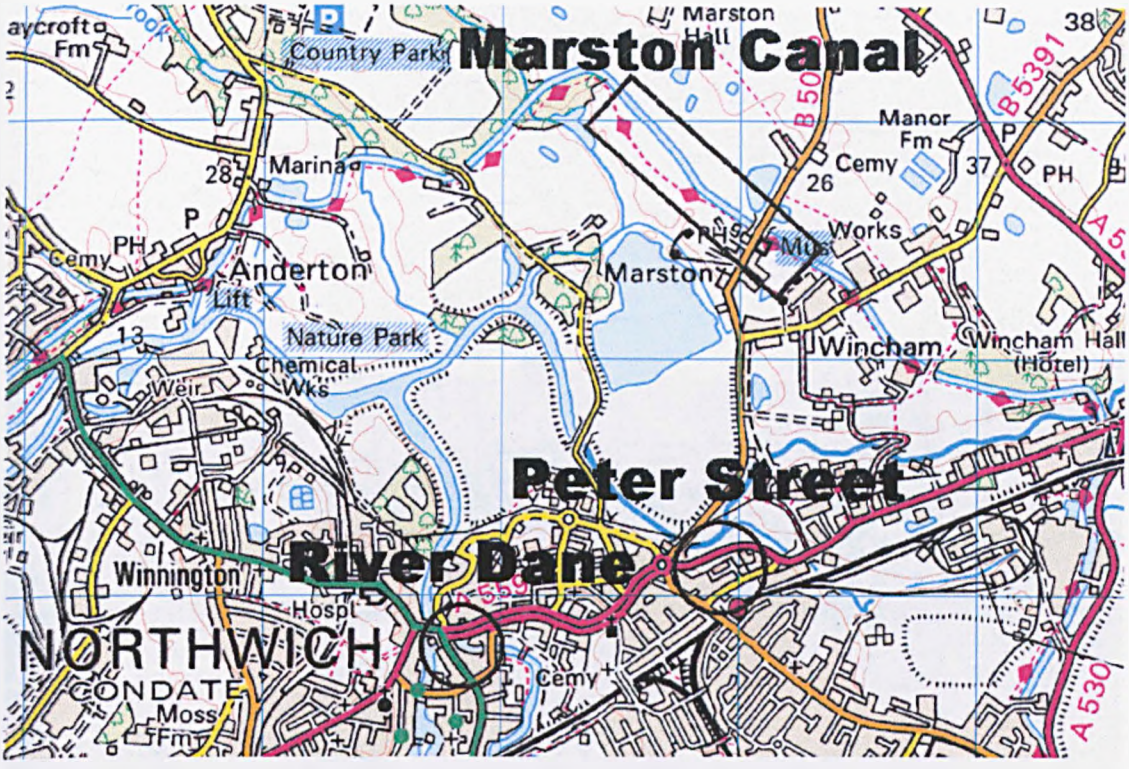




*Fig.6.5 Current Ordnance survey map for the area. The canal survey area is identified together with the location of other geophysical investigations undertaken as part of this investigation. It should be noted that the route of the canal has been straightened in the survey area and that a subsidence pool has now replaced the Adelaide mine.*

*Plate 6.2 Subsidence flashes that straddle the B5075 just north of the Trent and Mersey canal. Photo is taken looking north with the Trent & Mersey canal in foreground.*

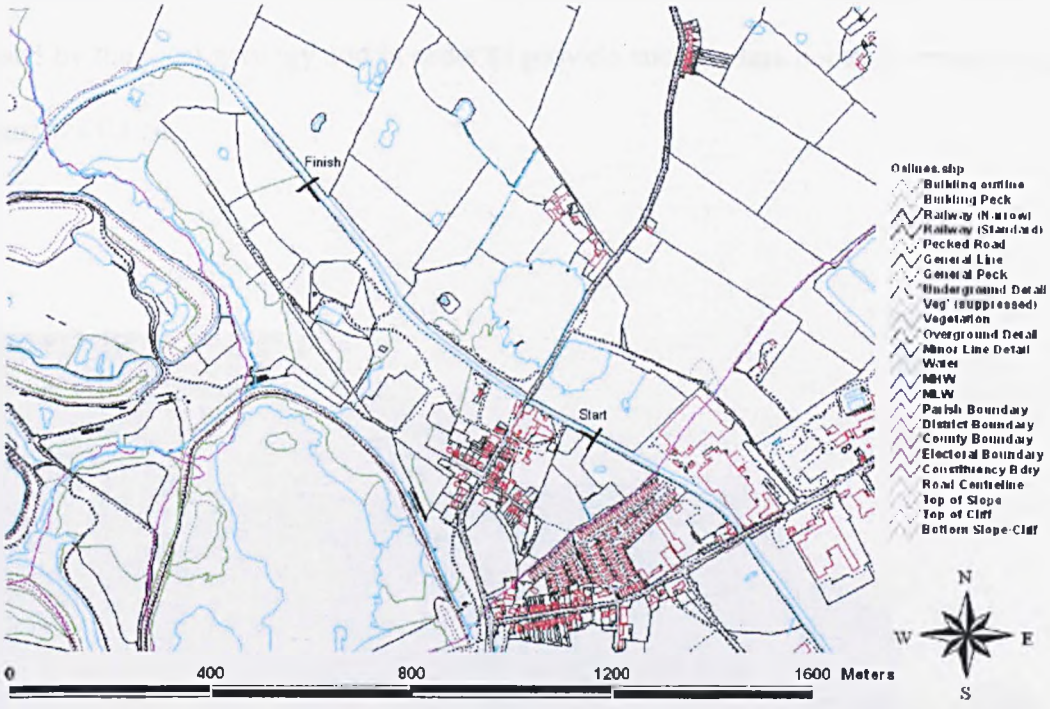




*Fig 6.6 Map showing the start and finish of the microgravity profile, acquired on the bank of the Trent & Mersey canal.*

The profile begins at chainage 2004 and continues in a NW direction along the canal (Figure 6.5). The first 320m (up to 1685 chainage) utilises a station spacing of 40m. The station spacing is then reduced to 5m for the next 200m (up to 1485 chainage) After 1485 chainage the station spacing is increased to 40m again and continues up to a chainage of 1244.

The distribution of the survey points along the acquisition profile results in a concentration of stations over the area that has been identified by British Waterways, to be subsiding. At this stage the depth or dimensions of a likely causative body were unknown and so a program of over sampling was adopted at this stage. The station spacing was

increased either side of the central part of the profile to a separation of 40m. These stations were included to provide information for the successful removal of gravitational effects caused by the local geology and in order to provide enough data points to close any gravity anomalies found.


*Plate 6.3 The profile ran along the towpath in a NW direction. Parts of the old Lion salt works that lined the canal banks are still standing. The bridge in the background is the same as shown in Plate 6.1.*

As this was a time-lapse microgravity program, the base station at St. Helens Church (Figure 6.7) was used as the base station to which the repeated surveys would be tied. The local base station was established on the bank of the canal a metre away from to

the west of survey nail 43. Survey nail 43 itself was not used, as it was too close to the bank and unsuitable for gravity surveying. The base station at St Helens church was revisited at the beginning and end of each survey and the local base station was revisited hourly.

Gravity was acquired along this profile on the May 11, July 12 and October 22, 2002. Topographic heights have been surveyed using a total station and tied in to survey nail 45.

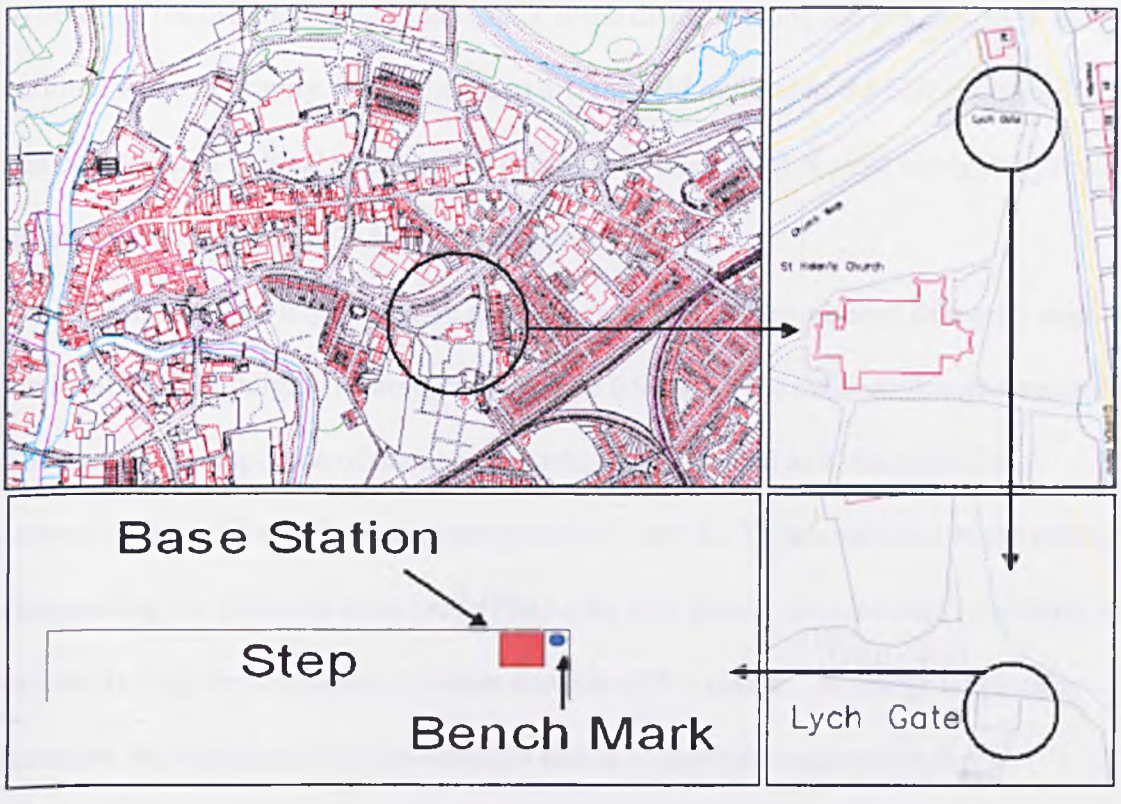




*Fig.6.7 Diagram showing the location of the St Helens base station. St Helens church is located on Church Road, Northwich.*

### 6.3.2 Gravity data

The reduced gravity data, acquired on the May 11, 2002 is presented in Figure 6.8. A strong local trend is present, increasing to the NW. This has been removed from the following data sets by subtracting the linear trend given by

$$y' = y - (0.0011x - 0.275). \qquad (6.1)$$

Where y is the original value of gravity, x is the distance along the profile and y' is the residual value of gravity. This equates to a 1.1mGal/km trend in the NW direction. This can be attributed to local variations in geology. In this case it is most likely to be result of dipping strata (see borehole section for further details).

Although the large negative anomaly is evident in the reduced data set, removing the local trend highlights its amplitude. Figure 6.9 shows the residual Bouguer anomaly. The maximum amplitude of the negative anomaly is located at 415m which is approximately mid-way between survey nails 40 and 41. This is adjacent to the compound surrounding the Adelaide mine head (Plate 6.4). The size of the anomaly, ~1.6mGal, is extremely large in comparison to other surveys of this nature. This large amplitude increases the significance of the anomaly and as a consequence requires further investigation.

*Plate 6.4 Compound surrounding the Adelaide mine head. The photograph is taken looking north across the canal. Subsidence is visible around the compound and is demonstrated by the deviation from horizontal of the compound fence and the position of the tree in the left of the picture. The area of ground between the canal and the compound has subsided considerably.*

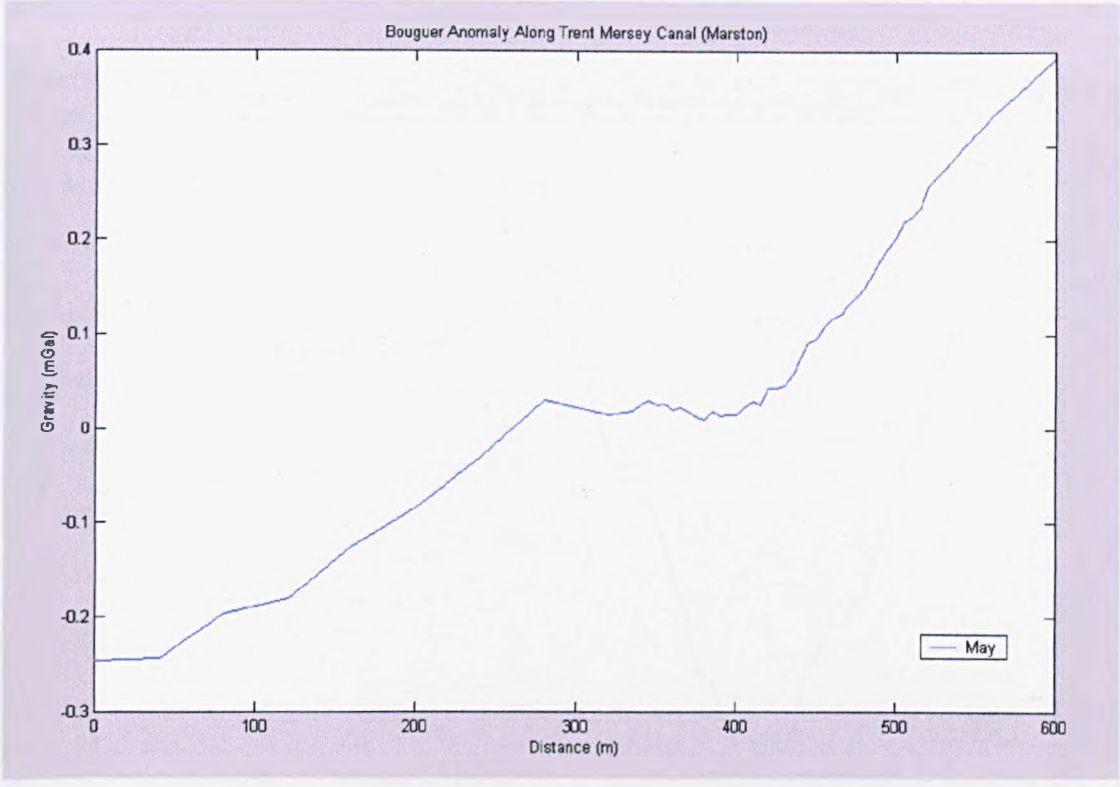


*Fig. 6.8 Reduced Bouguer anomaly recorded along the canal in May 2002. A 1.1mGal/km trend is present.*

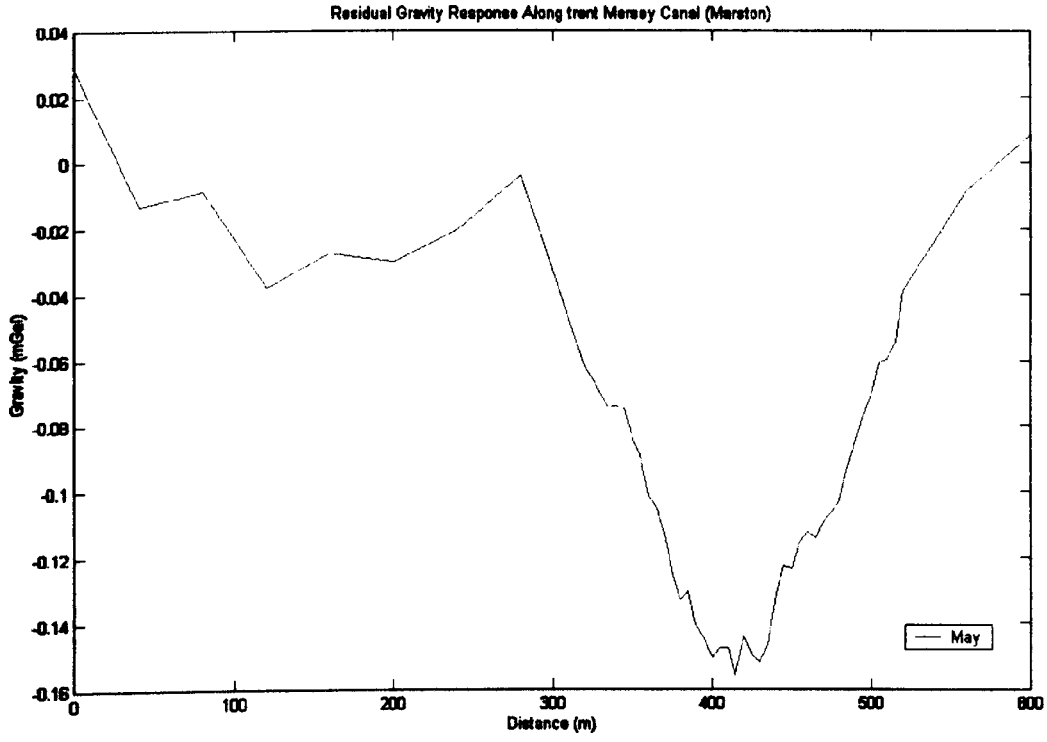


*Fig. 6.9 Residual Bouguer anomaly along canal after trend has been removed using formula 6.1.*

### 6.3.3 The terrain effect of the surrounding topography

Previous collapses as well as the current subsidence has resulted in the canal being raised above the surrounding area as its banks are raised to prevent them from bursting. To assess what proportion the terrain effect of the raised canal contributes to the measured gravity signal, the Parker method (Chapter 3) has been used to calculate the gravitational signal of the surrounding topography. This has been achieved by using the topographic data from the gravity profile as well as survey data of the surrounding area, provided by WS Atkins.

The maximum calculated effect of the surrounding terrain is 15μGal (Figure 6.10). However, this is well away from the profile along which the gravity was recorded. The maximum terrain effect experienced by the stations on the profile along the canal bank is only 5μGal opposite the Adelaide mine compound. Away form the compound the effect is between 1μGal and 2μGal. This value is insignificant when compared with the amplitude of the recorded gravity anomaly ~150μGal. The gravity data has therefore not been corrected for the terrain effect because of the relative insignificance of the effect and the fact that the data is to be used in time-lapse monitoring where terrain effects are eliminated.

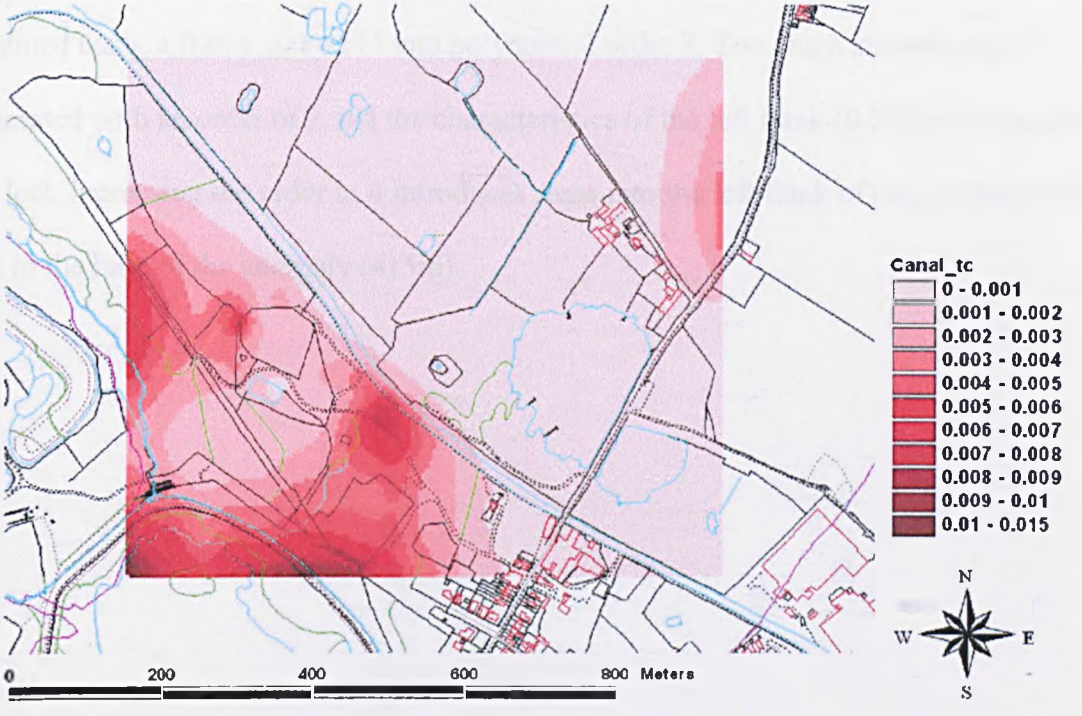




*Fig. 6.10 Plot showing the gravitational effect of the terrain surrounding the Trent Mersey canal. The terrain effect has been calculated using the Parker Method and has a maximum effect of 5μGal on the stations along the gravity profile.*

### 6.3.4 Filtering of gravity data

A Savitzky-Golay polynomial filter (Chapter 3) has been applied to the filter to remove some of the high frequency components of the data. Testing of the filter on the data resulted in a frame size of 11 and a polynomial surface with an order of 3 being chosen. Figure 6.11 and Figure 6.12 show the effect that the various parameters within the filter have on the data. A frame size of 11 or 15 was chosen so that no more than 3 data points were incorporated into the filter and so a single data point was only effected by its neighbours. Altering the polynomial order has the effect of smoothing the data set as it dictates what order of polynomial surface can be fitted to the data set. The lower the polynomial order the greater the smoothing. Figure 6.11, shows that the best result is obtained using a frame size of 11 and polynomial order 3. Too much smoothing is generated with an order of 2 and the characteristics of the left flank (0-200m) of the data are lost. Increasing the order to 4 introduces steps into the left flank of the anomaly (330m) and in the base of the anomaly (415m).

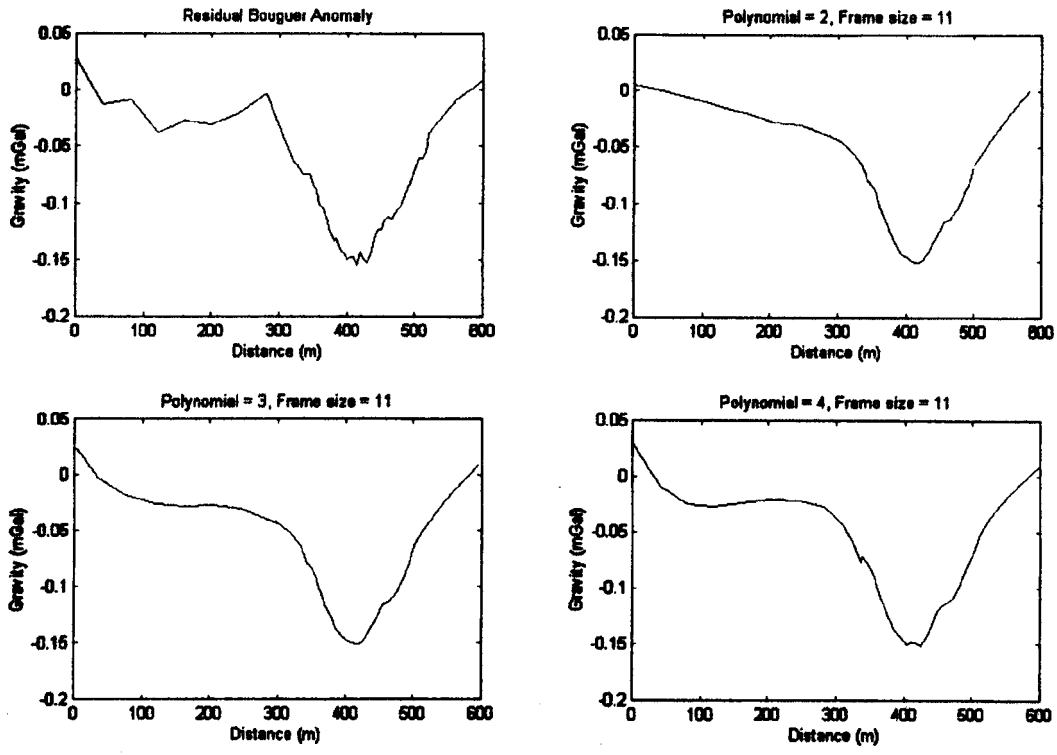


*Fig. 6.11 Filter testing of the May 11, 2002 data. The frame size has been kept constant while the polynomial order has been varied. The best result is obtained when using a polynomial order of 3 as the signal has been considerable smoothed but has kept the main characteristics of the data.*

The process has been repeated with a frame size of 15. In this test the polynomial order has been varied between 3 and 7 and it can be seen that a polynomial order of 5 produces the best results. In this test a polynomial order of 3 is too low and over smoothes the data, whereas a polynomial order of 7 has the same effect as the 4$^{th}$ order polynomial in the previous test; that is to introduce jumps into the data.

A filter with the a frame size of 11 and a polynomial order of 3 was chosen to apply to the data set as it produced the smoothest gradients whilst still retaining the main characteristics.

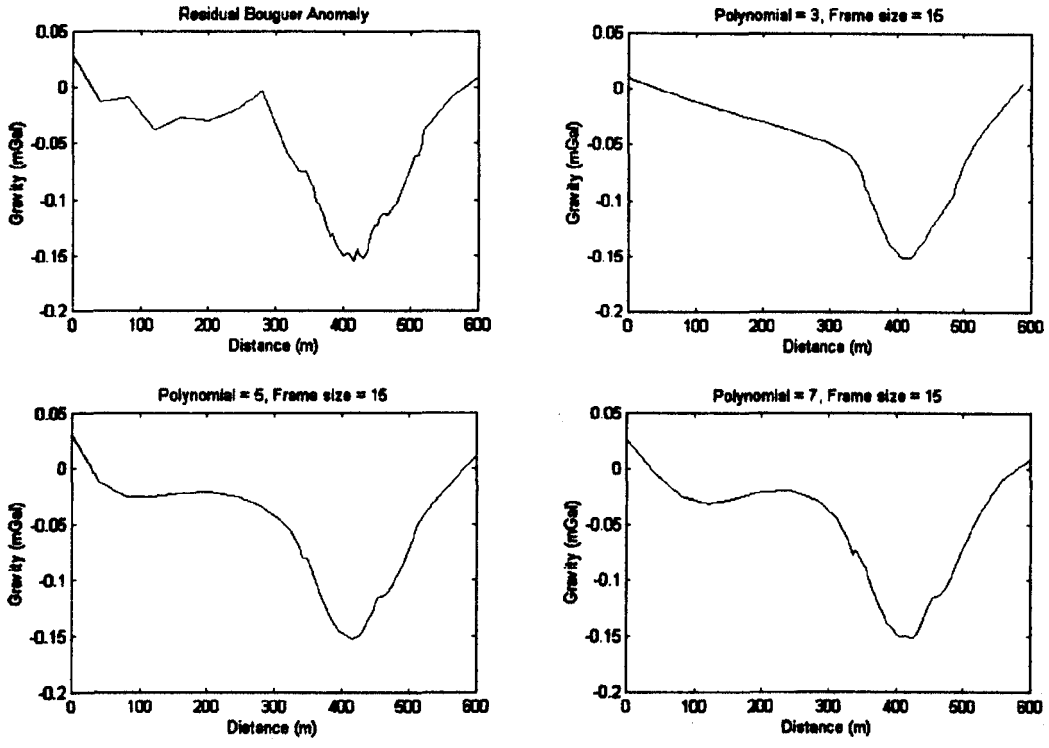


*Fig. 6.12 The results of testing the Savitzky-Golay polynomial filter on the May 11, 2002 data set. The frame size as been kept constant at 15 and the polynomial order has been altered between 3 and 7. It can be seen that an order of 5 gives the best results for this frame size.*

### 6.3.5 Borehole data

Several boreholes logs are available for the area around the canal (Table 6.1; Figure 6.13). They are confidential but the data derived from them gives us geological information about the area with which we can improve our interpretation. Importantly, this allows us to constrain the solution derived by using the 2.5D polygon modelling with plausible geological scenarios.

In general the strata dips towards the SE, although the boreholes are in one plane so it is difficult to state the true dip of the beds as the strike is not known. The top salt

horizon thickens to the SE as does the drift cover. Of some importance is a 5.2m high void which has formed at a depth of 71.53m below Ordnance datum, (95m below surface) in borehole 4. This void is located in the bottom salt bed and is most likely related to the Adelaide Mine




*Fig. 6.13 The location of the boreholes in the area around the investigation site.*

| **Borehole #** | **1** | **2** | **3** | **4** | **5** |
|---|---|---|---|---|---|
| Date | N/A | N/A | 08/96 | 08/96 | 08/96 |
| East | 66927 | 66707 | 66735 | 668911 | 67196 |
| North | 75733 | 75769 | 75833 | 75697 | 75530 |
| Ground Level (m). | 26.27 | 25.94 | 25.78 | 23.47 | 24.1 |
| Level base drift (m) | | | 12.78 | 6.17 | 8.3 |
| Level wet RH (m) | -13.62 | -17.40 | -16.22 | -19.93 | -17.72 |
| Level base top Bed (m) | -39.07 | -40.20 | -40.22 | -41.33 | -44.9 |
| Thickness of Top Salt (m) | 25.45 | | 24.00 | 24.4 | 27.18 |
| Level Base 30'Marl (m) | -47.03 | | | -48.93 | |
| Level Base Bottom Bed (m) | -74.28 | -76.17 | | | |
| Level top of Void (m) | | | | -71.53 | |
| Level Base of void (m) | | | | -76.73 | |

*Table 6.1. Summary of the borehole logs. Borehole locations are shown in Figure 6.13. Heights are relative to Ordnance Datum.*

### 6.3.6 Modelling of gravity data

The source of the anomaly has been investigated using Euler Depth Analysis and 2.5D polygon modelling in an attempt to get a estimate the size and depth of the causative body.

A Savitzky-Golay filter (polygon order 3, frame size 11) has been applied to the May 2002 data set before using the gradient of the data to solve Euler's equations for depth, obtaining a depth estimate of ~90m at a distance of ~400m along the profile. The

depth solution is presented in Figure 6.14 and is represented by the clustering of blue circles. A structural index of one (vertical tabular body) has been used to represent the shape of the body. A window length of 20 has been used with a tolerance of 0.2.

It is also possible to derive a satisfactory depth estimate of ~40m (i.e. one with sufficiently close clustering of blue circles) by using a window length of 10 and a tolerance of 0.027 with a structural index of 0.6 (stope). Although this estimate has a lower degree of confidence attached to it as it has less solutions clustering (Figure 6.15), it does, however, suggest that an anomalous body could be present at this shallower depth. Although reducing the structural index will have the effect of decreasing the depth of the solutions, this is not sufficient to explain a shallowing of 50m. It is not possible to get a clustering at 40m with a structural index of 1.0, neither is it possible to produce significant clustering at ~90m with a structural index of 0.6. It is my opinion that the result is caused by a body at ~40m depth which has a different shape to the deeper one.

This solution also relates well to the geology extracted from the borehole logs. The logs place wet rock head at a depth between 13.62m and 19.92m below O.D. which relates to 39.89m and 43.4m below surface respectively. It also fixes the known void (old mine) in the lower salt bed to a horizon between 71.53m and 76.73m below ordnance datum which relates to 95m and 100.2m below the surface respectively. This evidence suggests that the gravity anomaly is a result of solution at wet rock head superimposed onto the signal generated by the original mine.

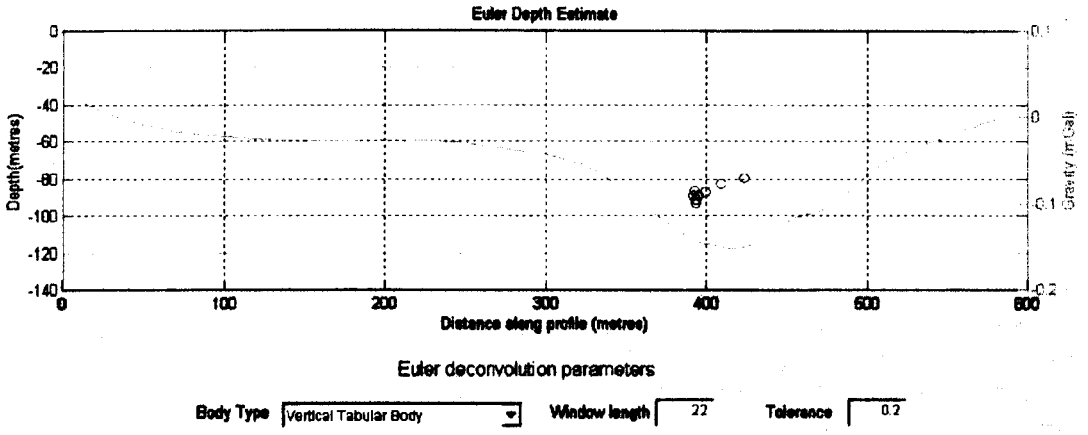


*Fig. 6.14 Euler depth estimate for the May 11, 2002 profile. Solutions cluster around 90m. Structural index=1, window length=22 and tolerance=0.2.*

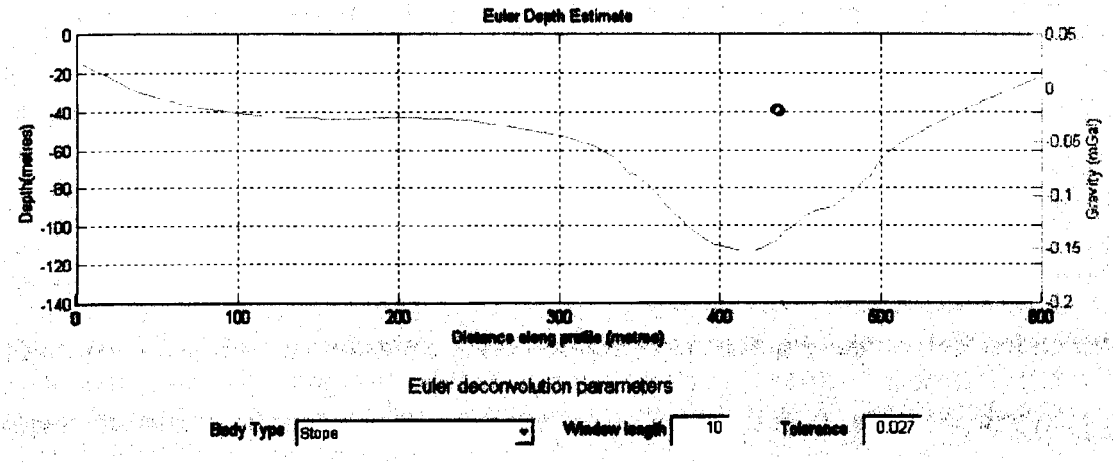


*Fig. 6.15 Euler depth estimate for the May profile. Solutions cluster around 40m. Structural index=0.6, window length=10 and tolerance=0.027.*

### 6.3.6 2.5D Modelling

Using the data extracted from the borehole logs we are able to create a geological model within GRAVMAG. Assigning properties (Table 6.2) to the geological units such as density and extent along strike, we are able to produce a gravity response for the model.

By matching the model's gravity response to the observed gravity enables us to hypothesise as to the cause of the gravity anomaly.

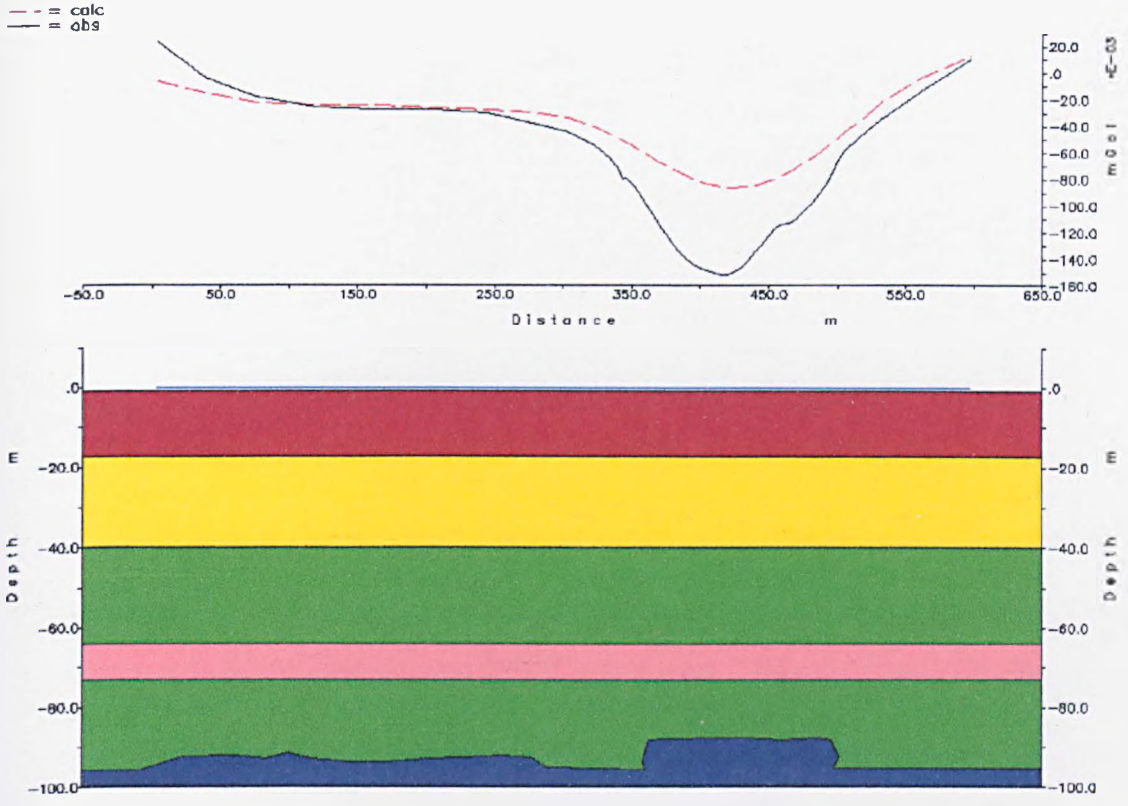


*Fig.6.16 GRAVMAG model of the Trent and Mersey canal at Marston. It is not possible to match the observed gravity with a single body of density 1Mg/m³ while keeping the top surface of the body below 90m. Properties are shown in Table 6.2.*

Assuming the void has a density of 1Mg/m³ (i.e. a water-filled cavern) it is not possible to match the observed gravity signal if we restrict the top surface of the void to a depth of 90m (Figure 6.16). In fact it requires the top surface for the void to rise above 75m in order to match the anomaly.

If a second void at wet rock head (i.e. 40m) is added to the model the observed gravity signal can be matched and the dimensions of the void kept within those suggested by the Euler depth analysis (Figure 6.17).

Although this solution is not unique it does agree with the estimates derived from the Euler depth analysis, that is, two bodies exist and lie at separate depth horizons.

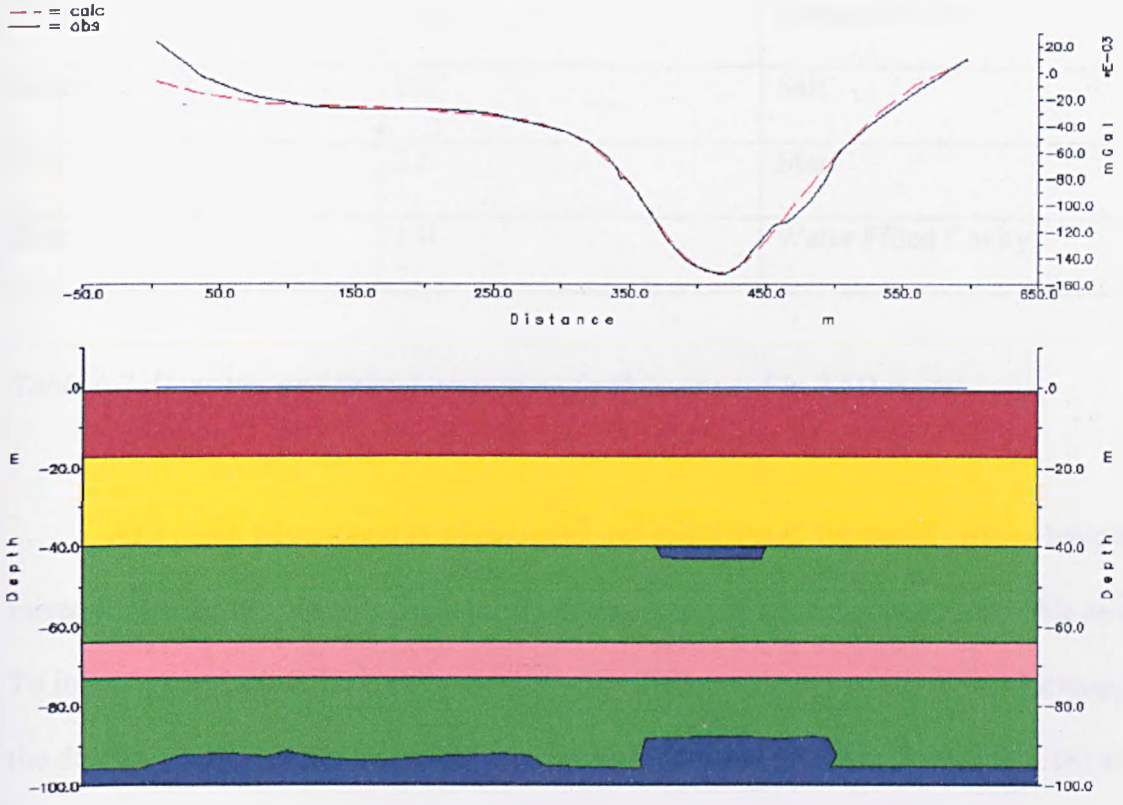


*Fig.6.17 GRAVMAG model of the Trent & Mersey canal at Marston. By adding a second body at a depth of 40m it is possible to match the observed gravity and keep the top surface of the lower body below 90m. Properties are shown in Table 6.2.*

| Polygon Colour | Density $Mg/m^3$ | Rock type |
|---|---|---|
| Brown | 1.6 | Drift |
| Yellow | 1.8 | Unnamed Unit |
| Green | 2.1 | Salt |
| Pink | 2.0 | Marl |
| Blue | 1.0 | Water Filled Cavity |

*Table 6.2. Densities and brief description of polygons used in 2.5D model*

As a result of continuous subsidence over many years, the canal's banks have been raised several times. As a consequence it is probable that the canal deepens in this area. To investigate whether the gravity anomaly recorded could be the result of an increase in the depth of the canal, the scenario has been modelled in GRAVMAG (Figure 6.18) as there is no bathymetry data available for this stretch of the canal.

The model assumes that the increase in canal depth would only be filled with water. The build up of sediment has not been incorporated into the model. Although it is highly unlikely that there would not be a build up of sediment during the subsidence of the canal, this model provides the minimum depth (maximum density contrast) by which the canal would need to subside in order to produce the gravity anomaly recorded.

The results of the modelling in GRAVMAG show that a minimum depth of ~18m would be necessary in order for the recorded gravity anomaly to be produced. This figure would probably double if sediment was considered. The canal currently stands 4m higher than the surrounding ground to the south, which gives a reasonable estimate of the total subsidence if we assume that the canal was not raised during its construction. Therefore

we can conclude with confidence that a deepening of the canal can not realistically produce the gravity anomaly.

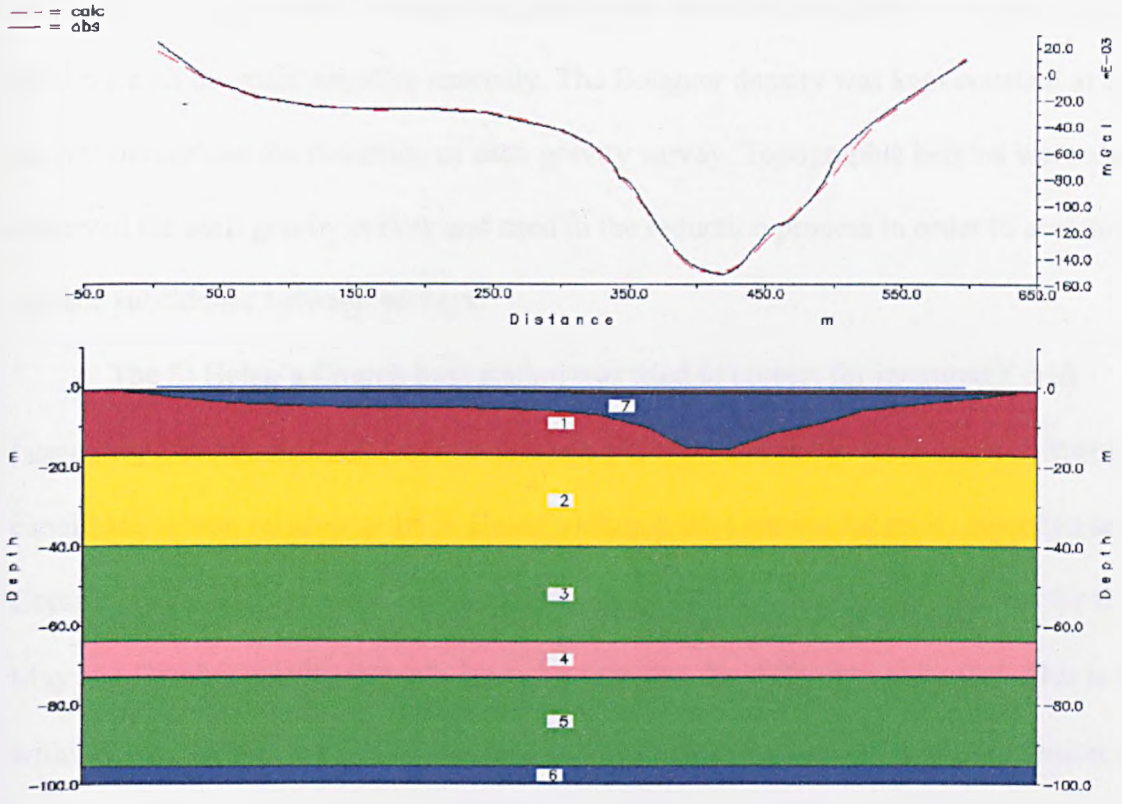


*Fig.6.18 GRAVMAG model of the Trent & Mersey canal at Marston. Although it is probable that the canal deepens in this area, the depth it would need to attain in order to produce the gravity signal recorded is too great. It has been possible to match the observed gravity signal by extending the depth of the canal to ~18m.*

### 6.3.7 Time-lapse microgravity

After establishing that a significant gravity anomaly was present and related to a low density feature located at depth, the plan to re-survey the profile was put in to action.

Gravity was re-acquired along the profile on two further occasions, July 12 and the October 22, 2002. The aim of the repeating the survey was to monitor the suspected void in order to determine if it was currently stable.

Gravity was acquired along the same profile using the same instrument and station locations. For the repeated surveys the profile was extended by 160m in order to be certain of closure on the main negative anomaly. The Bouguer density was kept constant at 2.2 $Mg/m^3$ throughout the reduction of each gravity survey. Topographic heights were also re-observed for each gravity survey and used in the reduction process in order to account for surface subsidence between surveys.

The St Helen's Church base station was used to correct for instrument drift (assuming it to be linear) and to calculate the gravity value of the local Trent & Mersey canal base station relative to the St Helen's Church base station for each respective survey. Comparing the average value of the local Trent And Mersey base station values for the May and October gravity surveys, it can be seen that the difference is 3 μGal. This is well within the expected errors of a repeated survey, suggesting that the local base station at the Trent & Mersey Canal has not changed in the period between surveys. It is necessary to average the local Trent And Mersey Canal base station values to account for Earth tides variations during the day (as the tidal variations are sinusoidal their average will be zero). Applying this correction also ensures that tares between surveys have not effected the instrument.

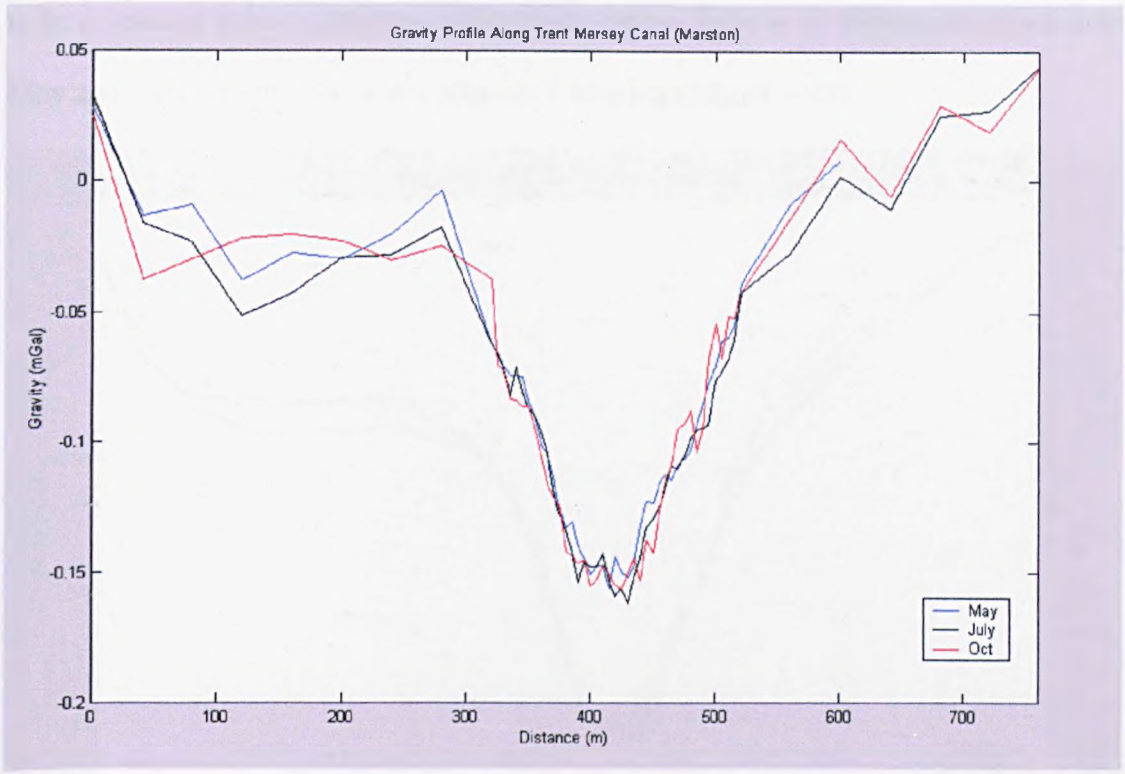


*Fig. 6.19 A graph combining the residual gravity profiles for the surveys acquired in May, July and October 2002.*

From the residual gravity plots shown in Figure 6.19 we can see that the main negative anomaly has been detected on each of the subsequent surveys. Its gradient and amplitude are in general agreement although because of the high frequency noise it is difficult to identify any significant change.

If the filtered data sets are plotted (Figure 6.20), it can be seen that there is a very good match between the data sets. In particular the gradient on the left limb of the main anomaly is constant across all three surveys. There is a small degree of variation in the right limb of the anomaly around 425m along the profile. The main area of noticeable change is on the July survey between 0 and 300m. This section of the profile has a spacing of 40m and consequently the change is likely to be due to an error in the gravity readings caused by the meter settling after being transported between stations. It would not appear

to be a result of sub-surface mass changes as there is little or no difference between the May and October surveys in this area after filtering (Figure 6.20).

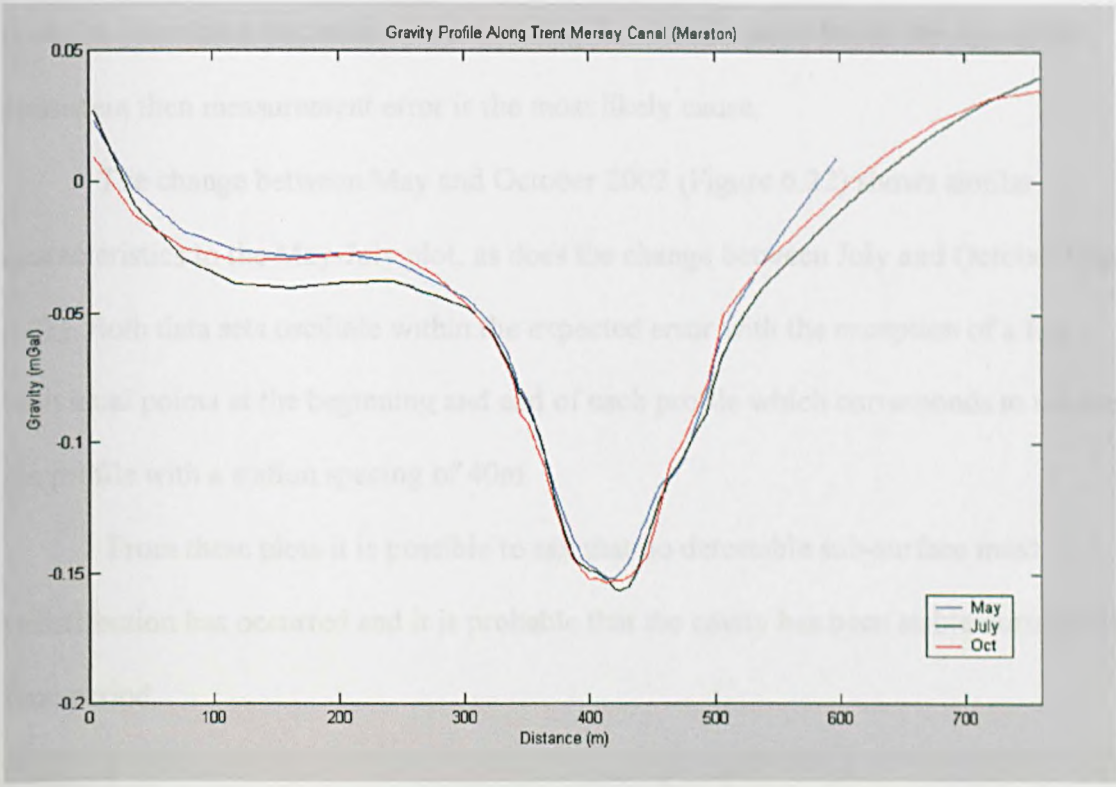


*Fig. 6.20 Plot showing the three gravity surveys after the Savitzky-Golay polynomial filter has been applied to each data set.*

In order to investigate further how the gravity signal has changed between these surveys, the reduced Bouguer anomalies from each survey have been subtracted from each other. No regional field has been subtracted from the data set as this should be accounted for in the subtraction as it will not have changed significantly in the intervening periods. In the same way any terrain effects associated with the surrounding topography will be accounted for. By removing these two contributing factors in this way, the accuracy of the survey is increased.

Examining the change in observed gravity between May and July 2002 (Figure 6.21), it becomes apparent that there is no pattern to the observed changes. Instead the

values appear to oscillate between -15µgal and +15µgal. This is just over the expected accuracy of a time-lapse survey (see Chapter 3). If the values were sign consistent then it could be postulated that mass movement may have taken place but as the sign is not consistent then measurement error is the most likely cause.

The change between May and October 2002 (Figure 6.22) shows similar characteristics to the May-July plot, as does the change between July and October (Figure 6.23). Both data sets oscillate within the expected error with the exception of a few individual points at the beginning and end of each profile which corresponds to the area of the profile with a station spacing of 40m.

From these plots it is possible to say that no detectable sub-surface mass redistribution has occurred and it is probable that the cavity has been stable during this time period.

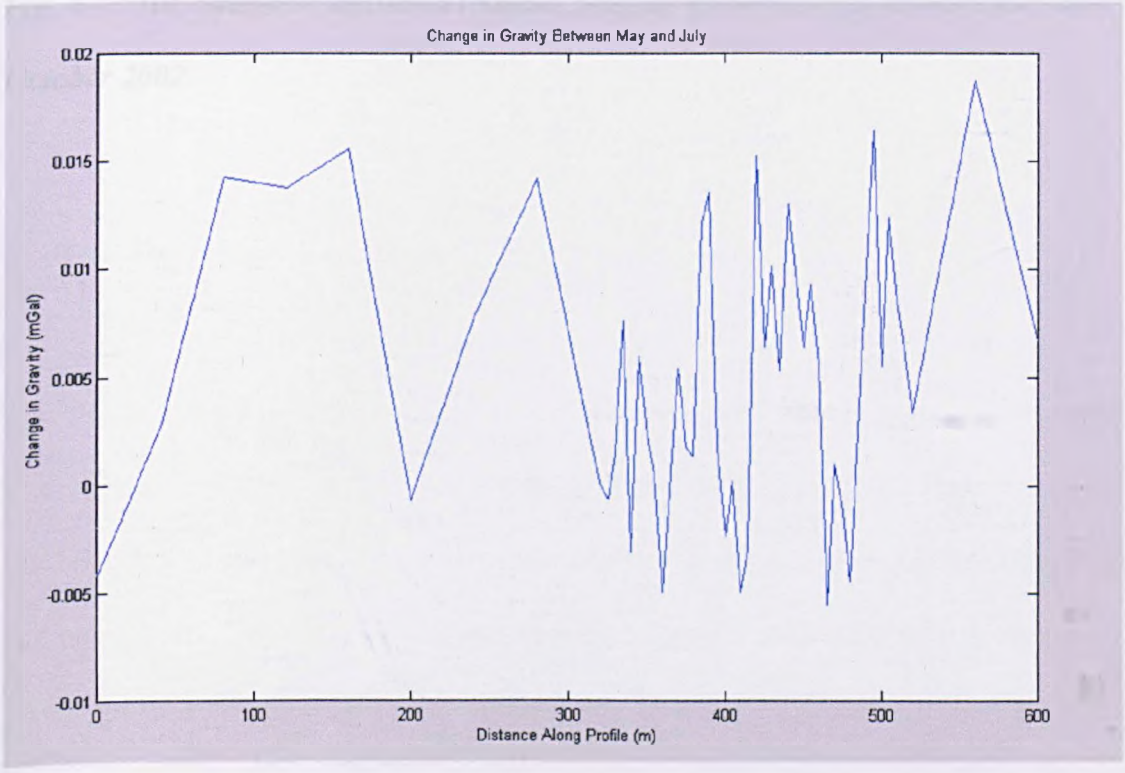


*Fig. 6.21 The change in unfiltered reduced Bouguer gravity values between May and July 2002.*

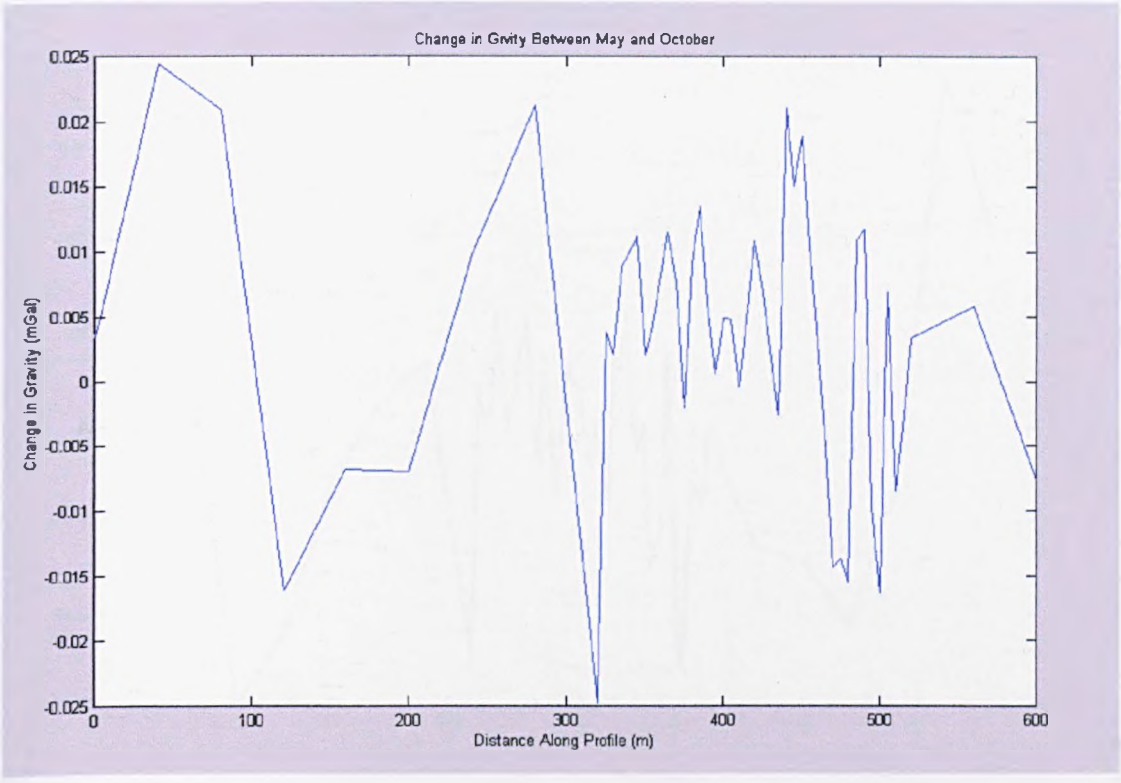


*Fig. 6.22 The change in unfiltered reduced Bouguer gravity values between May and October 2002.*

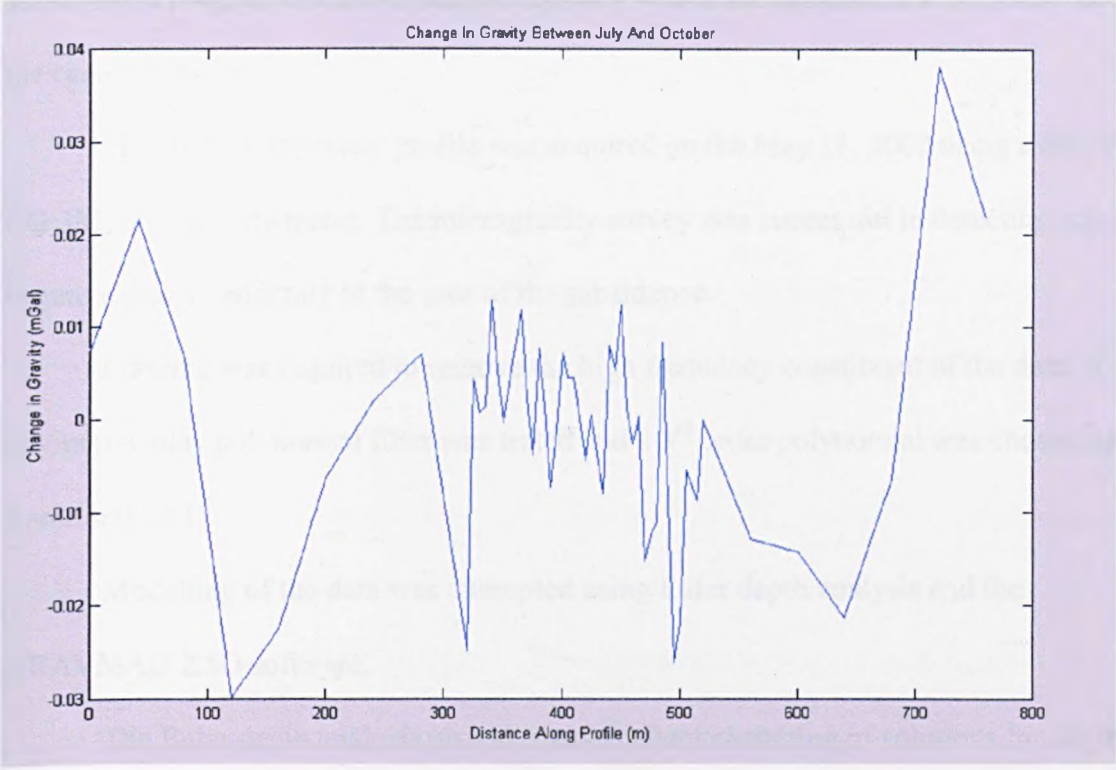


*Fig. 6.23 The change in unfiltered reduced Bouguer gravity values between July and October, 2002.*

### 6.3.8 Summary and conclusions

The Trent & Mersey canal was an important link in the development of the salt industry in and around Northwich. Reduced transport cost resulted in the establishment of numerous mines along the banks of the canal. The stretch of canal at Marston, Cheshire has experienced subsidence for many years and has in the past burst its banks, flooding the surrounding area. The canal was re-cut in 1958 to avoid further damage to property through subsidence. However, the stretch of the canal at Marston is currently experiencing subsidence.

result of a low density area and establish the causative bodies size and depth. If this proved successful a program of time-lapse microgravity would be implemented to try and assess the canals stability.

The first microgravity profile was acquired on the May 11, 2002 using a Scintrex CG 3M microgravity meter. The microgravity survey was successful in detecting a large negative gravity anomaly in the area of the subsidence.

Filtering was required to remove the high frequency constituent of the data. A Savitzky-Golay polynomial filter was tested and a 3$^{rd}$ order polynomial was chosen using a frame size of 11.

Modelling of the data was attempted using Euler depth analysis and the GRAVMAG 2.5D software.

The Euler depth analysis provides an excellent clustering of solutions for the depth of the causative body at ~90m below the surface using a structural index of 1 and a frame size of 22. However, using a smaller frame size (10) and a lower structural index (0.6) also produced a significant clustering of solutions at a depth of 40m below surface. No other combinations of frame size and structural index provided a significant clustering of solutions.

2.5D modelling using the GRAVMAG program confirmed that two separate bodies at different depths was a likely and plausible solution. Assuming a density of 1 Mg/m$^3$ it is not possible to match the observed data with a single body without placing the top surface much shallower than the Euler results suggest. However, it is possible to match the observed data with two individual bodies with densities of 1 Mg/m$^3$ by placing them at the depth suggested by the Euler depth analysis.

The two-body theory is also supported by borehole data available in the area. The borehole logs report that wet rock head is encountered at a depth of ~40m and that a void within the lower salt bed is located between 95m and 100.2m below surface.

The microgravity survey was repeated in July and October. The main negative anomaly discovered in May is also present in both of the surveys. Modelling of the July and October surveys is consistent with the solutions derived from the May survey. Analysis of the gravity data shows that the gravity signal has not changed significantly between each survey and is within the expected error for a survey of this kind.

It is likely therefore that the gravity low in the area is related to the subsidence being experienced along the Trent & Mersey canal at Marston. Modelling of the gravity low suggests that it is caused by the superposition of two water filled cavities at different depths below the surface. The first is located at ~90m below surface and is related to the original mine workings. Borehole data places the original roof at a depth of 95m. The shallowing of this contact would suggest that further collapse or spalling has occurred since the borehole was logged. The second cavity is located at a depth of ~40m below surface. This cavity corresponds to solution at wet rock head and is likely to have developed as a result of changes in the level of ground water or by fresh water being drawn through the area.

Reviewing the results from the GEMA trial, the preferential flow line that crosses the canal in the centre of Figure 6.22 corresponds spatially to the gravity low detected in the microgravity surveys acquired in 2002. This correlation adds credence to the postulation that the anomalous low density body, isolated by the microgravity survey, is a result of dissolution at wet rock head, accelerated by a brine flow orientated east west, between Marston Old Mine and Adelaide mine. At this stage the direction of flow is not known.

During the period in which the area has been monitored using microgravity the gravity signal has not changed significantly. However, the change in depth of the lower cavity relating to the original mine and nature in which the second cavity at wet rock head has been formed, suggests that over a longer period the area will continue to be dynamic. As a result the gravity signal will evolve as the size and depth of the causative bodies change. Further monitoring of the canal at Marston is recommended.

### 6.3.9 Future work

- Continued monitoring of the canal with microgravity.
- Forward modelling of the size of collapse needed to produce a detectable change in gravity.
- Ground proof of the existence of the shallower body.
- Geotechnical monitoring of the above borehole.
- Continued precise levelling of the area, extending to the ground north and south of the canal.

## 6.4 Second site in Marston area

The following section describes the results of a microgravity survey undertaken at a second site in the Marston area. It is not possible to name or give details of this site's location because of political sensitivities. This survey has been included in this chapter because of the similarity of the geology and ground subsidence observed with that along the Trent & Mersey canal.

### 6.4.1 Introduction

At the request of Mr. Gareth Ellis (Environmental Planning, Cheshire County Council) a second microgravity survey was acquired in the vicinity of Marston. It is not possible, at this stage, to identify the location of the survey due to political reasons, however, this survey has been included in this chapter because of its similarity to the Trent and Mersey canal survey.

The area of interest had been identified, through a program of precise levelling (in operation since October 1998), to have subsided by a maximum of 232mm over a 3-year period.

The aim of the microgravity survey was to investigate the cause of the subsidence and to provide information on the depth and size of the causative body. In order to reach this objective, the microgravity technique was chosen for this investigation because of its record of success in the identification of sub-surface mass contrasts, especially in the Northwich area.

The survey was intended to be a reconnaissance survey to determine whether the subsidence was related to a sub-surface mass deficiency, and whether this was detectable by a microgravity survey. In light of this, and as a consequence of the surrounding environment, a single profile was chosen on which to acquire the survey.

It is intended that if the survey is successful and the political climate allows, the survey will be extended to cover the whole of the effected area.

### 6.4.2 Survey procedures

Microgravity data acquisition was performed during the October 21, 2002 with a Scintrex CG-3M microgravity meter. The profile was centred on the survey pin showing the greatest subsidence and extended 300m to the north and 240m to the south. A profile length of 540m was thought to be necessary in light of the canal survey. A split spacing of 5m and 20m was used, similar to that implemented in the canal survey. For the main area of interest a station spacing of 5m was used. This was centred at the lowest point of the subsidence and extended for 100m to the north and 100m to the south, cutting the subsidence trough at right angles to its strike. A secondary station spacing of 20m was used to extend the profile to an area unlikely to be influenced by the gravitational signal of any sub-surface mass differences associated with the subsidence. This secondary station spacing extended for a further 200m in a northerly direction and 140m towards the south. Based on the work carried out alongside the Trent & Mersey canal, where a similar geological situation exists, this would enable delineation of a gravity anomaly associated with the subsidence.

A single base station was used and revisited at hourly intervals throughout the survey. This was located at the centre point of the profile. This base station was then re-occupied at approximately 60 minute intervals in order to account for the internal drift of the instrument.

Gravity was recorded for a period of 90 samples at each station and re-observations were regularly made in order to check the accuracy of the survey. The topographic heights of the survey points needed for the Free Air Correction were acquired using a Sokia Total Station with a closed loop accuracy of 5mm.

### 6.4.3 Gravity results

The purpose of the interpretation of the microgravity survey was to identify areas of the gravity profile indicative of low-density materials or cavities present in the sub-surface that might be responsible for the continued subsidence in the area. The gravity data was reduced to a Bouguer anomaly using a Bouguer density of 2.2 $Mg/m^3$. Two trends were removed in order to produce the residual anomaly. They were:

$$y' = y - (0.00165x + 0.001) \quad (6.2)$$

for gravity stations –240m to 95m, and

$$y' = y - (0.00105x + 0.007) \quad (6.3)$$

for gravity stations 100m to 300m.

The likely cause of this change in regional trend is a change in dip of the local geology. The residual Bouguer anomaly is presented in Figure 6.24.

The quality of the data acquired on October 21 was generally of a poor standard. The repeatability at any one station was between 15 and 20 μGal. There are three main factors that have contributed to this. The most likely cause is the disturbance caused by the traffic in the area. Passing vehicles degenerate the quality of data in two ways. Firstly the disturbance they create in the air causes the gravity meter to move, disturbing the levels. Secondly, their weight causes the ground to vibrate which in turn causes the instrument's internal mechanism to oscillate. Surface waves created by earthquakes swarms occurring in the Manchester area during the acquisition period area are another contributing factor to the poor data quality. During the period of acquisition on the October 21, 2002 seven earthquakes originating in the Manchester area were recorded. The largest magnitude recorded during this period was 3.9 at 11:42:35 am. The associated ground disturbance

the poor data quality. During the period of acquisition on the October 21, 2002 seven earthquakes originating in the Manchester area were recorded. The largest magnitude recorded during this period was 3.9 at 11:42:35 am. The associated ground disturbance causes the instruments internal mechanism to oscillate resulting in poor repeatability and the high frequency scatter evident in Figure 6.24.

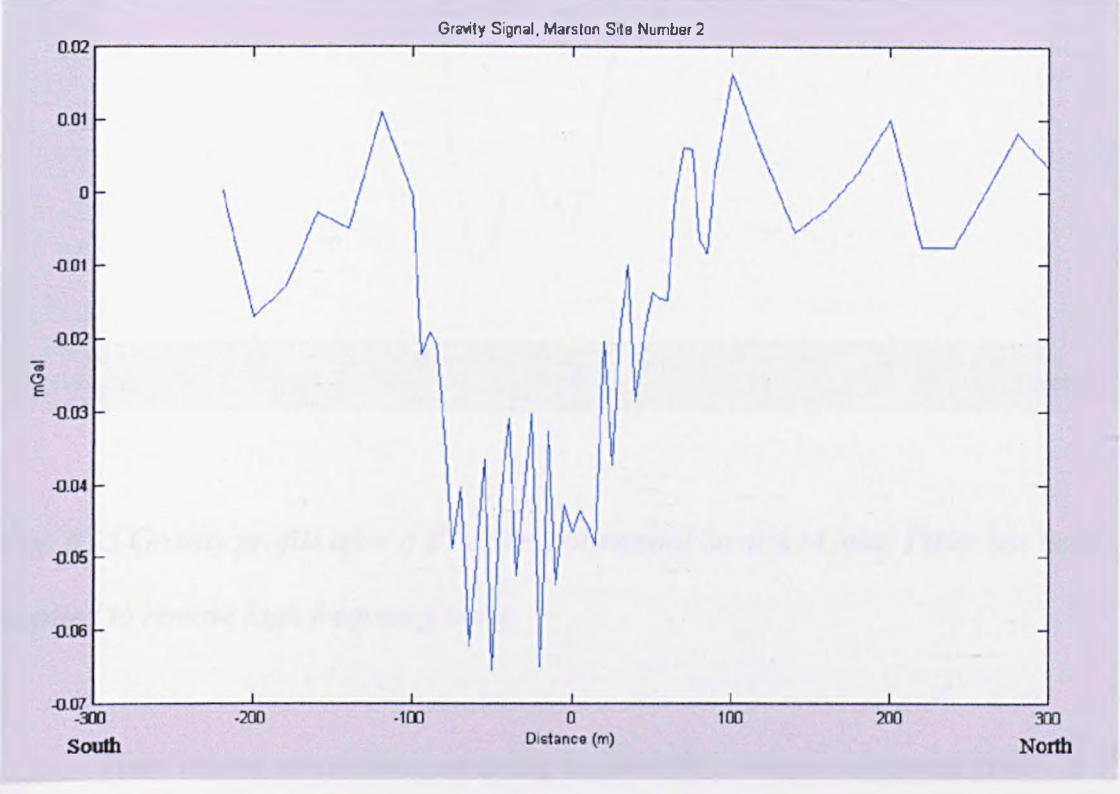


*Fig. 6.24 Residual Bouguer anomaly of the gravity data acquired on October 21, 2002.*

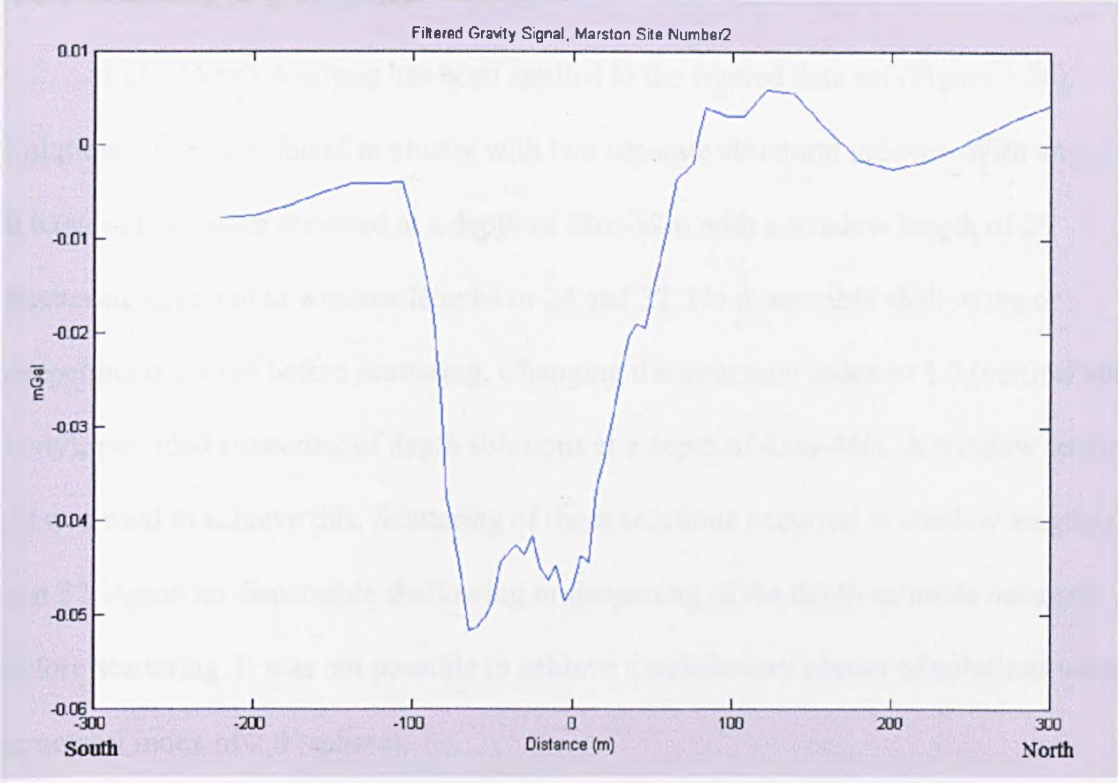


*Fig. 6.25 Gravity profile after a 3rd order polynomial Savitzky-Golay Filter has been applied to remove high frequency noise.*

Filter testing was carried out using the Savitzky-Golay Polynomial Filter. A 3rd order polynomial Savitzky-Golay Filter with a frame size of eleven was chosen as it gave the best compromise between smoothing of the high frequency noise associated with the disturbances, while retaining the main characteristics of the anomaly. The filtered data set can be seen in Figure 6.25.

Investigation of the residual Bouguer gravity data in Figure 6.25, reveals a significant gravity low between –100 and +80m along the profile. The anomaly has a maximum amplitude of –50μGal and appears to be a result of the summation of two separate gravity lows as a small positive feature is present at the centre of the anomaly (-40m).

### 6.4.4 Modelling of gravity data

Euler Depth Analysis has been applied to the filtered data set (Figure 6.26). Solutions have been found to cluster with two separate structural indexes. With an index of 0.6 (stope), a cluster occurred at a depth of 28m-32m with a window length of 28. Scattering occurred at window lengths of 24 and 32. No discernible shallowing or deepening occurred before scattering. Changing the structural index to 1.0 (vertical tabular body), provided clustering of depth solutions at a depth of 43m-46m. A window length of 30 was used to achieve this. Scattering of these solutions occurred at window lengths of 27 and 32. Again no discernible shallowing or deepening of the depth estimate occurred before scattering. It was not possible to achieve a satisfactory cluster of solutions using a structural index of 2.0 (sphere).

This is a similar situation to that encountered in the interpretation of the profile acquired along the canal, although the separation of the two depths is not as great. It is conceivable, however, that the anomaly is made up of two individual bodies of differing geometry (and therefore structural index), located at different depths, as postulated in the canal survey. The double negative within the main anomaly supports the interpretation that the anomaly is a result of two anomalous bodies. However, it is also possible that it is simply one body with the cluster being the result of incorrect structural index selection but this is unlikely from the profile shape.

It must be remembered, however, that the original data is not of a good quality and has been filtered considerably in order to achieve this solution. Interpretations drawn from this quality of data can only be an estimate or a guide and the interpretation re-considered, should further information become available.

An example of one area of contention caused by the poor quality of the data, is the lateral position of the depth estimates. The clustering of the solutions derived from the

Euler Depth Analysis consistently plotted between 30m and 50m north of the centre of the profile, i.e. 30m to 50m to the north of the centre of the measured subsidence. This is not inconceivable as the survey nails used for the topographic monitoring are sited at 40m intervals, however, it is counterintuitive as it appears to disagree with the position of the main gravity low which would place the causative body between –60m and 0m along the profile.

Although it appears that the lateral position of the depth solution is related to a flexure in the northern limb of the gravity anomaly, further filtering has shown that this is not the case. As a test, the data has been over filtered, removing all gradient changes from the main gravity anomaly's limb. The lateral position of the depth solution remains consistent with the less severe and more appropriate filter. At this time there is no explanation for this aberration.

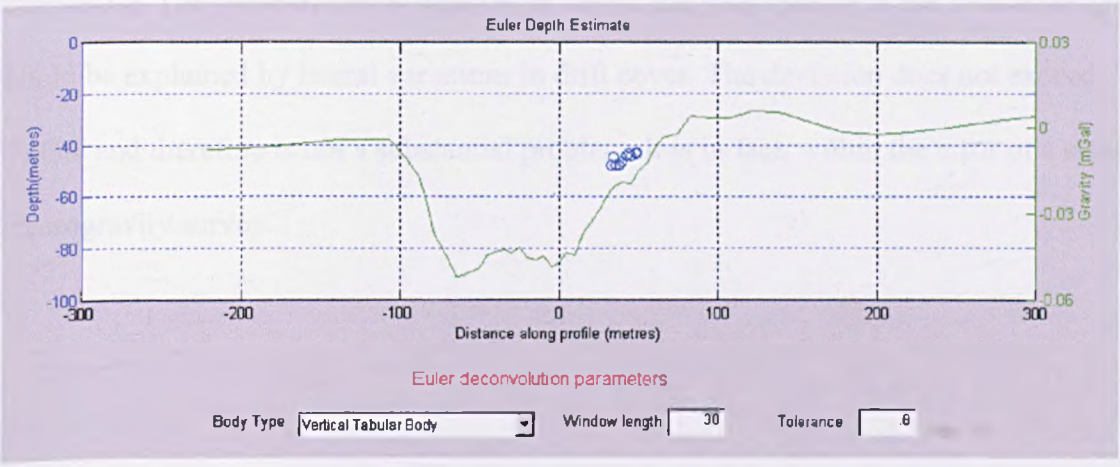


*Fig. 6.26 Euler depth estimates for Marston Lane. The solutions cluster between 43m and 46m depth.*

A 2.5D model has been created using GRAVMAG (Figure 6.27). No borehole information is available for this area and so this model uses borehole information taken from the Marston Canal site to create a basic geological cross section. Densities have been

estimated from the driller's log and are listed in Table 6.3. In this model the two salt beds are depicted by the green polygons. Wet rock head is at a depth of approximately 40m below the surface. A plausible solution has been created using this information and experience gained from other sites in the Northwich area.

A credible interpretation, using the information available at present, is that the gravity low is the result of two low-density areas (represented by blue polygons) at or near wet rock head. These areas have been modelled as water-filled cavities with a density of 1.0 $Mg/m^3$. The depth estimates from the Euler Depth Analysis have been used as the basis for the position of the voids. However, it is not possible to match the observed gravity by placing these bodies at the X co-ordinate suggested by the Euler Depth Analysis. Instead, they have been sited beneath the two gravity minima.

The observed and calculated gravity signals deviate from one another at the ends of the profile. The cause of this is likely to be due to the poor quality of the data although it could be explained by lateral variations in drift cover. The deviation does not exceed 7μGal and therefore is not a substantial problem. It is in fact, within the error of a standard microgravity survey.

| **Polygon Colour** | **Density Mg/m³** | **Rock type** |
|---|---|---|
| Brown | 1.6 | Drift |
| Yellow | 1.8 | Unnamed Unit |
| Green | 2.1 | Salt |
| Pink | 2.0 | Marl |
| Blue | 1.0 | Water Filled Cavity |

*Table 6.3. Densities and brief description of polygons used in 2.5D model*

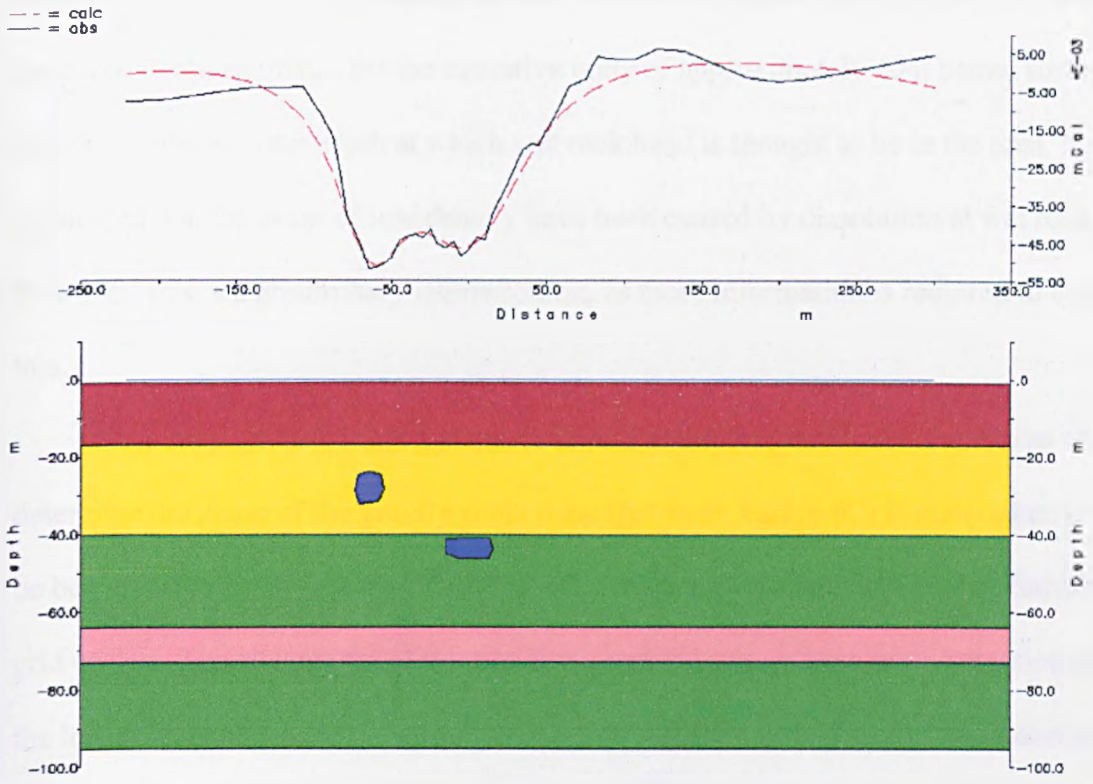


*Fig. 6.27 A 2.5D model of the possible cause of the gravity lows present in the data acquired on October 21, 2002. Borehole data from the Marston Canal site has been used to create a geological cross section in which the two salt beds are represented by the green polygons. Two water filled cavities are represented by the blue polygons. Geological descriptions and densities are presented in Table 6.3.*

### 6.4.5 Conclusions

The repeatability of the microgravity data is poor due to the seismic activity around Manchester. However, it clearly indicates a low density area located between –100m and +80m along the profile. This correlates with the topographic low identified by the precise levelling. The maximum amplitude of the northerly gravity low is located in the area where the maximum movement has been recorded by the 3-year precise levelling.

The data has been filtered using a Savitzky-Golay Filter to eliminate high frequency noise associated with traffic and earth movements. Modelling of the data has produced depth estimates for the causative body of approximately 40m below surface, which correlates to the depth at which wet rock head is thought to be in the area. It is postulated that the areas of low density have been caused by dissolution at wet rock head. However, this is a preliminary interpretation, as more information is required to confirm this.

It is recommended that a physical investigation programme is undertaken to determine the cause of the gravity anomalies. However, before this is undertaken it would be beneficial to extend the gravity survey into the areas that flank the profile forming a grid of data. The advantages of this are that, there is increased spatial information about the location and extent of the gravity low, which results in a higher degree of accuracy in the modelling process. As a direct result of this, sites for physical investigation can be selected with a higher degree of certainty, as the gravity minima are isolated. This can eliminate the possibility of missing the target by drilling on the limb of a larger gravity low.

Increased spatial information would also aid the interpretation of the cause of the gravity low. It would establish whether the anomaly is isolated or whether it was part of a linear feature.

# Chapter 7

# Characterisation of a Site in Northwich Using Microgravity

## 7.1. Introduction

This chapter details work carried out in Northwich town centre. It is slightly different from the preceding work at Peter Street and around the Trent & Mersey canal (Chapters 5 and 6 respectively) as it was not commissioned as a response to continuing subsidence. The purpose of the work was to assess the site for structural stability and also identify and delineate areas likely to pose problems to the public.

In the autumn of 2001, a retaining wall on the bank of the River Dane collapsed (Plate 7.1). As part of the site investigation for the rebuilding of this wall the engineer, WS Atkins, commissioned two percussion boreholes (BH10 and BH11, Figure 7.22) to investigate the ground conditions. The results from one of the boreholes (BH10) suggested that a void had been encountered at a depth of 12.8m (Table 7.1). The location of the collapse was in an area away from the known extent of the salt mine workings beneath Northwich town centre and their associated subsidence (Figure 7.1). It was therefore necessary to investigate the depth and lateral extent of the suspected void further as the area was previously thought to be solid ground. It was important to establish the size, depth and extent of the suspected void to determine whether this area is likely to be effected by further subsidence.

Gravity forward modelling of the site (section 7.3) concluded that the microgravity technique would be able to delineate areas of low density associated with the suspected

void reported in BH10. The gravity was acquired on the night of the 4th of December 2001 and processed using the method described in Chapter 3.

The use of Ground penetrating radar (G.P.R.) was felt unsuitable as the silty material, which made up the near surface deposits would impede the penetration of the radar. Therefore it was felt unlikely that the use of G.P.R would be able to further delineate the void detected at a depth of 12.5m

Section 7.4 outlines the survey procedures and processing used to reduce the gravity data to a Bouguer anomaly. It was necessary to account for the river cutting which abutted the survey area immediately to the south. Terrain effects of the river cutting were calculated using bathymetric profiles provided by the engineer.

The initial results (detailed in section 7.5) show that there is a gravity low in the vicinity of BH10 and the collapsed retaining wall. Initial modelling of the data is presented in section 7.6. Euler depth estimates have been calculated for the data. Estimates of the thickness of the body responsible for the gravity anomaly have also been calculated using the Cordell and Henderson Method. The missing mass associated with the anomalous area has been calculated as an aid for the remediation of the area.

However, initial depth estimates using Euler Deconvolution suggest that the causative body is located at a depth of 4m. This is shallower than expected and probably a result of loose material in the strata above the initial void. It is possible to remove the part of the gravity signal caused by the near surface effects by filtering the gravity data. In section 7.7 a low pass filter has been applied to the data. This removes the high frequency constituent of the signal caused by density contrasts close to the surface revealing the signature of deeper features. Euler deconvolution depth estimates using profiles taken

across the low frequency part of the anomaly suggest that the source of the anomaly lies at a depth of 12m. This is consistent with the depth of the void detected in the borehole.

Estimates of the thickness and lateral extent of the causative body using Cordell and Henderson (1968) modelling techniques (section 7.6.2) suggest that the anomalous material extends from 3m to a depth of up to 13m.

A targeted drilling program was completed, concentrating on the areas of low density identified by the microgravity survey. The results of this survey confirm the presence of a body of soft material coincident with the gravity anomalies. The maximum thickness of the anomalous material is in the area around the initial collapse (3-14m). To the east, the top of the anomalous material decreases in depth to 1.8m below the surface, with its base being at 6.8m.

The combination of microgravity and targeted ground proofing has lead to the identification of an area of low-density material around the collapsed retaining wall. Integrated processing and interpretation has identified anomalous areas of low density at two separate depths. The first body has a minimum depth of 3-4m and a base at 13m. Within this is a secondary body, at a depth of 12m. Drilling of the gravity anomalies supports the depth estimates.

*Plate 7.1 A photograph of the collapsed retaining wall which lead to the site investigation.*

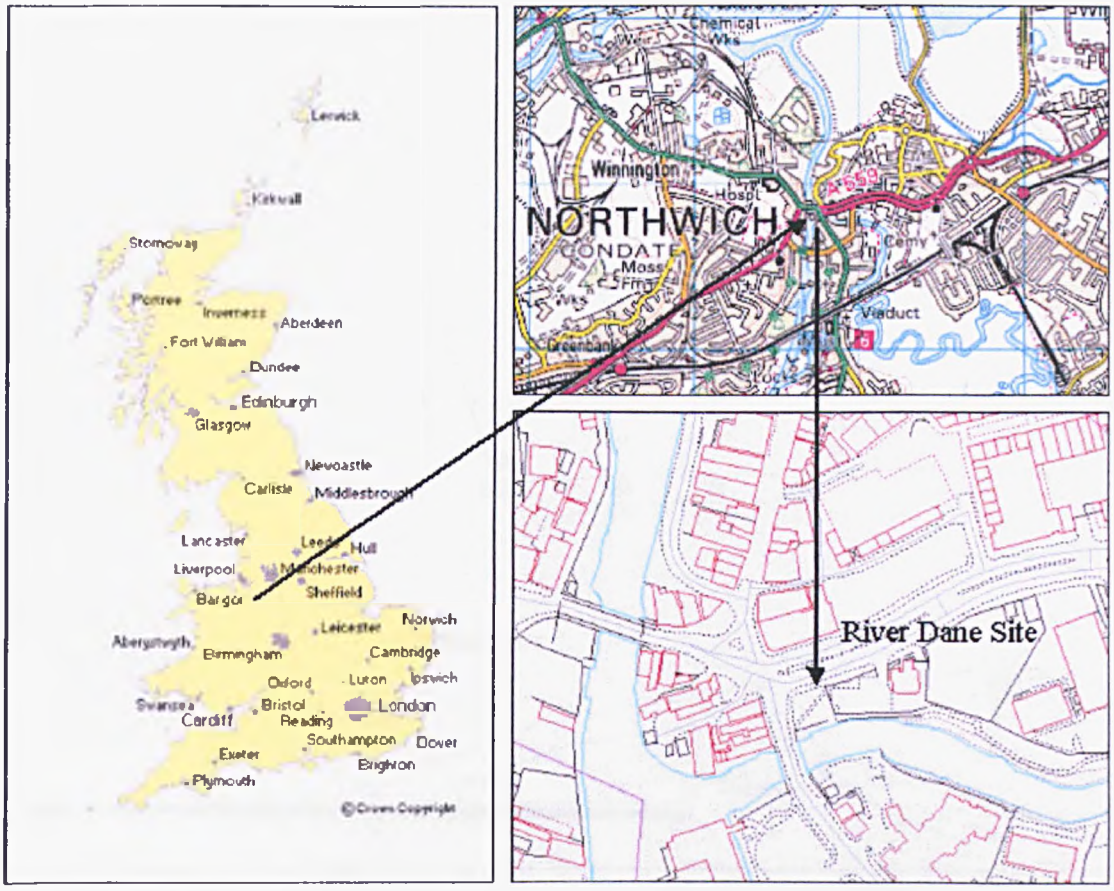




*Fig. 7.1 The site to of the survey area was located on the bank of the River Dane in Northwich, Cheshire.*

## 7.2. Borehole data

W.S. Atkins provided draft logs of the initial percussion boreholes to the Applied and Environmental Research Group at Keele University. These boreholes were drilled as part of the initial site investigation for the bank re-stabilisation. The borehole logs are listed in Tables 7.1 and 7.2. A plan of their location is shown in Figure 7.2.

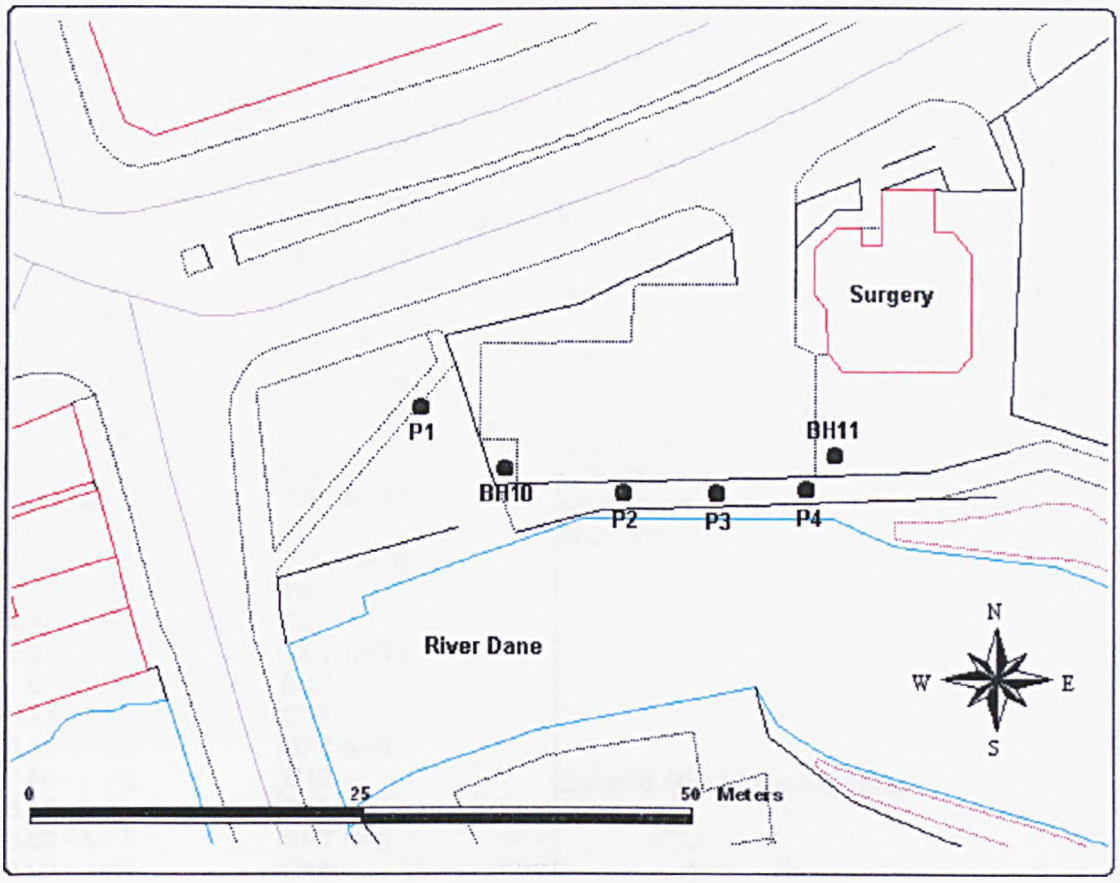




*Fig.7.2 Location of the boreholes drilled in this area. Borehole logs for BH10 and BH11 are provided in Tables 7.1 and 7.2. W.S. Atkins drilled boreholes P1-P4 as part of the secondary phase of investigation. The logs for P1-4 are provided in Tables 7.3 to 7.6.*

| **Date;** 17/10/01 | | **Borehole Number;** BH10 |
|---|---|---|
| **Driller;** Ian Farmer Associates | | **Site;** River Dane Northwich |
| **Boring Method;** Cable percussion | | **Engineer;** W. S. Atkins |
| | | |
| **Depth** | **Tests / Samples** | **Description** |
| 0.5 - 1.00 | B1 | MADE GROUND; Very loose dark brown slightly clayey gravely fine to coarse SAND. Gravel is angular and subangular fine to coarse including ash and brick |
| 1.00 - 1.45 | SPT N=2 | |
| 1.00 - 1.45 | D2 | |
| 1.45 - 2.00 | D3 | |
| 2.00 - 2.45 | SPT N=13 | |
| 2.00 – 2.45 | D4 | MADE GROUND; Medium dense brown sandy angular and subangular fine to coarse GRAVEL including ash, brick and sandstone. Occasional whole bricks. Water strike at 2.00m, rose to 2.00m in 20mins |
| 2.45 - 3.00 | D5 | |
| 3.00 - 3.45 | D6 | |
| 3.00 -3.45 | SPT N=13 | |
| 3.45 - 4.00 | D7 | |
| 4.00 - 4.45 | SPT N=10 | |
| 4.00 - 4.45 | D8 | |
| 4.45 - 5.00 | D9 | |
| 5.00 - 5.45 | SPT N=15 | |
| 5.00 - 5.45 | D10 | |
| 5.45 - 6.50 | D11 | |
| 6.50 - 6.95 | SPT N=8 | |
| 6.50 - 6.95 | D12 | Below 6.50m becoming loose |
| 6.95 - 8.00 | D13 | |
| 8.00 - 8.45 | SPT N=0 | |
| 8.00 - 8.45 | D14 | |
| 8.45 - 9.50 | D15 | Below 8.00m becoming VERY loose. SPT sank under weight of rods. |
| 9.50 - 9.95 | SPT N=0 | |
| 9.50 - 9.95 | D16 | |
| 9.95 - 11.00 | D17 | SPT sank under weight of rods. |
| 11.00 - 11.45 | SPT N=0 | |
| 11.00 - 11.45 | D18 | |
| 11.45 - 12.50 | D19 | SPT sank under weight of rods. |
| 12.50 - 12.95 | SPT N=0 | |
| 12.50 - 12.95 | D20 | |
| 12.95 - 14.00 | D21 | SPT sank under weight of rods. |
| 14.00 - 14.45 | SPT N=0 | Possible very loose or very soft strata (drillers notes possible void) SPT sank under weight of rods. |
| 14.00 - 14.45 | D22 | |
| 14.45 - 15.00 | D23 | |
| 15.00 - 15.45 | SPT N=10 | |
| 15.00 - 15.45 | D24 | |
| | | Loose to medium dense brown slightly silty gravely organic fine and medium SAND. Gravel is subangular and subrounded fine and medium including sandstone. Occasional peaty organic fragments. |
| | | At 16.00m: driller notes possible void, sampling gear fell by 2m. Bottom of void not encountered |

*Table 7.1. Log for borehole BH10.*

| **Date;** 16/10/01 | | **Borehole Number;** BH11 |
|---|---|---|
| **Driller;** Ian Farmer Associates | | **Site;** River Dane Northwich |
| **Boring Method;** Cable percussion | | **Engineer;** W. S. Atkins |
| | | |
| **Depth** | **Tests / Samples** | **Description** |
| 0.5 - 1.00 | B1 | Topsoil over MADE GROUND; Orange brown slightly gravely fine and medium SAND. Gravel is subangular and subrounded fine to coarse. Occasional plant roots |
| 1.00 - 1.45 | SPT N=5 | |
| 1.00 - 1.45 | D2 | MADE GROUND; Loose black gravely medium and coarse SAND. Gravel is subangular fine and medium including ash and brick |
| 1.45 - 2.00 | D3 | |
| 2.00 - 2.45 | SPT N=3 | |
| 2.00 - 2.45 | D4 | MADE GROUND; Medium dense brown sandy angular and subangular fine and medium GRAVEL including ash, sandstone and brick |
| 2.45 - 3.00 | D5 | |
| 3.00 - 3.45 | SPT N=10 | |
| 3.00 -3.45 | D6 | |
| 3.45 - 4.00 | D7 | |
| 4.00 - 4.45 | SPT N=11 | |
| 4.00 - 4.45 | D8 | |
| 4.45 - 5.00 | D9 | |
| 5.00 - 5.45 | SPT N=13 | |
| 5.00 - 5.45 | D10 | |
| 5.45 - 6.50 | D11 | |
| 6.50 - 6.95 | SPT N=14 | |
| 6.50 - 6.95 | D12 | |
| 6.95 - 8.00 | D13 | |
| 8.00 - 8.45 | SPT N=13 | |
| 8.00 - 8.45 | D14 | |
| 8.45 - 9.50 | D15 | |
| 9.50 - 9.95 | SPT N=14 | |
| 9.50 - 9.95 | D16 | |
| 9.95 - 11.00 | D17 | |
| 11.00 - 11.45 | SPT N=14 | |
| 11.00 - 11.45 | D18 | |
| 11.45 - 12.50 | D19 | |
| 12.50 - 12.95 | SPT N=19 | Medium dense dark brown silty gravely fine to coarse SAND. Gravel is subangular and subrounded fine to coarse including sandstone. (Possible mixing with overlying made ground in upper part). Below 14.00m becoming dense |
| 12.50 - 12.95 | D19 | |
| 12.95 - 14.00 | D21 | |
| 14.00 - 14.45 | SPT N=36 | |
| 14.00 - 14.45 | D22 | |
| 14.45 - 15.00 | D23 | |
| 15.00 - 15.45 | SPT N=24 | |
| 15.00 - 15.45 | D24 | Medium dense brown silty organic fine and medium SAND, occasional peaty organic fragments |
| | | Complete at 15.45m |

*Table 7.2. Log for borehole BH11.*

BH10 shows made ground down to a depth of 12.8m, composed of medium dense dark brown, sandy, angular and sub-angular fine to coarse gravel, including ash, brick and sandstone: the drillers log reports that this becomes loose below 6.5m, very loose after 8m and below 12.8m there is a possible void of 2m extent. Loose to medium dense, dark brown, slightly silty, gravely organic fine and medium sand and gravel is encountered at 14.8m before a second void is suspected at 16m. Whilst taking an undisturbed sample at the 14.8m horizon the driller reported that his sampling gear dropped by approximately 2m but that the base of the void was not encountered. The Standard Penetration Test (SPT) values (N) for this borehole drop from 10 - 15 to a value of 8 at a depth of 6.5m. At 8m, N drops to zero and continues at this level to the base of the borehole.

The Standard Penetration Test consists of driving a split-barrel sampler of 50mm outside diameter into the soil at the bottom of a cased borehole and is used in the determination of the state of compaction in cohesionless soils. The sampler is attached to a stiff drill rod and is driven into the soil by blows from 63.5 kg mass falling 0.76 m. The sampler is initially driven a distance of 150mm below the bottom of the borehole, it is then driven a further distance of 305mm. The number of blows required to drive this distance is termed the standard penetration value N (Wilun and Starzewski, 1975).

The log for BH11 reports made ground down to a depth of 12m, and below this a medium dense, dark brown, silty, gravely, fine to coarse sand that becomes denser after 14m depth where the borehole is terminated at 15.45m The standard penetration values for this hole are again in the range 10 – 14 down to a depth of 12.5m. Below this they increase up to 19 and then 36 at a depth of 14m.

## 7.3 Gravity forward modelling

The probable success of a survey in detecting the specified target was investigated before acquisition began. The survey was then designed to optimise the probability of detecting and characterising the anomalous area. Over sampling, with the associated additional work and costs, can also be avoided.

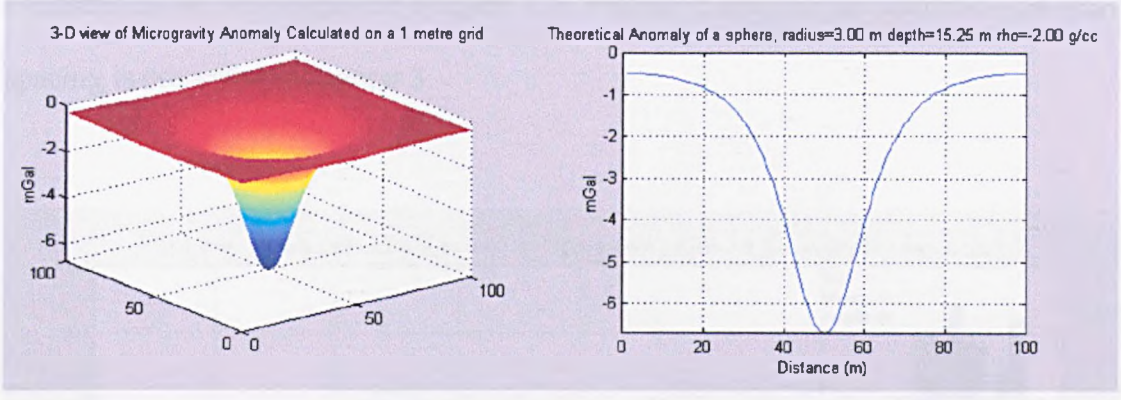


*Fig.7.3 Forward modelling of the suspected void in BH10. An anomaly of 6μGal is expected.*

Calculation of the maximum amplitude of the negative gravity anomaly likely to be present as a result of the material reported in BH10 showed it to be 6.5μGal, which is at the limit of detection for a Lacoste and Romberg Model D gravity meter (Figure 7.3). However, it is anticipated that the void will extend deeper than the base of the borehole and/or the gravitational anomaly will be increased by the *halo effect* caused by fracture or de-compaction of material around the void thus increasing the amplitude of the anomaly (Daniels 1988).

Consideration of the wavelength of the expected anomaly showed that an acquisition grid with a 10m grid spacing would sample the anomaly from a body whose

upper limit lies at 12.5m depth (centre 15.25m) with sufficient frequency to give an accurate representation of its shape and amplitude (Figure 7.4). However, the borehole log also reports that loose material is encountered at a depth of 6.5m Acquiring the gravity with a 10m grid spacing would not sample the anomaly from a body at this depth with a sufficient frequency to represent it accurately (Figure 7.5) and aliasing would occur. It was decided that an acquisition grid with a 2.5m grid spacing should be utilised in order to characterise the site adequately (Figure 7.6). Further discussion on selection of station spacing is presented in chapter 3.

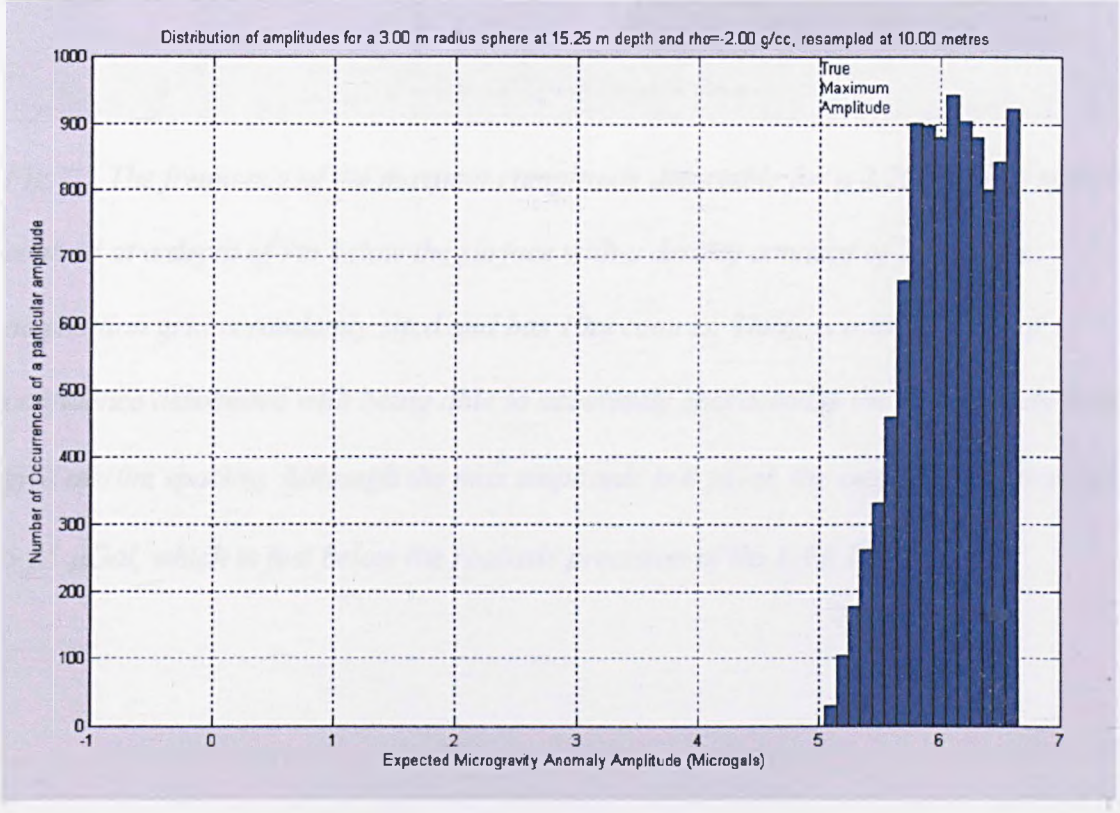


*Fig.7.4 The frequency of the maximum amplitude detectable on a grid with 10m centres for a body 2 m in radius centred at a depth of 15.75m below the surface and a density contrast of -2g/cc. The amplitude is on the limit of detection, however, the sampling rate is sufficient to represent the anomaly accurately.*

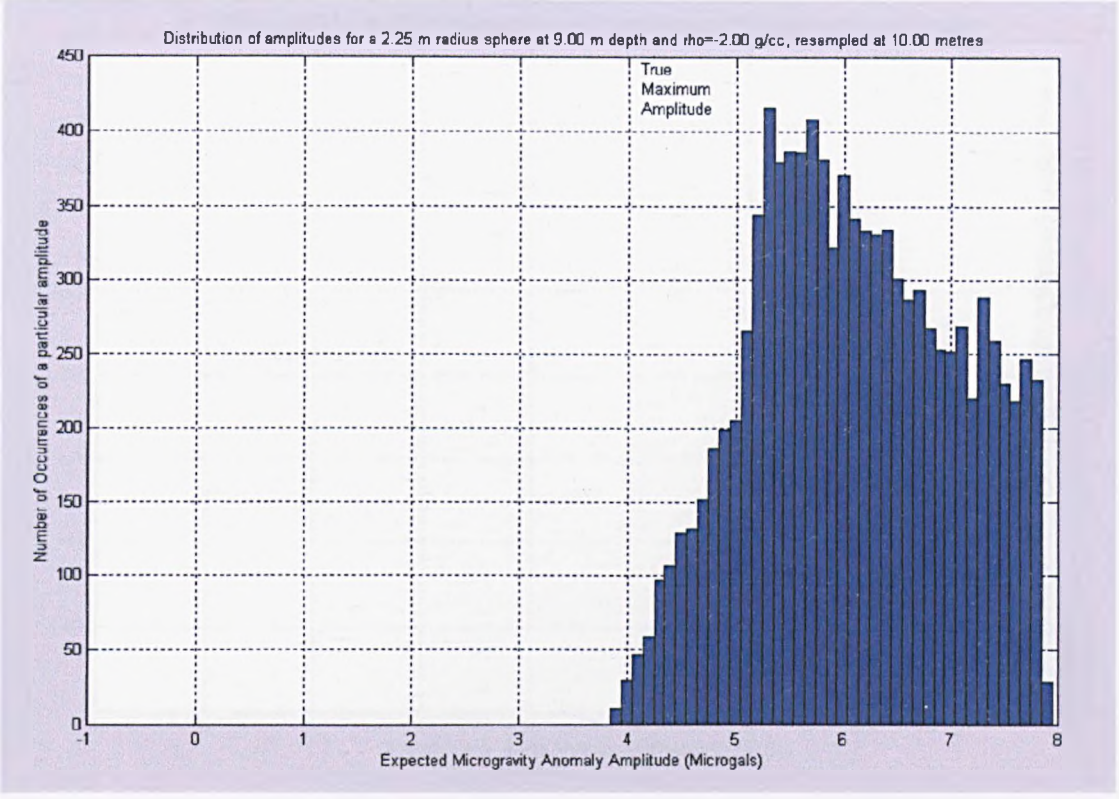


*Fig.7.5 The frequency of the maximum amplitude detectable for a 2.25m radius sphere centred at a depth of 9m below the surface with a density contrast of 2g/cc. The acquisition grid is randomly sited and has 10m centres. There is a low degree of confidence associated with being able to accurately characterise the source body with a grid of 10m spacing. Although the max amplitude is 8 μGal, the mode distribution lies at 5.25 μGal, which is just below the realistic precision of the L&R D meter.*

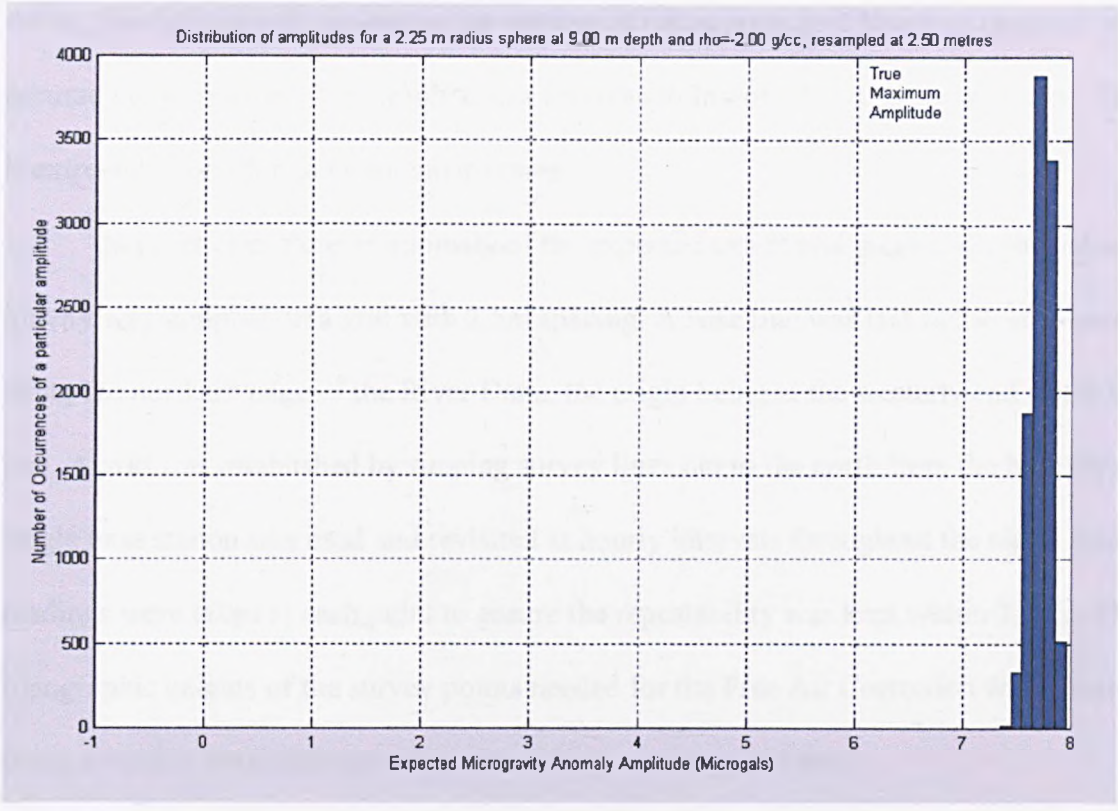


*Fig. 7.6 Frequency distribution of the maximum amplitude detectable for a 2.25m radius sphere centred at a depth of 9m below the surface, with a density contrast of 2.0 g/cc. The acquisition grid spacing is 2.5m. The spread of the distribution is small and the mode is located at 7.75 μGal. There is a high degree of confidence attached to the detection of this body with this acquisition grid.*

## 7.4 Field procedures and processing

A detailed microgravity survey was undertaken in order to investigate the extent of the suspected void in BH10. Microgravity data acquisition was performed during the night of 4th December 2001 with a Lacoste and Romberg model D microgravity meter (D-141). The west half of the site area consisted of an ornamental garden (Plate 7.2), the east half incorporated the car park to a local doctor's surgery (Plate 7.3). The survey was acquired

during the night in order to reduce the amount of urban noise and therefore improve the accuracy of the survey. This resulted in a reproducibility of ±5μGal being achieved. This is extremely good for an urban environment.

In order to capture an anomaly of the expected extent and magnitude, the value of gravity was sampled on a grid with 2.5m spacing. A base line was laid out west to east along the northern edge of the River Dane, the origin being at the westerly end of the base line. A grid was established by running survey lines out to the north from the base line. A single base station was used and revisited at hourly intervals throughout the night. Repeat readings were taken at each point to ensure the repeatability was kept within 3μGal. The topographic heights of the survey points needed for the Free Air Correction were acquired using a Sokkia Total Station with a closed loop accuracy of 5mm.

*Plate 7.2 Photograph showing the ornamental garden that made up the west half of the survey site. The photo is taken looking west. The position of BH10 is in the centre foreground.*

*Plate 7.3 A photograph showing the east half of the survey site. The survey was acquired at night due to the impracticality of surveying while the surgery was open. Again the photograph is taken looking west. The railing running alongside the left-hand edge of the photography leads onto the river cutting.*

The survey was reduced to produce a Bouguer gravity map where the effect of drift, elevation and the influence of topography have been removed. A value of 2.0 $Mg/m^3$ was used for the calculation of the Bouguer correction during processing.

It was also necessary to calculate the terrain effect caused by the river cutting to the south of the survey (Plate 7.4 and 7.5). The Bouguer correction uses the assumption that

the material below the survey station can be approximated by a slab of constant thickness and infinite length, in order to correct for the difference in height between the reference base and the station. However, the presence of the river cutting leads to an over correction as a result of the missing mass associated with the river cutting. This results in disproportionately low gravity values for the stations near the river.

The gravitational effect of the river cutting and surrounding area has been calculated and added to the measured gravity. WS Atkins supplied bathymetric profiles detailing the depth of the river along three profiles (Figure 7.7) from which the gravity response was modelled (Figure 7.8). The density used for the terrain correction was 2.0 $Mg/m^3$.

*Plate 7.4 A photograph of the river cutting which runs along the south of the survey site. The photograph has been taken looking west. The retaining wall can be seen through the trees, lit by the sunshine.*

*Plate 7.5 Photograph of river cutting looking down from survey site. Photograph was taken looking SW.*

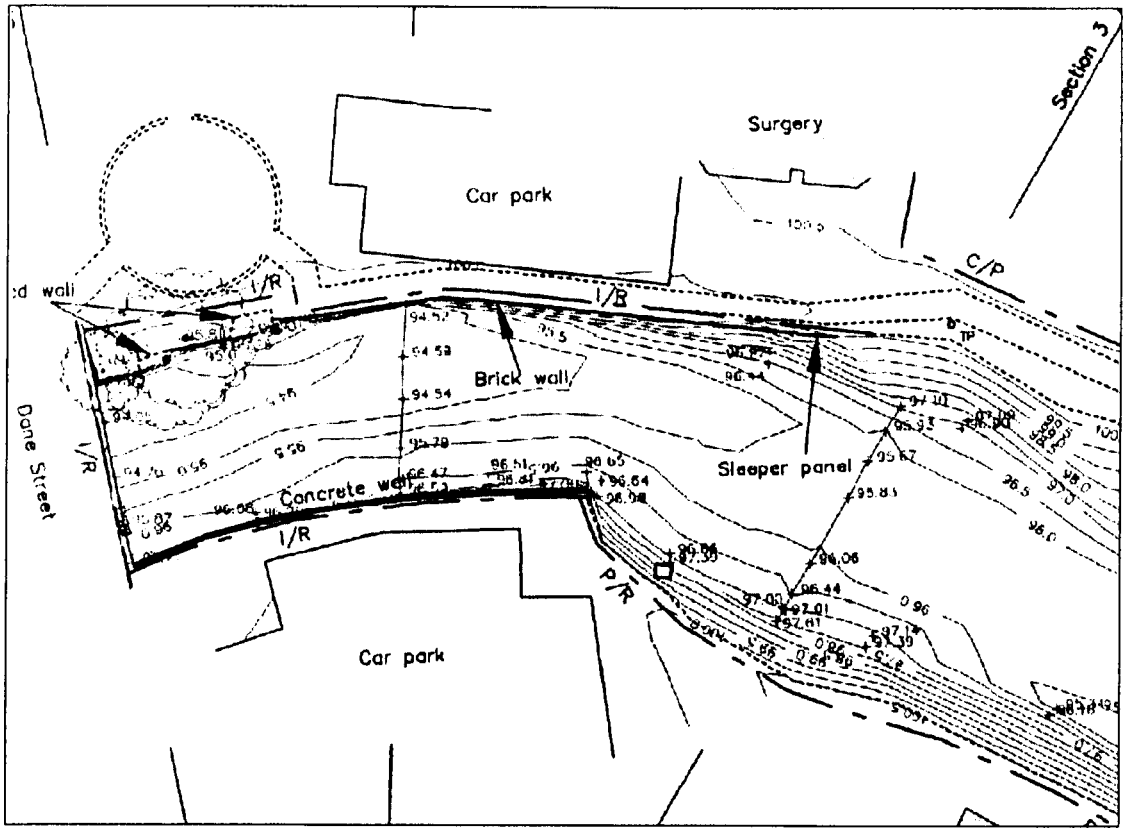


*Fig. 7.7 Plan showing the bathymetric profile of the River Dane adjacent to the survey site. Data supplied by WS Atkins.*

The correction has a "stripy" appearance because the data used to calculate it consists of 3 profiles. However, this does not effect the correction dramatically as the calculated terrain effect levels out into contours roughly parallel to the river cutting, once the position of the survey points has been reached. It can be seen in Figure 7.8 that the terrain effect of the river cutting is localised to the area within 5m of the bank with the majority of the terrain effect dying off after 1m.

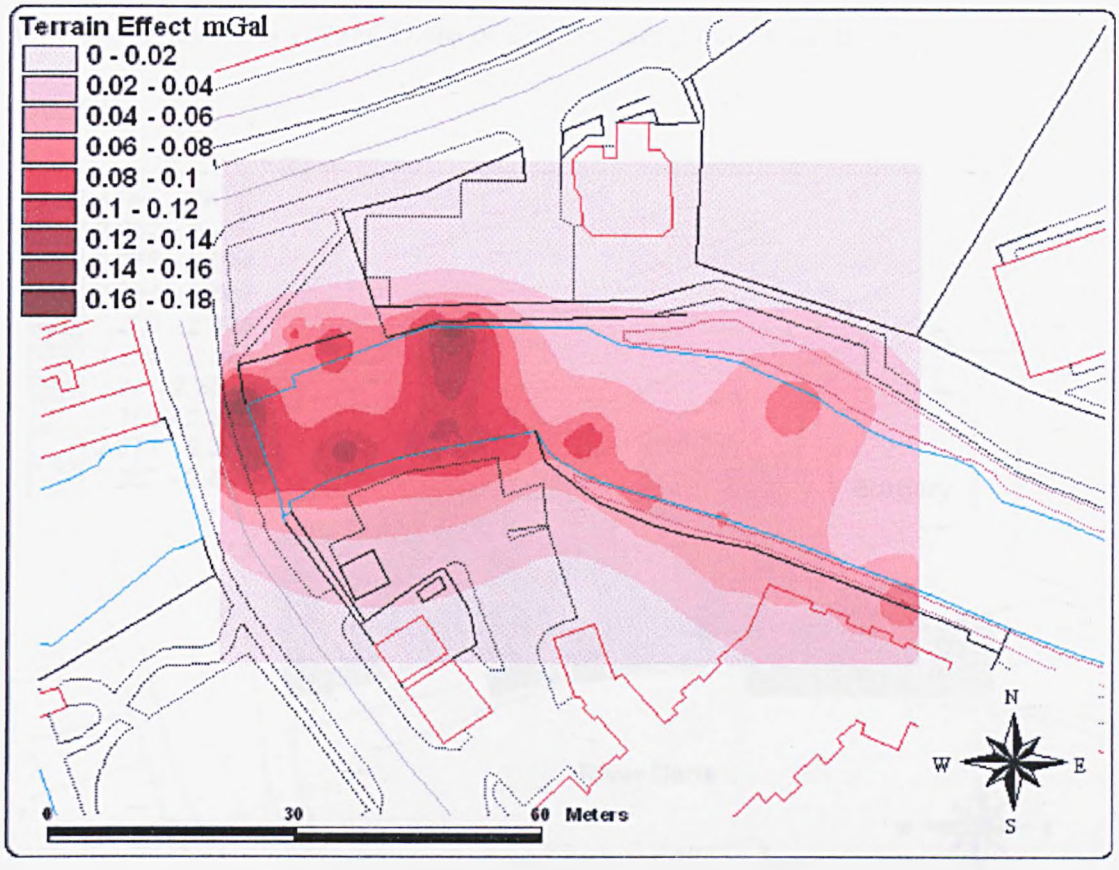




*Fig. 7.8 The terrain effect calculated using the bathymetric depths provided by WS Atkins.*

## 7.5 Gravity results

A first order polynomial surface has been removed from the data to produce a residual Bouguer anomaly. The polynomial surface decreases in a SW direction at approximately 0.16mGal/100m and can be thought as representing locally dipping strata. The residual Bouguer anomaly for the Dane River Survey is shown in Figure 7.9. Several areas of low density can be seen to extend to the north from the river bank. Anomaly A is located in the vicinity of BH10, and trends NW to join with anomaly B. Both of these anomalies are of considerable size and extent, having a maximum amplitude of ~50μGal, consequently they have a high degree of significance attached to them. To the east of

anomaly A, anomalies C and D are of smaller lateral extent but still have a magnitude of ~50μGal.

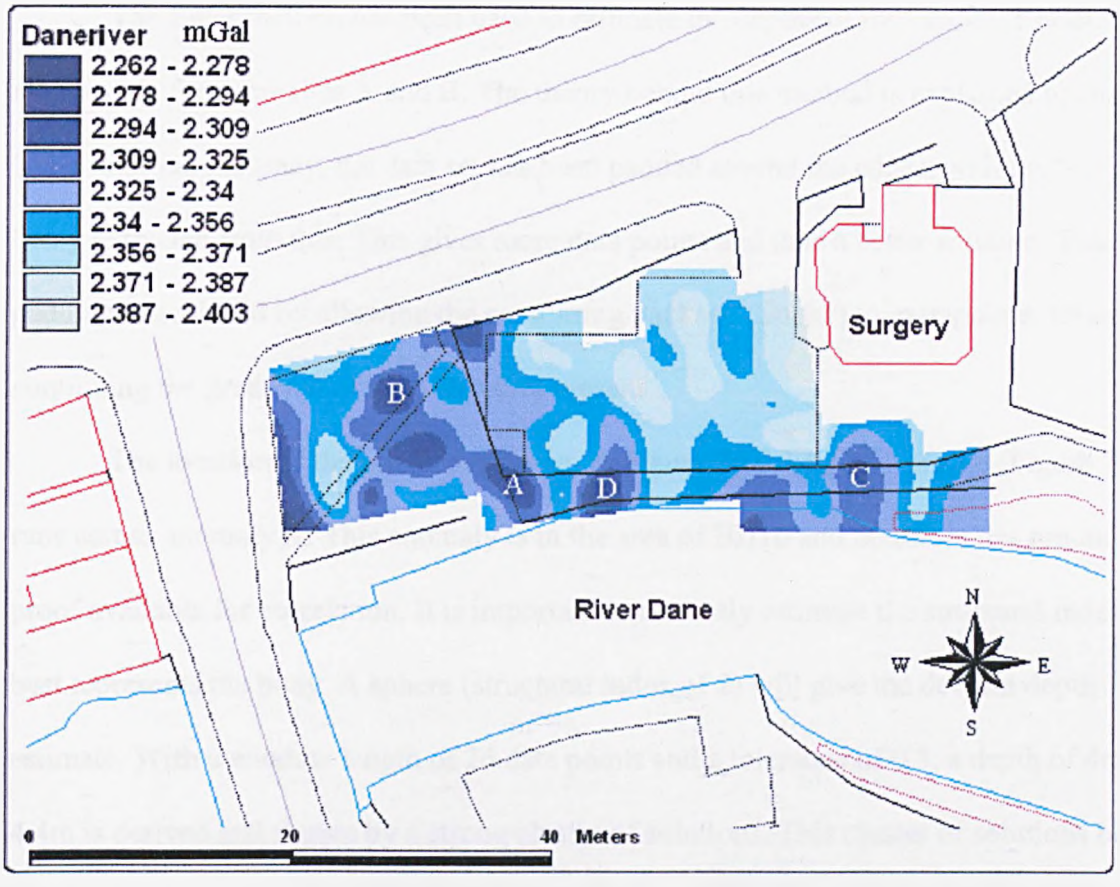




*Fig. 7.9 A contour map of the reduced Bouguer gravity for the area on the north bank of the Dane river. A first order polynomial surface has been removed to account to local geology.*

WS Atkins supplied service plans for the area dated 20/02/2000 and 02/03/2000. The plans show no evidence of household services passing through the area of the survey. This eliminates the possibility of the gravity anomalies being an artefact of man-made trenches.

## 7.6 Modelling of gravity data

### 7.6.1 Depth estimates

The Euler method has been used to estimate the depths of the causative bodies responsible for anomalies A and B. The theory behind this method is explained in chapter 3. To improve accuracy, the data set has been padded around the edges, with the profiles being extracted from this. This gives more data points and thus a better solution. The padding is achieved by allowing the contouring package (Surfer) to extrapolate, effectively continuing the gradients of the anomalies present

The location of the profiles is shown in Figure 7.10. The first profile (Figure 7.11) runs across anomaly A. This anomaly is in the area of BH10 and therefore has ground proof available for correlation. It is important to correctly estimate the structural index that best represents the body. A sphere (structural index of 2) will give the deepest depth estimate. With a window length of 26 data points and a tolerance of 0.3, a depth of 4m-4.4m is derived and shown by a strong cluster of solutions. This cluster of solutions begins to break apart at window lengths of 2 and 28. No shallowing of the cluster is achieved by changing the window length. Substituting structural indices of 1 (vertical tabular body) and 0.6 (stope), has the effect of shallowing the cluster of solutions to depths of 2.6m-2.8m and 2m respectively. This suggests that the body has a geometry which can be accounted for by the superposition of several geometrical shapes, all with different structural indices as is often the case. The tightest clusters of solutions is derived by using a structural index of 2 and so it is this depth estimate that has been deemed the most likely.

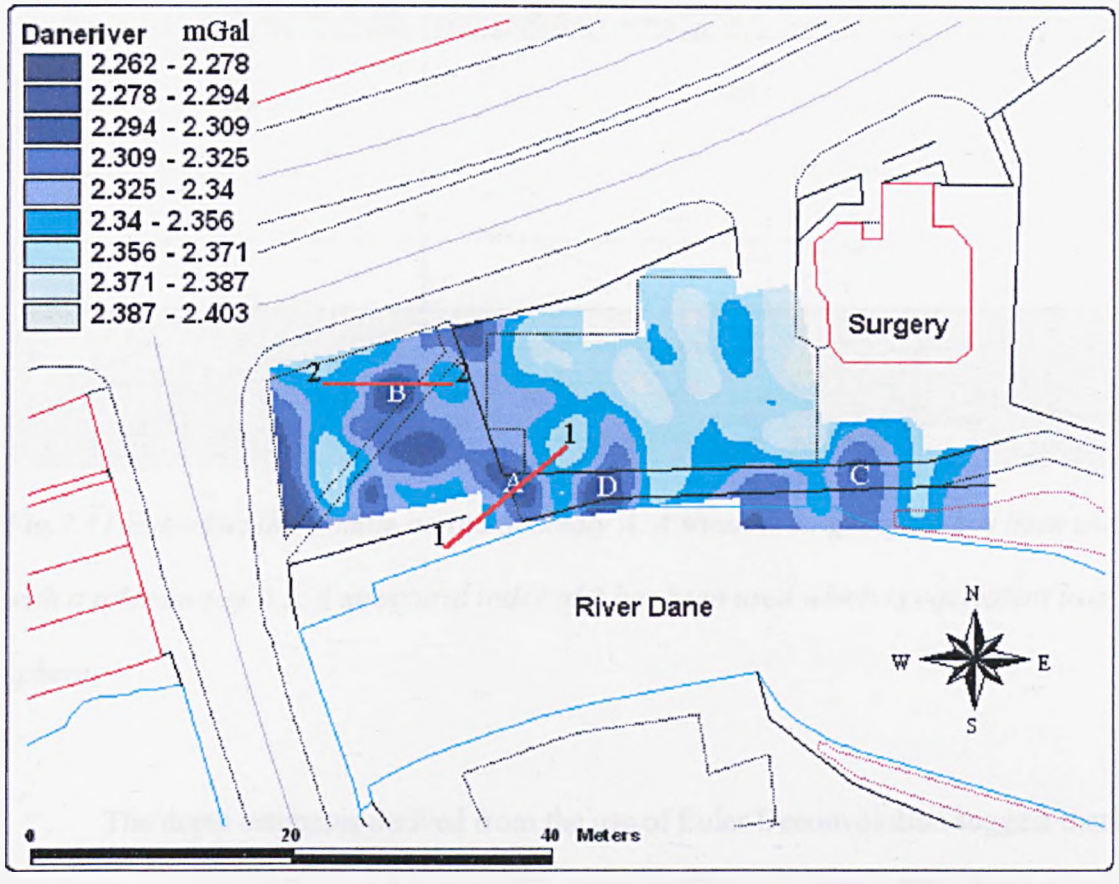




*Fig. 7.10 Map showing the location of the profiles used for the Euler depth analysis.*

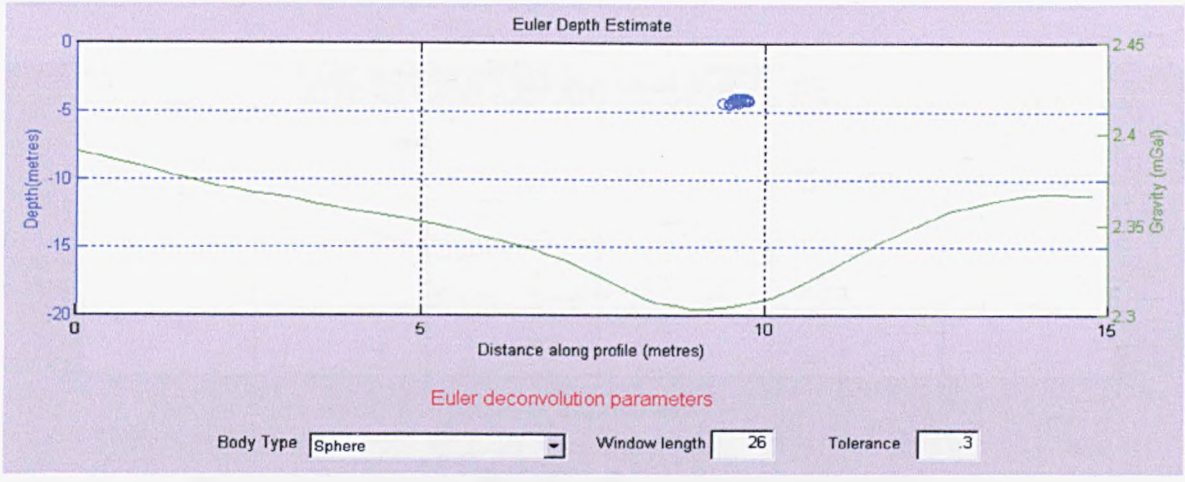


*Fig.7.11 Euler Depth estimate across anomaly A. A window length of 26 has been used with a tolerance of 0.3. A structural index of 2 has been used which is equivalent to a sphere.*

The depth estimates derived from the use of Euler Deconvolution suggest that the top of the anomaly is located between 4m and 5m below the surface. This is 3m to 4m above the depth that the draft drillers log (Table 7.1) reports the SPT values fall to zero.

The second profile (Figure 7.12) runs across anomaly B. The depth estimates derived from the use of Euler Depth Analysis suggest that the top of the anomalous body is located at a depth of 2.9m. A structural index of 2 has been used for this solution together with a window length of 31 and a tolerance of 0.6. The cluster of solutions associated with this depth estimate disperses once the window length has been increased/decreased to 35 and 24 respectively. No shallowing of the solution is associated with the altering of the window length. Changing the structural index to 1 (vertical tabular body) and 0.6 (stope) results in a shallowing to a depth of 1.8m and 1.25m respectively. These depth estimates are similar to anomaly A suggesting that there is a correspondence between the two. This relationship is investigated in greater detail later.

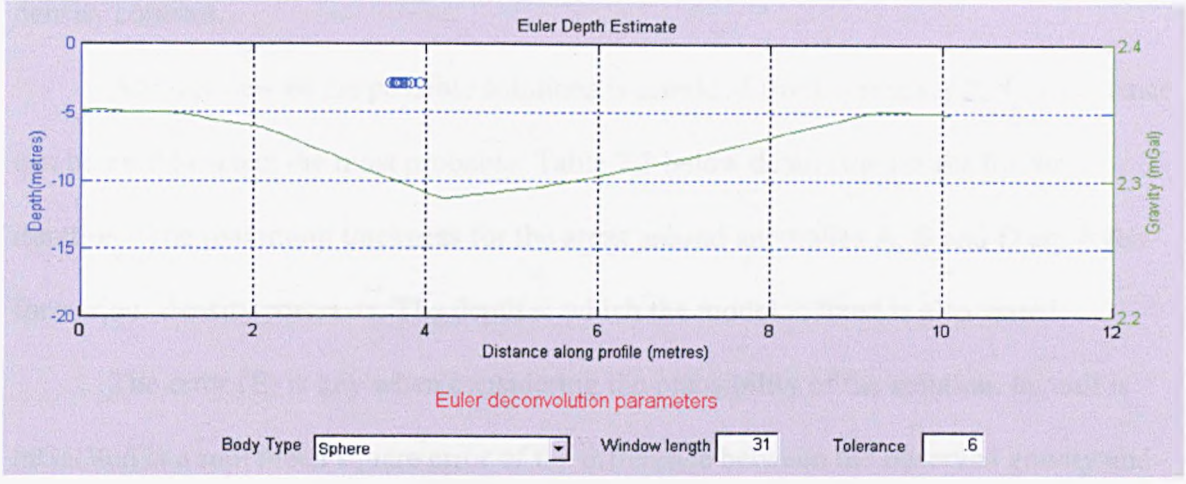


*Fig. 7.12 Euler Depth estimate across anomaly B. A window length of 31 has been used with a tolerance of 0.6. A structural index of 2 has been used which is equivalent to a sphere.*

### 7.6.2 Thickness estimates

The second modelling technique used gives an estimate of the thickness of the causative body by inverting the gravity data. The program iteratively calculates the thickness of the causative body using the Bouguer Slab equation. The depth horizon, to which the solution is pinned, must be assigned, as must the density contrast between the causative body and the host rock. Using this method in conjunction with the depth estimates derived using the Euler Depth Analysis enables a 3D image of the causative body to be created. Further details of the theory behind this method can be found in chapter 3.

As described in chapter 3, a measured potential field anomaly can have many possible causes. The Cordell and Henderson (1968) inversion has been conducted over a

range of values for the main two parameters, the depth of the top of the body and the density contrast.

An overview of the possible solutions is provided from which supportive evidence can be used to select the most probable. Table 7.3 below details the results for the iteration. The maximum thickness for the areas around anomalies A, B and D are given for various density contrasts. The depth at which the model is fixed is also varied.

The error (E) is key when considering the plausibility of the solution. Its unit is mGal and is a root mean square error of the difference between the observed gravity and the calculated gravity. A good guide is to discount solutions with an error of greater than 4μGal as they are not representing the observed gravity field correctly.

Solutions derived for depths of 12m (original depth of suspected void in BH10) were rejected as the solutions gave errors in the order of 10-20μGal for all density contrasts. It should also be noted that the thickness estimates for this depth were also nonsensical, being 20m to 30m for a density contrast ($\Delta\rho$) of $-1.0$.

| | Depth to top of the model 2m | | | | Depth to top of the model 3m | | | |
|---|---|---|---|---|---|---|---|---|
| Δρ | A | B | D | E ($\Delta 10^{-3}$) | A | B | D | E ($\Delta 10^{-3}$) |
| **-0.4** | 18 | 10.8 | 14.2 | 1.3 | 14.2 | 13 | 13.6 | 2.4 |
| **-0.6** | 8 | 6.7 | 7.4 | 0.8 | 13 | 8 | 9 | 1.5 |
| **-0.8** | 5.7 | 5.3 | 5.5 | 0.7 | 8 | 6.6 | 7.2 | 1.2 |
| **-1.0** | 4.6 | 4.5 | 4.6 | 0.7 | 6.5 | 5.8 | 6.0 | 1.1 |
| | **Depth to top of the model 4m** | | | | **Depth to top of the model 5m** | | | |
| Δρ | A | B | D | E ($\Delta 10^{-3}$) | A | B | D | E ($\Delta 10^{-3}$) |
| **-0.4** | 16 | 14.1 | 15.3 | 3.7 | 19.3 | 15.3 | 19 | 5.1 |
| **-0.6** | 15.5 | 10 | 12.6 | 2.4 | 15.5 | 10.2 | 15.1 | 3.4 |
| **-0.8** | 10.8 | 10.0 | 9.1 | 1.9 | 10.3 | 9.0 | 10.1 | 2.8 |
| **-1.0** | 9.5 | 7.1 | 7.7 | 1.7 | 10.7 | 8.4 | 9.6 | 2.5 |

*Table 7.3. Table detailing the various solutions attainable for the Cordell and Henderson thickness inversion. The values given are the depth to base of the body. The parameters that have been varied are the density contrast (Δρ) between the host rock and the anomalous material and the depth at which the model is pinned. Maximum thickness (m) has been given for the areas around anomalies A, B and D. The error (E) of the iteration is also given. Its units are mGal and give an indication of the success of the iteration.*

From the solutions provided in Table 7.3, it can be deduced that the majority of the thicknesses are plausible, with only the combination of maximum depth and minimum density contrast producing a solution that exceeds the error threshold of 4μGal.

Incorporating the Euler depth analysis results can narrow the possible solutions down. The profiles across anomalies A and B provided depth estimates between 1.25m and 4 m. However, the best clustering was achieved with a structural index of 2, giving a depth estimate of 2.9m and 4m, and thus the model with its top surface fixed at 3m or possibly 4m would give the most plausible solution. The second consideration is the density contrast ($\Delta\rho$). The borehole data we have available at the time (BH10) only indicates a possible void at 12.5m and 16m (although below 9m is extremely loose). Therefore density contrasts of greater than -0.8 $Mg/m^3$ can be discounted. Of the remaining solutions, the combination of a fixed depth to the top of the model of 3m and a density contrast of –0.6 $Mg/m^3$ has the lowest error.

Figure 7.13 is a plot showing the lateral extent and thickness of the anomalous material responsible for the gravity anomalies A, B and D. The parameters chosen for this visualisation are a minimum depth of 3m below the surface for the top of the model and a density contrast of 0.6 $Mg/m^3$.

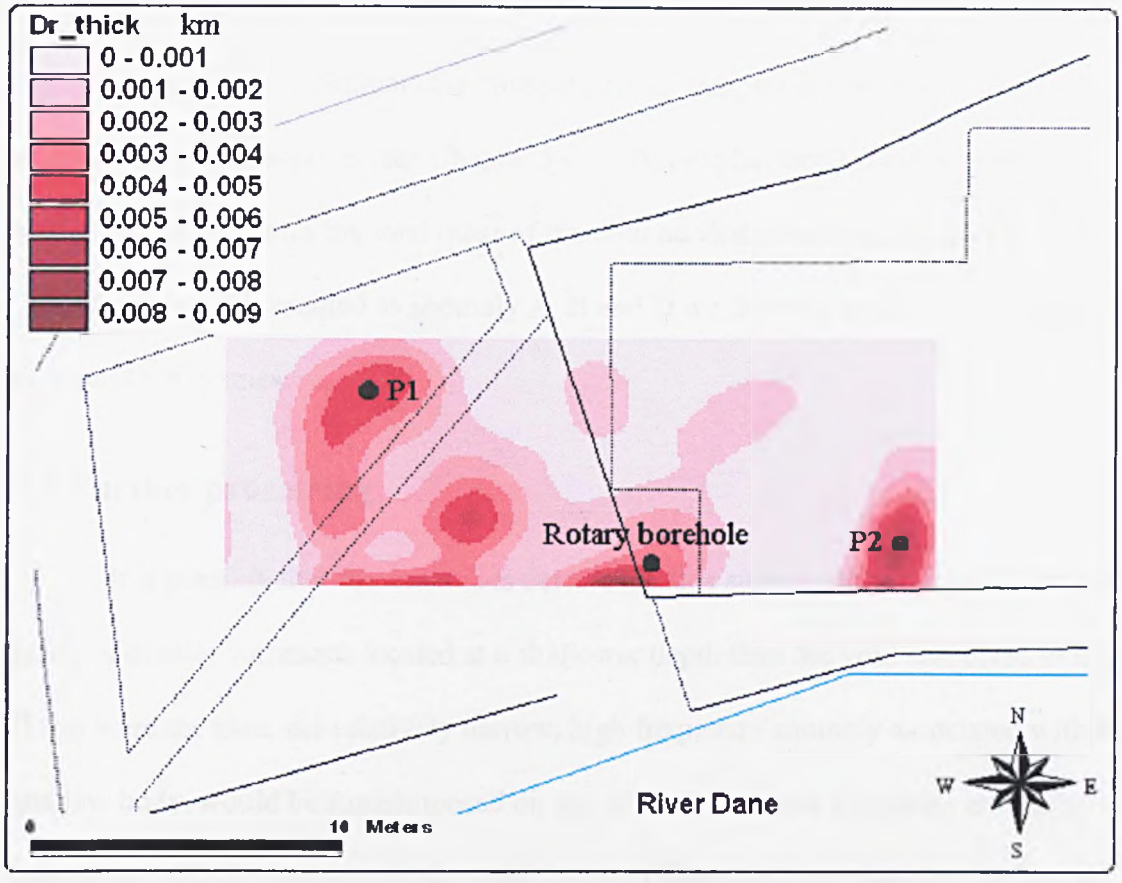




*Fig.7.13 The Figure shows the predicted thickness of the causative body related to anomalies A, B and D. A density contrast of –0.6 Mg/m³ has been assigned and the top of the solution has been fixed at 3m below the surface. The maximum thickness is 9m, with a base at 12m below the surface.*

### 7.6.3 Mass deficiency

It is possible to estimate the "missing mass" that is associated with the presence of negative gravity anomalies (see Chapter 3 for a full explanation). This is a particularly useful tool as it enables the total mass of material needed to remediate the sub-surface void. Applying this method to anomaly A, B and D we derive a value for the missing mass at around 600 tonnes.

## 7.7 Further processing

It is possible that the anomalies detected in this survey contain signals that are the result of density variations located at a shallower depth than the void suspected in BH10. If this were the case, the relatively narrow, high frequency anomaly associated with the shallow body, would be superimposed on top of the broad, low frequency anomaly associated with the deeper void. In order to investigate this a low pass spatial filter is applied to the data set striping away the high frequency contingent associated with shallow density contrasts.

Figure 7.14 shows the result of applying a Butterworth low pass filter with a corner frequency of 0.7 cycles per metre and an order of 10. The filter applied is shown in Figure 7.15. The effect of applying a low pass wavelength filter to the data set is to broaden anomalies A, B and D so that they become one anomaly trending NW across the site form the River Dane towards the A559. Anomaly C is little effected. Applying the Euler depth analysis to the low frequency constituent of the gravity anomaly provides depth estimates for the body responsible for the generation of this suite of frequencies.

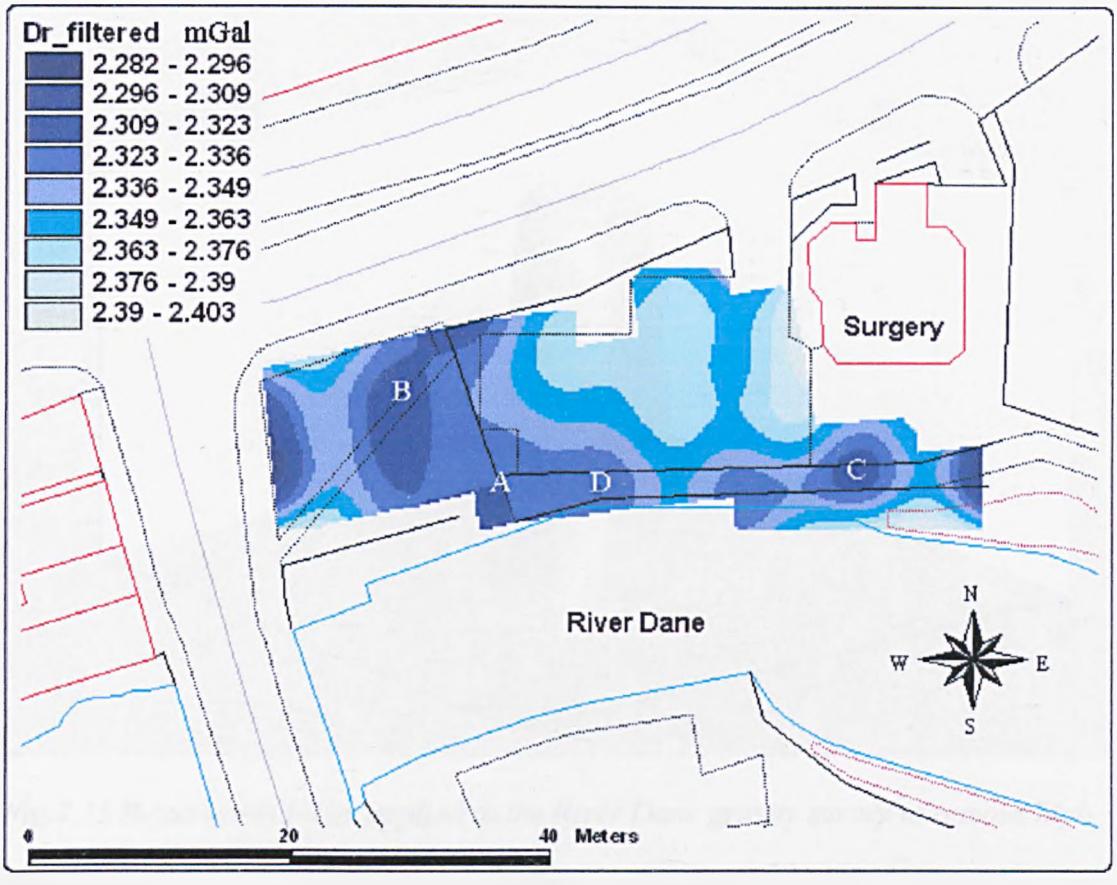




*Fig.7.14 The residual gravity map after applying a low pass filter to the data set.*

*Removing the high frequencies has had the effect of broadening the anomalies A and B.*

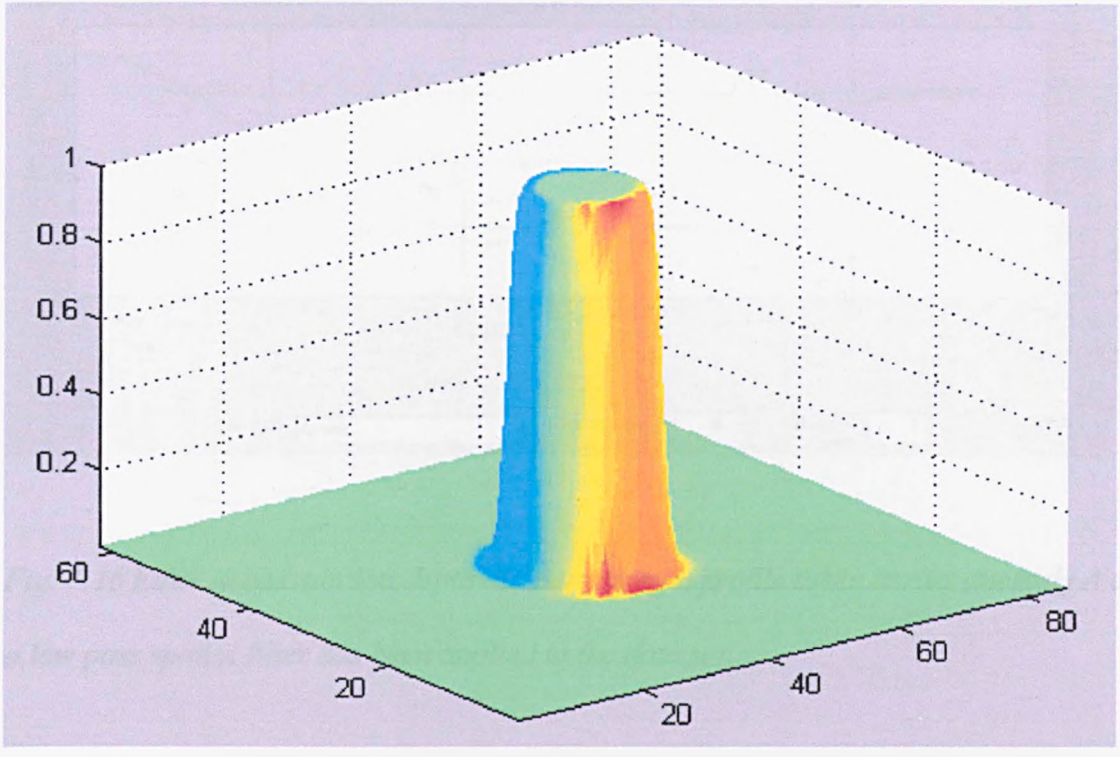


*Fig.7.15 Butterworth Filter applied to the River Dane gravity survey to remove high frequencies.*

The results of the Euler Deconvolution are shown in Figures 7.16 and 7.17. Using the Euler method across anomaly A, after filtering, results in the solutions clustering around a depth of 12m below the surface. This is at the same depth horizon as the suspected void recorded in the log of BH10.

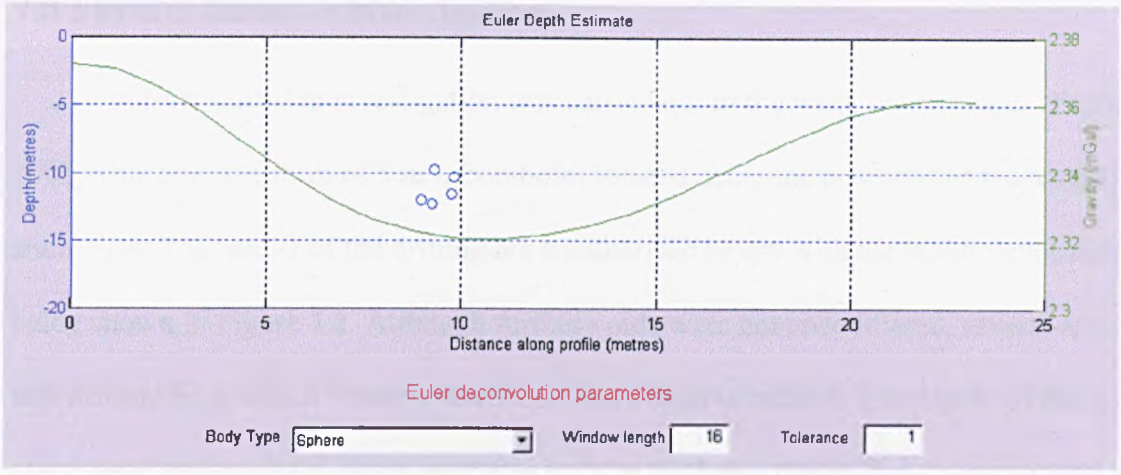


*Fig. 7.16 Euler deconvolution depth estimate using a profile taken across anomaly A after a low pass spatial filter has been applied to the data set.*

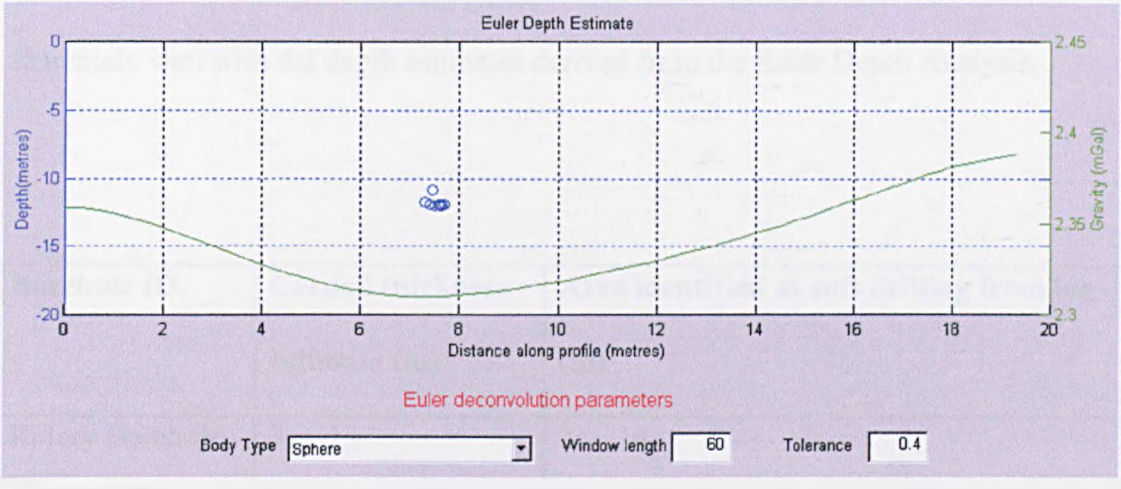


*Fig. 7.17 Euler deconvolution depth estimate using a profile taken across anomaly B. A low pass spatial filter has been applied to the data set.*

Applying the Euler method to a profile which cuts across anomaly B results in the solutions clustering around a depth of 12m also.

## 7.8 Further invasive investigation

Further intrusive investigation was carried out in the week beginning 2nd February 2002. This took the form of 5 new boreholes located using the positions of the identified anomalies. The results of the drilling are summarised below with the borehole locations being shown in Figure 7.2. Although further voids were not encountered, several areas of soft drilling from which "returns were lost" have been identified. The depths of these areas correspond well with the depth estimates and the thickness modelling. A comparison of the modelled depths and thickness with the results of the drilling program is made in Table 7.4.

Of particular interest is borehole P1 which is sited over anomaly B. The log records "lost flushings" from 2.5m to 9m and again between 12.10m and 12.50m. This matches extremely well with the depth estimates derived from the Euler Depth Analysis.

| **Borehole ID** | **Cordell thickness estimate (m)** | **Area identified as soft drilling from log (m)** |
|---|---|---|
| Rotary Borehole | 3 - 13 | 3 - 14 |
| P1 | 3 - 8 | 2.5 - 9 |
| P2 | 3 - 9 | 1.5 - 8 |

*Table 7.4. A comparison between modelled thickness and the results from the drilling program.*

Comparing the secondary drilling with the Cordell and Henderson thickness inversion we see that the combination of a minimum depth of 3m and a density contrast of –0.6 $Mg/m^3$ matches best with the new data set.

Further precautionary probing was carried out at P3 and P4 (Figure 7.2) to investigate the small localised negative anomaly in that area. No void was encountered but soft drilling with lost flushings was encountered as depths of 8m-9.2m and 9.2m–10m respectively. This is probably the cause of the anomaly but the small amplitude and extent of the anomalous material does not make it a high-risk anomaly.

**Rotary Borehole**

| | | | |
|---|---|---|---|
| GL | - | 1.00 | fill, brick |
| 1.00 | - | 3.00 | Soft black sand |
| 3.00 | - | 14.00 | Very soft drilling (no returns) |
| 14.00 | - | 16.00 | Hard drilling |
| 16.00 | - | 24.50 | Soft with hard bands (sand/clay) |
| 24.50 | - | 26.00 | Marl |
| 26.00 | - | 36.00 | Sand with gravel + marl bands |
| 51.00 | - | 51.50 | Rock salt |
| 51.50 | - | 60.00 | Marl |

**Borehole P1**

| | | | |
|---|---|---|---|
| GL | - | 1.00 | Fill, brick |
| 1.00 | - | 2.50 | Soft yellow sand |
| 2.50 | - | 9.00 | Soft drilling lost flush |
| 9.00 | - | 12.00 | Firm drilling |
| 12.00 | - | 12.10 | Hard obstruction |
| 12.10 | - | 12.50 | Soft drilling (no flush) |
| 12.50 | - | 21.00 | Firm drilling |

**Borehole P2**

| | | | |
|---|---|---|---|
| GL | - | 1.50 | Fill, brick and ash |
| 1.50 | - | 8.00 | Soft ash, clay and sand (50% flush) |
| 8.00 | - | 9.00 | Firm drilling (lost flush) |

**Borehole P3**

| | | | |
|---|---|---|---|
| GL | - | 2.00 | Fill, brick and ash |
| 2.00 | - | 7.00 | Soft drilling lost flush |
| 7.00 | - | 8.00 | Firm drilling |
| 8.00 | - | 9.20 | soft drilling (no flush) |
| 9.20 | - | 10.00 | Firm drilling |

**Borehole P4**

| | | | |
|---|---|---|---|
| GL | - | 1.80 | Brick and ash fill |
| 1.80 | - | 6.80 | Soft drilling lost flush |
| 6.80 | - | 9.20 | Firm drilling |
| 9.20 | - | 10.00 | Soft drilling (no flush) |
| 10.00 | - | 12.00 | Firm drilling |

## 7.9 Conclusions

The high-resolution gravity survey has detected 4 negative anomalies, associated with zones of low density. A high degree of confidence is attached to anomalies A and B. Anomalies C and D have a lower degree of confidence attached to them as a result of their limited lateral extent.

Euler Deconvolution depth estimates across anomalies A and B suggest that the causative bodies lie at a depth 2m to 4m and 1.25 to 2.9m respectively. This is considerably shallower than the suspected void reported in the log for BH10 (12m), but lies approximately 2-3m above the depth where the SPT values begin to decrease.

Thickness estimates of the area around anomalies A, B, and D suggest that this area of low density material extends from 3m below surface, down to a depth of ~16m below surface.

Applying a low pass filter to the data set has the effect of eliminating the high frequency signal of shallow density contrasts. This unmasks the signal of deeper density contrasts. Depth estimates using the Euler method across anomalies A and B after applying a low pass spatial filter, suggest that the causative bodies lie at a depth of 12m. This agrees well with the driller's log for BH10 (Table 7.1).

In summary the gravity lows are a superposition of two areas of anomalous, low-density contrasts located at different depth horizons. At a depth of 12 m around BH10 there is a void or an area of very loose material, as reported in the drillers log. However, above this there is an area of low-density material.

The top of this material is 3-4m below surface although the contact is likely to be diffuse. Using the Cordell and Henderson modelling method, the base of this loose, low-density material has been identified as being at a depth of 12m below the surface. This is coincident with the suspected void detected in BH10. It is highly likely that these two areas are linked.

This gravity low around BH10 extends laterally towards the NW and the area depicted by B in Figure 7.6. A shallowing is present in both the top and base of the low-density material towards the NW.

Further drilling of the site supports the interpretation of an area of loose, low density material extending across the site at a depth of ~3-12m below surface (section 7.8). The suspected void, encountered in BH10 was not encountered in the secondary drilling

program. It is therefore likely that the suspected void is localised to the area around the initial retaining wall collapse.

It is unlikely that the void encountered is related to (dry) salt mining. The gravity survey has identified that a low density area runs across the site, roughly trending NW from the river bank, however, the amplitude (too low) and lateral extent (too localised) of the gravity anomaly rules out the possibility of the cause being related to a mine gallery or adit. It is not clear at this stage whether the low-density material is a result of a propagating void generated by salt dissolution by ground water at wet rock head. However, the low density feature originates from the northern bank of the River Dane and continues across the site in a NW direction which suggests that the river is related to the origin of the low-density material causing the gravity low. The riverbed is located approximately 5m below the surface level on the bank, which is within the depth horizon of the anomalous material identified by the Euler Depth Analysis. It is possible therefore that the gravity low has been caused by the deposition of river sediment at an earlier time or by the ingress of water into the bank, destabilising or washing out material beneath the bank, resulting in this low density area.

The microgravity method in conjunction with well-targeted drilling and site investigation has proved to be a very effective technique for assessing ground conditions and identifying zones of low density.

# Chapter 8

# Passive Seismic Monitoring of Cavities in Salt

## 8.1 Introduction

Microseismic monitoring has long been established as a means of monitoring ground stability. The recording of micro-earthquakes, created by the fracturing of rock, is used to assess the stability of an area. It is possible to locate the source of these failures and hence establish which areas are microseismically active, hence defining which areas are actively fracturing. This information can be of great help in the assessment of the stability of an area and can indeed pinpoint the precise area in which further investigation or remediation is required (e.g. Wong, 1989).

The application of microseismic monitoring for the evaluation of cavern stability has been assessed at Preesall Brine Field. The aim of the program was to establish if it was possible to record microseismic events in that environment and to assess the practicality of using microseismic monitoring; either as a stand-alone technique or integrated with microgravity, to monitor the development of the unstable caverns in the brine field. The results from this programme of monitoring will be discussed in section 8.2 of the chapter.

Section 8.3 of this chapter will detail the microseismic monitoring conducted in Peter Street. This monitoring was established in order to assess the microseismicity of the area. It was installed in order to provide extra information about the surface subsidence experienced in this area and to further investigate the nature of the anomalous area detected by the microgravity surveys.

The Applied and Environmental Geophysics Research Group (Keele University) has implemented microseismic monitoring in Northwich Town centre (Network Northwich). Network Northwich is part of a larger project to remediate the salt mines, which lie beneath the town centre and is funded by Vale Royal Borough Council and English Partnerships. The supervising engineer is WS Atkins.

The aim of the Network Northwich is to monitor the remediation of the salt mines and assess its effect on the stability of the local geological environment. In order to achieve this, the background seismicity of the area has been monitored for many months. Work presented here from the Northwich network has been completed by S. Toon. It is not part of this thesis but has been included as a corroborative data set from which conclusions presented here have been drawn.

## 8.2 Passive microseismic monitoring at Preesall brine field

The aim of the microseismic monitoring at Preesall brine field was to establish whether microseismic activity was being generated by the succession of roof collapses identified by the hooking and dipping monitoring carried out by ICI. If it were possible to record such events it may be possible to locate the area of activity and use this information to assess the risk posed by the cavern. Areas of activity could be identified and their progress towards the surface tracked.

### 8.2.1 Phase 1

The recording system used during phase 1 of this experiment was a Vibrosound SP1 seismic monitoring system made by Magus Electronics Ltd., Crewe, Cheshire and designed in conjunction with the Applied & Environmental Geophysics Research Group. It can record up to six channels of data with 24 bit resolution. Attached to the first three

input channels was a single 3-component Lennartz seismometer. The recording system was trigger activated once the geophone input exceeded a certain threshold. Channel one recorded the vertical component of ground motion and also acted as the trigger channel. Channels two and three were the north and east components respectively. The system recorded 2.144 seconds of data (including a 0.5-second pre-trigger) to a flash card every time the input value exceeded the trigger level. The records were all sampled at 1024 Hz, which is the maximum sample rate allowed by the recording system giving a Nyquist frequency of 512 Hz above which aliasing of the signal will occur. The Vibrosound and geophone can be run from a twelve volt battery and the system has a battery life of around 14 days (or until the data card fills up). This flexibility allows them to be installed easily and discretely. Data is stored on a 20 Mbyte Flash-EPROM card, which holds up to 467 events before needing to be replaced. This system is capable of recording a maximum event rate of one event approximately every 20 - 30 seconds.

The recording system was installed 3m north of the well head at brine well (BW) 64 (grid ref. 335 630, 445 718) on April 23, 2000. A 0.5m deep pit was dug for the geophone and a concrete base installed to ensure good ground coupling. The geophone was levelled and orientated with regard to north before the pit was back filled. The system was in place for 3 months, during which time 74 seismic events were recorded. An example of a typical event recorded by the system is shown in Figure 8.1

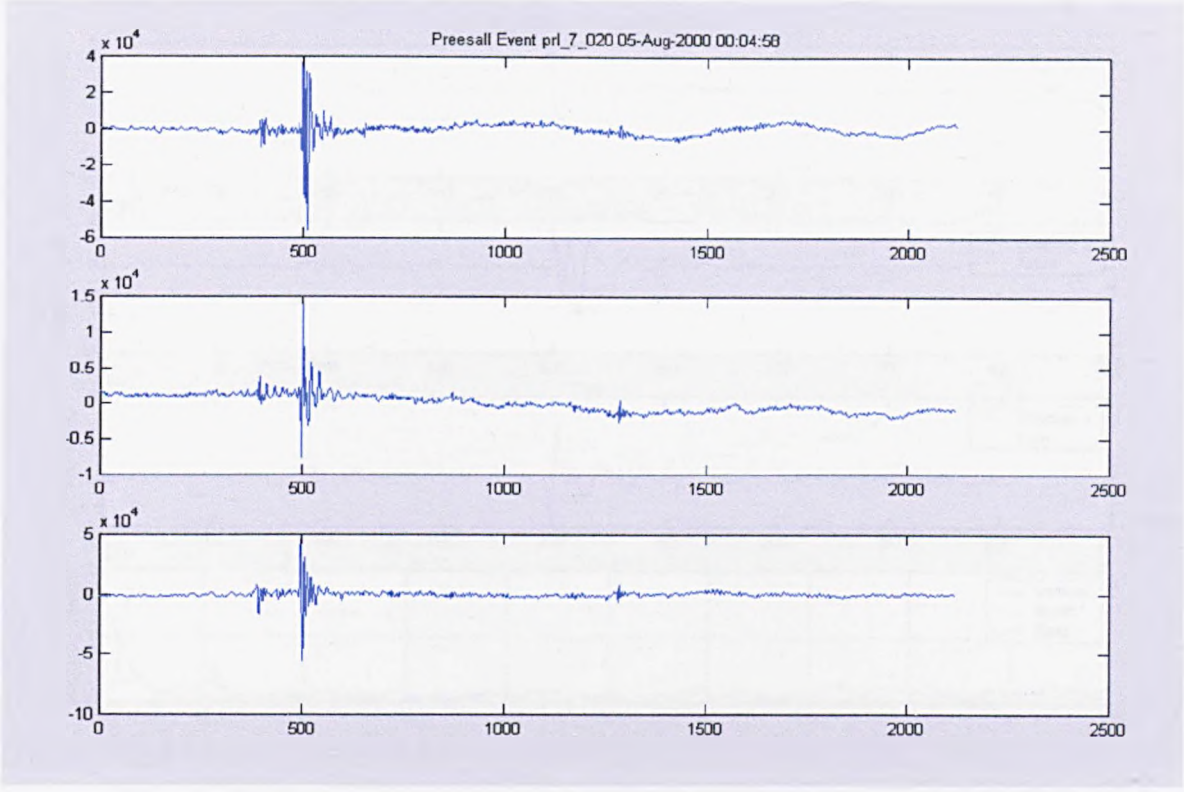


*Fig. 8.1 An example of a typical event recorded by the 3-componet geophone and Vibrosound recorder. The event was triggered at 500ms by an impulsive event. Event recorded at 4:58am on 05/08/00. Upper trace, vertical component of ground motion; middle trace, north-south component; lower trace, east west component.*

Zooming in on the data (Figure 8.2) it can be seen that the events are of short duration, lasting approximately 50ms. Investigating the frequency content of the recorded event reveals the event to be dominantly low-frequency, with the majority of frequencies being below 10Hz. The lack of high frequencies suggest that the event originates from some distance below the geophone, probably at mine depths and the extended path to the geophone has attenuated the high frequencies. Comparison with the other events gives similar results (Figures 8.3 to 8.6). All of the events recorded are short duration, relatively low-frequency events. The majority have simple waveforms with no clear P or S onsets.

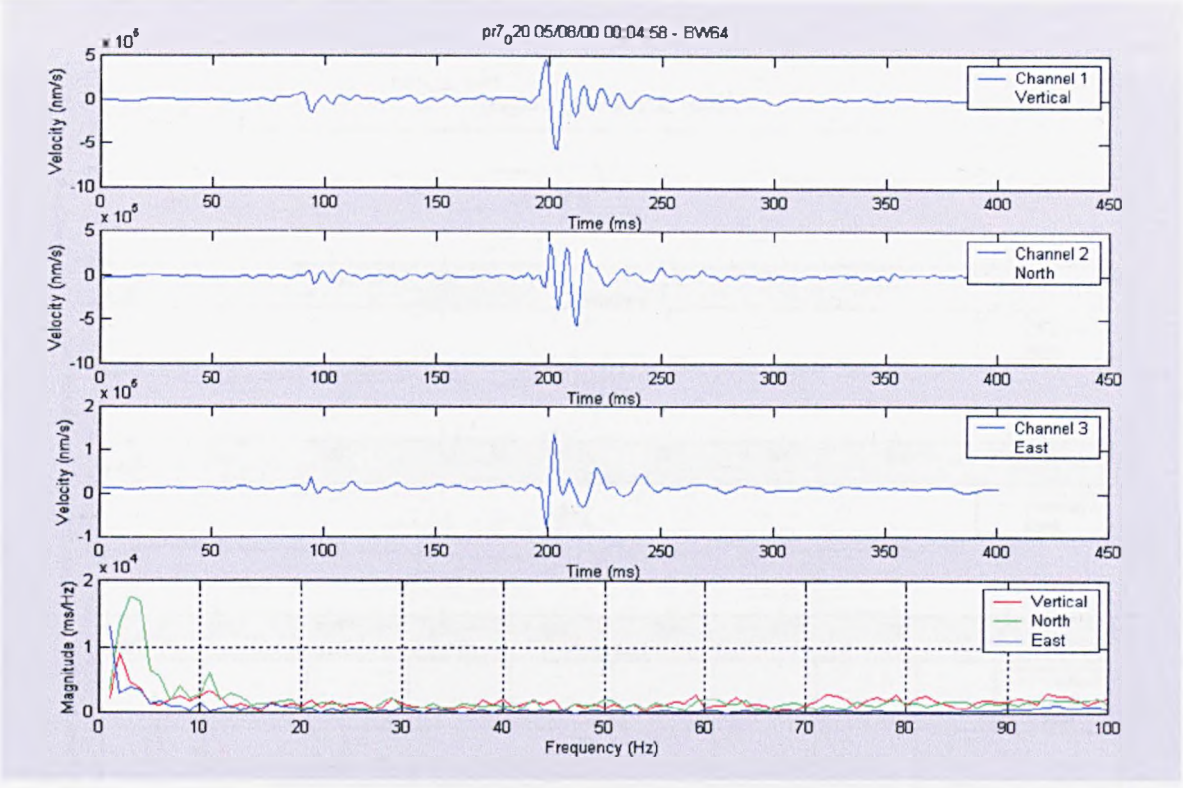


*Fig. 8.2 Enlarged image of the seismic event shown in Figure of 8.1 with frequency spectrum in lowest panel.*

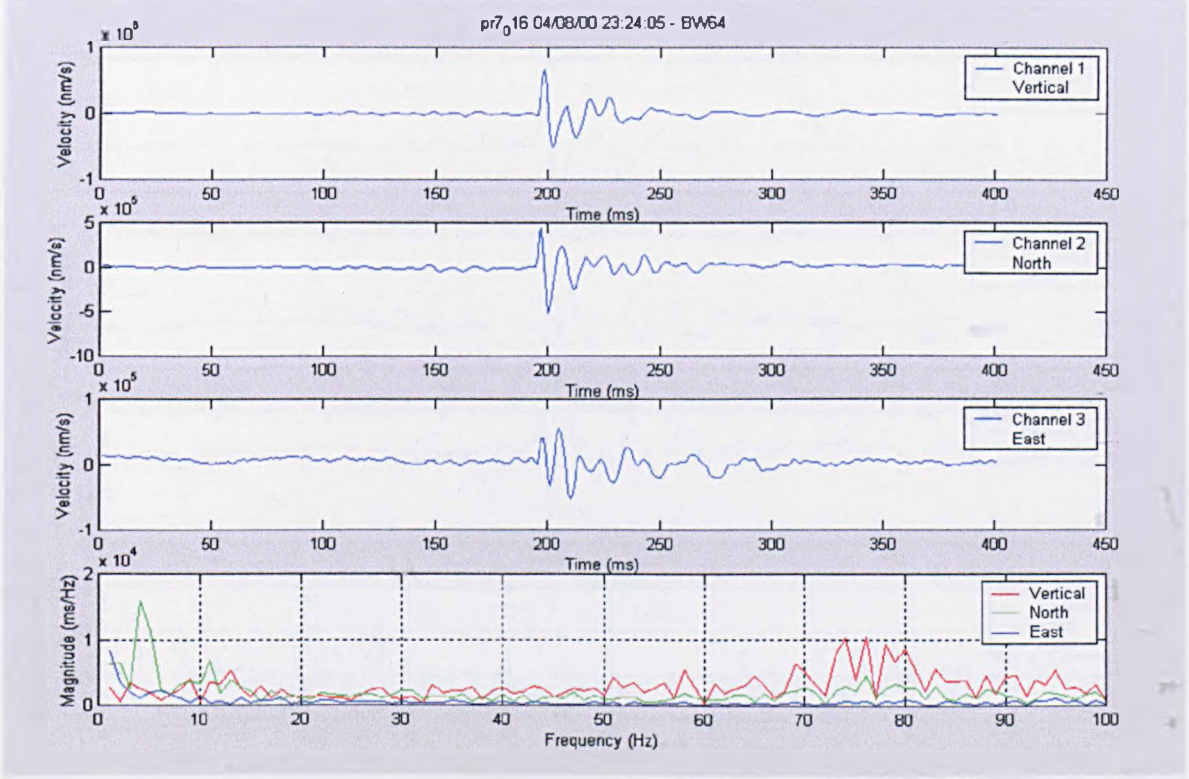


*Fig. 8.3 Event triggered at 23:24 on 04/08/00.*

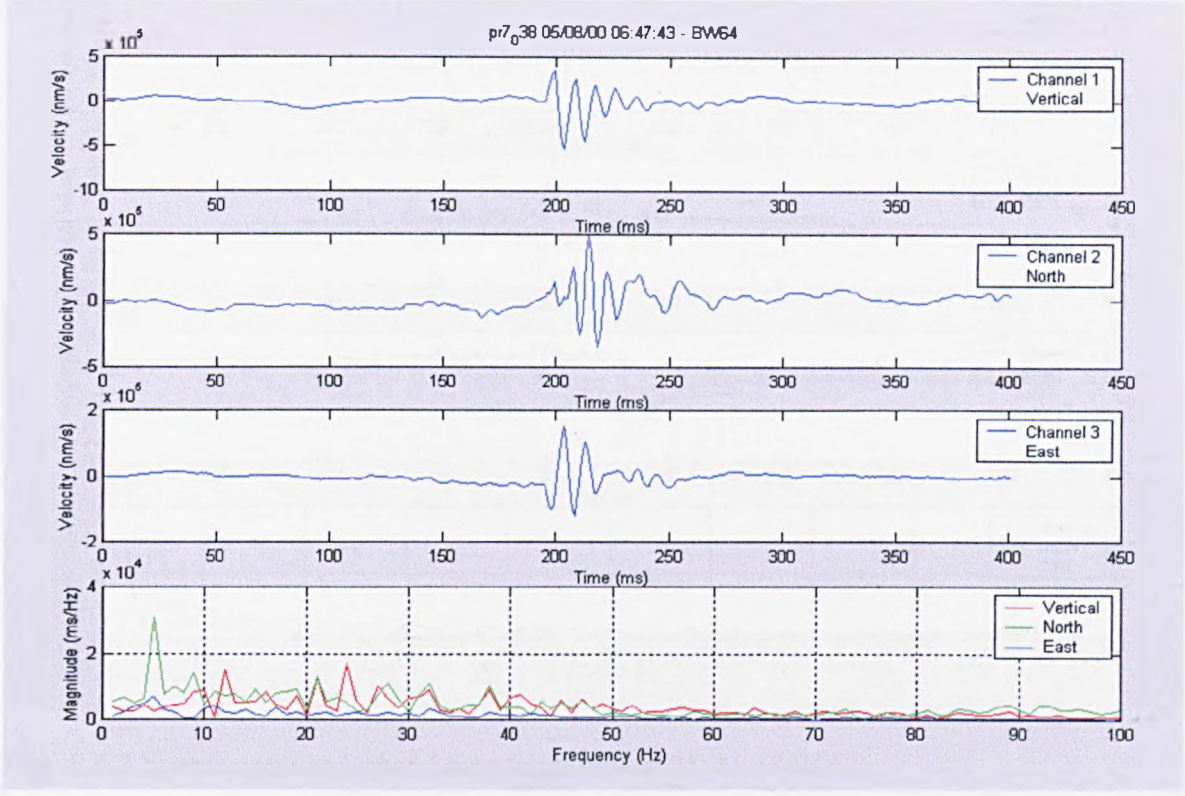


*Fig. 8.4 Event triggered at 06:47 05/08/00.*

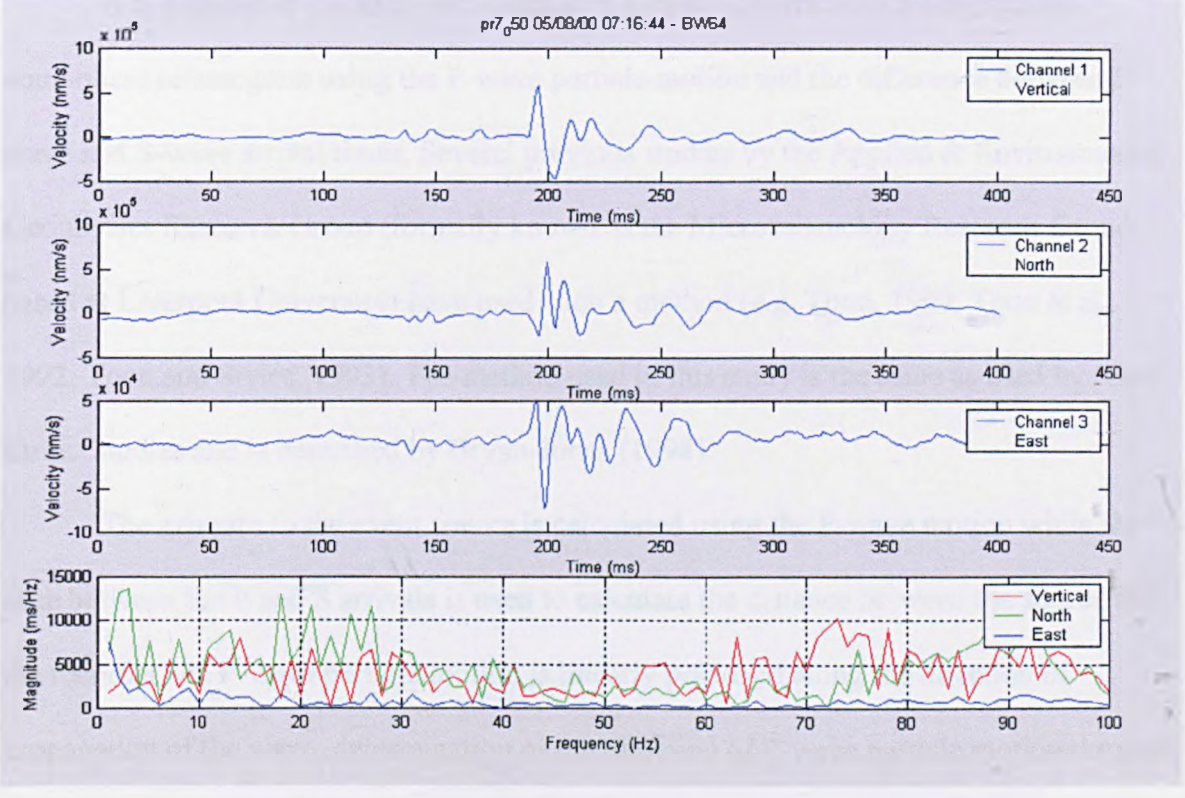


*Fig. 8.5 Event triggered at 07:16 05/08/00.*

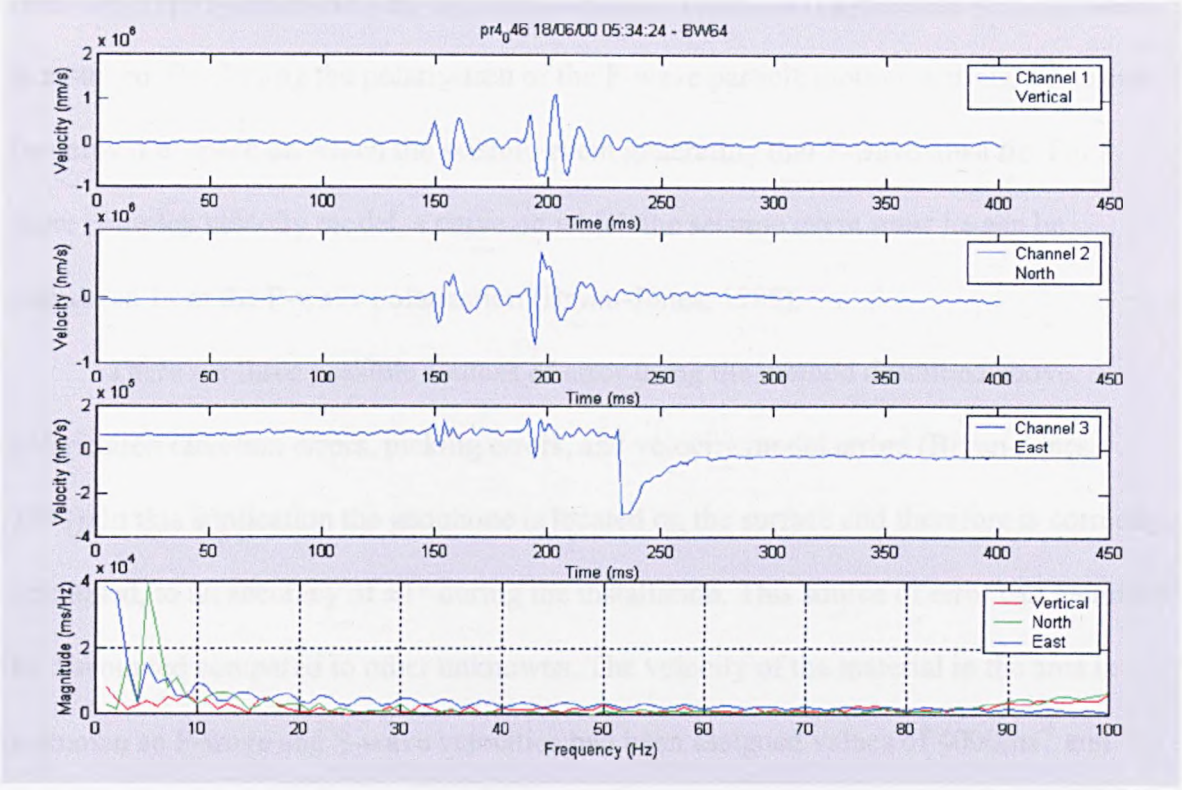


*Fig. 8.6 2 Events captured after being triggered at 05:43 18/06/00.*

It is possible to calculate the location of a seismic event from a single three-component seismogram using the P-wave particle motion and the difference between P-wave and S-wave arrival times. Several previous studies by the Applied & Environmental Geophysics Research Group (formally known as the Microseismology Research Group based at Liverpool University) have used such a method (e.g. Toon, 1990; Toon et al., 1992; Toon and Styles, 1993). The method used in this study is the same as used by these earlier studies and is described by Bryan-Jones (1998).

The azimuth to the event source is calculated using the P-wave motion while the time between the P and S arrivals is used to calculate the distance between the source and the recorder. As P-wave particle motion is linearly polarised along the direction of propagation of the wave, determination of the direction of P-wave particle motion through polarisation analysis also determines the direction of propagation of the P-wave. The

direction of propagation will be the source-receiver direction if a constant velocity model is assumed. By finding the polarisation of the P-wave particle motion, a straight line can be defined in space on which the seismic event generating that P-wave must lie. For a more complex velocity model, a curve on which the seismic event must lie can be calculated from the P-wave polarisation (Bryan-Jones, 1998).

There are three possible sources of error using the method described above, polarisation direction errors, picking errors, and velocity model errors (Bryan-Jones, 1998). In this application the geophone is located on the surface and therefore is correctly orientated, to an accuracy of $\pm 1°$ during the installation. This source of error can therefore be discounted compared to other unknowns. The velocity of the material in the area is unknown so P-wave and S-wave velocities had been assigned values of $4000ms^{-1}$ and $2310ms^{-1}$ respectively.

The size of the picking error depends greatly on the quality and nature of the data. If the event signal is an order of magnitude greater than the level of background noise then the arrival of the P and S waves can usually be determined with ease and the error will be governed by one or two samples (±2 ms). If, however, the event signal is of a similar order of magnitude to the background noise then it can be very difficult to distinguish the arrivals of the P and S phases. In this case then the picking error will be increased.

However, a hodogram can be used to identify the change in particle motion associated with the arrival of the S-wave. A hodogram is a cross-plot of two components of particle motion over a time window. As the particle motion associated with P and S waves is at 90° to each other, the two phases can be separated and the onset of the S-waves recognised.

In this situation the events that were recorded by the Vibrosound system were of a very low magnitude. As a result of this, and the nature of the signal, it has been very

difficult to distinguish the arrival of the S-wave, (if indeed there was shear phase). However, it has been possible to produce an estimate of the location of the source by using the hodogram plot to distinguish at which point the S-wave arrives (when applicable).

Analysis of the P-wave polarisation within the recorded events identifies that the source of the events is located below the geophone on a bearing that intersects the position of BW64. Therefore it is highly likely that the events are associated with activity around the cavity. By estimating the S-wave arrival time, we can establish whether it is feasible that they originated from a depth coincident with the cavity.

Plotting these locations in 3D (Figure 8.7) and cross section (Figure 8.8) shows the spatial distribution of their sources. Although the confidence attached to these locations is low because of the proportionately large errors attached to the pick of the S wave arrival, the spatial distribution of the events supports the hypothesis that the recorded events are real and that they are related to the cavity associated with BW64.

Estimates of the S-wave arrival time located the source of the events at a depth of between 50m and 160m below the surface. This corresponds well to the depth estimates derived from the microgravity surveys over the same area. In the horizontal plane the events are concentrated in an east-west orientation and match well with gravity minima recorded in 2002 (Figure 8.9 and Chapter 4).

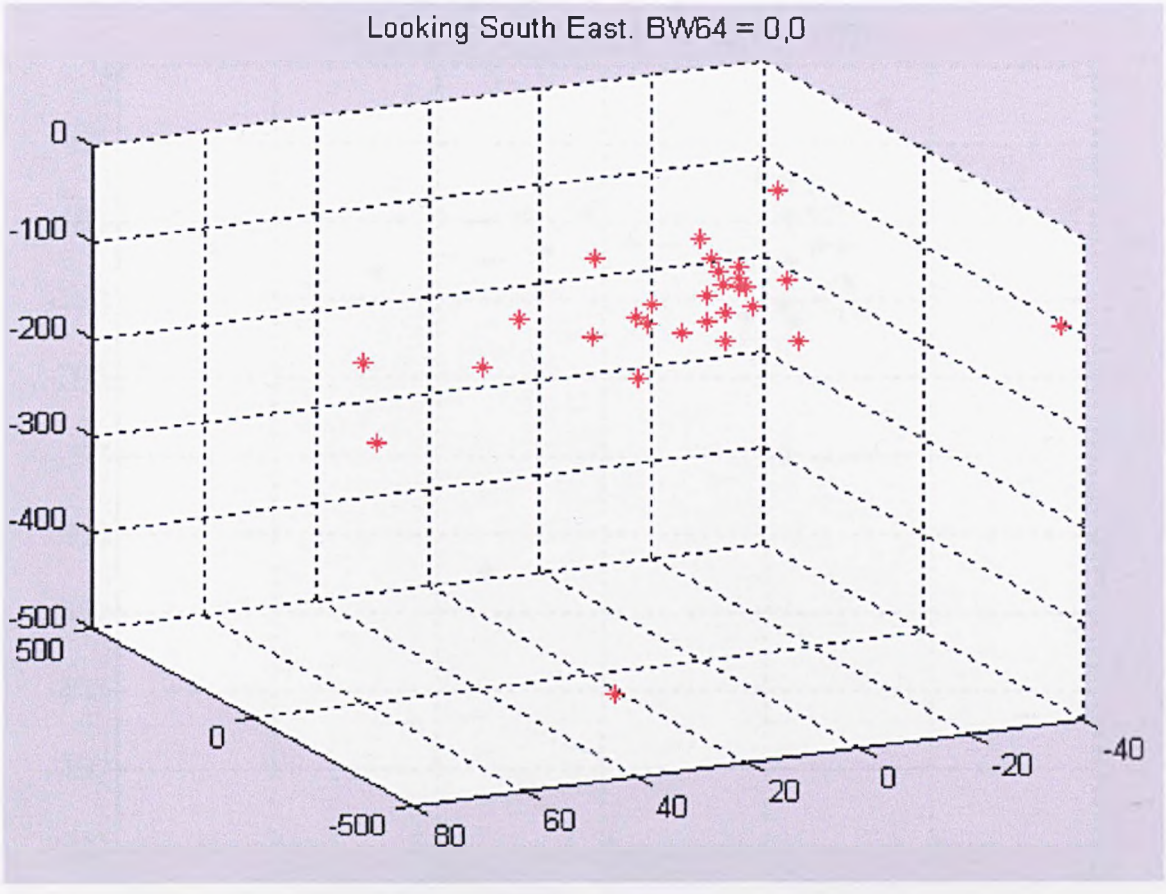


*Fig. 8.7 3D image of the estimated locations of the sources responsible for the events recorded during the first phase of microseismic monitoring at Preesall.*

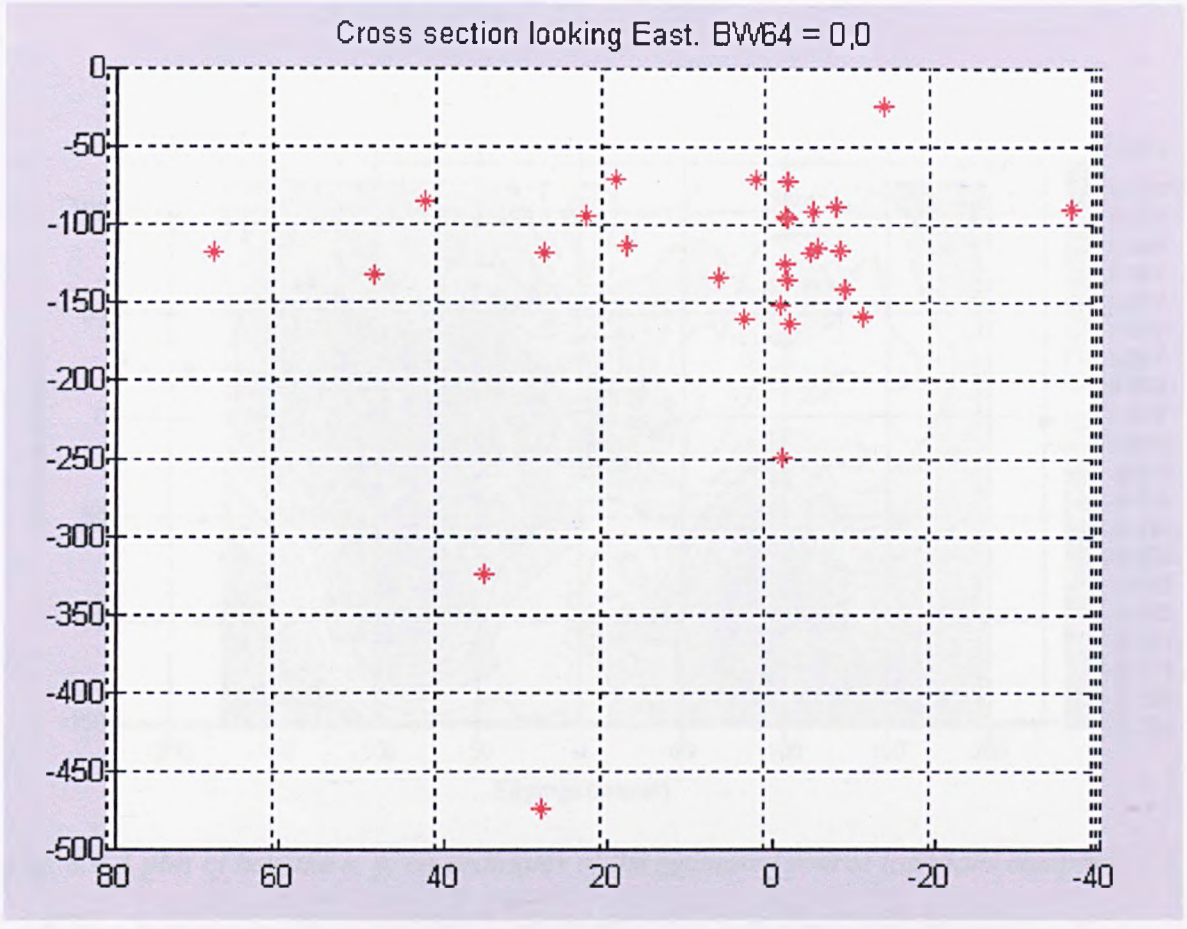


*Fig. 8.8 Cross section of the estimated source locations. The Figure is orientated so that east is into the page.*

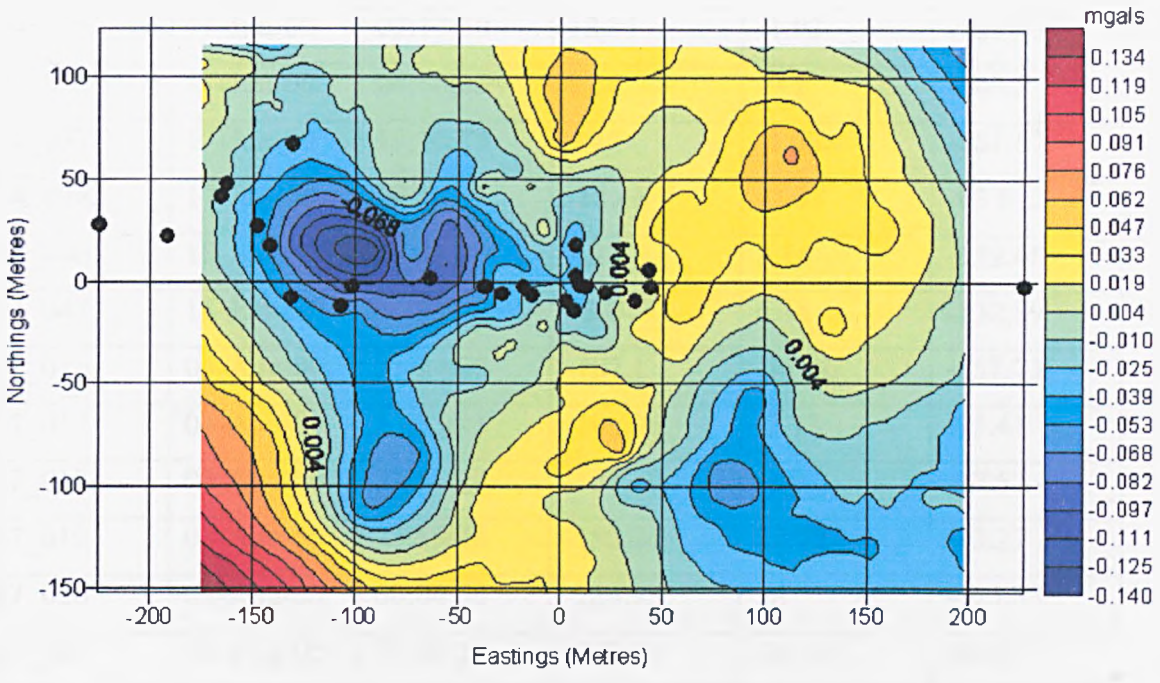


*Fig. 8.9 A plot of how the x, y, co-ordinates of the estimated source locations compare with the gravity anomalies recorded in 2000. The source locations can be seen to cluster around the negative (blue) gravity anomalies. The geophone is located at 0, 3.*

The events used for the location analysis are listed in Table 8.1. They were recorded on four days, the majority occurred late at night on the 4th of August 2000 and early in the morning of the 5th of August. These events were chosen because they contain high quality recordings on all three channels, which was relatively rare during the monitoring. The clustering of these events suggests that a collapse event occurred during this period resulting in a burst of events being recorded by the Vibrosound system.

| File | Date | Time | x | y | z |
|---|---|---|---|---|---|
| b4_021 | 17-Jun-00 | 02:16:53 | 21.85 | -5.09 | -117.25 |
| b4_022 | 17-Jun-00 | 02:17:30 | 12.35 | -1.92 | -125.03 |
| b4_023 | 17-Jun-00 | 04:56:23 | 2.34 | -9.2 | -140.3 |
| b4_037 | 17-Jun-00 | 19:10:15 | 9.46 | -1.53 | -151.57 |
| b4_038 | 17-Jun-00 | 19:12:31 | -18.46 | -2.03 | -93.8 |
| b4_046 | 18-Jun-00 | 05:34:24 | 7.23 | 3.14 | -159.45 |
| b4_047 | 18-Jun-00 | 05:35:08 | 43.04 | 6.18 | -132.79 |
| b7_016 | 04-Aug-00 | 23:24:05 | -107.1 | -11.46 | -157.73 |
| b7_017 | 04-Aug-00 | 23:35:45 | -101.96 | -2.12 | -95.41 |
| b7_018 | 04-Aug-00 | 23:51:28 | -131.19 | -7.9 | -87.52 |
| b7_019 | 04-Aug-00 | 23:55:48 | -192.26 | 22.58 | -93.27 |
| b7_020 | 05-Aug-00 | 00:04:58 | -224.93 | 28 | -473.83 |
| b7_021 | 05-Aug-00 | 00:07:24 | -492.01 | -36.29 | -89.37 |
| b7_022 | 05-Aug-00 | 00:08:11 | -147.6 | 27.7 | -118.02 |
| b7_023 | 05-Aug-00 | 00:18:33 | -37.76 | -2.23 | -134.43 |
| b7_028 | 05-Aug-00 | 06:31:03 | 411.72 | 34.17 | -324.36 |
| b7_038 | 05-Aug-00 | 06:47:43 | 7.32 | 18.72 | -70.31 |
| b7_050 | 05-Aug-00 | 07:16:44 | 43.86 | -2.36 | -72.04 |
| b7_051 | 05-Aug-00 | 07:17:43 | 226.88 | -1.81 | -249.85 |
| b7_052 | 05-Aug-00 | 07:18:42 | 36.42 | -8.81 | -115.47 |
| b7_055 | 05-Aug-00 | 07:21:30 | -63.76 | 1.79 | -71.08 |
| b7_056 | 05-Aug-00 | 07:22:40 | -165.96 | 42.08 | -84.66 |
| b7_074 | 05-Aug-00 | 07:36:14 | -14.25 | -5.91 | -114.74 |
| b7_075 | 05-Aug-00 | 07:41:01 | -28.3 | -5.35 | -91.05 |
| b7_079 | 05-Aug-00 | 07:58:41 | -35.92 | -2.37 | -163.2 |
| b7_127 | 05-Aug-00 | 15:12:45 | -130.88 | 67.75 | -117.96 |
| b7_130 | 05-Aug-00 | 15:33:03 | -141.45 | 17.55 | -112.82 |
| b7_131 | 05-Aug-00 | 15:34:25 | -162.85 | 48.26 | -131.62 |
| b7_135 | 05-Aug-00 | 15:43:50 | 6.94 | -14.08 | -23.34 |

*Table 8.1. List of the events used in the location analysis.*

The results of this preliminary investigation were promising. Although there is not absolute confidence in the locations derived from the single 3-component seismometer, it had been established that the area was seismically active and it is highly probable that the source of the events was related to the evolution of the cavity associated with BW64.

### 8.2.2 Phase 2

To combat the problem of the recorded events not having an easily distinguishable shear wave phase an array of six 3-component geophones was installed around the perimeter fence of BW64. The purpose of this much larger array was to locate the events by using only the P-wave arrivals. The azimuth of the source would be calculated in the same way as before by using the particle motion from the P-wave. However, if the event was recorded on more than one geophone, P-S wave separation would not be needed to calculate the distance from the geophone to the source. Instead it would be possible to determine the location of the source by finding the intercept of two or more azimuths or by using the P-wave arrival times from three or more seismometers.

The equipment used for this experiment was loaned from the NERC geophysical equipment pool in Edinburgh (loan number 679). The array was installed at Brine Well 64 on October 18, 2000. Six units were installed around the perimeter fence (Figure 8.10). Each unit consisted of 1 PDAS 100 recording unit, 1 REF TEK hard drive (500 Mbytes), 1 GPS clock, 1 12V battery a solar panel and a Lennartz 3Dlite geophone. The geophone was buried 0.5m below the surface in a protective tube with a cement bottom. This in turn was cemented into the ground.

The PDAS units were set to record continuously at a sample interval of 100 Hertz. This allows for a maximum of 12 days continuous recording. The batteries had a life

expectancy of 10 days although this could be prolonged if the weather was bright and extra energy could be drawn from the solar panels. In general the batteries were changed and the hard drives downloaded every seven to ten days.

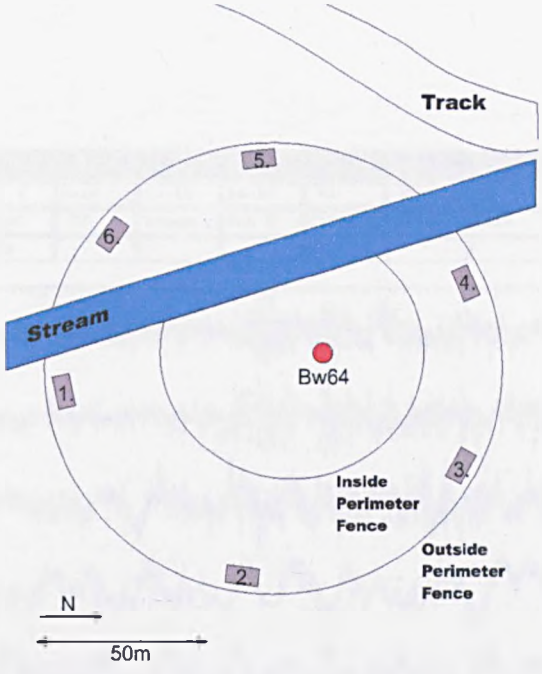


*Fig. 8.10 Schematic diagram showing the layout of the PDAS units around BW 64.*

Throughout the field season a number of problems were encountered while recording. The main problem was water ingress into the PDAS units. Towards the end of October the area around the investigation site, like much of the rest of the country, flooded. This lead to four out of the six units being disabled. This was later reduced to three out of the six units by pooling the undamaged circuitry to make one functioning unit. There were also continued difficulties with excessive power drain caused by the cold weather. After a few days the units were shutting down, as there was insufficient power to boot up and write to the hard drive. This led to patchy coverage throughout the recording period and was thought to be caused by the cold nights.

The data quality recorded in the Preesall Brine field is generally good. The individual events recorded by the units show the same characteristics as the events recorded by the Vibrosound, (impulsive with a single-phase arrival). Importantly, however, few of these events are recorded across two or more PDAS units. An example of this is shown in Figure 8.11.

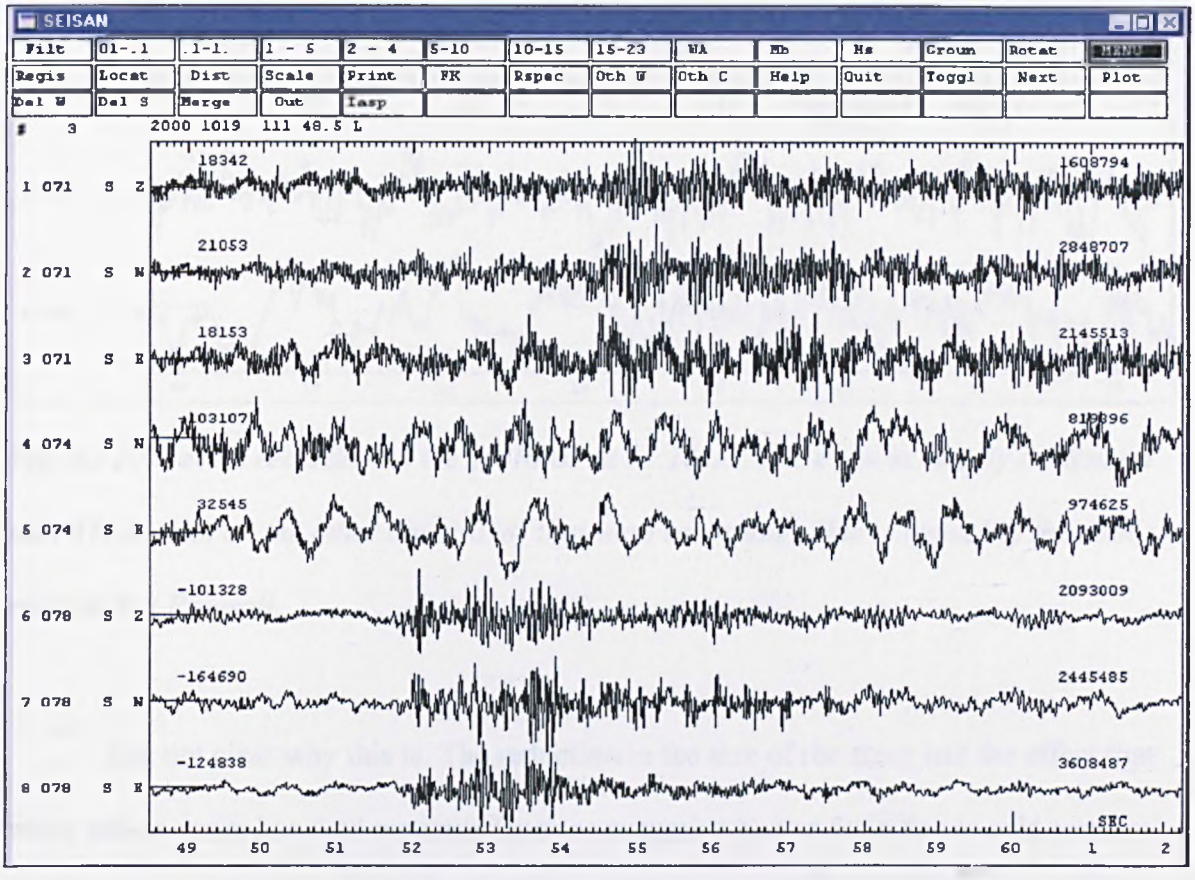


*Fig. 8.11 An event recorded on the 19/10/00 at 01:00:48. The event is clearly evident on unit 078 but not on the other units (071 & 074) that were recording. This is typical of the data recorded at Preesall.*

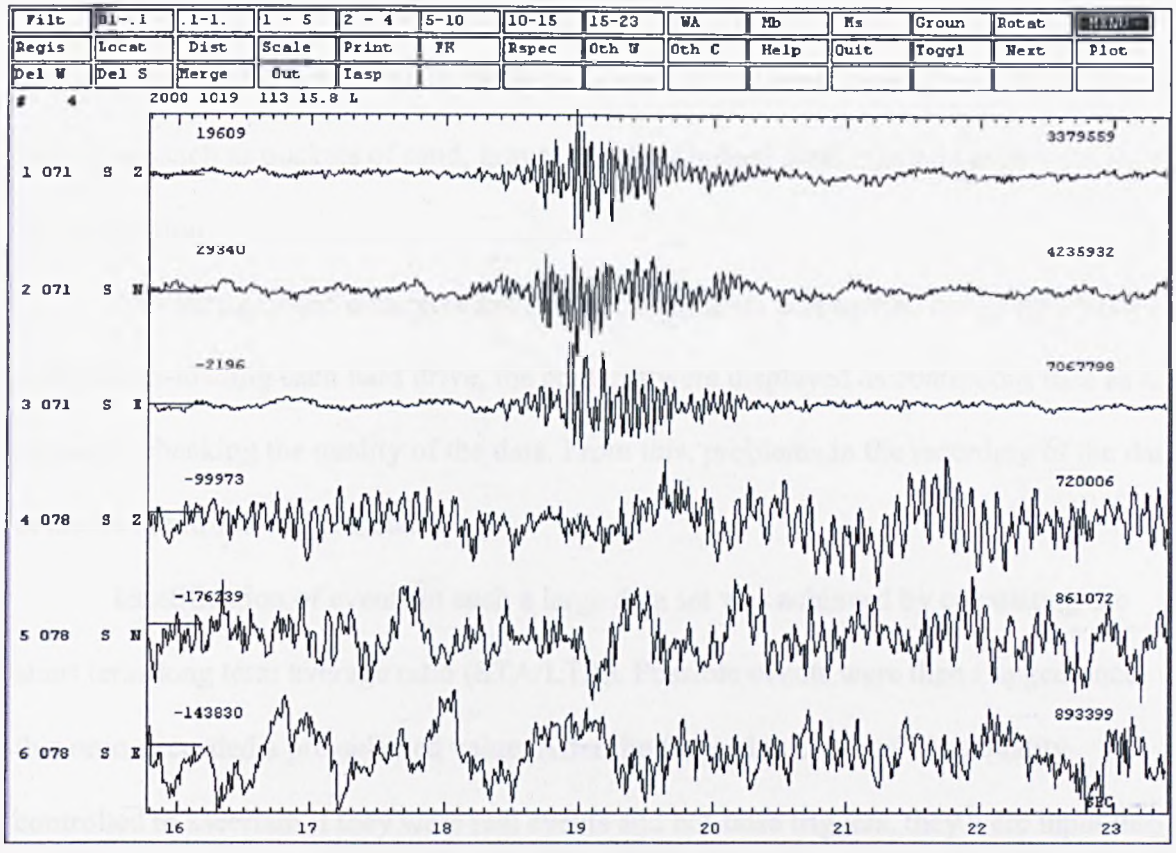


*Fig. 8.12 An event recorded on the 19/10/00 at 01:13:15. The event is clearly evident on unit 071 but not on the other units (078) that were recording. This is typical of the data recorded at Preesall.*

It is not clear why this is. The reduction in the size of the array had the effect that when minor errors knocked out units (such as excessive power drain due to cold weather, bugs in programs or loss of GPS clock) coverage was reduced to one or two units only. However, for periods of full coverage events were not detected on more than one unit. This maybe a result of timing errors or a reflection of the small magnitude of the events. If it is a result of timing errors, it is likely to be either a result of an error in the timing of the event during recording (potentially caused by the GPS clock or the PDAS's internal processing software) or errors within the merging of events within SEISAN (a windows based seismic analysis package which was used to process the data). It is conceivable,

however, that the events are of such a magnitude that they are not propagating to all of the receivers around the array. This is likely to be a result of lateral heterogeneities within the mudstone, such as pockets of sand, gravel or salt or indeed further small cavities caused by bed separation.

Processing of the data recorded by the PDAS units was carried out using Matlab. After down-loading each hard drive, the contents were displayed as continuous data as a means of checking the quality of the data. From this, problems in the recording of the data could be identified and corrected.

Identification of events in such a large data set was achieved by calculating the short term/long term average ratio (STA/LTA). Possible events were then flagged once this ratio exceeded a pre-selected value. After the flagged events had been quality controlled to ascertain if they were real events and not false triggers, they were input into SEISAN for conversion and merging. It has not been possible to produce satisfactory locations for the events because of the timing problems discussed earlier.

## 8.3 Passive microseismic monitoring at Peter Street, Northwich

Microseismic monitoring equipment was installed at Peter Street on August 1, 2001. The aim of the installation was two fold. The principal aim was to monitor the seismicity of the area in an attempt to substantiate the hypothesis that the body responsible for the gravity anomaly detected by the microgravity survey, was migrating towards the surface. The second aim of the experiment was to establish whether electroseismic signals could be detected in the area. This was part of ongoing work conducted by Baggaley (2002).

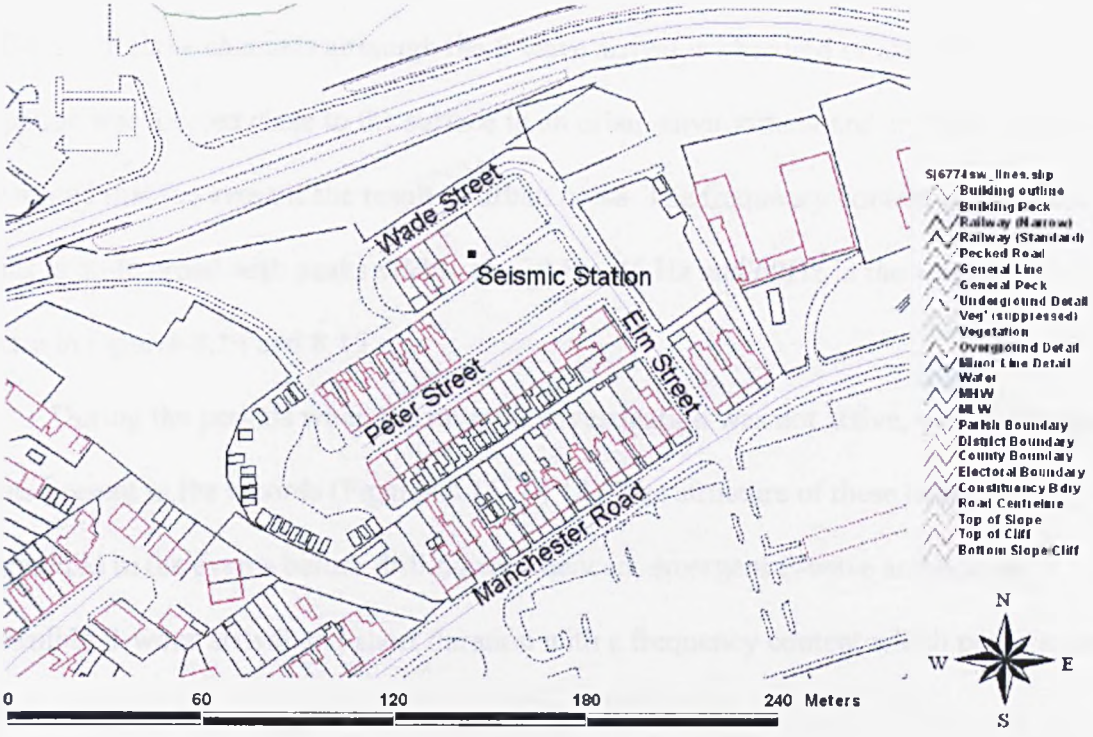




*Fig. 8.13 Map of Peter Street showing the location of the seismic station (grid ref. 366923, 374128).*

The equipment used in the experiment was the same as that used in phase 1 of the microseismic monitoring at Preesall Brine Field. The seismic station was located north of the gravity anomaly identified in the microgravity surveys (Figure 8.13). A 3-component, Lennartz geophone was buried beneath the surface in a small pit with a concrete base. The geophone was attached to a Vibrosound recorder, which recorded 2.144 seconds of data including a one-second pre-trigger at a sampling rate of 1000 Hz.

The seismic monitoring coincided with the invasive investigation of the microgravity anomaly identified in Chapter 5. Consequently, the majority (~90%) of the records downloaded from the Vibrosound are related to this activity. Examining data recorded before the commencement of the drilling, very clear seismic events can be seen.

Figures 8.14 and 8.15 show examples of such events. The arrival of the P-wave is clearly visible on all three channels although the S wave arrival is obscured or absent. The geophone was located close to the surface in an urban environment and so it can not be discounted that the event is the result of urban noise. The frequency content of these two events is quite broad with peaks visible at ~30 Hz, 45 Hz and 60Hz in the waveform spectra in Figures 8.14 and 8.15.

During the periods when the invasive investigation was not active, we see similar events present in the records (Figures 8.16 – 8.18). The structure of these events is comparable to the events before drilling commenced; emergent P-wave arrivals, no discernible S-wave arrival and short duration with a frequency content which peaks around 25 Hz.

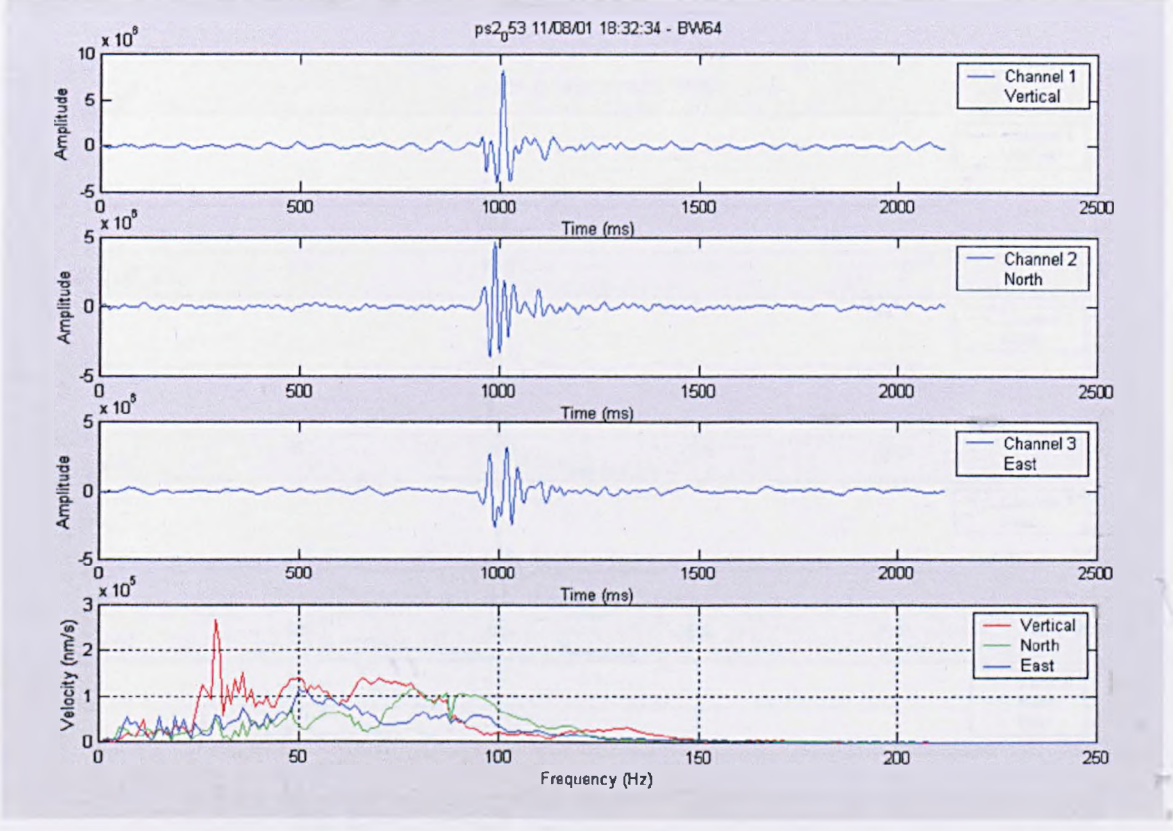


*Figure 8.14 Event recorded at 18:32 on 11/08/01.*

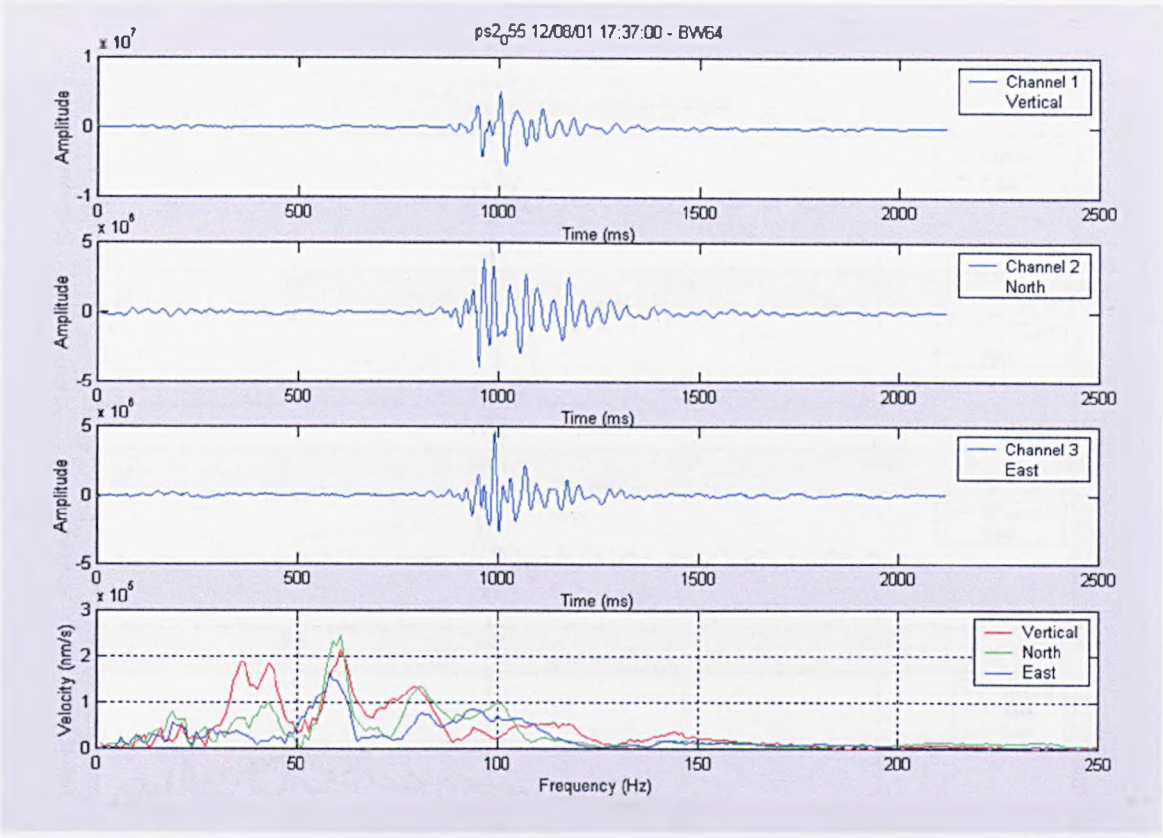


*Figure 8.15 Event recorded at 17:37 on 12/08/01.*

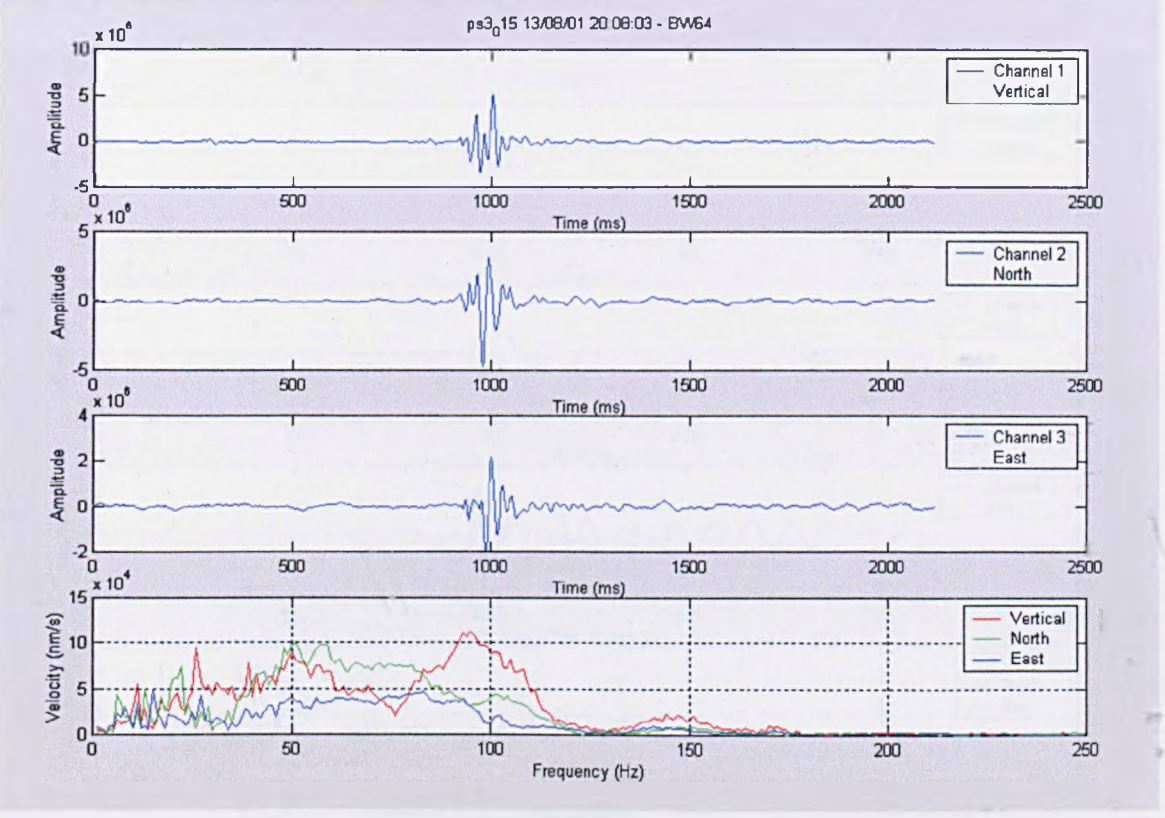


*Fig. 8.16 Event recorded at 20:08 on 13/08/01.*

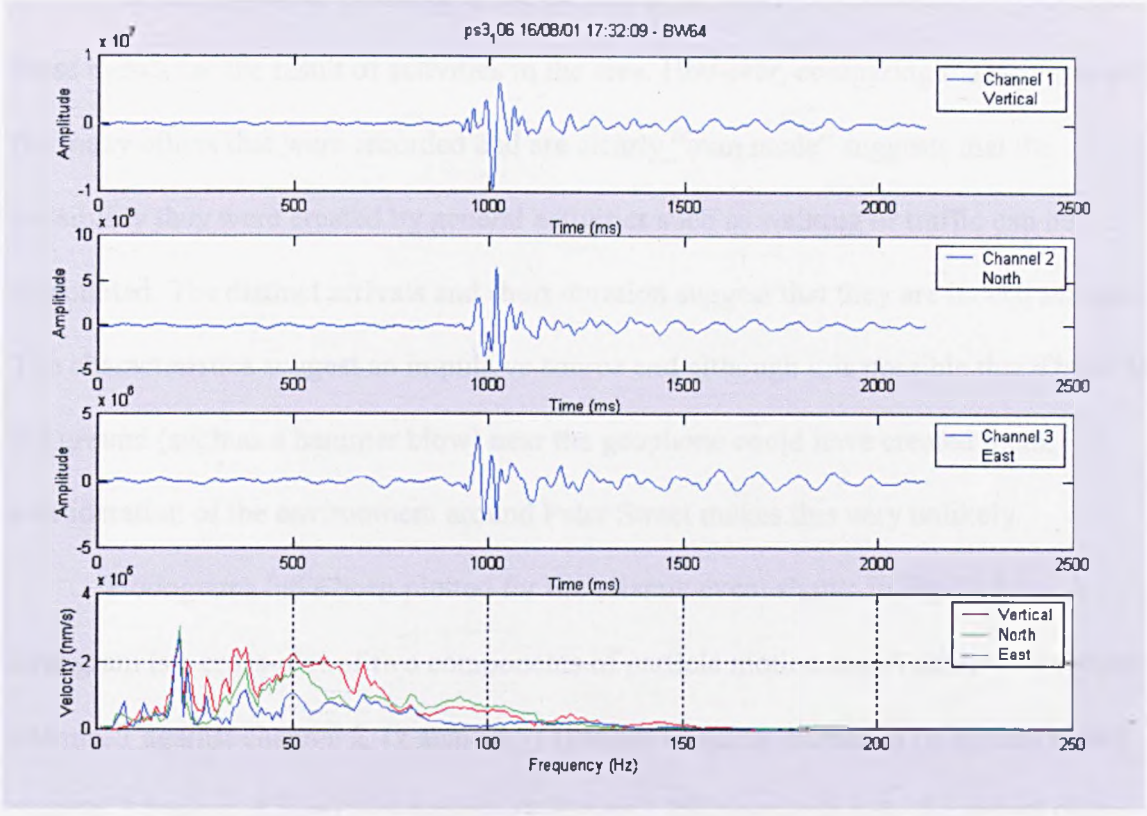


*Fig. 8.17 Event recorded at 17:32 on 16/08/01.*

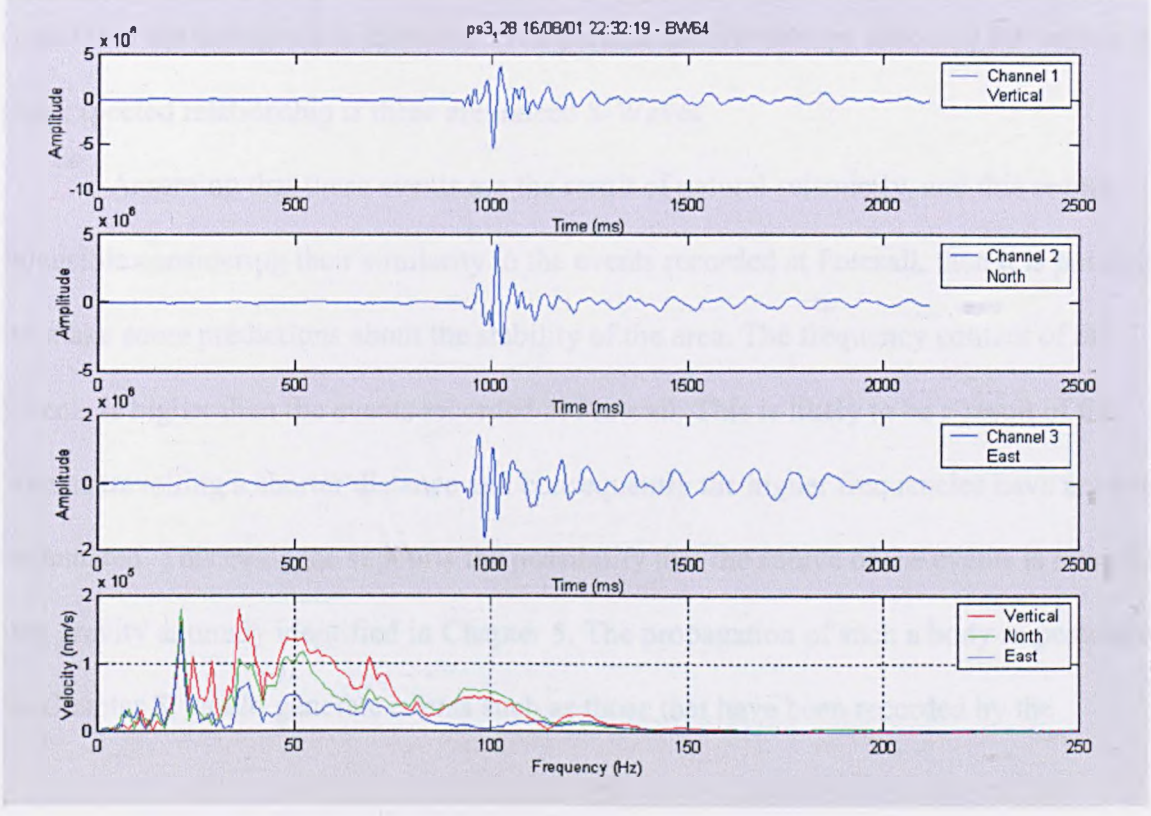


*Fig.8.18 Event recorded at 22:32 16/08/01.*

As the geophone is located at the surface in an urban environment it is possible that these events are the result of activities in the area. However, comparing these events with the many others that were recorded and are clearly "man made" suggests that the possibility they were created by general activities such as walking or traffic can be discounted. The distinct arrivals and short duration suggest that they are indeed seismic. The characteristics suggest an impulsive source and although it is possible that a blow to the ground (such as a hammer blow) near the geophone could have created them, consideration of the environment around Peter Street makes this very unlikely.

Hodograms have been plotted for the seismic event shown in Figure 8.14. A hodogram is a cross-plot of two components of particle motion and is achieved by plotting channel 1 against channel 2, (x against y) channel 1 against channel 3 (x against z) and channel 2 against channel 3 (y against z). Figure 8.19 shows that here the arrival of the event starts with a unidirectional particle moment. Figure 8.20 shows the result if the data input into the hodogram is extended. The particle motion sweeps round by 90° which is the expected relationship if these are indeed S-Waves

Assuming that these events are the result of natural seismicity, and this seems plausible considering their similarity to the events recorded at Preesall, then it is possible to make some predictions about the stability of the area. The frequency content of the events is higher than the events recorded at Preesall. This is likely to be a result of the events travelling a shorter distance and consequently the higher frequencies have not been attenuated. This evidence supports the possibility that the source of the events is related to the gravity anomaly identified in Chapter 5. The propagation of such a body as postulated in Chapter 5, would generate events such as those that have been recorded by the

Vibrosound system. Although we can not be certain that they are related, the information recorded by the Vibrosound is supportive of this hypothesis.

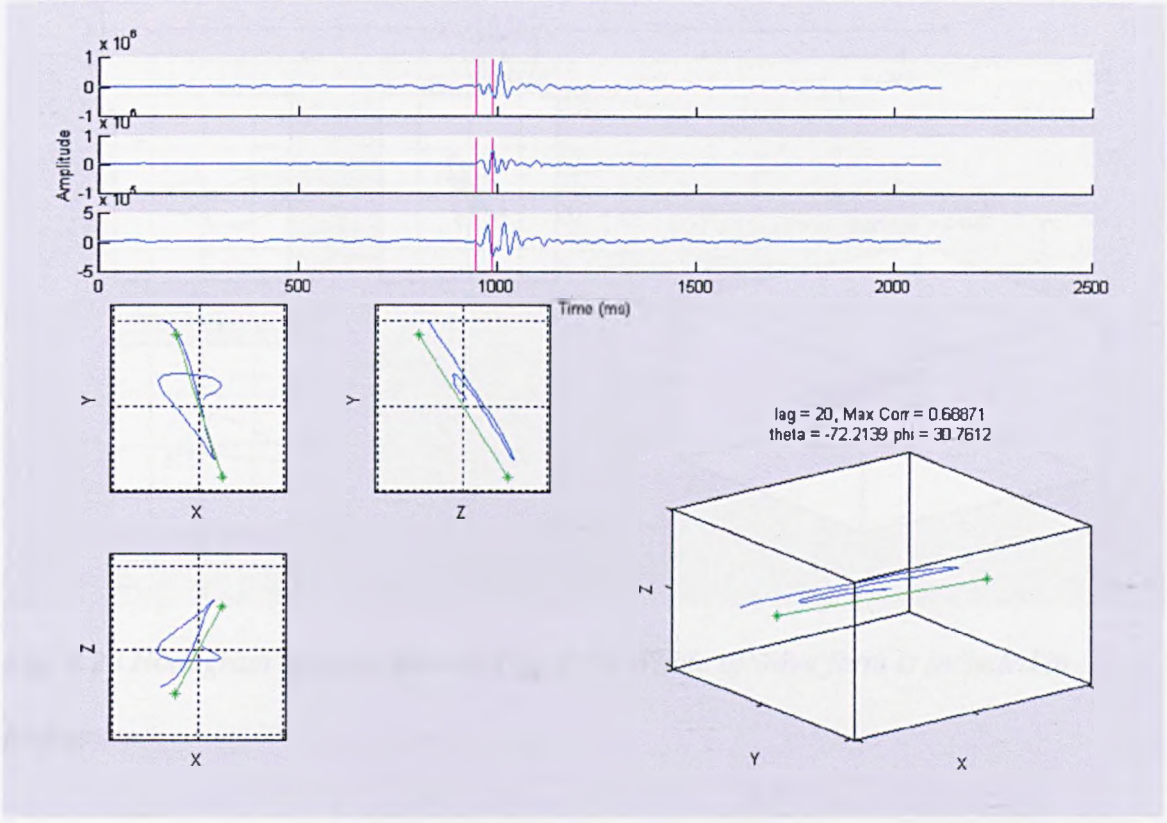


*Fig 8.19 Hodogram of event shown in Fig 8.13 Only first motions are included in hodogram.*

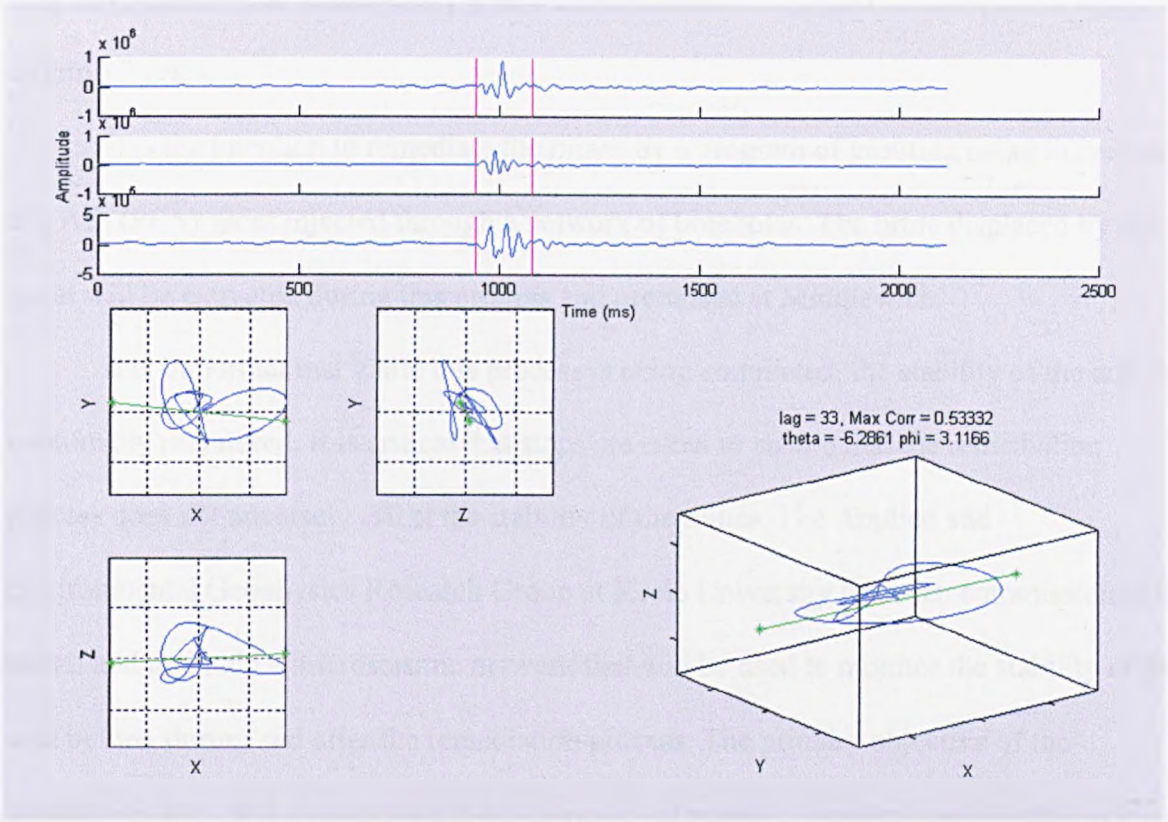


*Fig. 8.20 Hodogram of event show in Fig. 8.13. Whole of wave form is included in hodogram.*

## 8.4 Passive microseismic monitoring in Northwich town centre

Vale Royal Borough council and English Partnerships have commissioned work in Northwich to identify the remediation action necessary to stabilise the region and guarantee against further subsidence as a result of mine collapse.

Through sonar measurements and boreholes it has been identified that many of the supporting pillars in the mines which lie beneath the town (Figure 8.21) are deteriorating. This has the potential to result in the eventual collapse of the mines in a similar fashion to the catastrophic collapses that characterised the Northwich landscape in the early 20$^{th}$ century. In the case of Witton Bank Mine it was concluded that the onset of pillar failure

may have entered the tertiary creep phase and subsidence may start to occur at the surface within 15 years.

It is the intention to remediate the mines by a program of grouting using Pulverised Fly Ash (PFA) grout injected through a network of boreholes. The brine displaced by the grout will be extracted during this process and processed at Middlewich.

It is important that while this process is being completed, the stability of the area is continually monitored. It is critical that steps are taken to ensure that the remediation process does not adversely effect the stability of the mines. The Applied and Environmental Geophysics Research Group at Keele University has been commissioned to install and maintain a microseismic network that will be used to monitor the stability of the area before, during and after the remediation process. The primary objective of the installation is to give warning of the development of possible incipient instabilities within and around the salt mines and to give warning of such developments which will aid in the implementation of contingency procedures to prevent mine collapse.

At the time of writing, the network consists of nine seismic stations. Each station consists of 1 or 2 borehole geophones connected to an ISSI SAQS (Integrated Seismic Systems International, Stand Alone Quake Seismometer) at the surface. Geophones are grouted into boreholes at depths above and/or below the mine workings. Each station communicates to a central computer in the town centre where the validity of the trigger is assessed. The individual station can also store data internally should communications break down.

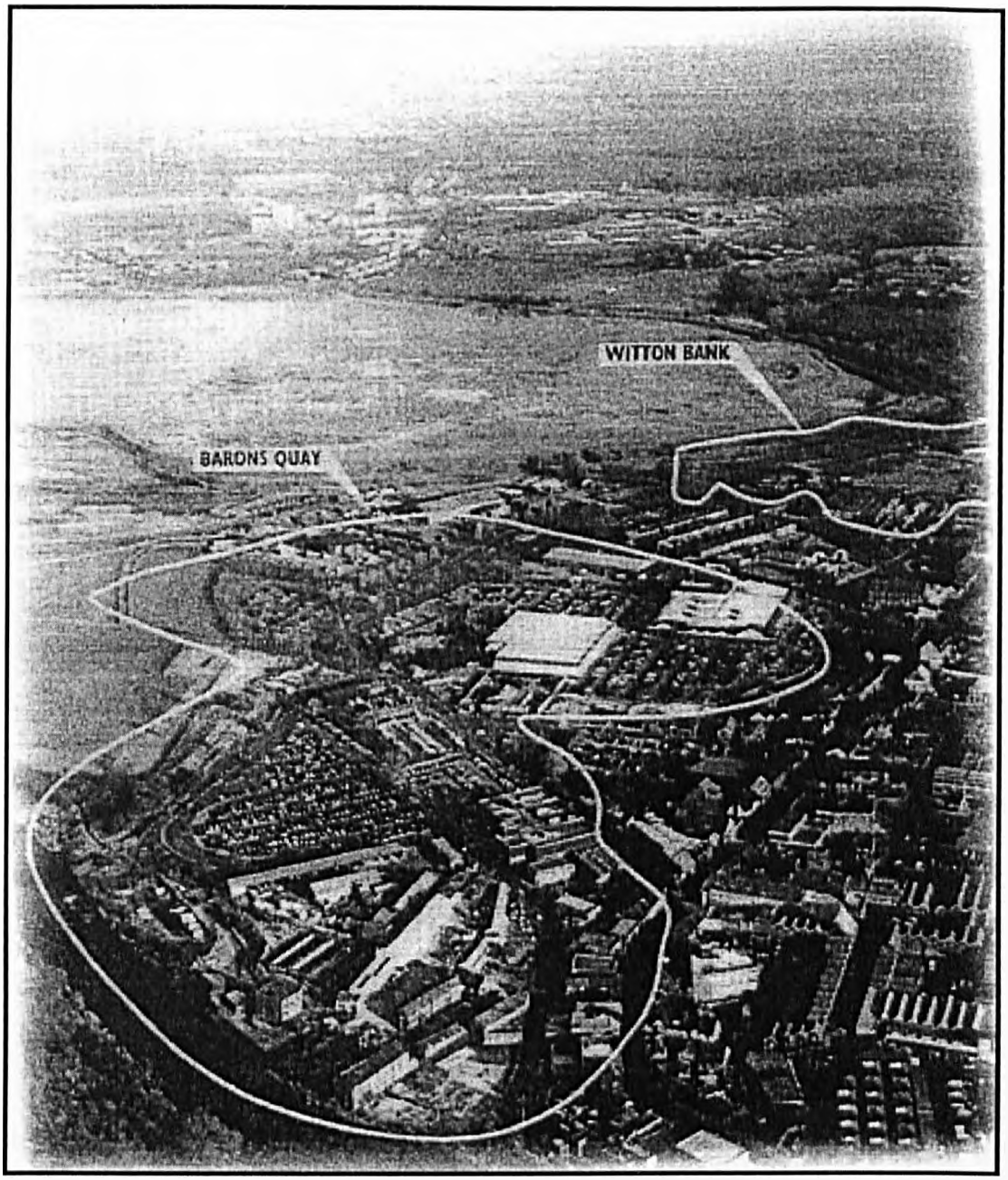


*Fig.8.21 Figure showing the extent of the Witton Bank and Barons Quay mines overlain on a photo of Northwich.*

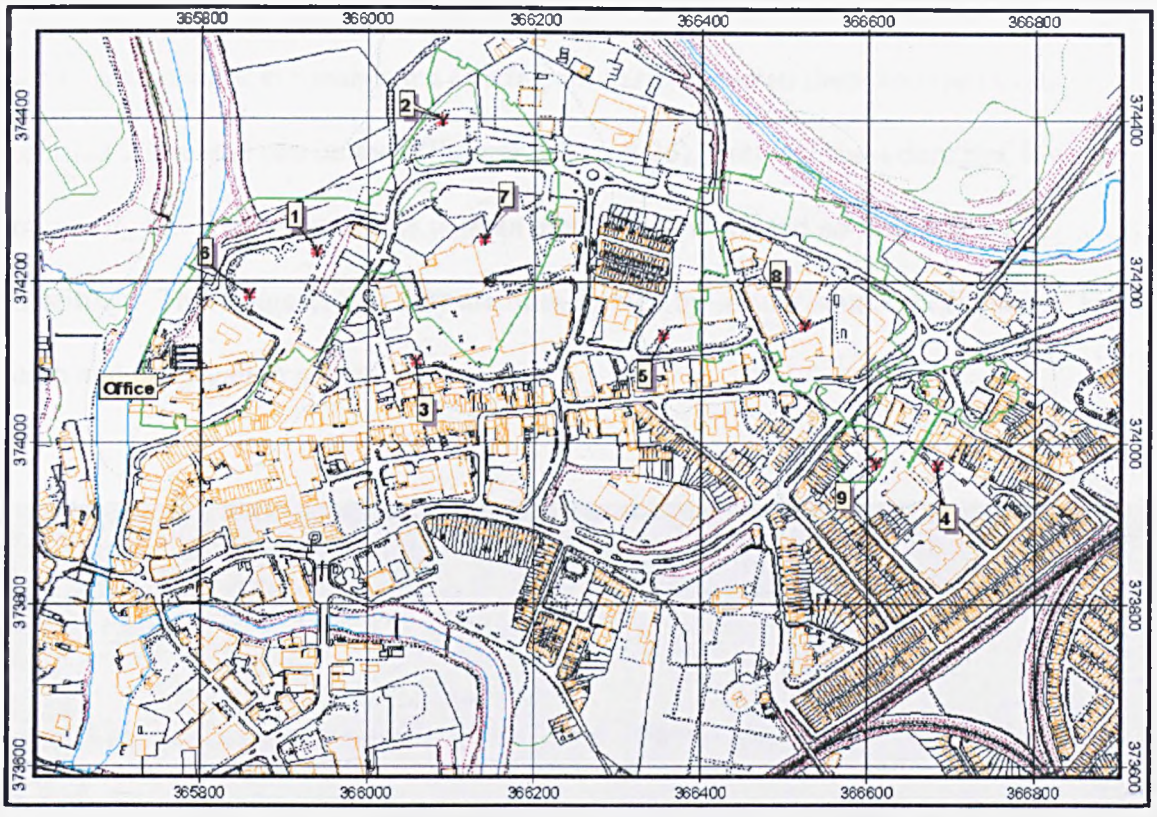




*Fig. 8.22 Figure showing the location of the seismic station within the Northwich network (Styles, 2002).*

To date, the activity detected during the monitoring period has been relatively low. On average 20-40 events have been recorded per day with the majority of the data being recorded around the Gladstone Club (Station 9) and the rear of Station Road (Station 4). Seismic station locations are shown in Figure 8.22.

The network has also recorded several large regional events. Although these are not of direct interest to this study they do prove that the system is functioning correctly. Of greater interest is the large volume of low magnitude events that have been recorded throughout the monitoring period.

These events are described as "unusual but interesting" (P. Styles, pers. Comm.) as they do not appear to have an S arrival, or have one which can not be distinguished from

the P wave. If some of the low magnitude events that have been recorded by the Northwich network are analysed a striking similarity between them and the events recorded at Preesall can be seen (Figures 8.23 – 8.26). Both are short duration, low amplitude, low frequency events with an emergent P wave and no visible S wave constituent. This suggests that they are both formed by similar source mechanisms, source depth and propagation paths.

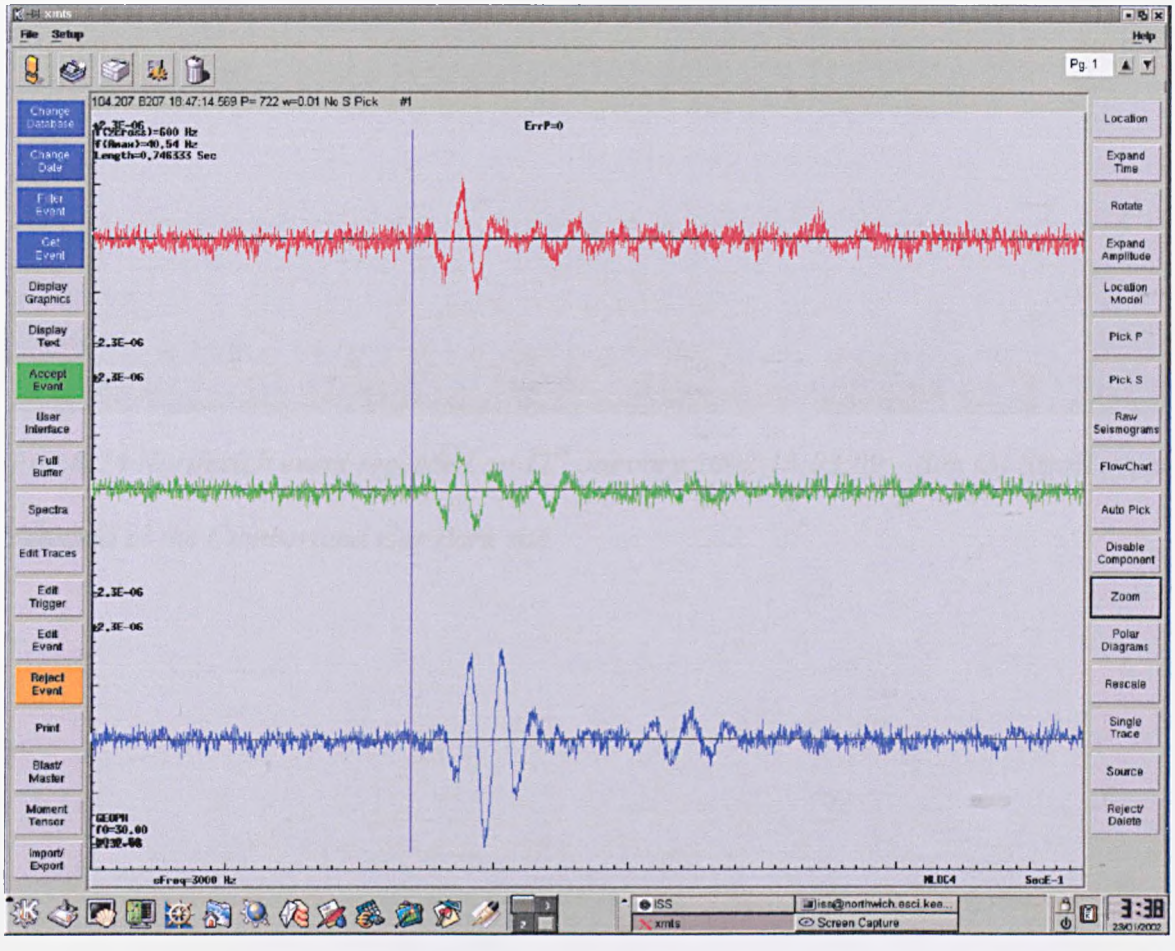


*Fig. 8.23 Northwich event recorded on 3rd January 2002 18:47:14 –This event was detected on only Site 7.*

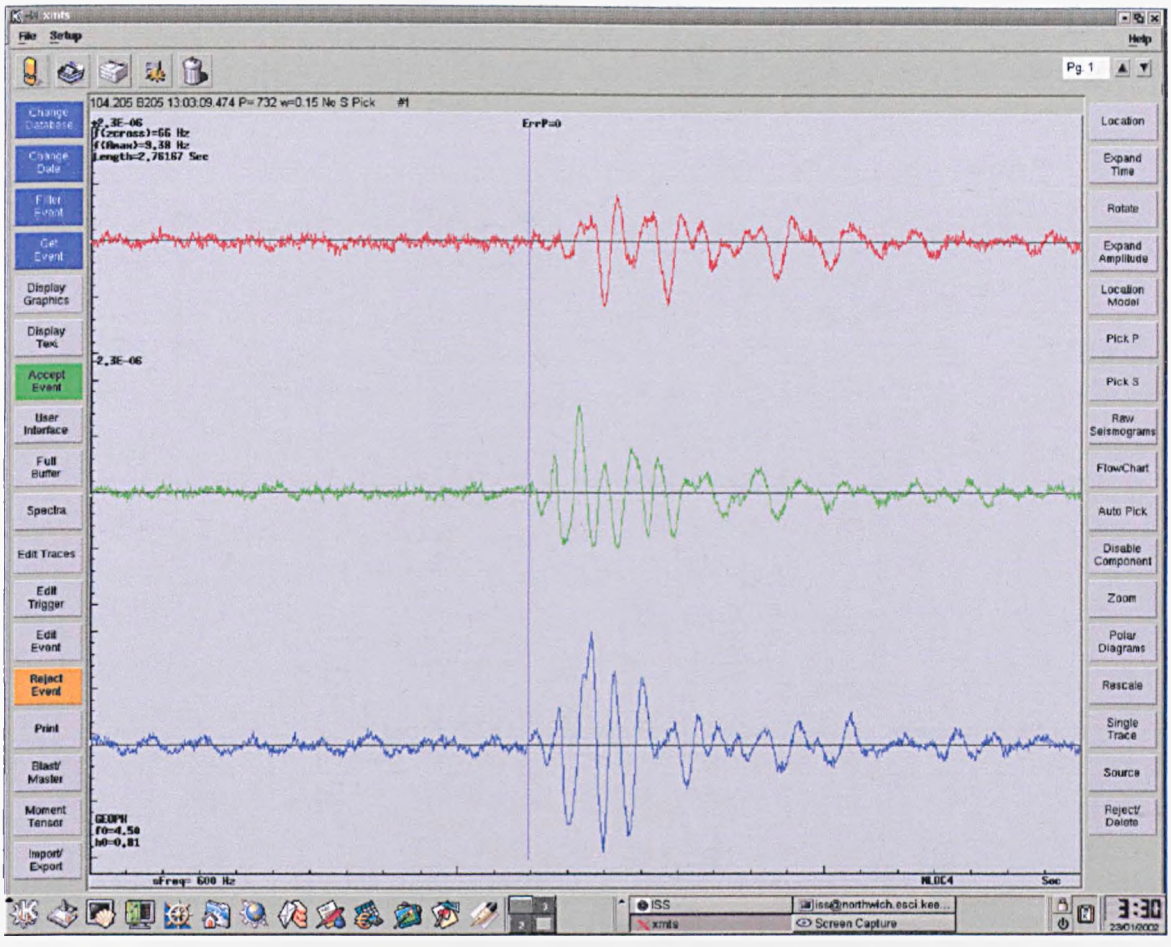


*Fig. 8.24 Northwich event recorded on 11th January 2002 13:03:09 – Site (5) Small event detected at the Cumberland Car Park site.*

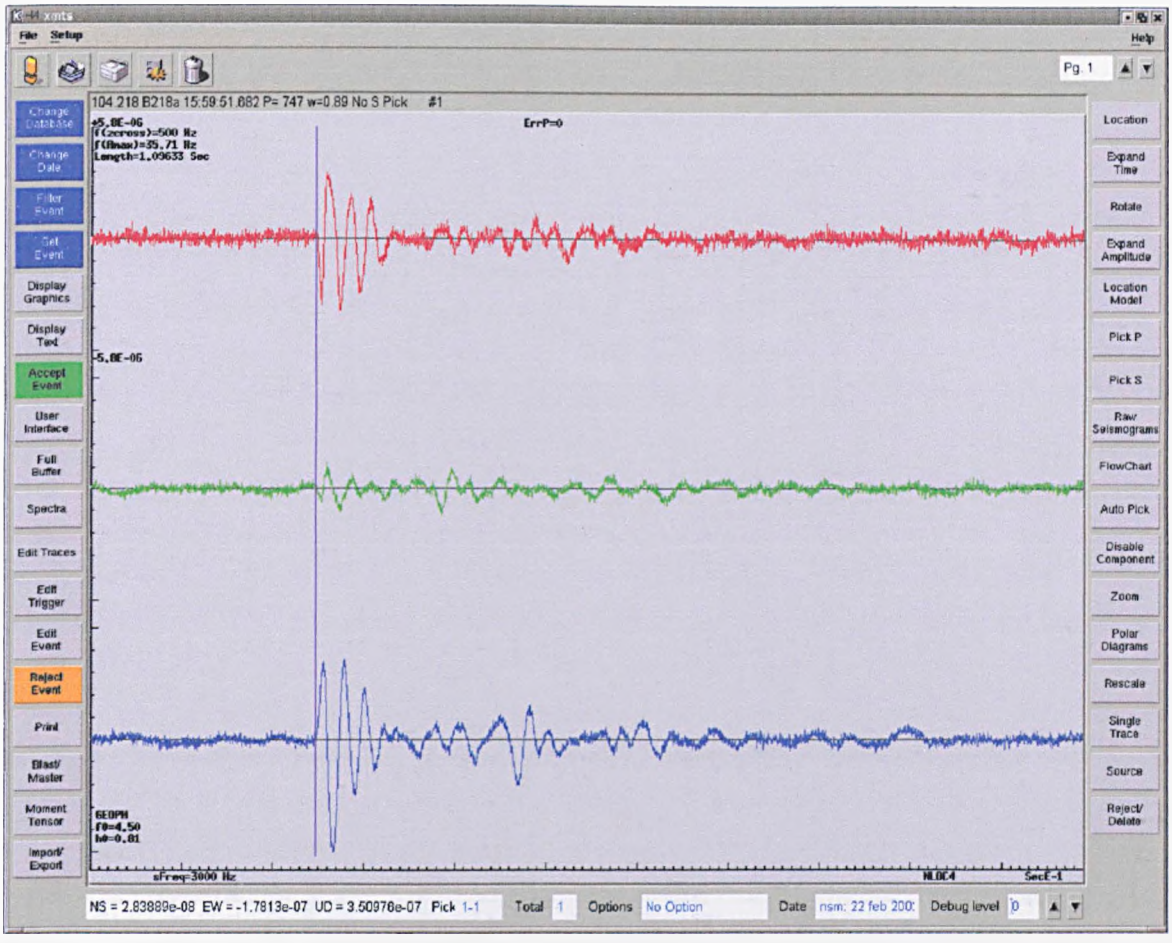


*Fig. 8.25 Northwich event recorded on Event detected at Stonemasons (4) on the 22nd Feb 2002 15:59:51.*

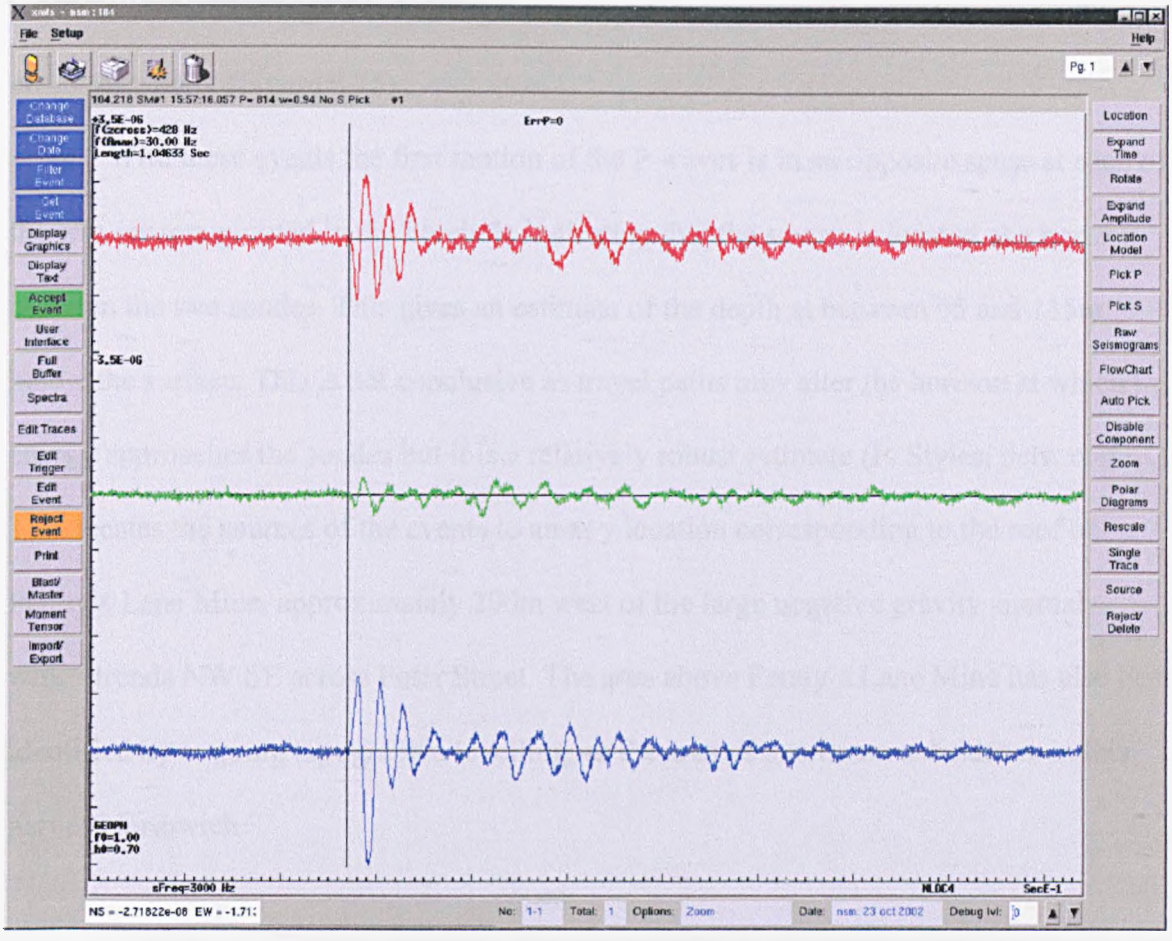


*Fig. 8.26 Northwich event recorded on Event recorded on 16th October 2002 at 14:23. This event was detected at Stonemasons (4) and Gladstone Club (9).*

It has not been possible to achieve an exact solution for the location of these sources with the Northwich network as it is rare for them to appear on enough sensors. Many of the events originate above both sondes (S. Toon, pers. comm.) which would suggest that the mechanism responsible for the events is related to dissolution at wet rock-head and not instability in the mine roof and pillars.

During November 2002 the number of events with these characteristics being detected increased dramatically. Some of these events were recorded on both the geophones at station 212 (Gladstone Club) and site 218 (Stonemasons). Analysis of the polarisation of the P waves (by S. Toon) made it possible to extract the azimuth to the

events sources. Plotting these bearings on a map gives an estimate of the source at the cross-over point (Figure 8.25)

With these events the first motion of the P waves is in an opposite sense at each of the two sensors grouted in the borehole indicating that the source is located at a horizon between the two sondes. This gives an estimate of the depth at between 65 and 115m below the surface. This is not conclusive as travel paths may alter the horizon at which the energy approaches the sondes but it is a relatively robust estimate (P. Styles, pers. comm.). This locates the sources of the events to an x, y location corresponding to the roof of Penny's Lane Mine, approximately 200m west of the large negative gravity anomaly which trends NW SE across Peter Street. The area above Penny's Lane Mine has also been identified by ongoing topographic levelling, as the area of maximum subsidence in this part of Northwich.

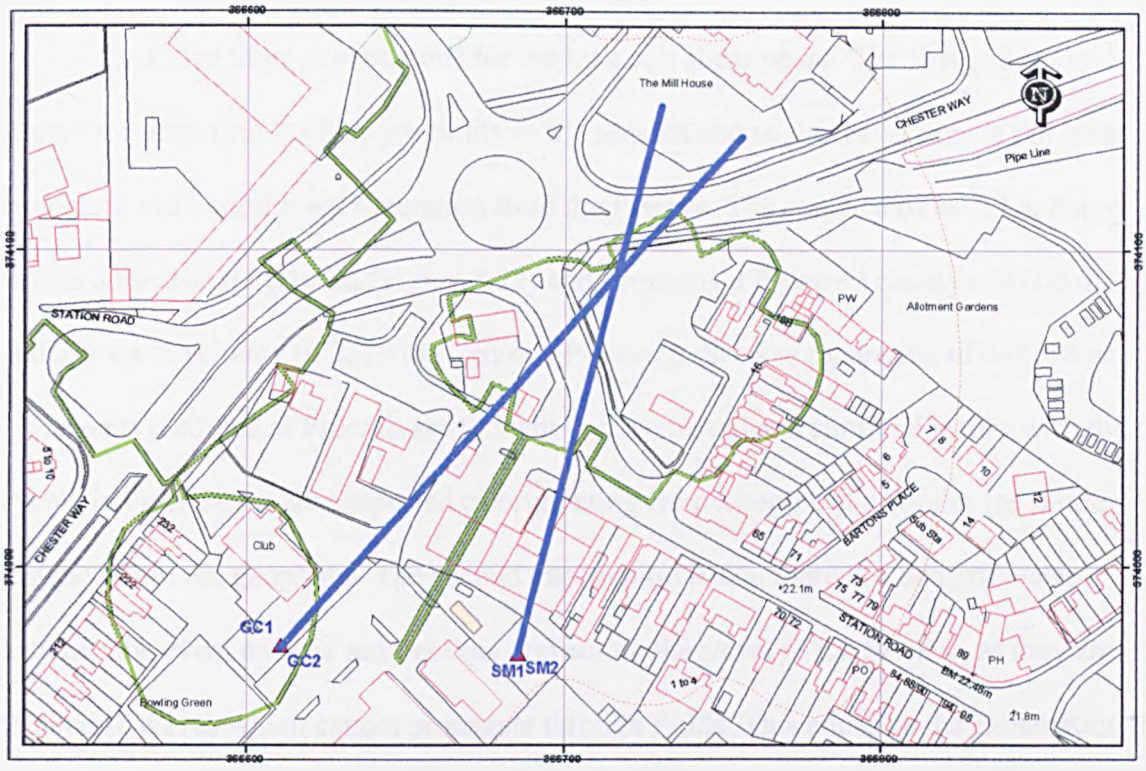




*Fig. 8.27 Map showing the direction to events for Gladstone Club (9) and Stonemasons (4). The intersection of the blue lines shows the location of the seismicity. (Styles, 2002).*

## 8.5 Discussion and conclusions

Throughout the monitoring of these three sites, there has been a dominant waveform type present in the records. The characteristics of this waveform are; short duration, low frequency, low magnitude, emergent P-waves without a clearly distinguishable S-wave arrival.

The first three characteristics are quite easy to interpret. They suggest that it is a small impulsive event (low magnitude, short duration) that has travelled some distance

(high frequencies attenuated). However, the lack of a defined shear wave phase allows for greater speculation on the mechanism of the source.

There are three explanations for the lack of a shear phase. The first is that the events are occurring in close proximity to the sensors and so the travel time is not great enough to see a significant separation from the P-wave. The distance travelled at Penny's lane is approximately 100m (Figure 8.27) and assuming a P-wave velocity of 4000 $ms^{-1}$ and a S-wave velocity of 2310 $ms^{-1}$ gives a P-wave to S-wave separation of only 18ms. The events recorded at Preesall are thought to have travelled a similar distance with the events in Peter Street are suspected or originating from a source at a similar (or shorter) distance from the geophone. The second explanation is that there is a body of water between the event and the sensors thus preventing the travel of the S-wave, as they are transverse waves which cannot propagate through fluids. This could be the explanation in the case of Preesall and Northwich Town centre. It is known that the cavities in Preesall are filled with brine in an attempt to slow down further dissolution. If the events were occurring at the base of the cavity then the shear wave portion of the energy generated would not be able to pass through the body of brine in the main cavity and therefore would not be detected by the geophone at the surface. This hypothesis has further credence if the hooking and dipping data recorded for BW64 is studied (Figure 8.28). This shows that the principal mode by which the cavity is changing in volume is not by roof collapse but by floor up-welling; therefore it is expected that the majority of seismic activity would originate from below the main body of water within the cavity. However, the time-lapse microgravity detected an increase in the negative gravity anomaly to the NE of the well head which could be supplying sediment to the area directly below the well head (and sampled by the dipping measurement). This would result in the apparent up-welling we see recorded in the dipping data.

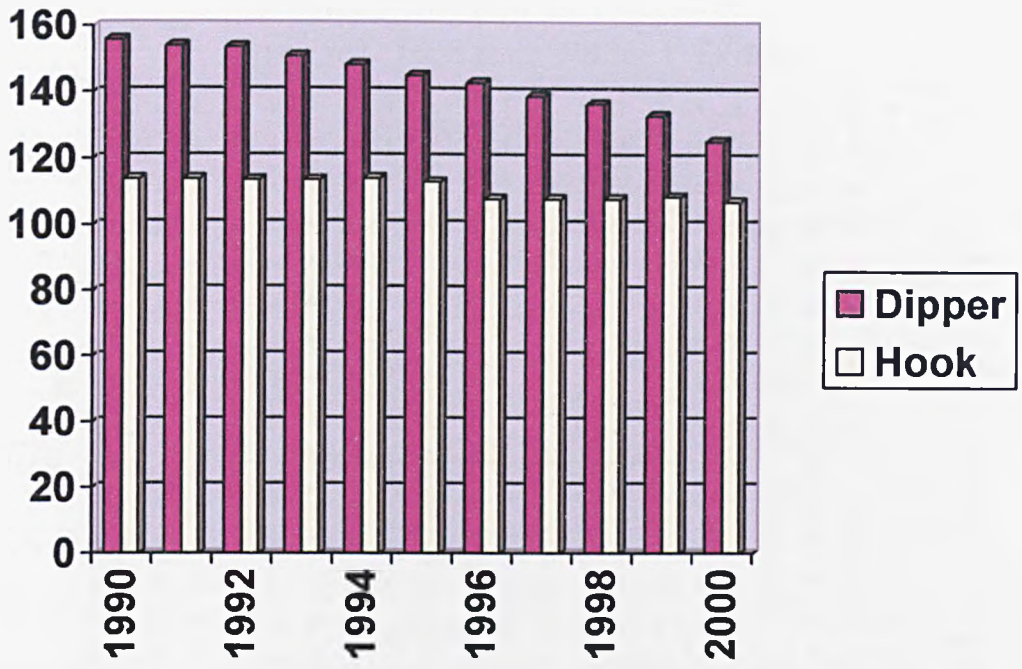


*Fig. 8.28 Plot of the hooking (roof) and dipping (floor) data for BW 64 for the period between 1990 and 2000 (Data supplied by ICI).*

This theory could also be applied to the events recorded under Northwich town centre. The mines below Northwich are again saturated and thus contain large bodies of water. However, in this case sensors are located above and below the mine and so we would expect to see one event with an S-wave arrival and one without, i.e. if the event originated below the mine then we would expect to see an event with both phases being recorded by the bottom sensor and an event with just the P wave arrival being recorded at the top sensor and vice versa. However, this is not seen. Instead both sensors are recording the same event apparently without the shear wave phase present. Therefore it is unlikely that this phenomenon is responsible for the data recorded under Northwich town centre. In the case of Peter Street there is no body of water large enough to obstruct the shear wave phase and consequently this theory can not be applied.

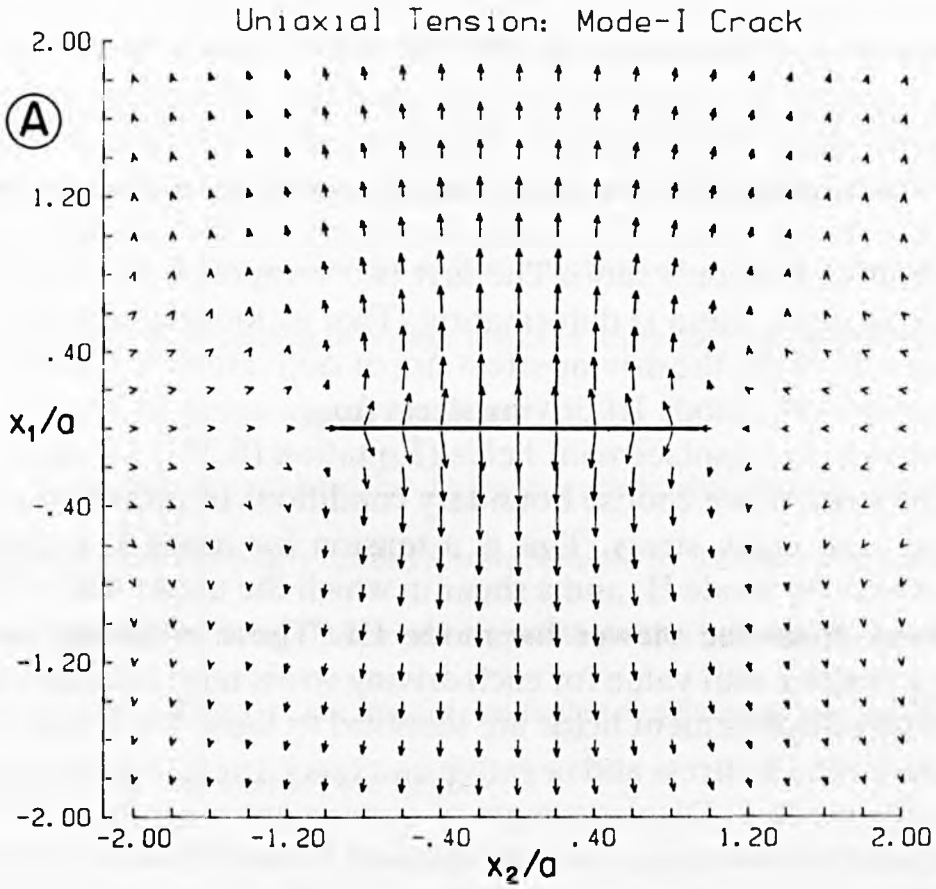


*Fig. 8.29 Displacement field for mode 1 crack deformation. The crack has a unit half width., 2a =1; the elastic shear modulus has unit value, $\mu = 1$. For the purpose of the illustration the displacements are greatly exaggerated from what is to be expected in rock. Taken from (Atkinson, 1987).*

The third possibility is that the events are associated with Mode 1 tensional fracturing where shear waves are poorly stimulated (Atkinson, 1987). Mode 1 fractures develop when an extensional force is applied to a body. The fracture develops perpendicular to the applied forces and little or no shear motion is involved. Figure 8.29 shows the displacement field for a mode 1 fracture. Displacement is perpendicular to the developing fracture with no shear components of significant magnitude visible.

Considering the fracture mechanisms involved in the 3 scenarios described above it is likely that mode 1 fracturing is dominant. In the case of Preesall and Peter Street, time-lapse microgravity (and hooking and dipping data at Preesall) has shown that cavities (an area of low density in the case of Peter Street) are propagating towards the surface. If the propagation is generated by the separation of beds/material at the top of the cavity, then it is likely that the driving mechanism of fracturing is mode 1. This fracture mechanism would result in the recording of seismic events in which the S wave is poorly defined, which is what the current evidence suggests.

It can then be postulated that the low magnitude, short duration, events with an emergent P wave and poorly defined S wave recorded by the Northwich network are also a result of mode 1 fracturing. This would suggest that either bed separation is occurring above the roof of Penny's Lane mine or that further dissolution at wet rock head is occurring in the area west of Peter Street.

# Chapter 9

# Conclusions

## 9.1 Introduction

This chapter concludes the achievements of this thesis in the context of the original aims. Consideration is given to the implications of the results and the potential development areas.

## 9.2 Aim 1 - Viability of time-lapse microgravity

The main aim of this project was to assess the viability of time-lapse microgravity surveys in environmental and geotechnical applications. Work at Preesall, Peter Street and Marston described in chapters 4, 5 and 6 show that time-lapse microgravity is an accurate, non-invasive technique that is rapid, cost effective, and beneficial to the identification and monitoring of sub-surface bodies related to subsidence.

## 9.3 Aim 2 - Precision of time-lapse microgravity surveys

In order to achieve this primary aim, it was important to establish the precision obtainable during a time-lapse microgravity survey. This was achieved by implementing controlled repeatability tests at Keele University over stable ground. These tests have identified that changes in gravity between time-lapse surveys which are above 15 μGal, can be interpreted as significant and a result of sub-surface mass movement. Field trials at Preesall brine field confirmed that this level of precision is attainable during a survey.

## 9.4 Aim 3 - Suitability of microgravity to identify the causes of subsidence

The assessment of risk posed by subsidence in an area requires the accurate identification of the cause of the subsidence. It was an aim of this thesis to ascertain whether microgravity could be used to identify the cause of subsidence in areas underlain by salt

Surveys completed around Northwich (chapters 5, 6 and 7) have identified the key role microgravity has in characterising sites effected by subsidence related to salt. Microgravity has been successfully applied in these areas to identify and characterise the causes of surface subsidence in environments that would have restricted the use and accurate interpretation by other techniques.

## 9.5 Aim 4 - The role of time-lapse microgravity

This project has demonstrated through the Peter Street case study that time-lapse microgravity is a practical and beneficial technique for use in environmental applications. Although it is easy to record the progress of subsidence it is often difficult to identify and constrain the cause of the subsidence. Time-lapse microgravity can provide a solution to this problem as well as providing information on the risk posed by future development of subsidence in the area.

## 9.6 Aim 5 - Further testing of the viability and application of microgravity and time-lapse microgravity

Further testing along the Trent and Mersey canal at Marston has demonstrated the viability and application of microgravity and time-lapse microgravity to the investigation of subsidence.

The results from the three Northwich case studies have directly increased the understanding of the causes of surface subsidence in the area and its development over time. The information obtained from these case studies has greatly improved the validity of the risk assessments in these areas.

## 9.7 Implications of this work and suggested future work

This thesis set out to investigate the practicalities and benefits of time-lapse microgravity as applied to environmental investigations. Through work documented in this thesis this project has proven the benefits of applying a long-term strategy to the problem of subsidence. Although it is beneficial to record the topographic development of surface subsidence it is more important to establish its cause and identify the potential risk posed by the sub-surface environment producing surface subsidence. Time-lapse microgravity provides the geophysicist with the means to map and monitor sub-surface density contrasts in a cost effective, non-invasive manner.

Although it is unlikely that the monitoring methods at Preesall will (or need to be) altered to incorporate time-lapse microgravity, the field tests conducted there were productive in that the unique situation present at Preesall allowed for the success of time-lapse microgravity to be assessed. The boreholes present at Preesall allow for the direct evaluation of the cavities in that area and so the added benefit of time-lapse microgravity is limited. However, regular surveys, with a suitable time gap (ten years) would give

valuable information about the development and long-term stability of the cavities and would give an indication of the state of the material surrounding the pre-existing cavity i.e. increased bed separation above the known cavity.

The work carried out at Peter Street (chapter 5) has proved to be extremely successful. Microgravity has shown that subsidence is not related to previous mine workings but is likely to be the result of dissolution of salt by the movement of groundwater (at this stage it is not possible to distinguish whether the ground water movement is natural or a result of brine extraction). Time-lapse microgravity has shown that the subsidence is related to a low density body located beneath the surface. It has been shown that this body has shallowed and then reduced in volume between 1998 and 2002. Although it is possible that this area of low-density material may be the result of a void, there is no evidence that a void currently exists. It is probable that the subsidence is a result of the compaction of loose material, generated by the backfilling of a void, which propagated up from the local wet rock head. It is unlikely that the continued subsidence of the area will result in catastrophic collapse. As a result, further remedial work is not planned.

Although limited in duration, the time-lapse program at Marston (chapter 6) and the derived interpretation has great implications for the future of the canal. The identification of such a large negative anomaly has alarming consequences when the associated missing mass is considered. The location of the anomaly (above the known extent of the mines) indicates the possibility that accelerated dissolution of salt at wet rock head is taking place. Although the time-lapse program did not yield significant results with regard to mass movement (largely due to the short time scale), it is strongly recommended that further surveys be undertaken in order to monitor this potentially catastrophic situation.

Work carried out at the second (unnamed) Marston site has led to Cheshire County Council investigating the possibility of extending the gravity survey. The aim of an extended, second survey, would be to delineate the anomaly identified in chapter 6 across a wider area. This would aid in the location of targeted drilling from which a detailed analysis and risk assessment of the area could be carried out. There is a strong case for a program of time-lapse microgravity to be established in this area as continued subsidence could again have catastrophic consequences, potentially resulting in the loss of life.

The work documented in chapter 7 resulted from a void being detected by a borehole, drilled as part of work being carried out to investigate the collapse of a riverbank retaining wall. The results obtained from the microgravity investigation enabled the characterisation of the site in a rapid, efficient and cost effective manner with minimal disturbance to the area. The void encountered in the original borehole was not found to extend further across the site, although several low amplitude, negative gravity anomalies were recorded. These were later identified as loose, low-density material by a second program of targeted drilling.

The microseismic monitoring, run concurrently with the microgravity surveys, has lead to the increased understanding of the mode of material breakdown leading to subsidence. Work carried out at Preesall and Peter Street has aided the interpretation of results recorded by the Northwich seismic network. Analysis of the data recorded at Preesall and Northwich has shown that the events are most likely to be the result of bed separation resulting in the generation of mode 1 (tensional) fractures.

The microgravity work carried out in Peter Street has strengthened the argument that activity at wet rock head is the current cause of microseismic activity in the area and not the failure of the mine roofs. This has serious implications for the current program to stabilise the mines below Northwich town centre. The Northwich network is an ongoing

project, which will continue to monitor the area and build on the results derived from the microseismic work conducted during this project and from the microgravity work carried out around Peter Street.

The use of time-lapse microgravity as a tool for monitoring the remediation of the salt mines below Northwich town centre is currently being discussed. The proposition is for microgravity surveys to be acquired before, during and after the stabilisation programme, which involves the pumping of PFA grout into the mines. Time-lapse microgravity may be used as a control to assess the success of the grouting and to identify areas that have not been successfully filled. This would facilitate the efficient and accurate location of remedial boreholes needed to assure the successful completion of the Northwich mine stabilisation program. The fact that time-lapse microgravity is being considered in such a high profile program is confirmation that the work carried out during this project and documented in this thesis has been successful in establishing that time-lapse microgravity is both practicable and beneficial to the geotechnical and engineering community.

The technique of time-lapse microgravity could be improved by the development and introduction of new gravity meters, which use modern data logging and filtering software. This has the potential to improve both the ease of data acquisition and the quality of data by filtering external noise. Instruments currently being introduced onto the market have the potential to revolutionise microgravity acquisition, eliminating the dependence of the technique on favourable weather conditions and allowing data to be acquired in hostile environments without a reduction in data quality.

Another area in which advancement towards making (time-lapse) microgravity an easily accessible tool for regular use in geotechnical solutions is the development of integrated inversion software that uses anomaly gradients together with anticipated density

contrasts and geological information to produce plausible geological solutions to the cause of the gravity anomaly. This could perhaps go someway towards de-mystifying the art of gravity interpretation, opening up the technique to a much wider audience. It is essential, however, that the principles and limitations of a technique are fully understood for their successful utilisation within a carefully considered engineering geology appraisal.

# References

Adams, S., P. A. Hart and P. W. McDowell (1992). Ground conditions at Lion salt works site, Marston, Cheshire. Proc. 4th Int. Conf. on ground movements and structures, Cardiff.

ADInstruments (2002). The Savitzky_Golay extension for Chart 4, ADInstruments. http://www.adinstruments.com/updates/appnotes/cfm4appnotes/SavitzkyGolay(4)AppNoteM.pdf

Al-Rawi, F. R., A. S. Al-Badri and J. S. Rezkalla (1989). Application of microgravimetric survey in Samawa salt deposit, Iraq. Geophysics 54(4): 440-444.

Albright, J. and C. Pearson (1981). Microseismic activity observed during depressurisation of an oil storage cavern in rock salt. Third Conference on Acoustic Emission / Microseismic Activity in Geological Structures and Materials, The Pennsylvania State University.

Arzi, A. A. (1975). Microgravimetry for engineering applications. Geophysical Prospecting 23: 408-425.

Atkinson, B. K. (1987). Fracture Mechanics of Rock. London, Academic press Inc.

Baggaley, P. (2002). Field measurements of electroseismic phenomena generated by active and passive acoustic sources. Ph.D. Thesis, School of Earth Sciences and Geography, Keele University.

Bannister, A. and S. Raymond (1967). Surveying. London, Sir Isaac Pitman and Sons.

Baranov, W. (1975). Potential fields and their transformations in applied geophysics. Geoepl. Monographs, Series 1, no. 6, Berlin, Geopublication Associates.

Bell, F. G. (1975). Salt and subsidence in Cheshire, England. Engineering Geology 9: 237-247.

Bell, F. G. (1988). Subsidence associated with the abstraction of fluids. Engineering Geology of Underground Movements, Geological Society Engineering Geology Special Publication. F. G. Bell, M. G. Culshaw, J. C. Crips and M. A. Lovell. London, Geological Society: 363-376

Bell, F. G., T. R. Stacey and D. D. Genske (2000). Mining Subsidence and its Effect on the Environment: Some Differing Examples. Environmental Geology 40.

Beres, M., M. Luetscher and R. Olivier (2001). Integration of ground-penetrating radar and microgravimetric methods to map shallow caves. Journal of Applied Geophysics 46: 249-262.

Bilham, R. (1999). NSF Absolute Gravity Facility. http://cires.colorado.edu/~bilham/GravFac.html

Bishop, I., P. Styles, S. J. Emsley and N. S. Ferguson (1997). The detection of cavities using the microgravity technique: case histories from mining and karstic environments. Modern Geophysics in Engineering Geolgy. Geological Society Engineering Geology Special Publication No. 12. London, Geological Society: 155-168.

Blakely, R. J. (1996). Potential theory in gravity and magnetic applications. Cambridge, Cambridge University Press.

Bryan-Jones, A. (1998). Evaluation of rock mass behaviour using borehole microseismic monitoring : an application to longwall coal mining. Ph.D. Thesis, Department of Earth Sciences, Liverpool.

Burton, A. N. and P. I. Maton (1975). Geophysical methods in site investigations in areas of mining. Site Investigations in Areas of Mining Subsidence. F. G. Bell. London, Butterworth and Co.

Butler, D. K. (1984). Microgravimetric and gravity gradient techniques for detection of subsurface cavities. Geophysics 49 (7): 1084-1096.

Carbone, D. and H. Rymer (1999). Calibration shifts in a Lacoste and Romberg gravimeter: comparison with a Scintrex CG-3M. Geophysical Prospecting 47: 73-83.

Cooper, A. H. (2002). Halite karst geohazards (natural and man-made) in the United Kingdom. Environmental Geology 42: 505-512.

Cordell, L. E. and R. G. Henderson (1968). Iterative three-dimensional solution of gravity anomaly data using a digital computer. Geophysics 33: 596-601.

Daniels, J. (1988). Locating caves, tunnels and mines. Geophysics: the Leading edge of Exploration 7: 32-37.

Debeglia, N. and F. Dupont (2002). Some critical factors for engineering and environmental microgravity investigations. Journal of Applied Geophysics 50: 435-454.

El-Behiry, M. G. and S. M. Hanafy (2000). Geophysical surveys to map the vertical extension of a sinkhole: a Comparison Study. Proceedings of the Symposium of the Application of Geophysics to Environmental and Engineering Problems, February 20-24, 2000 Crystal City Hyatt, Arlington, VA: 341-350

Elkins, T. A. (1951). The second derivative method of gravity interpretation. Geophysics v. 16: 29-50.

Emsley, S. J. and S. Corrie (1998). Geophysical Investigation of the Ground Subsidence land at Peter Street, Northwich, Cheshire. Maidenhead, Golder Associates (UK) Ltd.

Ervin, C. P. (1986). Temporal variations in the gravitational field of the Mississippi Embayment. Journal of Geophysical Research 91(B9): 9161-9168.

Ferguson, N. S. (1992). The detection and delineation of subterranean cavities by the microgravity method, Ph.D. Thesis, University of Liverpool.

Gehle, R. and R. L. Thoms (1981). Monitoring cyclic load effects on rock salt insitu. Third Conference on Acoustic Emission / Microseismic Activity in Geological Structures and Materials, The Pennsylvania State University.

Gelderen, M. V., R. Haagmans and M. Bilker (1999). Gravity changes and natural gas extraction in Groningen. Geophysical Prospecting 47: 979-993.

Ghatge, S. L. (1993). Microgravity method for detection of abandoned mines in New Jersey. Bulletin of the Association of Engineering Geologists 30(1): 79-85.

Goodkind, J. M. (1986). Continuos measurement of non-tidal variations of gravity. Journal of Geophysical Research B9(91): 9125-9134.

Gritto, R. and E. Majer (2000). Seismic mapping of subsurface cavities. Proceedings of the Symposium of the Application of Geophysics to Environmental and Engineering Problems, February 20-24, 2000 Crystal City Hyatt, Arlington, VA: 331-339

Hare, J. L., J. F. Ferguson, C. L. Aiken and J. L. Brady (1999). The 4-D microgravity method for waterflood surveillance: A model study for the Prudhoe Bay reservoir, Alaska. Geophysics 64(1): 78-87.

Harrison, J. C. (1960). The measurement of gravity at sea. New York, Interscience Publishers.

Harwood, G. and N. F. Johnson (1996). ICI Brinefields, stage2 - Geological Assessment, Strata Surveys Ltd.

Harwood, G. and N. F. Johnson (1997). ICI Brinefields, stage 1 - volume 1 - Data Study, Strata Surveys ltd.

Harwood, G. and N. F. Johnson (1997). ICI Brinefields, stage 3 - Risk Assessment, Strata Surveys Ltd.

Heick, C. and D. Flach (1989). Microseismicity in a flooded potash mine, the Hope Mine, Federal Republic of Germany. PAGEOPH 129(3/4): 475-496

Hente, B., A. Quijano and K. Dürr (1985). Microseismic observations in a rock salt mine with reference to the mine survey results. Fourth Conference on Acoustic Emission / Microseismic Activity in Geological Structures and Materials, The Pennsylvania State University.

Jeffrey, A. (1985). Mathematics for Engineers and Scientists, Wokingham, Van Nostrand Reinhold.

Johnson, K. S. (1981). Dissolution of salt on the east flank of the Permian Basin in the southwestern U.S.A., Journal of Hydrology 54: 75-93

Kaiser, J. (1953), Erkenntnisse unde folgerungen aus der messung von gerauschen bei zungbeanspruchung von metallischen werkstoffen, Archiv. Fur das Eisenhuttenwasen, 43-45.

LaCoste, L. (1967). Measurement of gravity at sea and in the Air. Reviews of Geophysics: 477-526.

Lacoste and Romberg (1998). Instruction manual model G & D gravity meters.

Lamont-Black, J. (1999). Report on trial geophysical works on evaluation of the GEMA geophysical techniques in Northwich Cheshire, UK, Department of Civil Engineering, University of Newcastle.

Lange (1999). Geophysical studies at Kartchner Caverns State Park, Arizona. Journal of Cave and Karst Studies 61(2): 68-72.

Loke, M. H. and R. D. Barker (1996). Rapid least-squares inversion of apparent resistivity pseudosections by a quasi-Newton method. Geophysical Prospecting 44: 131-152.

Longman, I. M. (1959). Formulas for computing the tidal accelerations due to the moon and sun. Journal of Geophysical Research 64: 2351-2355.

Maisons, C., E. Fortier and M. Valette (1997). Induced microseismicity and procedure for closure of brine production caverns. Pure Applied Geophysics 150: 585-603.

Merriam, J. B. (1992). Atmospheric pressure and gravity. Geophysical Journal International 109: 488-500.

Noel, M. and B. Xu (1992). Cave detection using electrical resistivity tomography. Cave Science 19(3).

Parker, R. L. (1995). Improved Fourier terrain correction, Part 1. Geophysics 60(4): 1007-1017.

Patterson, D. A., J. C. Davey, A. H. Cooper and J. K. Ferris (1995). The investigation of dissolution subsidence incorporating microgravity geophysics at Ripon, Yorkshire. Quarterly Journal of Engineering Geology 28: 83-94.

Phillips, C., G. Cascante and J. Hutchinson (2000). Detection of underground voids with surface waves. Proceedings of the Symposium of the Application of Geophysics to Environmental and Engineering Problems, February 20-24, 2000 Crystal City Hyatt, Arlington, VA.

Poeter, E. P. (1990). A new tool: delineation of textural heterogeneities in unconfined aquifers, using microgravity surveys during pumping. Bulletin of the Association of Engineering Geologists 27(3): 315-325

Pool, D. R. and J. H. Eychaner (1995). Measurement of aquifer-storage change and specific yield using gravity surveys. USGS publication. 33.

Qianshen, W., Z. Chijun, J. Fuzhen and Z. Wenhu (1996). Microgravimetry. Beijing, Science Press.

Ravat, D. (1996). Analysis of the Euler method and its application in environmental magnetic investigations. JEEG 1(3): 229-328.

Reid, A. B., J. M. Allsop, H. Granser , A. J. Millett, I. W. Somerton, (1990). Magnetic interpretation in three dimensions using Euler deconvolution: Geophysics, 55, (1), 80-91.

Rochester (n.d.) Subsidence and Salt. Cheshire, Salt Museum, Cheshire Libraries and Museums.

Rowell, G. A. and L. P. Yoder (1981). The effect of geophone emplacement on the observed frequency content of microseismic signals. Third Conference on Acoustic Emission / Microseismic Activity in Geological Structures and Materials, The Pennsylvania State University.

Rybakov, M., V. Goldshmidt, L. Fleischer and Y. Rotstein (2001). Cave detection and 4-D monitoring: A microgravity case history near the Dead Sea. The Leading Edge. 20: 896-900.

Rymer, H. (1989). A contribution to precision microgravity data analysis using Lacoste and Romberg gravity meters. Geophysical Journal 97: 311-322.

Rymer, H., J. Murray, G. Brown, F. Ferrucci and W. McGuire (1993). Mechanisms of magma eruption and emplacement at Mt Etna between 1989 and 1992. Nature 361: 439-441

Rymer, H. (1994). Microgravity change as a precursor to volcanic activity. Journal of Volcanology and Geothermal Research 61: 311- 328.

Schoor, M. V. (2002). Detection of sinkholes using 2D electrical resistivity imaging. Journal of Applied Geophysics 50: 393-399.

Sharma, P. V. (1997). Environmental and engineering geophysics, Cambridge University Press.

Speed, R. C. (1970). Gravity anomalies from cavities in salt beds. I. The surface Field. Northern Ohio Geological Society Third Symposium on Salt.

Steventon, H. and J. Dottridge (1997). Review of hydrogeologogy and geology of Preesall salt deposits, ICI and Hydrogeology Group, University College London.

Styles, P. (2002). Microseismic monitoring and its potential for application for the assessment of brine cavern stability, Keele University.

Talwani, M. and M. Ewing (1960). Rapid computation of gravitational attraction of three-dimensional bodies of arbitrary shape. Geophysics 25: 203-225.

Thompson, D. T. (1982). EULDPH: A new technique for making computer-assisted depth estimates from magnetic data. Geophysics 47(No 1): 31-37.

Toon, S. M. (1990). The location of faults in coal seams using microseismic activity. B.Sc. Dissertation *(unpublished)*, Department of Earth Sciences, Liverpool.

Toon, S. M., P. Styles and P. Jackson (1992). Microseismic imaging of fractures around longwall coal faces using downhole three component geophones. XVIIth General Assembly, European Geophyical Society, Edinburgh.

Toon, S. M. and P. Styles (1993). Microseismic event location around longwall coal faces using borehole in-seam seismology. Rockbursts and Seismicity in Mines, Rotterdam.

Vance, J. B. (1983). Application of microseismic techniques in potash mines. 1st international conference on Potash Technology.

Wallwork, K., L. (1956). Subsidence in the Mid-Cheshire industrial area. Geographical Journal 122: 40 - 53.

Wallwork, K., L. (1960). Some problems of subsidence and land use in the Mid-Cheshire industrial Area. Geographical Journal 126.

Wassman, T. H. (1980). Mining subsidence in Twente, east Netherlands. Geologie en Mijnbouw 59: 225-31.

Wilson, A. A. and W. B. Evans (1990). Geology of the country around Blackpool. Memoir of the British Geological Survey, sheet 66, HMSO London.

Wilun, Z. and K. Starzewski (1975). Soil Mechanics in foundation engineering, Surrey University Press in association with International Textbook Company Ltd.

Wong, I. G. (1989). Microseismicity and subsidence associated with a potash solution mine, southeastern Utah USA. Proceedings of the 4th conference of AE/MS activity in geological structures and materials 1985.

Yaramanci, U. (2000). Geoelectrical exploration and monitoring in rock salt for the safety assessment of underground waste disposal sites. Journal of Applied Geophysics 44: 181-196.

Yule, D. E., M. K. Sharp and D. K. Butler (1998). Microgravity investigations of foundation conditions. Geophysics 63(1): 95-103.

to be a result of sub-surface mass changes as there is little or no difference between the May and October surveys in this area after filtering (Figure 6.20).

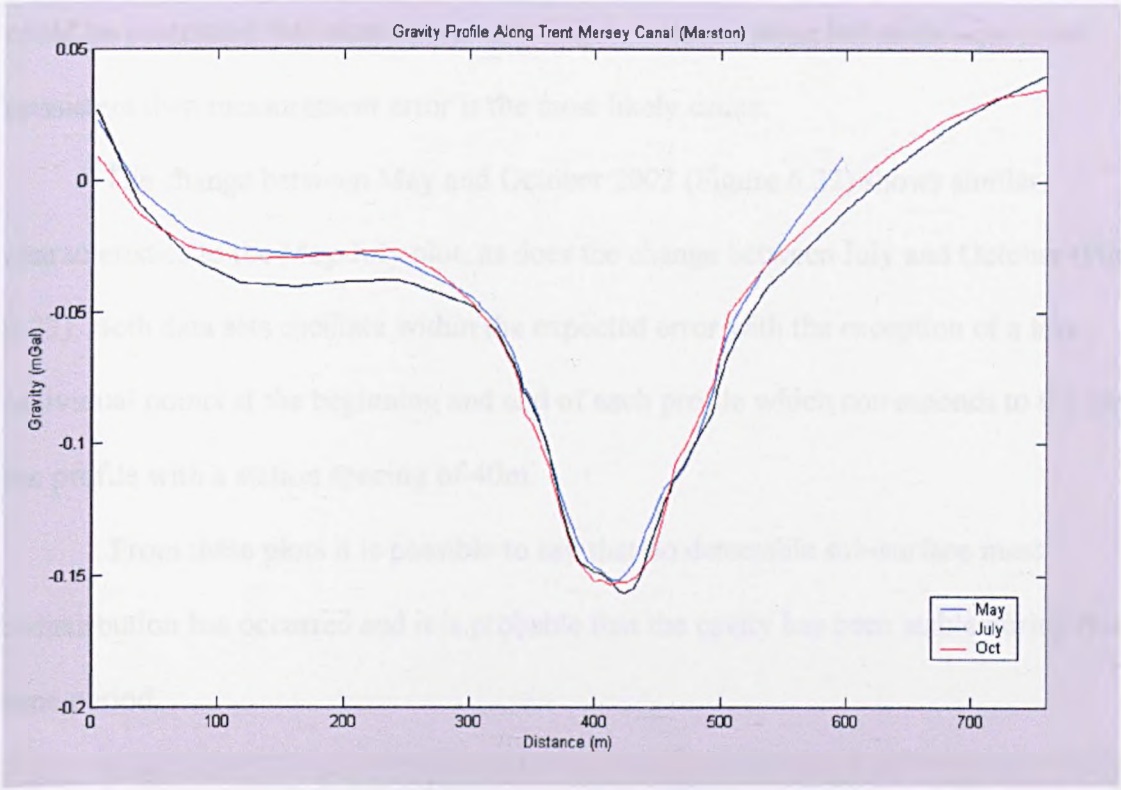


*Fig. 6.20 Plot showing the three gravity surveys after the Savitzky-Golay polynomial filter has been applied to each data set.*

In order to investigate further how the gravity signal has changed between these surveys, the reduced Bouguer anomalies from each survey have been subtracted from each other. No regional field has been subtracted from the data set as this should be accounted for in the subtraction as it will not have changed significantly in the intervening periods. In the same way any terrain effects associated with the surrounding topography will be accounted for. By removing these two contributing factors in this way, the accuracy of the survey is increased.

Examining the change in observed gravity between May and July 2002 (Figure 6.21), it becomes apparent that there is no pattern to the observed changes. Instead the